University of Dundee

University of Dundee

DOCTOR OF PHILOSOPHY

Signalling pathway of FBXO7 and its role in hereditary Parkinsonism

Sammler, Esther

Award date:
2014

Link to publication

General rights
Copyright and moral rights for the publications made accessible in the public portal are retained by the authors and/or other copyright owners and it is a condition of accessing publications that users recognise and abide by the legal requirements associated with these rights.

- Users may download and print one copy of any publication from the public portal for the purpose of private study or research.
- You may not further distribute the material or use it for any profit-making activity or commercial gain
- You may freely distribute the URL identifying the publication in the public portal

Take down policy
If you believe that this document breaches copyright please contact us providing details, and we will remove access to the work immediately and investigate your claim.

Download date: 05. May. 2023

DOCTOR OF PHILOSOPHY

Signalling pathway of FBXO7 and its role in hereditary Parkinsonism

Esther Sammler

2014

University of Dundee

Conditions for Use and Duplication
Copyright of this work belongs to the author unless otherwise identified in the body of the thesis. It is permitted to use and duplicate this work only for personal and non-commercial research, study or criticism/review. You must obtain prior written consent from the author for any other use. Any quotation from this thesis must be acknowledged using the normal academic conventions. It is not permitted to supply the whole or part of this thesis to any other person or to post the same on any website or other online location without the prior written consent of the author. Contact the Discovery team (discovery@dundee.ac.uk) with any queries about the use or acknowledgement of this work.

Signalling Pathway of FBXO7 and its role in hereditary Parkinsonism

Esther M. Sammler

A thesis submitted for the degree of Doctor of Philosophy

University of Dundee

June 2014

II. List of Figures

III List of Tables

IV REFERENCES

V Declarations

I hereby declare that the following thesis is based on the results of investigations conducted by myself, and that this thesis is of my own composition. Work other than my own is clearly indicated in the text by reference to the researchers or their publications. This dissertation has not in whole, or in part, been previously presented for a higher degree.

Esther M. Sammler

I certify that Esther Sammler has spent the equivalent of a least nine terms in research work in the College of Life Sciences, University of Dundee, and that she has fulfilled the conditions of the Ordinance General No. 14 of the University of Dundee and is qualified to submit the accompanying thesis in application for the degree of Doctor of Philosophy.

Dario R. Alessi

VI Acknowledgments

My sincere thanks goes to my PhD supervisor Professor Dario Alessi for giving me the opportunity to pursuit my scientific interest in his research group and the stellar environment of the MRC Protein Phosphorylation and Ubiquitylation Unit. As a clinician I am particularly intrigued by our inability to offer early diagnosis and effective treatments to our patients. This is mainly due to our limited understanding of the underlying disease mechanisms at a molecular level. I am ever so grateful to Dario for introducing me to his conceptual approach of how to tackle these problems by focusing on proteins and genes that arise from the genetic analysis of human diseases with a Mendelian mode of inheritance. This is the way forward towards making a difference to the growing number of patients with neurodegenerative diseases in the future.

I have been funded by the Wellcome Trust Clinical PhD programme of the University of Dundee and it has been a very special experience to be a part - no matter how small - of this amazing organization. I would like to thank my Wellcome Trust Clinical PhD programme directors Professor Sara Marshall, Professor Doreen Cantrell, and Professor Jeremy Lambert as well as my thesis monitoring committee members, Professor Kate Storey and Professor Julian Blow.

I wish to thank all members of the Alessi lab and everybody in the MRC and DSTT unit in Dundee for their tremendous support, fruitful discussions and good time together. My particular thanks goes to every single one of those people who magically make the impossible happen by cloning, sequencing (genes as well as proteins), making antibodies, producing and purifying proteins, looking after the laboratory animals, running the tissue culture facility, and keeping the lab going. I am grateful to all those helping me with my proteomic experiments.

My PhD thesis is dedicated to my daughter Maya and my husband Sheriar.

VII AMINO ACID CODE

Amino acid	Three letter symbol	One letter symbol
alanine	Ala	A
arginine	Arg	R
asparagine	Asn	N
aspartate	Asp	D
cysteine	Cys	C
glutamate	Glu	E
glutamine	Gln	Q
glycine	Gly	G
histidine	His	H
isoleucine	Ile	I
leucine	Leu	L
lysine	Lys	K
methionine	Met	M
phenylalanine	Phe	F
proline	Pro	P
serine	Ser	S
threonine	Thr	T
tryptophan	Trp	W
tyrosine	Tyr	Y
valine	Val	V

VIII Summary

Parkinson's Disease (PD) is the second most common neurodegenerative disorder after Alzheimer's and old age is the strongest risk factor for developing PD. PD has traditionally been seen as a motor disorder, but its non-motor symptoms such as dysautonomia, sensory dysfunction, sleeping problems and neuropsychiatric features equally add to the disease burden. There is no cure for PD and this is probably a reflection of our poor understanding of the disease pathogenesis. One way of tackling this is to focus on the small, but significant number of PD patients with a family history compatible with Mendelian autosomal inheritance (10-15%). Hereditary and sporadic PD share important clinical and neuropathological features, and there is reasonable hope that dissecting molecular pathways of PD gene products will have more general implications for the pathophysiology of PD associated neurodegeneration and help device new treatment strategies.

Mutations in the FBXO7 gene have recently been shown to cause an autosomal recessive early onset Parkinsonian-pyramidal syndrome and FBXO7 has been designated as PARK 15 (Di Fonzo et al., 2009). FBXO7 is a member of the F-box protein family, which functions as the variable subunit of Skp1-Cullin1-F-box protein (SCF) E3 ubiquitin ligase complexes and as such dictate substrate specificity. The canonical outcome of ubiquitylation is proteasomal degradation and my working hypothesis is that FBXO7 may be involved in protein quality control in the brain. A perturbation thereof may be a first step towards FBXO7 dependent disease.

At the time of starting with my PhD project, little was known about the molecular function of FBXO7 and how mutations in FBXO7 result in neurodegeneration. In order to learn more and dissect the signalling pathway of FBXO7 I have used tagged stable overexpression cell lines of the FBXO7 wildtype as well as human disease mutant proteins for tag-pulldowns followed by mass-spectrometry to identify interacting partners and possible substrates. With this approach I have been able to confirm the interaction between FBXO7 and its core SCF E3 ligase partners as well as some of the previously reported interacting partners. I have been able to show that not only the FBXO7 wildytpe protein, but also all of the so far reported human disease mutants are able to assemble into an SCF complex. Hence, my fist conclusion

is that the human disease mutants do not exert their pathogenicity by SCF complex disruption.

Next, a knock-in (KI) mouse model of one of the pathogenic *FBXO7* mutations (R378G) was generated and evaluated by molecular and biochemical approaches as well as motor and behaviour phenotyping. In particular, I have used the *Fbxo7* mouse model for extensive proteomic screens to identify wildtype (wt) and KI Fbxo7 interactors: endogenous Fbxo7 immunoprecipitations from mouse brain lysates and subsequent fingerprint mass-spectrometry; differential whole proteome: *ex vivo* differential dimethyl labelling of wt and KI brain samples, and Fbxo7-dependent ubiquitinome analysis: quantitative di-GLY capture proteomics combining *in vivo* SILAC labelling with antibody-based affinity enrichment of "di-GLY remnant motifs"-containing peptides prior to proteomic profiling of the wild-type in comparison to the homozygous R379G *Fbxo7* KI ubiquitinome in MEF lysates. The di-GLY remnant motif is the signature peptide of ubiquitinylated protein sites at peptide level after tryptic digestions. Some of my findings are:

- For the first time I show that endogenous Fbxo7 actually assembles into an Skp1-Cullin1-Fbxo7 complex and that the pathogenic R378G does not disrupt $SCF^{Fbxo7\text{-}KI}$ complex formation *in vivo*. This is true for the Fbxo7 KI mouse model, but also for patient derived immortalized cell lines carrying the R378G FBXO7 mutation.

- Endogenous Fbxo7 interacts with the Sumo E3 ligase complex RanBP2/ RanGAP1*Sumo1/Ubc9 complex.

- In the differential enrichment of ubiquitylated protein species in SILAC labelled wild-type and homozygous R379G *Fbxo7* KI MEFs, I have clearly identifies 2 highly conserved lysine residues, which are conserved amongst VDAC 1, 2, and 3 in mouse as well as human homologous, to be preferentially ubiquitinylated in a *Fbxo7* wild-type background (in collaboration with Dr. Patrick Pedrioli, MRC Programme leader).

- There is a significant difference in motor performance between wildtype and homozygous R379G KI Fbxo7 mice at 10 months of age (in collaboration with Dr. Steve Martin, Neuroscience Division, Dundee).

- Furthermore, I have successfully set up an *in vitro* FBXO7 dependent ubiquitinylation assays.

1 Introduction

1.1 Parkinson's Disease

1.1.1 **Historical perspective**

It was the English physician James Parkinson who first captured the clinical symptoms of Parkinson's disease (PD) by describing 6 cases in his famous monograph "An Essay on the Shaking Palsy" published in 1817(Parkinson, 2002):

Involuntary tremulous motion, with lessened muscular power, in parts not in action and even when supported; with a propensity to bend the trunk forward, and to pass from a walking to a running pace: the senses and intellects being uninjured.

Apparently, James Parkinson did not have the opportunity to examine the patients he described or else he would have noticed that muscle power was in fact normal. Also, today we appreciate that senses and intellect may be affected in PD. The French neurologist Jean-Martin Charcot subsequently named the illness after James Parkinson (in 1879) and also added the description of increased "rigid" muscle tone to the syndrome. James Parkinson speculated that the "supposed proximate cause…was a disease state of the medulla spinalis" (medulla spinalis = spinal cord). It was in the early 20th century that the substantia nigra in the midbrain was firmly established at the primary site of pathology, and characteristic intraneuronal inclusions had already been described by Lewy in 1912(Greenfield and Bosanquet, 1953; Hassler, 1937; Lewy, 1912). Subsequently, the neurotransmitter dopamine was found to be present in the brain and *"concerned with the function of the striatum and thus with the control of movement(Bertler and Rosengren, 1959)".* These discoveries form basis for the hypothesis of dopaminergic loss in the pathogenesis of PD and the rational for alleviating symptoms with levodopa and dopamine-based therapies.

1.1.2 **Etiological classification of Parkinsonian syndromes**

PD is characterized by paucity and slowness of movement accompanied by muscle stiffness and resistance to passive movement and as such is the prototype of the akinetic-rigid syndromes. The clinical signs and symptoms of Parkinsonism can occur

in different settings, and the current classification aims to stratify patients according to the underlying aetiology. This is important for clinical practice – especially for prognosis and management – but also for basic and clinical research into molecular pathways, treatments or biomarkers for the disease. For example, age of symptom onset and distinguishing whether pure Parkinsonism or Parkinsonism with additional clinical signs and symptoms points to a hereditary cause in the former and helps to distinguish idiopathic Parkinsonism from the so called Parkinsonism-Plus syndromes. A variety of drugs, in particular neuroleptic antipsychotic medications, and other underlying conditions may cause secondary Parkinsonism:

- Idiopathic Lewy body Parkinsonism: 70% of all patients
- Familial PD: There is a positive family history in about 10% of cases; this can be with autosomal recessive or autosomal dominant inheritance pattern.
- Parkinson-plus syndromes: examples include Multiple Systems Atrophy, Progressive supranucelar palsy, Corticobasal degeneration, and Lewy body dementia.
- Secondary PD: examples include drug- or toxin induced, PD in the context of infection, deranged metabolism, trauma, cerebrovascular disease, or Wilson's disease.

1.1.3 **Clinical features**

Idiopathic PD is characterized by the gradual onset and progression of tremor, rigidity, akinesia and impairment of posture and locomotion in conjunction with non-motor symptoms. The onset of motor symptoms is unilateral with progressive persistent asymmetry throughout the disease course. There is a good and sustained response to levodopa and eventually levodopa-induced dyskinesias. Idiopathic PD would be excluded if there was no response to levodopa, if a positive family history of PD was present and if dementia, postural imbalance and falls, as well as dysautonomia were prominent features during the early stages of the illness. Also idiopathic PD would be excluded if eye movement abnormalities, and pyramidal or cerebellar signs were present. However, the gold standard for the diagnosis of PD is its distinct neuropathology with degeneration of pigmented brainstem nuclei – including the dopaminergic substantia nigra pars compacta – with the presence of Lewy bodies in remaining nerve cells.

1.1.4 **Epidemiology and risk factors**

PD is a common and often disabling disease, which affects mainly people of middle and old age and occurs worldwide. About 1% of people older than 60 years of age or 3 in 1000 of the general population are affected PD, and its crude incidence is between 5-20 new cases per year for every 100 000 of the population (de Lau and Breteler, 2006). Given the demographic trends – ageing in the developed and ageing plus growing in the developing world – the prevalence of PD and associated socioeconomic burden are expected to rise exponentially(Dorsey et al., 2007). Most studies report men to be slightly more often affected than females. Pesticide and other toxin exposure have been postulated to increase the risk of developing PD(Massano and Bhatia, 2012). Likewise, there may be protective factors and the most robust association exists for smoking (Morens et al., 1995). However, the strongest risk factors for developing PD are old age and a positive family history.

1.1.5 **Monogenetic forms of Parkinsonism**

Heredibility in PD has been acknowledged for more than 100 years. The British neurologist William Gowers noted already in 1902 that 15% of his patients stated a positive family history of PD(Bhatia, 2012). Although historically a number of large PD families exhibiting autosomal-dominant inheritance were known, it was not until 1996/1997 that the first PARK gene (PARK to denote the putative link to PD) was mapped and identified to indisputably demonstrate heredibility in PD(Duvoisin, 1996; Polymeropoulos et al., 1996; Polymeropoulos et al., 1997). Since then, 28 distinct chromosomal regions have been linked to PD, but only 6 of these regions contain genes with mutations that conclusively cause monogenetic disease(Klein and Westenberger, 2012): *SNCA, LRRK2, PARKIN, PINK1, DJ-1, ATP13A2*. Although altogether mutations in these 6 genes only account for 3-5% of all PD patients, a lot of research focuses on mapping the pathways in which the aberrated gene products function and whether they intersect with the reasonable expectation to draw more general conclusions for the molecular basis of PD associated neurodegeneration. Table 1-1 gives an up to date overview of the chromosomal regions with a putative link to PD according to the current genetic classification of PD.

PARK	Gene locus	Gene	Inheritance	Onset	Comments	Pathology
PARK1	4q21-22	*SNCA*	AD	EO	Confirmed	Lewy bodies, atypical in some cases (MSA like)
PARK2	6q25.2-q27	*PARKIN*	AR	EO	Confirmed	In general no Lewy bodies
PARK3	2q13	Unknown	AD	Classical PD	Unconfirmed since 1998	
PARK4	4q21-q23	*SNCA*	AD	EO	Erroneous locus / same as PARK1	
PARK5	4q13	UCHL1	AD	EO	Unconfirmed since 1998	
PARK6	1q35-p36	*PINK1*	AR	EO	Confirmed	So far only one brain for autopsy (Lewy bodies)
PARK7	1p36	DJ-1	AR	EO	Confirmed	Unknown
PARK8	12q12	LRRK2	AD	Classical PD	Confirmed; pathogenic mutations as well as risk variants	Heterogenous, typical Lewy bodies in most cases
PARK9	1p36	ATP13A2	AR	Complex PD with EO	Confirmed	So far only one brain for autopsy (ceroid lipofuscinosis)
PARK10	1p32	Unknown	Risk factor		Confirmed susceptibility locus	
PARK11	2q36-27	Unknown	AD	Late onset PD	Unconfirmed	
PARK12	Xq21-p25	Unknown	Risk factor		Confirmed susceptibility locus	
PARK13	2p12	HTRA2	AD or risk factor	Classical PD	Unconfirmed	
PARK14	22q13.1	PLA2G6	AR	EO plus dystonia	Confirmed	Typical Lewy bodies, iron accummulation
PARK15	22q12-q13	FBXO7	AR	Complex PD with EO	Confirmed	Unknown
PARK16	1q32	Unknown	Risk factor	Classical PD	Confirmed susceptibility locus	
PARK17	16q11.2	VPS35	AD	Classical PD	Confirmed	Unknown
PARK18	3q11.2	EIF4G1	AD	Classical	Unconfirmed, likely not	

Table 1-1 Overview of PD associated chromosomal regions: PARK loci

Up to date list of PARK loci (modified according to(Klein and Westenberger, 2012)): The current genetic PD nomenclature denotes specific genetic regions with a putative link to PD as "PARK loci" and numbers them in chronological order of their discovery. It is neither comprehensive as there are other confirmed genes with a link to PD not listed amongst the PARK loci as well as erroneous – PARK 4 was designated as a novel loci but eventually found to be identical with PARK1. Some of the have been identified by genetic linkage analysis in large families, others by candidate gene approaches or genome wide association studies. EO – early onset, AR – autosomal recessive, AD – autosomal dominant. Pathology has only been reported for confirmed monogenetic Parkinsonism.

1.1.6 **Autosomal dominant PD**

Mutations in the α-synuclein gene (SNCA) and in leucin-rich repeat kinase 2 (LRRK2) cause autosomal dominant forms of PD.

- α-synuclein mutations are rare and include point mutations (PARK1) and whole-locus multiplications (PARK4)(Chartier-Harlin et al., 2004; Polymeropoulos et al., 1997; Singleton et al., 2003). The seminal discovery of the A53T point mutation in the α-synuclein gene was made in one of 2 large related kindreds from Itlay with 41 affected people over four generations(Polymeropoulos et al., 1997). The same point mutation has so far been found in 8 Greek, 2 Korean, and 1 Swedish families(Klein and Westenberger, 2012). Two further missense mutations in α-synuclein have been reported in single families from Germany (A30P) and from Spain (E46K)(Klein and Westenberger, 2012). Duplications have been found in 13 PD families and 4 in sporadic disease; whereas triplications of α-synuclein have been detected in 3 independent families(Klein and Westenberger, 2012). Clinically, patients with α-synuclein mutations tend to have early-onset PD (≤50years) and rapid disease progression. The associated clinical spectrum is broad ranging from classical PD to Parkinson-plus syndromes and penetrance tends to be high and brain pathology is characterized by abundant α-synuclein-positive neuronal inclusions. The physiological function of the α-synuclein protein remains unknown, but a role in lipid membranes and their stabilization has been suggested(Bhatia, 2012). Interestingly, abnormal filamentous aggregates of misfolded α-synuclein protein are a major component of Lewy bodies in sporadic PD(Jellinger, 2003; Spillantini et al., 1997).
- LRRK2 (PARK8) mutations in PD families were first discovered in 2004; and are the most common cause of autosomal dominant PD explaining 10% of cases (Di Fonzo et al., 2006; Paisan-Ruiz et al., 2004; Zimprich et al., 2004). The LRRK2 gene has 51 exons and encodes a large protein (>250kDa), called lrrk2 or dardarin. Over 50 variants have been identified in LRRK2 so far, but only some of them can be considered clearly pathogenic. Amongst them is the G2019S mutation, which has an

incomplete, age-related penetrance (ranging from 20% to70% by 80 years of age in differed studies) and can thus be found in familial as well as seemingly sporadic disease. The G2019S mutation is very common with a frequency of 2% of in general North American clinical populations and British Parkinson's Disease Brain Bank specimens and particularly frequent in Ashkenazy Jewish, Portuguese, and North African Arabian PD patients even in the absence of a clear family history(review:(Hardy et al., 2006)). In general, the clinical characteristics of patients with LRRK2 gene mutations - in particular those with the common G2019S mutation – are very similar to those of idiopathic PD. Nigrostriatal cell loss and gliosis are common findings in patients with LRRK2 mutations, and most of them also have Lewy bodies. However, there are also cases with no Lewy bodies, where only tau- or ubiquitin positive inclusions are observed(Zimprich et al., 2004). The lrrk2 protein contains a GTPase and kinase enzymatic domains and at least 2 protein-protein interaction domains. The common G2019S mutation lies within the kinase domain and results in a small increase in kinase activity *in vitro*(Nichols et al., 2010). Despite extensive efforts the physiological function of lrrk2 remains unknown and to date, no *in vivo* substrates of its kinase domain has been identified.

1.1.7 **Autosomal recessive PD**

Mutations in PARKIN (PARK2), PINK1 (PARK6), and DJ1 (PARK7) cause autosomal recessive forms of PD. Furthermore, mutations in ATP13A2 (PARK9), PLA2G6 (PARK14), and *FBXO7* (PARK15), cause more rare forms of recessive disease with usually very early onset (<30 years of age) and complex phenotype(Kitada et al., 1998; Paisan-Ruiz et al., 2009; Ramirez et al., 2006; Shojaee et al., 2008; Valente et al., 2004).

- Parkin mutations (PARK2) are a common cause of autosomal recessive parkinsonism with early onset. Various point mutations as well as large genomic rearrangements resulting in exon deletions and multiplications have been detected in the homozygeous as well as compound heterozygeous state. About half of the reported changes affect the region that encodes the UBL domain (459/887), amongst them is the most frequent of all PARKIN mutation: deletion of exon 3 (88/887, in 17 different

screens). The second most common mutation (c.C924T) lies outwith the UBL domain in RING1 of the protein. Additionally, there are numerous reports of cases with only a single mutation with then apparent autosomal dominant inheritance(Farrer et al., 2001; Hardy et al., 2006). Parkin mutations explain up to half of the familial cases with autosomal recessive inheritance and early disease onset (<45 years of age), and in about 15% of the sporadic cases with early disease onset (<45 years of age)(Periquet et al., 2003). The clinical phenotype associated with *PARKIN* mutations is characterized by Parkinsonism of early onset, good and prolonged response to levodopa, and in general no profound cognitive or autonomic declines. Late onset cases have been reported but not systematically screened for. The pathology associated with Parkin has only been studied in a small number of cases and has usually been regarded as a severe nigropathy – neuronal cell loss and gliosis in the substantia nigra – with lewy bodies present only in a minority of patients(Doherty and Hardy, 2013; Hattori et al., 2000). Parkin encodes for a 465 AA protein with a modular architecture comprising a carboxy-terminal domain with 3 RING (really interesting new gene) domains, one IBR (in between ring) domain and a aminoterminal ubiquitin like (UBL) domain(Wauer and Komander, 2013). As such Parkin may physiologically function as an E3 ligase with the ability to control protein turnover via polyubiquitin chain addition. However, pathological substrates responsible for neuronal death have yet to be identified *in vivo*.

- PINK1 (PARK6) mutations are the second most common cause for autosomal recessive PD with early onset with variable frequency between 1% and 9% depending on which population is examined(Klein and Westenberger, 2012). Most patients carry homozygeous point mutations – so far 60 different missense and nonsense mutations in >170 patients- but also a number of single heterozygous mutations as well as genomic rearrangements have been found. Clinically, patients resemble parkin cases, and with regards to PINK1 related pathology, it has to be noted that so far only one case with nigrostriatal neuronal loss and gliosis with only a few Lewy bodies and Lewy dendrites identified(Samaranch et al., 2010). PINK 1encodes for a protein called phosphatase and tensin homolog (PTEN)-induced,

putative kinase 1 with 581 AA. It consists of an aminoterminal mitochondrial targeting motif, a conserved serine-threonine kinase domain and a carboxy-terminal autoregulatory domain. The majority of mutations are loss-of-function mutations affecting the kinase domain. It is now assumed that PINK1 and Parkin share a mechanistic pathway in the pathogenesis of PD.

- DJ-1 (PARK7) mutations account for 1% to 2% of early-onset familial PD with autosomal recessive inheritance(Pankratz et al., 2006). About 10 different point mutations and exonic deletions have been described, mostly in the homozygeous or compound heterozygeous state. Overall, DJ-1 associated disease resembles that of the other early onset autosomal recessive syndromes caused by PINK1 and PARKIN(Hardy et al., 2006). DJ-1 codes for a uniquitously expressed protein of 189 AA that may function as a cellular sensor for oxidative stress. Mutant DJ-1 proteins are frequently misfolded, unstable, and readily degraded by the proteasome(Anderson and Daggett, 2008).
- ATP13A2 (PARK9) mutations cause a rare early onset and rapidly progressive atypical PD syndrome that is also called Kufor-Rabek disease after the region in Jordan where it was first described. Less than 10 families with PARK9 disease have been described so far and all affected cases present early (around 15 years of age) with levodopa responsive parkinsonism with additional spasticity, supranuclear upgaze paresis and dementia. There may be brain atrophy, and in at least 2 cases iron deposition in the basal ganglia has been described(Behrens et al., 2010; Schneider et al., 2010). The associated pathology is still unknown. ATP13A2 encodes a large protein with putative ATP-ase activity in the lysosomal membrane with 10 transmembrane domains(Ramirez et al., 2006). Its function is unknown, but its transcript is highy expressed in the substantia nigra, and it appears to be upregulated in idiopathic PD(Ramirez et al., 2006).
- *FBXO7* mutations (PARK15) are associated with an early onset pyramidal-parkinsonian syndrome. 3 different homozygeous and compound heterozygeous mutations have been identified so far in only a handful of families worldwide. *FBXO7*

encodes for a subunit of an E3 ubiquitin ligase and may as such be involved in protein quality control. *FBXO7* will be discussed in great detail in section 1.3.

There are a number of other genes with a link to familial PD. Amongst the ones with PARK designation are UCHL1 (PARK5), GYGYF2 (PARK11), and OMI/HTRA2 (PARK13). Additionaly, mutations in synphilin-1, NR4A2/Nurr1, POLG, mortalin, and PARL are considered to contribute to the pool of very rare causes of familial PD(Klein and Westenberger, 2012). UCHL (ubiquitin carboxy-terminal hydrolase L1) is a neuronal protein and has been suggested to binds and stabilize neuronal monoubiquitin. It is also found to be a component of Lewy bodies(Osaka et al., 2003). Also, mutations in the GBA gene encoding for the lysosomal enzyme geta-glucocerebrosidase is a recognized risk factor for PD. Pathogenic loss-of-function mutations can cause Gaucher disease with dysfunction of liver, blood, bone marrow, spleen, lung, and the central nervous system(Klein and Westenberger, 2012).

1.2 The Ubiquitin system

1.2.1 **Posttranslational modifications and cellular signaling**

The complexity and diversity of all the proteins in a living organism can be greatly increased by the covalent attachment of posttranslational modifications (PTMs). PTM is a swift way to alter activation status, turn over, subcellular localization, interacting partners or even conformational change of a protein to allow prompt adjustment and response to internal and external stimuli(Deribe et al., 2010). Important representatives of PTMs are protein phosphorylation and protein ubiquitination. Together, they govern most aspects of a living cell, but disturbances in their control mechanism can also have detrimental consequences and be linked to cancerogeneis and numerous other diseases and make a perfect target for research into understanding human diseases and developing therapies(Cohen and Tcherpakov, 2010).

1.2.2 **Ubiquitin**

Aaron Ciechanover, Avram Hershko and Irwin Rose were awarded the Nobel Prize in Chemistry in 2004 for their discovery of the ubiquitin proteasom pathway(Ciechanover,

2005; Hershko, 2005; Rose, 2005). Ubiquitin is a small, highly conserved - 76 amino acids - polypeptide of about 8500 Da – and is encoded by 4 different genes in mammals: the *UBB* and *UBC* genes encode polyubiquitin precursors, while *UBA52* and *UBA80* encode single copy ubiquitin in fusion with ribosomal proteins(Redman and Rechsteiner, 1989). In the end, these precursors are then cleaved to release identical monomeric ubiquitin units. Ubiquitin is characterized by seven Lysine residues at positions K6, K11, K27, K29, K33, K48, and K68; and these Lysines as well as the Methionine at position 1 can be involved in colalent linkages either between ubiquitin and its target proteins or the formation of ubiquitin polymers (Figure 1). It should be noted that there are many ubiquitin-like proteins that also serve as posttranslational modifiers. Despite limited sequence homology of some of these proteins with ubiquitin, they display structural homology and undergo an analogues enzymatic cascade in order to be transferred to a target protein(Ding et al., 2005; Whitby et al., 1998).

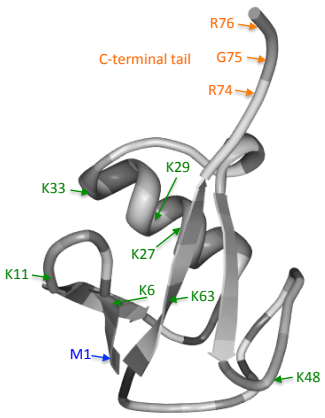

Figure 1: Structure of Ubiquitin

Ribbon representation of ubiquitin indicating the C-terminal tail and showing the seven Lysine residues (K6, 11, 27, 29, 33, 48, and 63) in green and the Methionine at position 1 in blue. These residues are used in different ubiquitin chain formations (Protein Data Bank (pdb) code 1ubq)(Vijay-Kumar et al., 1987). The

RGG motif at its C-terminal end is important for MS/MS detection of ubiquitylated species and this will be discussed in more detail in 5.1.

1.2.3 **The Ubiquitinylation Cascade**

Ubiquitin is covalently attached to other proteins in a cascade of events called ubiquitination (Figure 2). In the first instance, ubiquitin is activated by the formation of a thioester bond between its C-terminal carboxylate group and either the thiol or sulhydryl group of a cysteine residue of an E1 activating enzyme. Second, the ubiquitin is then transferred to the active site cysteine of an E2 congugating enzyme. In the third step, the E2 conjugating enzyme interacts with an E3 ligase in order to attach the C-terminal glycine of ubiquitin to the ε-amino group of a lysine of its target protein. By attaching one ubiquitin moiety to a substrate lysine, the outcome is monoubiquitylation. Multiple lysine residues of a particular substrate can be modified during multi-monoubiquitylation. If, however, the N-terminal Methionine or any of the seven Lysine residues of an ubiquitin molecule that is attached to a substrate becomes modified, polymeric ubiquitin chains are being formed. These can vary in length - from 2 to about 10 moieties – and also differ in architecture, depending on the linkage between the ubiquitin molecules. It is the topology, mode of linkage, and number of ubiquitin monomers or polymers attached that encode quite versatile information about the fate of a protein undergoing ubiquitylation (Figure 3). The outcome of ubiquitylation will be discussed in detail in 1.2.4.

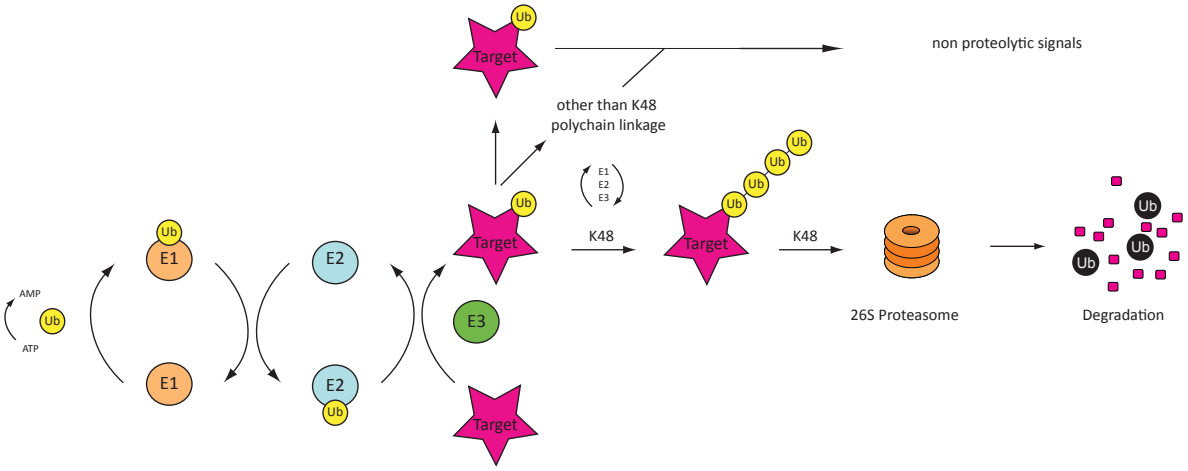

Figure 2: The ubiquitin conjugating system and functional outcomes

The ubiquitination of target protein is a three-step enzymatic reaction: Activated ubiquitin is transferred to the E2 conjugating enzyme. The E2~Ubiquitin then interacts with the E3 ligase resulting in the covalent attachment of Ubiquitin to its target protein. Monoubiquitinated proteins can either dissociate from the ubiquitination machinery or can undergo multiple rounds of ubiquitination with the effect of multi-monoubiquitin or polyubiquitin chain attachment. K48-polyubiquitination usually directs targets towards degradation by the ubiquitin proteasome pathway, whereas monoubiquitination and other ubiquitin chains (for example K63) signal towards other biological outcomes.

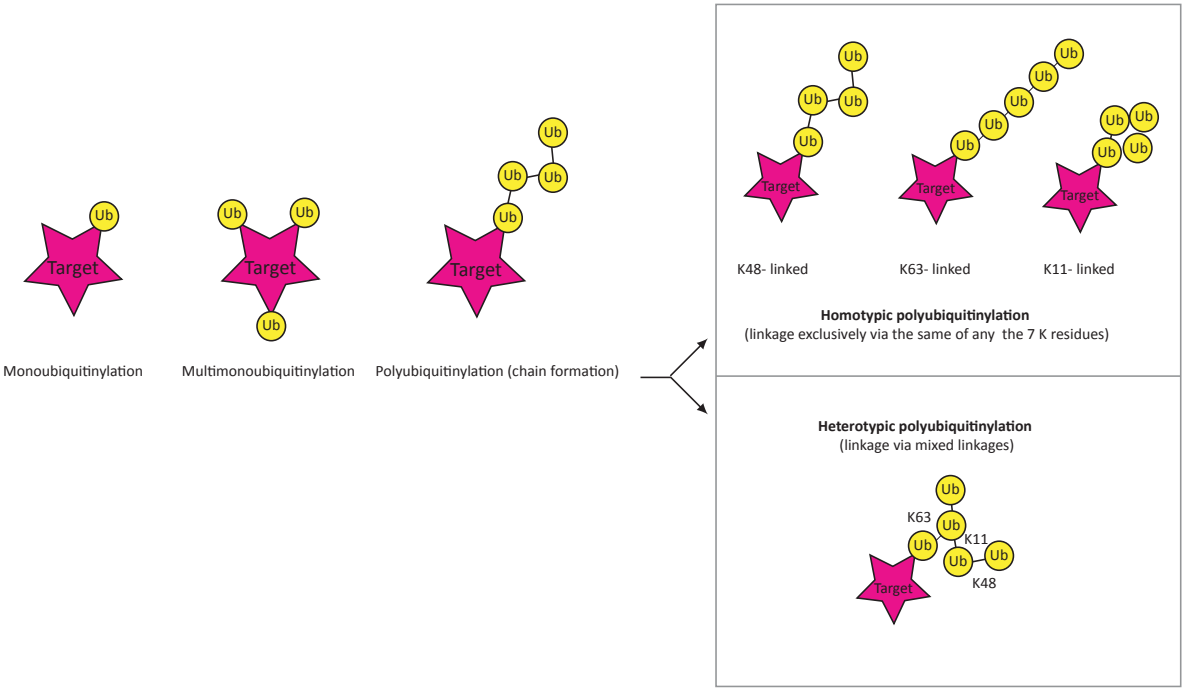

Figure 3: Different ubiquitin topologies

Depending on number and linkage type, the outcome of ubiquitylation can be mono-, multimono- and polyubiquitylation. Polyubiquitylation can result in homogtypic (polymers of the same linkage) or heterotypic ubiquitin chains and the examples of either type on the right illustrate the difference in topology and hence encoded signal.

1.2.3.1 The Ubiquitin activating enzyme

The first step in the ubiquitinylation cascade is catalysed by the ubiquitin activating enzyme E1. The human genome encodes 2 E1s; the *UBE1* and *UBE1L2* genes(Pelzer et al., 2007; Pickart, 2001). Interestingly, mutations in the *UBE1* gene have been associated with a lethal infantile form of spinal muscular atrophy, a neuromuscular disorder that is charcaterized by the degeneration of the anterior horn cells of the spinal cord(Ramser et al., 2008).

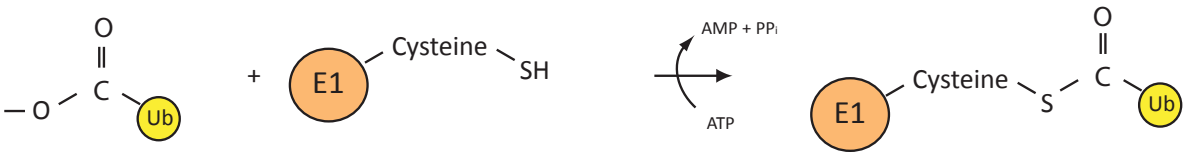

Figure 4: Ubiquitin activation

Ubiquitin activation by E1 + ATP to form E1-thioester

1.2.3.2 The Ubiquitin Conjugating Enzyme

The ubiquitin is then transferred from the E1 enzyme to the E2 conjugating enzyme by means of yet another thiol beyond between a cysteine residue of the E2 and Ubiquitin(Figure 5). There are at least 38 ubiquitin conjugating enymes in humans and at least one is associated with Mendalian disease: mutations in the UBE2A gene are associated with a X-linked syndromic mental retardation(Budny et al., 2010). The specificity in terms of the outcome of ubiquitylation – number of ubiquitin molecules attached and type of linkage – can either be attributed to the E2 alone, the E3, or a particular E3-substrate complex. An example of an E2 enzyme being the critical determand of the outcome of ubiquitylation is the E2 UBE2W: the E3 enzymes BRCA-1-BARD1 and CHIP catalyze monoubiquitylation if UBE2W is the corresponding E2, but produce ubiquitin chains with the unspecific UBE2D E2(Christensen et al., 2007; Scaglione et al., 2011). E2 enzymes can differentiate and have a preference for either

one of the 2 E1 enzymes and a single E2 can function together with several different E3s (Ye and Rape, 2009).

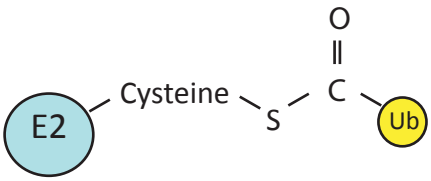

Figure 5: The Ubiquitin conjugating enzyme

Formation of a thiol bond between the acceptor Cysteine residue of the E2 and ubiquitin

1.2.3.3 The Ubiquitin Ligating Enzyme

E3 ubiquitin ligases are involved in the final step of the ubiquitylation cascade, when ubiquitin is transferred to a substrate. There are 2 major classes of E3 ubiquitin ligases defined by the presence of a RING (really interesting new gene) or HECT (homology to E6AP carboxyl terminus) domain(Deshaies and Joazeiro, 2009; Rotin and Kumar, 2009). HECT-type E3 enzymes form an obligatory thioester intermediate with ubiquitin, wheras RING-type E3 ligases lack cathalytic cysteines and mediate the direct transfer of ubiquitin to a substrate (Figure 6)(Deshaies and Joazeiro, 2009; Metzger et al., 2012). More recently, another distict type of E3 ligases has been discovered: RING-in-between-RING E3 ligases, which are hybrids in terms of how the ubiquitin is transferred from the E2 onto a substrate(Wenzel et al., 2011). It is estimated that there are over 600 human genes that encode E3 ligases, of which the vast majority belongs to the class of RING E3 ligases(Li et al., 2008). Many E3 ligases are involved in disease, which has raised interest in exploiting them as therapeutic targets(Kirkin and Dikic, 2011; Lipkowitz and Weissman, 2011). FBXO7 as part of an E3 RING complex, PARKIN as a RING-in-between-RING E3 ligase, and HECT2 as a HECT E3 ligase are all examples of E3 ligases being involved in monogenetic Mendelian neurodegenerative diseases: the former 2 in PD and the latter in an Angelman syndrome like neurodevelopmental disorder(Harlalka et al., 2013; Lucking et al., 2000; Puffenberger et al., 2012; Shojaee et al., 2008).

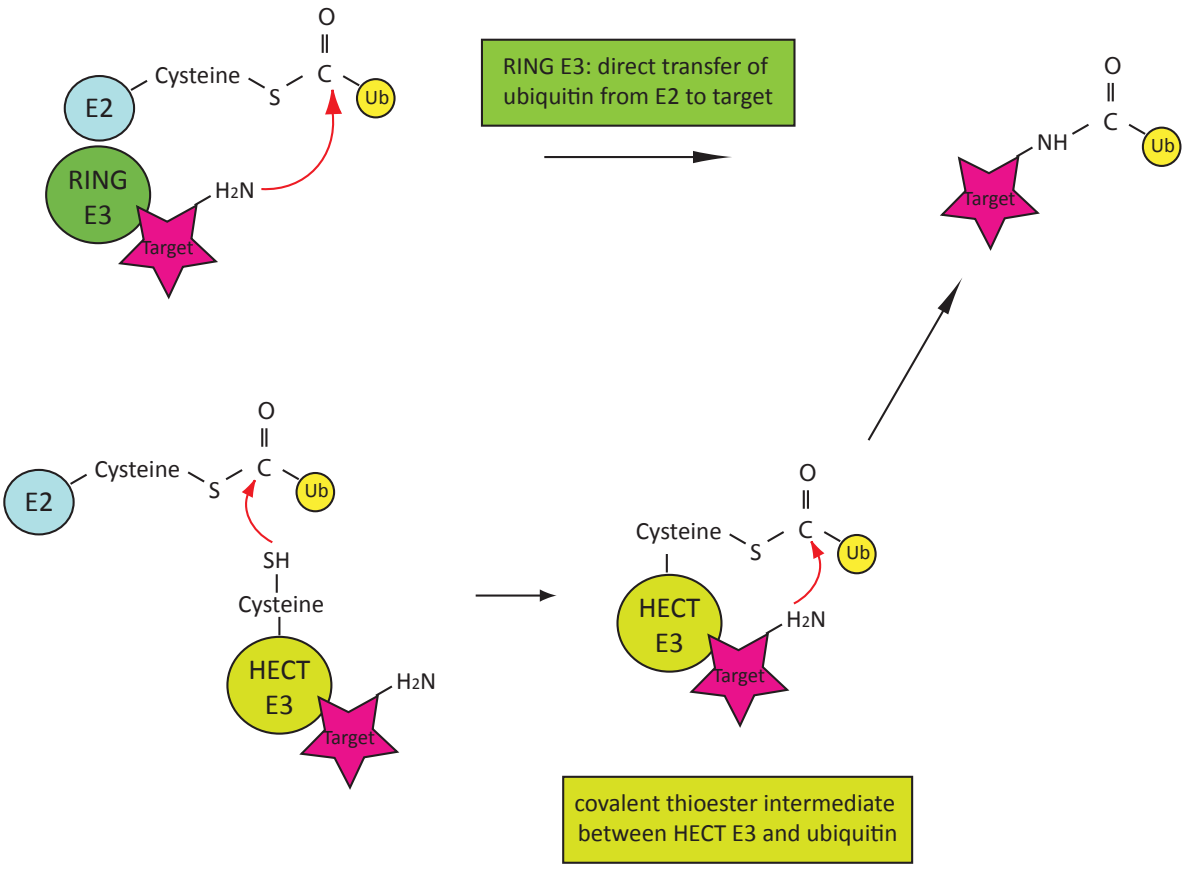

Figure 6: The 2 main classes of Ubiquitin ligating enzymes: RING and HECT E3 ligases

RING E3 ligases do not posses a catalytically active cysteine residue and facilitate the direct transfer pf ubiquitin to the ε-amine group of a substrate lysine. HECT E3 ligases posses an active site cysteine group which serves as an acceptor site for ubiquitin by means of an intermediate thiolester. The ubiquitin is then transferred from the HECT E3 ligase to the ε-amine group of a substrate lysine.

1.2.4 Outcome of ubiquitylation depending on topology

Ubiquitinylated proteins are recognized by at least 20 specialized ubiquitin-binding domains, which help decoding and translating the various ubiquitylation signals(Hurley et al., 2006). Ubiquitinylation had first been discovered and studied in the context of proteasomal degradation(Hershko and Ciechanover, 1998). This is mostly the case when the ubiquitin signal is encoded as K48 polyubiquitin chains(Chau et al., 1989; Hershko and Ciechanover, 1998). However, it has recently been found, that even K48 linkages can encode for non-proteolytic signals, for example in transcription factor regulation,

while K63 and K11 linked chgains as well as to a lesser extend K29-linked chains can also contribute to protesomal degradation(Flick et al., 2006; Komander, 2009). In cells, all possible linkages of ubiquitin chains have been detected and at least for some – monoubiquitylation and K11, K48, K63 linkges - distinct cellular outcomes have been ascertained. For other chain types - K6, K27, K29, or K33 – a clear pattern in terms of downstream effects has not been established as yet(Komander and Rape, 2012).

Mono- and multimonoubiquitylation are involved in receptor trafficking and DNA damage response pathways. Fanconi anaemia is a rare, heterogeneous chromosomal instability syndrome, which predisposes affected individuals to cancer. The Fanconi pathway contains a multiprotein core complex that functions as an E3 ligase to monoubiquitylate the heterodimeric FANCD2 / FANCI complex with subsequent initiation of replicative DNA crosslink repair(Moldovan and D'Andrea, 2009). In this context, monoubiquitylation is considered the signal for translocating the complex to the nucleus and linking it to the BRCA1 repair machinery. This is deficient in patients with Fanconi anaemia. Multimonoubiquitylation is involved in cell-surface receptor's lysosomal degradation and recycling by means of the ESCRT (endosomal sorting complex required for transport) machinery(Haglund et al., 2003a; Haglund et al., 2003b). K11 linked chains are involved in endoplasmatic reticulum associated degradation (ERAD) and cell cycle regulation; K48 linkages mostly in proteasomal degradation, and K63 linked polyubiquitinylation plays a rold in signalling, trafficking, as well as DNA damage response reviewed in: (Komander and Rape, 2012).

Ubiquitination is reversible and the cleavage of ubiquitin from proteins ("deubiquitination") is catalyzed by deubiquitinases or DUBs. Proteins that posses an ubiquitin-binding domain or ubiquitin-like domain further add to the complexity of the ubiquitination machinery by influencing the fate of ubiquitinated proteins via noncovalent interactions with ubiquitin(Grabbe and Dikic, 2009).

1.2.5 **The Ubiquitin system and human disease**

It has become increasingly evident that altered functions of components of the ubiquitin system play an important role in human diseases. Hence, the ubiquitin proteasome

system is subject of intense drug discovery programmes and harbours huge potential for devising new treatments in cancer, but possibly also in neurodegenerative diseases(Cohen and Tcherpakov, 2010; Kessler, 2013; Nalepa et al., 2006). Altered gene expression and mutations have been identified in proteins functioning as tumor suppressors such as F-box protein FBW7 or the E3 ligase von Hippel Lindau (*VHL* gene) with an heightened risk for cancer in general in the former and increased susceptibility to pheochromocytoma in the latter(Latif et al., 1993; Welcker and Clurman, 2008). Oncogenes such as *MDM2* – encoding an E3 ligases - or *SKP2* – a F-box protein - can also be found to be dysregulated in cancer and thereby ineffectively promote degradation of proteins that negatively regulate cell division (p53 and p27)(for review see:(Nalepa et al., 2006)). Mutations in the DUB CLYD (USP4) cause rare forms of cancer arising from skin appendages(Bignell et al., 2000). The breast cancer type 1 susceptibity protein (BRCA1) has E3 ligase activity and is involved in DNA repair and genome integrity(for review see:(Nalepa et al., 2006)).

There are many examples of neurodegenerative diseases that are linked with mutations in the ubiquitin proteasome system: Mutations in the E3 ligase PARKIN are frequently associated with early onset PD and had first been described in 1998 (see: 1.1.7 and (Kitada et al., 1998)). The *UCHL1* gene encodes for a ubiquitin C-terminal hydrolase has at least been implicated in one German family with early onset PD, but so far has not been replicated in other affected individuals(Leroy et al., 1998). Interestingly, homozygeous *UCHL1* mutations that are predicted to affect the function of the ubiquitin binding domain have recently been found in a Turkish family with childhood onset neurodegeneration with optic atrophy but no parkinsonism(Bilguvar et al., 2013). Muations in the F-box protein FBXO7 – subject of this thesis – are also associated with early onset complex Parkinsonism (see: 1.1.7 and (Shojaee et al., 2008). Angelman's syndrome is a complex neurodevelopmental disorder that can be caused by various genetic mechanisms and a subset of cases is caused by mutations in the E3 ligase E6-AP (UBE3A)(Malzac et al., 1998). Another mental retardation syndrome is caused by mutations in the E3 ligase HUWE1(Froyen et al., 2008; Parsons et al., 2009). Additionally, pathogenic polyglutamine expansions in *ATXN3*, which encodes a protein ATAXIN that

has deubiquitinase activity, causes autosomal dominant Spinocerebellar Ataxia(Kawaguchi et al., 1994). It has also been suggested that pathogenic expansions in the ATXN3 gene may be associated with PD depending on ethnic background based on one reported family of African descent(Gwinn-Hardy et al., 2001). All this only illustrates how important the ubiquitin system is and how fine a balance it keeps between health and disease.

1.3 FBXO7

1.3.1 **Clinical spectrum of *FBXO7* associated PD**

Mutations in the *FBXO7* gene were first shown to cause an autosomal recessive Parkinsonian-Pyramidal syndrome with early onset in 2008: Shojaee and colleagues reported homozygeous *FBXO7* missense mutations (p.R378G) in a large consanguineous family from Iran that cosegregated with the disease in 11 affected family members over 2 generations(Shojaee et al., 2008). Subsequently, one Italian and one Dutch family (each with 2 affected siblings) associated with homozygeous nonsense mutations in the former (p.R498G) and compound heterozygeous mutations in the *FBXO7* gene in the latter have been identified(p.T22M and IVS7+1g/t)(Di Fonzo et al., 2009). Additionally, a family from Pakistan and one from southeast Turkey each with homozygeous nonsense mutations (p.R498X) have been found(Paisan-Ruiz et al., 2010). Clinically, all affected individuals from the Iranian index family presented with equinovarus foot deformities since childhood. All exhibited pyramidal tract abnormalities mainly of the lower limbs (or spastic paraparesis) including spacticity, brisk deep tendon reflexes, and positive Babinski signs. No cerebellar nor supranuclear gaze abnormalities, as well as no dementia were reported. Onset of the pyramidal symptoms was always before the third decade of life. 3 of the 10 living affected family members developed extrapyramidal Parkinsonian symptoms 5-20 years after the appearance of the pyramidal signs. There was sustained levodopa responsiveness over at least 4 years in the only patient with extrapyramidal symptoms that was aminable for treatment. Structural imaging was unremarkable in the 3 patients with Parkinsonism. All other family members did not show any abnormal neurological signs or symptoms(Shojaee et al., 2008). The clinical

description for 2 out of 4 affected sibelings from the Italian family (p.R498X) states equinovarus foot deformities in one case and a combination of pyramidal and parkinsonian features from the age of 10 in the sister and 13 from the brother onwards. Additionally, there were dystonic symptoms, eye movement abnormalities and possibly cerebellar signs. The 2 Dutch sibelings (compound heterozygous mutations) developed symptoms at the age of 18 (sister) and 19 (brother). There was no dystonia, though. All 4 patients reported by Di Fonzo and colleagues had in common that there was no dementia and that structural imaging of the brain was unremarkable. A DaTSCAN-Spect (assessing biochemical integrity of presynaptic dopaminergic neurotransmitter system) was performed only in 1 of the Dutch sibelings and was abnormal. There was also levodopa responsiveness as well as levodopa-induced side effects – dyskinesias, motor fluctuations and behavioural disturbances – in all 4 patients(Di Fonzo et al., 2009). The family from Pakistan (p.R498X) includes 3 affected individuals over 3 generations with symptom onset between 17 and 22 years of age. They all display a combination of pyramidal and parkinsonian signs and symptoms and have a marked response to levodopa including the usual levodopa-induced side effects. Additionally, there was cognitive decline and some behavioural / psyichiatric deaftures in all 3, dysarthria in all 3, cataracts in 2, and cervical dystonia in 1. Structural imaging of the brain was normal in 1 and showed general atrophy in the other 2. Symptom duration was about 20 years at the time of the report. There was one affected member with homozygeous p.R498X *FBXO7* mutations in the Turkish family. He developed symptoms at the age of 17 and died 10 years later due to aspiration. He also had a combination of pyramidal and parkinsonian signs, mild eye movement abnormalities and no cognitive symptoms. Structural brain imaging was normal and there was leavodopa responsiveness and induction of side effects(Paisan-Ruiz et al., 2010).

In summary, the core features of *FBXO7* associated disease are a combination of progressive parkinsonism and pyramidal tract signs with early onset (range 10 to 22 years of age). Additional features may include supranuclear eye movement abnormalities, dystonia, cognitive decline, incontinence and dysarthria / dysphagia. Generally, there is levodopa responsiveness and suseptability to levodopa-induced side

effects. Also structural imaging of the brain is normal or shows general atrophy. Functional imaging suggests that there is a defect in the presynaptic dopaminergic neurotransmitter system. To date, there is no autopsy report available as yet. Thus, parkinsonism is cleary a core feature of *FBXO7* associated disease justifying it's designation as a PARK gene – but the associated phenotype is cleary more complex than the pure Parkinsonism seen in other autosomal recessive PARK genes such as PINK1, PARKIN or DJ-1.

1.3.2 **FBXO7 gene mutations in diease families and polymorphisms across populations**

In the *FBXO7* index family the associated disease was first linked to chromosome 22 before direct sequencing of candidate genes revealed mutations in FBXO7 gene as the culprit(Shojaee et al., 2008). The mutant allele (p.R378G) was not found in 800 control individuals – 600 of them were unrelated healthy controls over the age of 60 and 200 were unrelated Iranian PD patients(Shojaee et al., 2008). The truncating mutation (p.R498X, c.C1492T) was not found in 364 chromosomes tested from the Italian general population and of the 2 alterations that constitute the compound heterozygous FBXO7 mutation in the Dutch family, the splice site mutation IVS7+1G/T was not seen in 300 and the c.C65T (P.T22M) was not found in 348 chromosomes from the general Dutch population(Di Fonzo et al., 2009). More systematic screens have looked at populations in China, Taiwan and the South of Spain(Gomez-Garre et al., 2013; Lin et al., 2013; Luo et al., 2010): none of the known disease causing Fbxo7 mutations were found in 135 Chinese early-onset ($\leq$ 40 years of age) PD patients and 200 controls, 448 PD patients (mean age of symptom onset 57.4 years of age) and 452 age-matched controls from Taiwan, nor 338 PD patients and 330 unrelated controls from Southern Spain **Table 1-2**). All together variants in the FBXO7 gene in heterozygosis were only found in a small proportion of subjects and probably don't have a significant impact in the etiology of PD on a population level.

Reference	AA change and effect on protein	Nucleotide change	Carrier state	Affected individuals	Controls
Iranian family (Shojaee et al., 2008)	p.R378G / missense mutation	c.C1132G	Hom	11 in 2 generations	800
Dutch family (Di Fonzo et al., 2009)	p.T22M / missense mutation (isoform 1 only)	c.C65T	compound het	2 in 1 generation	348
	IVS7+1G/T / disrupts mRNA splicing	Splice site	compound het		300
Italian family (Di Fonzo et al., 2009)	p.R498X / nonsense	c.C1492T	hom	2 in 1 generation	364
Turkish family (Paisan-Ruiz et al., 2010)	p.R498X / nonsense	c.C1492T	hom	1 in 1 generation	N/A
Pakistani family (Paisan-Ruiz et al., 2010)	p.R498X / nonsense	c.C1492T	hom	3 in 3 generations	N/A

Table 1-2 Pathogenic *FBXO7* mutations

List of pathogenic *FBXO7* gene mutations that have been identified so far in a small number of families from different ethnicities, associated amino acid change and number of affected individuals per family and population matched controls. Mutations in *FBXO7* with reference to GenBank accession number NP_036311.3 [Homo sapiens].

1.3.3 FBXO7: transcripts and protein

1.3.3.1 FBXO7 transcripts

The *FBXO7* gene is located on the long arm of chromosome 22 (22q12-q13) where also one of the other rare autosomal recessive PARK genes is located (PARK14/PLA2G6). It is composed of 9 exons and spans a genomic region of about 24 kilobases. Alternative splicing at the 5' end is expected to yield 3 complete protein coding FBXO7 isoforms, which are annotated by NCBI: (NM_001033024.1, NM_001257990.1, NM_012179.3)(Di Fonzo et al., 2009). By convention, FBXO7 gene variants and mutations are named

after the longest mRNA transcript: isoform 1(GenBank accession numbers NM_012179.3 for the transcript and NP_036311.3 for the protein). One of the pathogenic missense mutations (p.T22M) only affects the longer isoform 1 and leaves any shorter isoforms unaltered. The splice site mutation (IVS7 + 1G/T) is expected to disrupt mRNA splicing as it removes an invariable splicing donor of intron 7(Di Fonzo et al., 2009).

1.3.4 **FBXO7 belongs to the family of F-box proteins**

FBXO7 belongs to the family of F-box proteins. F-box proteins are characterized by the presence of a F-box domain, which mediates binding to SKP1 and subsequent assembly into ***S***kp1-***C***ullin1-***F***-box-protein-Rbx1 (SCF) ubiquitin E3 ligase complexes(Zheng et al., 2002). F-box proteins usually form the variable substrate recognizing subunit of SCF ubiquitin E3 ligases of the RING type (1.2.3.3) with the canonical outcome of ubiquitin-mediated proteolysis(Ho et al., 2006; Skaar et al., 2013). However, functioning within the ubiquitin-proteasome-pathway is not a necessary or at least not exclusive function of F-box proteins, and there are ample examples in the literature(Hermand, 2006; Jonkers and Rep, 2009; Nelson et al., 2013). F-box proteins are a divers group of proteins and can be further classified into 3 subfamilies depending on the presence of additional domains other than the F-box: FBXW with an additional WD40 domain, FBXL with a leucin-rich-repeat domain and F-box only proteins(FBXO)(Jin et al., 2004). More recently, it has become clear that some members of the FBXO family actually do have additional domains hence calling them 'F-box proteins with other domains' is more appropriate than 'F-box only proteins '(Skaar et al., 2013). In humans, there are about 70 F-box proteins; 12 of them are members of the FBXW, 21 of the FBXL, and 36 of the FBXO family(Skaar et al., 2009a). However, if an F-box protein functions as an E3 ubiquitin ligase, it requires assembly into an SCF complex as the substrate recognizing subunit. It then plays its part in the concerted action of ubiquitin-activating (E1), ubiquitin-conjugating (E2) and ubiquitin-ligating (E3) enzymes with the outcome of ubiquitylation and subsequent proteasomal degradation of its substrates.

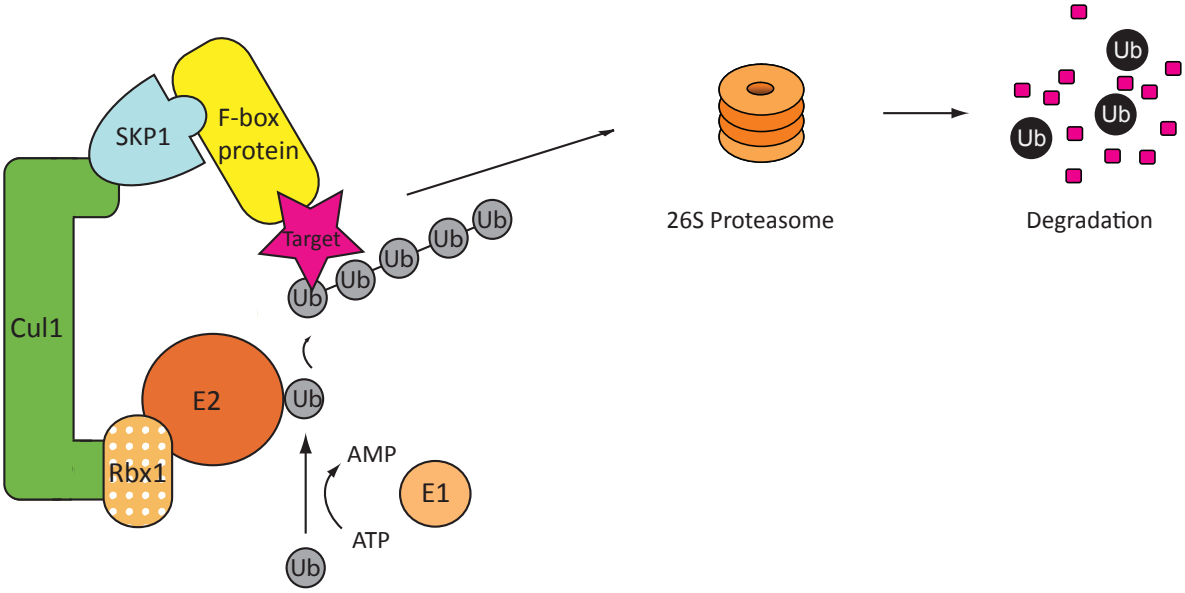

Figure 7: The SCF E3 ubiquitin ligase complex and proteasomal degradation

Cullin 1 (Cul1) serves as a scaffold bringing the E2 conjugating enzyme via RBX1 at its carboxy-terminal end in proximity to its target by recruiting the F-box protein via SKP1 to its amino-terminal end. Substrate specificity is hence dictated by the F-box protein; and the modular assembly of SCF complexes allows ubiquitinylation of many different substrates depending on which F-box protein participates. The E2 transfers ubiquitin to the target for ubiquitin-mediated degradation by the 26S proteasome(Zheng et al., 2002).

1.3.4.1 Protein and domain architecture of FBXO7

There are at least 3 Fbxo7 isoforms with differing N-terminal domains and consisting of between 408 and 522 AA(Di Fonzo et al., 2009). Only the longer isoform 1 contains an additional N-terminal Ubiquitin-like domain (UBL; AA 1-78); otherwise there are the F-box domain for binding to SKP1 (AA 329-379), the FBXO7 and PI31 interacting domain (FP, AA 180-324), a Cdk6-interacting motif, and a C-terminal, most likely unstructured proline-rich-region (PRR, AA 423-522), which are shared by all 3 isoforms (Figure 8). There is no structural information available on FBXO7 as yet; the crystal structure of the FP domain of PI31 has been solved, and the corresponding FBXO7 domain is on its way of being reported(Kirk et al., 2008; Shang et al., 2013).

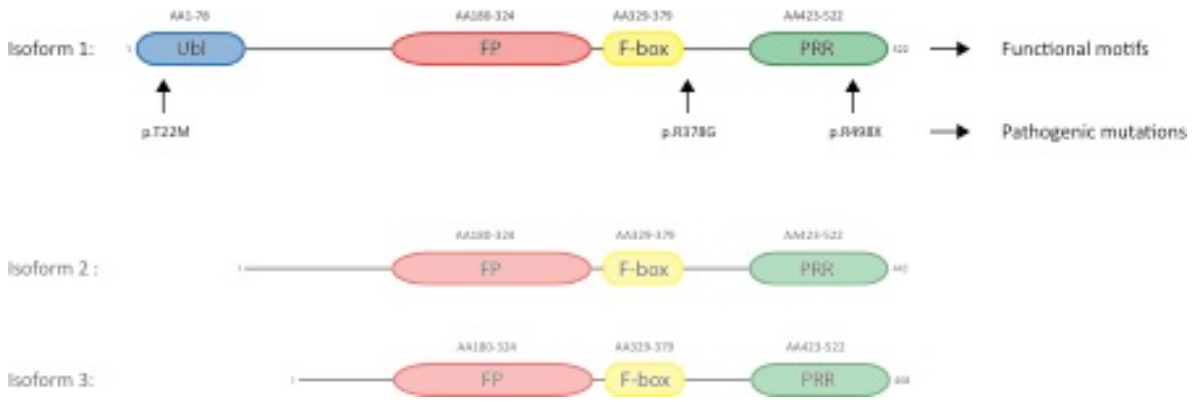

Figure 8: The human FBXO7 protein, domain arichtecture and pathogenic mutations

Schematic representation of the FBXO7 transcripts (NM_001033024.1, NM_001257990.1, NM_012179.3) with functional domains and position of all so far reported pathogenic *FBXO7* mutations. By convention, FBXO7 gene variants and mutations are named after the longest mRNA transcript: isoform 1(GenBank accession numbers NM_012179.3). UBL (Ubiquitin-like domain, AA 1-78), FP (FBXO7 and PI31 interacting domain, AA 180-324), F-box (AA 329-379) and proline-rich-region (PRR, AA 423-522).

1.3.5 Putative function and reported interacting partners of FBXO7

FBXO7 was identified as a member of the F-box protein family in the context of systematic screening for other SKP1 binding poteins after the initial discovery of the first F-box protein, cyclin F, in 1999(Cenciarelli et al., 1999; Winston et al., 1999). While FBXO7 had been the subjects of only a few publications before its link to human disease in 2008 / 2009, this has changed in recent times, at least in terms of number of citations and related publications.

1.3.5.1 FBXO7 and its link to the ubiquitin-proteasome system

The first reported substrate of FBXO7 / SCF^{Fbxo7} was HURP (Hepatoma up-regulated protein)(Hsu et al., 2004). It was shown that HURP is a mitotic phophoprotein, which co-immunoprecipitates specifically with tagged FBXO7, but not with several other F-box proteins. Endogenous Cullin1 and endogenous SKP1 were also shown to co-immunopreicipitate with overexpressed FBXO7. The binding site for HURP was mapped to the C-terminal proline rich region of FBXO7 and binding was dependent on HURP phosphorylation as a phosphomutant, in which all 9 previously mapped cdk1-cyclinB-mediated phosphosites of HURP were mutated to Alanine, abolished this interaction.

Furthermore, HURP expression levels stabilized in the presence of proteasomal inhibition and higher molecular weight species of tagged HURP co-immunoprecipitated with tagged Ubiquitin in Hek 293 cells. Also, knockdown of Fbxo7 was suggested to stabilize endogenous HURP. In summary, HURP was proposed to be the first identified FBXO7 substrate, which requires cdk1-cyclinB-mediated phosphorylation for its recognition. It was initially identified as a putative oncogene in hepatocellular carcinoma. Whether it is physiological substrate of FBXO7 and its role – if at all – in FBXO7 mediated pathology is unknown.

FBXO7 has further been suggested to be involved in the ubiquitinylation of the cellular inhibitor of apoptosis (cIAP1) and TNF receptor associated factor 2 (TRAF2)(Kuiken et al., 2012): First, FBXO7 was identified as a negative regulator of NFκB signalling in a siRNA screen amongst E3 conjugating and deconjugating enzymes. This was linked to FBXO7 function within a SCF^{FBXO7} E3 ubiquitin complex as overexpression of the FBXO7 wt, but not a F-box motif-deficient mutant (predicted to disrupt SCF complex formation) diminished the activity of a NFκB luciferase assay in U2OS cells. Subsequently, the interaction between overexpressed FBXO7 and either cIAP1 or TRAF2 was investigated as both proteins associate with activated TNF-α receptor 1 complex (TNFR1) - cIAP1 being recruited via TRAF2 - and hence find there place in the complicated NFκB signalling cascade(Wertz and Dixit, 2010). Also, cIAP1 had previously been reported to interact with FBXO7 in co-expression experiments(Chang et al., 2006). It was shown that co-expressed FBXO7 -wt as well as mutant - and cIAP1 coimmunoprecipiate, but that the wt associates with higher molecular weight, ubiquitin-modfied species of cIAP1 whereas the mutant doesn't. Similarly, overexpression experiments demonstrated an interaction between TRAF 2 and the wt as well as the mutant FBXO7. When tagged TRAF2, ubiquitin with either wt or mutant FBXO7 were co-transfected, an increase in TRAF2 ubiquitylation in the wt, but not the mutant FBXO7 was demonstrated. Hence, it was concluded that FBXO7 ubiquitylates cIAP1 and TRAF2. NFκB signalling is involved in many pathologies and a link to FBXO7-associated neurodegeneration is an intriguing hypothesis warranting further investigation.

1.3.5.2 Cyclin D and FBXO7: potential involvement in the cell cycle

The first physical interaction at endogenous levels was shown between FBXO7 and cyclin D in U2OS cells(Laman et al., 2005). It was also shown that coexpressed Flag-FBXO7 and T7-RBX1 into U2Os cells interacted with each other and also with endogenous Skp1 in support of SCF^{FBXO7} complex formation *in vivo*. FBXO7 was thus seen in the context of cell cycle regulation. The same authors further speculated that FBXO7 might have oncogenic potential. This was based on the observation that exogenous overexpression of FBXO7 in mouse fibroblasts was associated with cellular transformation and tumour formation in nude mice, and also that certain tumour biospsie of human lung and colon cancer were positive for FBXO7 while it was absent in corresponding normal tissues(Laman, 2006; Laman et al., 2005).

1.3.5.3 FBXO7 and PI31: proteasomal pathways

As a member of the F-box family and supported by previous reports on its potential involvement in ubiquitylation of other proteins, FBXO7 may play a critical role in the ubiquitin-proteasome pathway. Further evidence that places FBXO7 in the context of proteasmal pathways comes from its domain architecture: the presence of a putative UBL and FP domain. Isoform 1 of FBXO7 has been suggested to contain a UBL domain, although no function has been reported with it as yet. PI31 on the other hand has been found to share sequence homology in a region of about 150 AA with FBXO7 with 24% identity and 45% similarity (FBXO7: AA 180-324 and PI31: AA 1-151). As this region mediates binding between the 2 proteins, it has been termed FP domain (for FBXO7 and PI31 dimerization domain). Its crystal structure has been solved for PI31 and reveals a globular domain with an unusal α/β fold(Kirk et al., 2008). What the *in vivo* function of the interaction between FBXO7 and PI31 may be is unclear. However, studies in Drosophila demonstrate a functional relationship of their orthologues DmNutcracker and DmPI31 in a proteasomal regulatory complex involved in non-lethal caspase activity in the final step of spermatogenesis, a cellular remodelling process that eliminates excess organelles and cytoplasm(Bader et al., 2011). Binding via the FP domain was conserved, and this interaction was indispensable for DmPI31 stability: in the absence of Nutcracker or a mutant deficient of binding, DmPI31 levels were greatly reduced – the

opposite of what one would expect if DmPI31 was a substrate of SCF^{FBXO7} proteasomal degradation. Also, C-terminal cleaved forms of DmPI31 appeared in the Nutcracker deficient and mutant forms. Ultimatively, the conclusion was that Nucracker functions through DmPI31 stabilization of especially the C-terminal end of DmPI31 to promote caspase activation and sperm differentiation. Contrary to the original characterization of PI31 as a proteasomal inhibitor, DmPI31 was found to have activating effects *in vivo* and a C-terminal HbYX motif was thought to be important in this context. This motif resembles the proteasome-interacting, gate-opening domains of the proteasome-regulatory ATPases, which are proteasome activators. In DmPI31 the HbYX motif is located within in the C-terminal end that is stabilizes via its interaction with FBXO7. Understanding the FBXO7 / PI31 interaction as a mechanism to regulate proteasomal activity is very interesting for formulating hypothesis of how FBXO7 mutations cause human pathology. Abnormal protein aggregation is a key feature of neurodegenerative diseases including PD and the ubiquitin proteasome system has been implicated in disease pathogenesis by failing to clear potentially neurotoxic molecules(Ebrahimi-Fakhari et al., 2012; Ross and Poirier, 2004).

1.3.5.4 FBXO7 and possible links to PD/PARK associated pathways in mitophay

So far the mitochondrial damage repair pathway has been implicated as a theme in the pathogenesis of several monogenetic PD genes. In fact, there is now compelling evidence that at least 2 of the autosomal recessive PD gene products – PINK1 and PAKIN - act in the same pathway involved in mitochondrial quality control: In genetic Drosophila models, Dm*PINK1* as well as Dm*PARKIN* knockout flies display similar phenotypes with reduced longevity, degeneration within the dopaminergic system, motor deficits, and male sterility as well as mitochondrial dysfunction in particular in the former Clark, 2006 #160}(Park et al., 2006). Furthermore, the double-knock out of both genes presents with a very similar phenotype and overexpressing either fly or human *PARKIN* was able to rescue the *PINK* null phenotype, but not vice versa and hence, that both gene products act in series with *PARKIN* downstream of *PINK1*(Yang et al., 2006). Further studies in mammalian cells have shown that PINK1 senses depolarized / damaged mitochondria, and recruits and activates PARKIN, which functions as a RING-

IBR-RING E3 ubiquitin ligase, to ubiquitinylate proteins in the outer mitochondrial membrane(Chan et al., 2011; Chen and Dorn, 2013; Narendra et al., 2010; Poole et al., 2010; Sarraf et al., 2013; Seibler et al., 2011; Tanaka et al., 2010). The end result is then selective autophagy of damaged mitochondria called mitophagy.

More recently, FBXO7 has been implicated to interact with PARKIN as well as PINK1 and also be involved in mitophagy(Burchell et al., 2013). In analogy to the genetic drosophila studies that eluded the functional dependency of PINK1 and PARKIN, ectopic expression of FBXO7 was shown to be able to rescue the PARKIN locomotor and mitochondrial phenotype. This was not achieved when any of the disease mutants was expressed instead, possibly suggesting a pathomechanistic clue. As before shown by Bader et al. knockdown of the FBXO7 ortholog DmNutcracker resulted in male sterility with no other overlap with the PD phenotypes of PINK1 and PARK knockdown(Bader et al., 2011), which could not be rescued by ectopic FBXO7 expression which led to the authors' conclusion that DmNutcracker is not a functional homolog of FBXO7(Burchell et al., 2013). Furthermore a direct physical interaction between FBXO7 and PARKIN was demonstrated in coimmunoprecipitations assays in double overexpression cell culture systems and also for endogenous FBXO7 with overexpressed PARKIN in HEK293 cells. The site of interaction was mapped to the N-terminal end of FBXO7 (AA1-88) which includes its UBL domain and which is only present in the longer isoform 1 of FBXO7.

With regards to genetic Drosophila studies aiming to elucidate the interaction between FBXO7 and PINK1, it was shown that FBXO7 was unable to rescue the PINK1 knockdown phenotype. However, the fact that FBXO7 overexpression enhanced the "rough eye" phenotype that is seen with PINK1 overexpression was seen as a potential genetic link between the 2 nonetheless. In fact, FBXO7 overexpression was unable to rescue the phenotype of the double knockout *PINK1/PARKIN*, which was interpretated that PINK1 activity was required for proper FBXO7 functioning(Burchell et al., 2013). Please refer to the schematics and table below for a summary of the insight into genetic links between PINK1, PARKIN and FBXO7 that has been gained from Drosophila melanogaster studies (Figure 10, Figure 9,Table 1-2).

PD locus	Gene	Inheritance	Fly homolog	Fly homolog
PARK2	*PARKIN*	AR	Dm*PARKIN / CG10523*	42% identidity 50% similarity
PARK6	PINK1	AR	Dm*PINK1 / CG4523*	32% identity 50% similarity
PARK15	FBXO7	AR	Dmnutcracker* / CG10855	28% identity 45% similarity

Table 1-3 Drosophila homologs of the PARK genes PINK1, PARKIN and FBXO7

Fly homologs are referenced according to Flybase(Marygold et al., 2013). With regards to FBXO7 (*), DmNutcracker may not be a functional ortholog, as it does not cause a neurodegenerative / locomotor phenotype as for example PINK1 and PARKIN. Nutcracker and FBXO7 share the F-box and FP domain, but Nutcracker lacks the C-terminal Proline rich region of FBXO7.

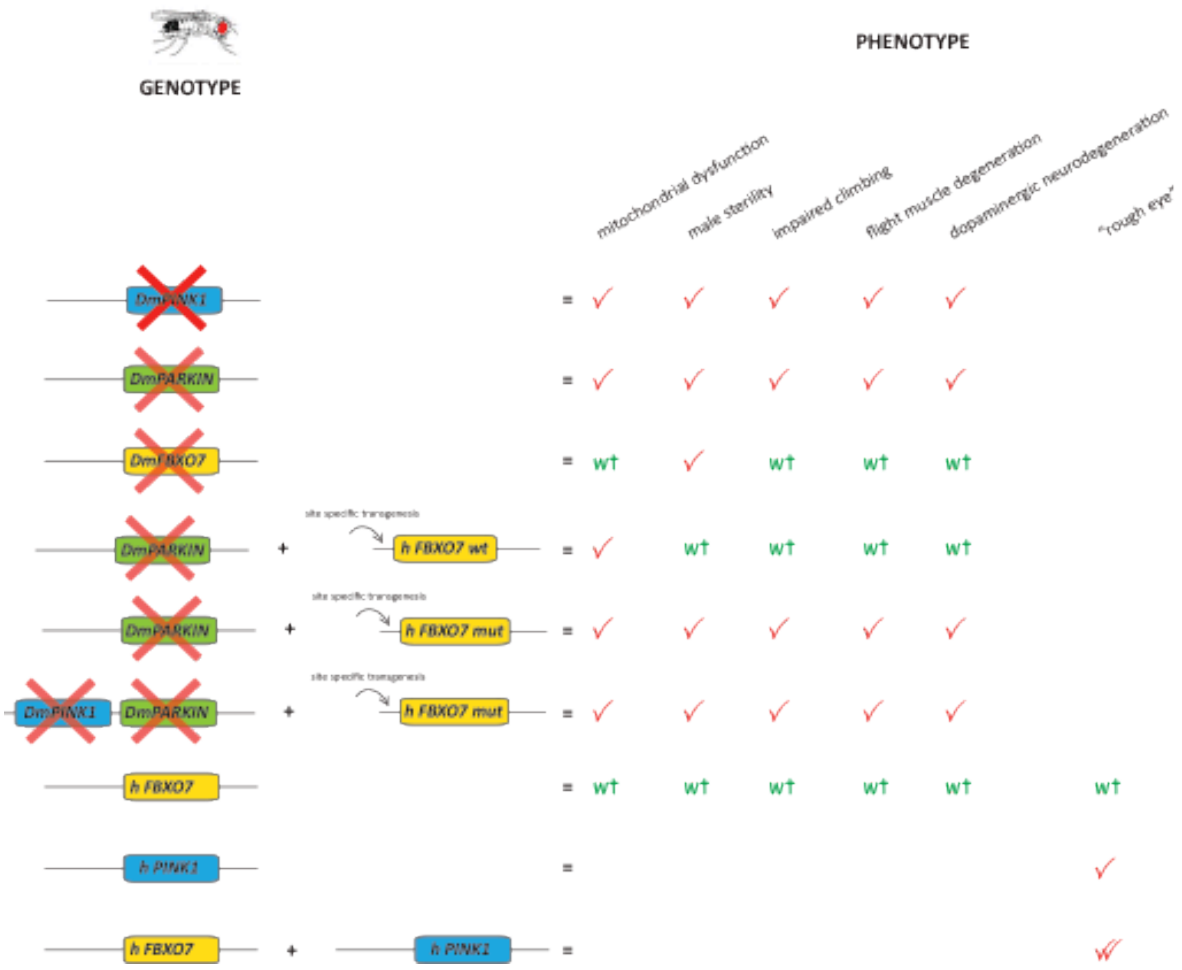

Figure 9 Genetic insights from Drosophila studies into PD pathways

Summary of the effects of genetype (gene knock-out: red cross; or transgenic expression: coloured boxes) on phenotype (wt: no difference to wildtype; red tick: abnormality present) in Drosophila

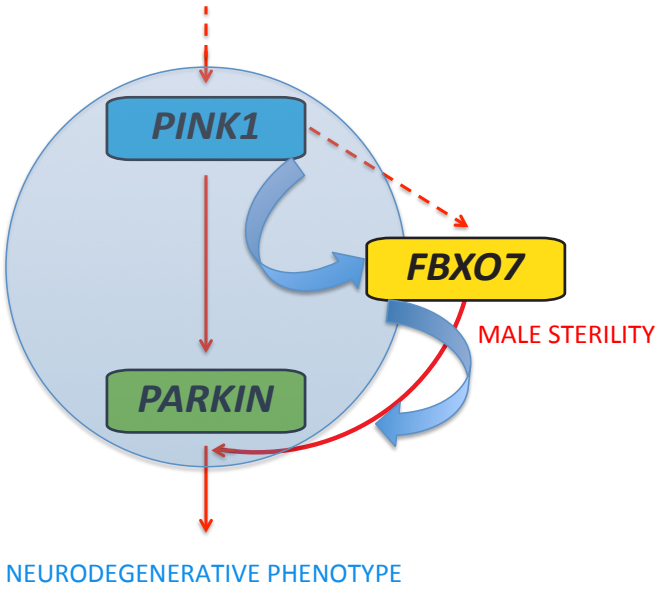

Figure 10 Genetic drosophila model of PINK1, PARKIN and FBXO7 interaction

PINK1 and PARKIN loss of function mutations each cause a similar neurodegenerative phenotype. PARKIN overexpression can rescue the PINK1 phenotype, but not vice versa. FBXO7 loss of function mutations do not result in a neurodegenerative phenotype, but FBXO7 overexpression rescues the PARKIN knockout phenotype, but not the double knockout of PINK1 and PARKIN together.

2 Materials & Methods

2.1 Materials

2.1.1 **Commercial reagents**

Acetone, ethanol, formic acid, glycerol, glycine, 4-(2-Hydroxyethyl)piperazine-1-ethanesulfonic acid (Hepes), isopropanol, methanol, 2-mercaptoethanol, orthophosphoric acid, potassium chloride, sodium chloride, sodium ethylenediaminetetraacetic acid (EDTA), magnesium acetate, sodium ethylene glycol tetraacetic acid (EGTA), sodium fluoride, sodium β-glycerophosphate, sodium orthovanadate, pentobarbital, puromycin, adenosine 5'-triphosphate sodium salt (ATP), anti-HA-agarose, ammonium bicarbonate, ammonium persulphate (APS), ampicillin, benzamidine, bovine serum albumin (BSA), bromophenol blue (BPB), dexamethasone,

doxorubicin, dimethyl pimelimidate (DMP), dimethyl sulphoxide (DMSO), hydrogen peroxide, iodoacetamide, MISSION™ shRNAs, phenylmethanesulphonylfluoride (PMSF), Ponceau S, sodium dodecyl sulphate (SDS), sodium tetraborate, N, N, N', N'-Tetramethylethylenediamine (TEMED), triethylammonium bicarbonate, Nonidet P40, Triton-X-100 and Tween-20 were from Sigma-Aldrich (Poole, UK). Sucrose and Tris(hydroxymethyl)methylamine (Tris) were from BDH (Lutterworth, UK). Cellophane films, i-Script Kit, SsoFast™ EvaGreen® Supermix, polymerase chain reaction (PCR) plates and Precision Plus protein markers were from BioRad (Herts, UK). 3-[(3-Cholamidopropyl)dimethylammonio]-1-propanesulfonate (CHAPS) was from Calbiochem (Merck Biosciences, Nottingham, UK). Insulin-like growth factor (IGF1) was from Cell Signaling Technology (New England Biolabs, Herts, UK). Polybrene was from SantaCruz Biotechnology (Heidelberg, Germany). Cell culture dishes and flasks, cryovials and Spin-X columns were from Corning (NY, USA). Cell scrapers were from Costar (Cambridge, USA). 40% (w/v) 29:1 Acrylamide:Bis-Acrylamide solution was from Flowgen Bioscience (Nottingham, UK). Protein A-agarose, Protein G-sepharose, Glutathione-sepharose, Enhanced chemiluminescence (ECL) kit, Hyperfilm MP, Protran nitrocellulose membrane, P81 paper, 3mm chromatography paper and [γ32P]-labelled ATP were from GE Healthcare (Piscataway, USA). Cell dissociation buffer, Dulbecco's modified eagle medium (DMEM), RPMI-1640 medium, Phosphate buffered saline (PBS), Trypsin/EDTA, L-glutamine, Lipofectamine 2000, non-essential amino acids, sodium pyruvate, antibiotic/antimycotic, NuPAGE Novex SDS Bis-Tris gels, NuPAGE MOPS running buffer, NuPAGE reducing agent, NuPAGE LDS sample buffer and primers were from Invitrogen (Paisley, UK). Photographic developer (LX24) and liquid fixer (FX40) were from Kodak (Liverpool, UK). X-ray films were from Konica (Japan). Polyethylenimine (PEI) was from Polysciences (Warrington, PA). Skimmed milk (Marvel) was from Premier Beverages (Stafford, UK). Plasmid Maxiprep and RNeasy kits were from Qiagen Ltd (Crawley, UK). Acetonitrile (HPLC grade) was from Rathburn Chemicals (Walkerburn, UK). Protease inhibitor cocktail was from Roche (Lewes, UK). Horseradish peroxidase (HRP)- and Alexafluor-conjugated secondary antibodies, Bradford reagent and Fetal Bovine Serum (FBS) were from Thermo-scientific (Essex, UK). CellTiter 96® AQueous One Solution Cell

Proliferation Assay (MTS) and trypsin (mass spectrometry grade) were from Promega (Southhampton, UK). Matrigel™ invasion chambers were from BD Biosciences #354483 (Oxford, UK). Reastain Quick-Diff kit was from Reagena (Finland). InstantBlue protein staining solution was from Expedeon (Harston, UK).

2.1.2 **Tissue culture reagents**

6 well plates, cell culture dishes and cryovials were from Corning Incorporated (NY, USA). Cell scrapers were from Costar (Cambridge, USA). Dulbecco's modified eagle medium (DMEM), Opti-MEM reduced serum media, Foetal bovine serum (FBS), tissue culture grade Dulbecco's phosphate buffered serum (PBS), Trypsin/EDTA solution, L-glutamine, non-essential amino acids, vitamins, sodium pyruvate and antibiotic/antimycotic were from GIBCO (Paisley, UK). Polyethylenimine (PEI) was from Polysciences (Warrington, PA). Penicillin/streptomycin solution, hygromycin, tetracycline, blasticidin, Zeocin, Lipfectamine 2000 were from Invitrogen. Dialysed Foetal Calf Serum (FCS) and DMEM w/o Arg, Lys and Met were from Biowest. Following unlabeled and isotopically labeled amino acids were purchased for SILAC experiments; L-arginine and L-lysine (Sigma–Aldrich) for R0K0 (light); L-arginine-HCl (U-13C6) and L-lysine-2HCl (4,4,5,5,D4) for R6K4 (medium); and L-arginine-HCl (U-13C6, 15N4) and ^{13}C-Llysine-2HCl (U-^{13}C6, ^{15}N2) for R10K8 (heavy) (Cambridge Isotope Laboratory). Polybrene, puromycin, and the MISSION™shRNA and siRNA constructs were from Sigma-Aldrich. The following chemicals used to induce mitochondrial depolarization were purchased from SIGMA: Oligomycin, Antimycin, Valinomycin, FCCP, CCCP, Dopamine, 6-OHDA, MPP+Iodide, Rotenone, Ionomycin, 3-N- Propionic acid, L-BSO (L-Buthionine Sulfoxime), H202, Diamide, Doxorubicin. Phenformin (SIGMA) and Deferiprone (SIGMA).

2.1.3 **In-house reagents**

Luria Bertani (LB) broth and LB agar plates supplemented with 200 μg/mL ampicillin were from media kitchen. Primers were synthesised by the University of Dundee oligonucleotide synthesis service. Bacterial culture medium Luria Bertani (LB) broth and LB agar plates were provided by the University of Dundee media kitchen facility. The Protein Production Team at Division of Signal Transduction

and Therapy (DSTT) expressed and purified all proteins used in any of the *in vitro* ubiquitinylation assays.

2.1.4 **Antibodies**

In-house antibodies (Table 2-1)were raised in sheep and affinity purified on the appropriate antigen by the DSTT. In-house antibodies were used at 1 µg/mL in 5% (w/v) skimmed milk in TBST. Commercial antibodies (Table 2-2)were used at 1:1000 dilutions. The α-UBC9 antibody was a gift from Professor Ron Hay (University of Dundee).

Antibody	Immunogen	DU	Sheep	Bleed
FBXO7	GST- human full lenth FBXO7	34108	S916C	3rd
FBXO7	GST- human full lenth FBXO7	34108	S038D	3rd, 4th
FBXO7	GST- mouse full lenth FBXO7	34179	S917D	3rd
PI31	GST- human full length PI31	34918	S194D	3rd
SKP1 A	GST – SKP11	22343	S408D	2nd
RanBP2	GST – RanBP2 (2553-2838)	41169	S363D	3rd, 4th
NogoB	GST – human full length NogoB	92	S845A	3rd
GFP tag	GST – GFP (2-238)	1574	S268B	1st

Table 2-1: In house DSTT produced antibodies

Antibody	Company	Catalog #	Host	Dilution
Flag	Sigma-Aldrich	F3165	Rabbit	1:1000
Rbx1	Thermo Scientific	RB-069-P1	Rabbit	1:1000
VDAC	Cell Signaling	D73D12	Rabbit	1:1000
SKP1	Cell Signalling	2156	Rabbit	1:1000
Cullin1	Invitrogen		Mouse	1:1000
HURP DLG7	New Balance	NB 110-40572	Mouse	1:1000
Ubiquitin				
Exportin 1 / CRM1	Cell Signalling	Sc-74454	Mouse	1:1000
Neurabin 2	Santa Cruz	Sc-14774	Goat	1:1000
GAPDH	CST	2118	Rabbit	BSA
RanGAP1	Epitomics	2771-1	Rabbit	1:1000
PI31	Epitomics	S0243	Rabbit	1:1000
CIAP1				
Integrin beta 5	Cell Signalling	csD24A5	Rabbit	1:1000
Sentrin specific protease	Acris	Ap06461PU-N	Rabbit	1:1000
VEGRF1	Abcam	Ab32152	Rabbit	1:1000

Table 2-2: Commercial antibodies

Antibodies against Sumo1, Ubc9, were kindly provided by Professor Ron Hay, CLS,

2.1.5 **Plasmids**

Dr M. Deak, Dr. N. Wood, Mr T. Macartney, and Dr. S. Weidlich performed the cloning, subcloning and mutagenesis of the constructs described in this thesis. Constructs used are shown in Table (Table 2-3). All constructs encoded the human version of the gene.

The mammalian expression vector, pEBG6P, was generated by Dr M. Deak. This is a modified version of the pEBG2T vector (Sanchez et al., 1994) that allows the expression of proteins with an N-terminal GST tag followed by a PreScission cleavage site. A mammalian expression vector under the control of the cytomegalovirus promoter called pCMV5A was also utilised, encoding an N-terminal hemagglutinin (HA)-tag (Andersson et al., 1989). For retroviral transduction of cells pBABE vector encoding puromycin selectable marker was used. The pBABE vector is based on the Moloney murine leukemia virus (MoLV) and the genes are expressed from the MoLV long terminal repeat (LTR) (Morgenstern and Land, 1990).

Protein expressed	**Vector expressed**	**Clone number**
Flag-Fbxo7 wildtype (human)	pcDNA5-FRT/TO	DU35005
Flag-Fbxo7 T22M (human)	pcDNA5-FRT/TO	DU35006
Flag-Fbxo7 R378G (human)	pcDNA5-FRT/TO	DU35007
Flag-Fbxo7 R498X (human)	pcDNA5-FRT/TO	DU35008
Flag-Fbxo7 wildtype (mouse)	pCMV5	pEBG
Flag-Fbxo7 T22M (mouse)	pCMV5	pEBG
Flag-Fbxo7 R378G (mouse)	pCMV5	pEBG
Flag-Fbxo7 R498X (mouse)	pCMV5	pEBG
Flag-Fbxo7-wt	pCMV5	DU35005
Flag-Fbxo7-T22M	pCMV5	DU35006
Flag-Fbxo7-R378G	pCMV5	DU35007
Flag-Fbxo7-R498X	pCMV5	DU35008
Flag-Fbxo7-Δ329-375 (f-box)	pCMV5	DU38462
Flag-Fbxo7-P336/A	pCMV5	DU38516
Flag-Fbxo7-D348/A	pCMV5	DU38523
Flag-Fbxo7-D361/A	pCMV5	DU38527
Flag-Fbxo7-E338/A	pCMV5	DU38517
Flag-Fbxo7-I343/A	pCMV5	DU38519
Flag-Fbxo7-L335/A	pCMV5	DU38515
Flag-Fbxo7-L346/A	pCMV5	DU38521
Flag-Fbxo7-L347/A	pCMV5	DU38522
Flag-Fbxo7-L353/A	pCMV5	DU38525
Flag-Fbxo7-L355/A	pCMV5	DU38526
Flag-Fbxo7-L370/A	pCMV5	DU38528
Flag-Fbxo7-L371/A	pCMV5	DU38529
Flag-Fbxo7-R342/A	pCMV5	DU38518
Flag-Fbxo7-R345/A	pCMV5	DU38520
Flag-Fbxo7-R350/A	pCMV5	DU38524
Flag-Fbxo7-R373/A	pCMV5	DU38530
Flag-Fbxo7-I343/A,L346/A, L347/A, V349A	pCMV5	DU37985
Flag-Fbxo7-L332/A,L335/A,L337/A,L339A,L341/A	pCMV5	DU37984

Flag-Fbxo7-I343/A,L346/A, L347/A, V349A	pcDNA5-FRT/TO	DU41285
Flag-Fbxo7-L332/A,L335/A,L337/A,L339A,L341/A	pcDNA5-FRT/TO	DU41284
Flag-Fbxo7-I343/A, L346/A, L347/A, V349A-R378G	pcDNA5-FRT/TO	DU41287
Flag-Fbxo7-L332/A,L335/A, L337/A, L339A, L341/A-R378G	pcDNA5-FRT/TO	DU41286

Table 2-3: List of constructs in mammalian expression vectors

Constructs refer to the human protein if not otherwise specified.

Recombinant Protein Expressed	Vector	Clone number
DAC-TEV human FBXO7-wild-type, human Skp1 (untagged)	pFBDM / Baculovirus	DU23910
DAC-TEV human FBXO7-R378G, human Skp1 (untagged)	pFBDM / Baculovirus	DU23909
DAC-TEV human FBXO7-R498X, human Skp1 (untagged)	pFBDM / Baculovirus	DU24109
DAC-(blunt)TEV-human Cullin1, human Rbx1, human Skp1	pFBDM / Baculovirus	DU23403
DAC-(blunt)TEV-human Cullin1, human Rbx1,	pFBDM / Baculovirus	DU23290

Table 2-4: List of constructs for insect cell expression

Recombinant Protein Expressed	Vector	Clone number
6HIS_TEV-PI31	pET28a	DU23357
Human UBE1 (N-terminal 6HIS)	pFBHTb	DU3026
Human UBE2R1 (N-terminal 6HIS)	pET28a	DU4317

Table 2-5: List of constructs for bacterial expression

2.1.6 **Inhibitors / Treatments**

Inhibitors used in this thesis are shown in Table 2.4. Compounds were dissolved in DMSO and stored at -80°C. MLN4924 is a deneddylating agent of Cullins. Cullin neddylation is required for SCF E3 ubiquitin ligase activity and hence MLN4924 specifically inhibits E3ligases of the SCF type. Cullin 1 immunoblotting can be used as a positive control as the neddylated form disappears upon MLN4924 treatment. CCCP is used to uncouple mitochondria.

Inhibitor	Target	Brutto	Source	Reference
MLN4924	NEDD8-E1 activating enzyme	$C_{21}H_{26}ClN_5O_4S$	DSTT	(Soucy et al., 2009)
CCCP				

Table 2-6 Inhibitors

2.1.7 **Buffers**

Tris-based CHAPS lysis buffer: CHAPS (0.3% [w/v]), 50 mM Tris-HCl pH 7.5, 1 mM EGTA, 1 mM EDTA, 1 mM sodium orthovanadate, 10 mM sodium-ß-glycerophosphate, 50 mM sodium fluoride, 10 mM sodium pyrophosphate, 0.27 M sucrose, 0.15 M NaCl, 0.1% 2-mercaptoethanol and either 1 mM benzamidine and 0.1 mM phenylmethylsulphonylfluoride (PMSF) or complete protease inhibitor cocktail. For some experiments when specifically indicated CHAPS was replaced by the harsher detergent 1% (v/v) Triton-X100.

HEPES lysis buffer: (for ubiquitinylation assays) 40 mM Hepes pH 7.5, 1 mM EDTA, 0.3% (w/v) CHAPS, 0.5 mM sodium orthovanadate, 10 mM sodium-ß-glycerophosphate, 50 mM sodium fluoride, 10 mM sodium pyrophosphate, 0.27 M sucrose, 0.12 M NaCl and 1 mM benzamidine and 0.1 mM PMSF.

Lysis buffer inhibits proteases, kinases, phosphatases and other divalent cation-dependent enzymes ensuring that the phosphorylation and expression levels of proteins are fixed at the levels in which they are found *in vivo*. Benzamidine and PMSF or complete protease inhibitor tablets prevent the action of metallo, aspartic, cysteine and serine proteases. EDTA chelates Mg^{2+} and EGTA chelates Ca^{2+}. Sodium fluoride, sodium-ß-glycerophosphate and sodium pyrophosphate are Ser/Thr phosphatase inhibitors. Sodium orthovanadate is Tyr phosphatase inhibitor. Sodium orhovanadate was prepared, as recommended by manufacturer, by repeated rounds of boiling and cooling until the solution was colourless at pH10 at room temperature to ensure that it is in the monomeric state that favours Tyr phosphatase inhibition.

Buffer A: 50 mM Tris-HCl pH 7.5, 0.1 mM EGTA, and 0.1% 2-mercaptoethanol

Hepes kinase buffer: (for mTOR kinase assays) 25 mM Hepes pH 7.5, 50 mM KCl

Tris buffered saline (TBS): 50 mM Tris-HCl pH 7.5, 0.15 M NaCl

5x sodium dodecyl sulfate (SDS) sample buffer: 5% (w/v) SDS, 5% (v/v) 2-mercaptoethanol, 250 mM Tris-HCl pH 6.8, 32.5% (v/v) Glycerol, bromophenol blue

Tris-glycine SDS running buffer: 25mM Tris-HCl pH 8.3, 192mM Glycine, 0.1% (w/v) SDS

Tris-glycine transfer buffer: 48mM Tris-HCl, 39mM Glycine, 20% (v/v) Methanol

2.1.8 **Cell lines**

Human heterozygeous and homozygeous, patient derived FBXO7 R378G fibroblasts and FBXO7 R498X lymphoblasts were kindly provided by Professor Henry Houlden, UCL London. All other cell lines were supplied by the MRC Protein Phosphorylation and Ubiquitylation Unit (University of Dundee).

2.1.9 **Animals**

Mice obtained from Taconic-Artemis (Cologne, Germany) were maintained under specific pathogen-free conditions and routine animal tail and ear notching was carried out by staff in the College of Life Science Transgenic Unit (University of Dundee). Mrs G. Fraser and Mrs E. Forsyth carried out genotyping from tail biopsies. All procedures were carried out in accordance with the regulations set by the University of Dundee and the United Kingdom Home Office.

2.1.10 **Instruments**

Centrifuge tubes, rotors and centrifuges were from Beckmann (Palo Alto, USA). Trans-Blot Cells, iQ5 real time PCR detection system and gel dryer apparatus were from BioRad (Herts, UK). SpeedVac was from CHRIST (Osterode, Germany). Thermomixer IP shakers were from Eppendorf (Cambridge, UK). The Biofuge microcentrifuge was from Haraeus Instruments (Osterode, Germany). pH meters were from Horiba (Kyoto, Japan). X-Cell SureLock Mini-cell electrophoresis systems and X-Cell II Blot modules were from Invitrogen (Paisley, UK). Polytron was from Kinematica (Brinkmann, CT, USA). X-omat autoradiography cassettes were from Kodak (Liverpool, UK). The Konica automatic film processor was from Konica Corporation (Japan). Li-Cor Odyssey^{TM} Infrared Imaging System was from Li-Cor Biosciences (Cambridge, UK). CO_2 incubators were from Mackay and Lynn (Dundee, UK). Tissue culture class II safety cabinets were from Medical Air Technology (Oldham, UK). The PCR thermocycler (PTC-200) was from MJ Research. The 96-well Versamax plate reader was from Molecular Devices (Wokingham, UK). Proxeon EasynLC chromatography system, LTQ-Orbitrap Classic mass spectrometer and

Nanodrop were from Thermo Scientific (Essex, UK). Scintillation counter (Tri-Carb 2800 TR) was from Perkin-Elmer.

2.2 Methods

2.2.1 **Transformation of chemically competent *Escherichia coli* (*E.coli*)**

Calcium competent *E.coli* DH5α (Inoue et al., 1990) cells were provided by the DSTT. Approximately 10-50 ng DNA was added to 50 µl of competent cells and incubated on ice for 5 min. Cells were then subjected to heat shock at 42°C water bath for 90 seconds to induce the uptake of DNA and briefly placed back on ice. Cells were streaked onto LB agar plates containing 200 µg/mL ampicillin and plates incubated at 37°C overnight.

2.2.2 **Purification of plasmids from *E.coli***

Transformed DH5α *E.coli* were cultured in 200 mL LB containing 200 µg/mL ampicillin at 37°C while shaking at 200 rpm overnight. Cells were pelleted by centrifugation at 6000 ***g*** for 15 min at 4°C. Plasmid DNA was purified using the Qiagen plasmid Maxiprep kit according to the manufacturer's instructions.

2.2.3 **Measurement of DNA and RNA concentration**

DNA and RNA concentrations were measured using NanoDrop as per manufacturer's instructions. RNA and DNA absorb at 260 nM. Absorbance was also measured at 280 nM because calculation of 260/280 ratio allows estimation of purity. Ratios of greater than 1.8 are accepted as pure. Lower ratios may indicate the presence of phenol, protein or other contaminants.

2.2.4 **DNA mutagenesis**

Site-directed mutagenesis was performed using QuikChange kit (Stratagene) and KOD polymerase (Novagen). Mutations were verified by sequencing.

2.2.5 **DNA sequencing**

Sequencing was performed by DNA Sequencing and Services (www.dnaseq.co.uk) using Applied Biosystems Big-Dye v. 3.1 chemistry on an Applied Biosystems model 3730 automated capillary DNA sequencer.

2.2.6 **Cell culture**

All procedures were carried out in aseptic conditions meeting biological safety category 2 regulations. Cells were maintained at 37°C in a 5% CO_2 water saturated incubator. For the passaging of cells, cells were washed with PBS and then incubated with Trypsin/EDTA to detach the cells. Detached cells were resuspended in cell culture medium and split at a 1:2 – 1:20 ratios for continued culture. All breast cancer cell lines were cultured in RPMI-1640 and human embryonic kidney 293 (HEK293), HeLa and MEF cells in Dulbecco's modified eagle medium (DMEM). All cell lines were grown in the presence of 10% (v/v) foetal bovine serum (FBS), 2 mM L-glutamine, 100 U/mL penicillin and 0.1 mg/mL streptomycin. For primary MEF culture medium was additionally also supplemented with 1x non-essential amino acids and 1 mM sodium pyruvate.

2.2.7 **Freezing / thawing cells**

Detached cells were centrifuges at 1000 rpm for 5 min and resuspended in growth medium supplemented with 10% DMSO. 1 mL aliquots were stored in cryovials at -80°C prior to long-term storage in liquid nitrogen. Cells were thawed in a 37°C water bath, resuspended in growth medium and allowed to adhere overnight prior to medium change.

2.2.8 **Transfection of cells using polyethylenimine (PEI)**

Cells were transiently transfected using the polyethylenimine (PEI) method (Durocher et al., 2002). 1 mg/mL PEI stock was prepared in 20 mM Hepes (pH 7). For transfection of cells grown on 10 cm dishes, 5 µg of DNA was mixed with 20 µL 1mg/mL PEI and 1 mL serum-free DMEM and left for 15 min at room temperature before being added to cells. Cells were harvested 36 hrs post transfection.

2.2.9 **Generation of stable cell lines**

To ensure low-level uniform expression of recombinant proteins, manufacturer's instructions (Invitrogen) were followed to generate stable cell lines that express FLAG-tagged forms of proteins (cDNA subcloned into pcDNA5-FRT-TO plasmid) in a tetracycline inducible manner. Flp-In T-REx-293 host cells containing integrated FRT recombination site sequences and Tet repressor, were co-

transfected with 9 µg of pOG44 plasmid (which constitutively expresses the Flp recombinase), and 1 µg of pcDNA5/FRT/TO vector containing a hygromycin resistance gene for selection of the gene of interest with FLAG tag under the control of a tetracycline-regulated promoter. Cells were selected for hygromycin and blasticidin resistance three days after transfection by adding new medium containing hygromycin (100 µg/ml) and blasticidin (7.5 µg/ml). After 3 weeks of selection, colonies were trypsinized and expanded. Expression of the recombinant protein was induced with 0.1 µg/ml of tetracycline for 24 hours.

2.2.10 **Treatment of cells with inhibitors and other agents**

Cells were treated with 10 µM CCCP or DMSO control for 4 hr (or other time point if otherwise indicated) before whole cell lysis. Alternatively, cells were treated with the Cullin-deneddylation agent MLN4926 at a concentration of 3uM for 4 hours and DMSO as a control.

2.2.11 **SILAC (Stable isotope labelling of amino acids in cell culture)**

SILAC DMEM (high glucose without NaHCO3, L-glutamine, arginine, lysine and methionine; Biosera #A0347) was supplemented with methionine, glutamine, NaHCO3, 10 % dialysed FBS (Hyclone) and the following combinations of unlabeled and isotopically-labeled arginine (84 µg/ml) and lysine (146 µg/ml): L-arginine and L-lysine (Sigma–Aldrich) for R0K0 (light); L-arginine-HCl (U-13C6) and L-lysine-2HCl (4,4,5,5,D4) for R6K4 (medium); and L-arginine-HCl (U-13C6, 15N4) and 13C-Llysine-2HCl (U-13C6, 15N2) for R10K8 (heavy). The SILAC medium was filtered through a 0.22-µm filter and cells cultured for five passages in these media for maximum incorporation of labeled amino acids. Labelling efficacy was tested by mass-spectrometry.

2.2.12 **Cell / tissue lysis and mitochondrial fractionation of cell lysates**

Cells were lysed using mammalian cell lysis buffer as listed in 2.1.7. Lysates were clarified by centrifugation at 13,000 rpm for 10 min at 4 °C and the supernatant was collected. For mitochondrial fractionation, cells were lysed in mitochondrial fractionation buffer (refer to Table 2.5) at 4 °C. Cells were disrupted using a glass hand held homogeniser (20 passes) and lysates clarified

by centrifugation for 10 min at 800g at 4°C. The supernatant was removed and further centrifuged at 16,600g for 10min. The resultant supernatant was retained as the cytosolic fraction. The pellet containing the mitochondrial fraction was resuspended in buffer containing 1% Triton X-100 and centrifuged at 13,000 rpm for 10 min. This final supernatant contained solubilized mitochondrial proteins. All lysates were snap-frozen at -80°C until use. Lysates intended for mass spectrometry analysis were processed immediately without snap freezing to avoid possible protein complex disruption.

2.2.13 **Quantification of protein concentration with Bradford assay**

The protein concentration of lysates was estimated using the Bradford assay {Bradford, 1976 #90). Binding of coomassie dye to protein in an acidic medium shifts the absorption maximum from 465 to 595 nm. A standard curve was generated by plotting absorbance against BSA standards. Lysate samples diluted in water were assayed in triplicates using 200 µL of Bradford reagent per sample and absorbance at 595 nM was measured. Sample concentrations were calculated using the standard curve.

2.2.14 **Purification of recombinant proteins**

Baculovirus / insect cell expression was used to generate sufficient SCF^{FBXO7} components for biochemical assays. Another advantage is thatthis system allowed simultaneous expression of up to 3 proteins. Baculoviruses containing the open reading frames of the respective constructs with or without tags (Table 2-4) were transformed into DH10Bac cells and grown under antibiotic selection on plates containing X-gal. White clones, which indicated that bacmids had formed, were picked and after a second round of selection were used to prepare bacmid DNA. Bacmid DNA was transfected into Sf21 cells using Cellfection II (Invitrogen), and the transfection was left for a week to prepare a P0 virus. The cells and the medium were harvested and separated by centrifugation. The medium was used to infect fresh Sf21 cells at a dilution of 1:50. After several dayS (4-5), the cells were collected and used for protein purification. The medium was kept and used as a P1 virus stock. For purification of DAC tagged proteins, ampicillin sepharose had to be prepared: Ampicillin Sepharose was prepared by coupling ampicillin (o.2 M fc) to NHS-activated sepharose. Briefly, NHS-activated

Sepharose was washed in 1 mM HCl. The Sepharose was equilibrated in 0.1 M $NaHCO_3$, mixed with an equal volume of 0.4 M ampicillin in 0.1 M $NaHCO_3$ (pH 7.5), and incubated for 4 h at 22 ° C. The unbound ampicillin was washed away with 20 volumes of 0.1 M Tris-HCl (pH 7.5). The Sepharose was washed with 20 volumes of 20% EtOH and stored at 4 ° C in 20% EtOH. Ampicillin Sepharose stored at 4 ° C in 20% EtOH is stable for at least 6 months. Prior to use, ampicillin Sepharose was washed three times with 10 volumes of H_2O. Cell extracts were diluted to 2 to 4 mg/ml. The cell extract was brought to ambient temperature (20-23 ° C) and added to the ampicillin Sepharose. The extract was mixed for 50 min with ampicillin Sepharose at ambient temperature in a tube roller. The Sepharose was sedimented by centrifugation and washed three to five times with wash buffer (40 mM Tris-HCl [pH 7.5], 150 mM NaCl, and 0.03% Brij-35) at ambient temperature. Small sediments (<50 μl) in 1.5-ml reaction tubes were washed four times with 1 ml of buffer. Larger sediments were washed in 15-ml centrifuge tubes. The total washing time did not exceed 15 min in order to minimize losses. Proteins were released by allowing the β-lactamase activity of PBP5 to cleave the bond with ampicillin under conditions where PBP5 cannot easily bind to another immobilized ampicillin. This was achieved by either competing with mobile ampicillin or cooling the sample on ice. Any release or elution buffer contained 100 mM NaCl, a mild detergent, and 5% glycerol (e.g., 40 mM Tris-HCl [pH 7.5], 0.1 M NaCl, 0.03% Brij-35, and 5% glycerol). After elution or release, the proteins were analyzed by SDS-PAGE. Proteins were stained for 1 h with Instant Blue (Expedeon), followed by washing in water{Lee, 2012 #389}. Proteins were dialysed overnight at 4 °C into storage buffer, snap-frozen and stored at -80°C until use. His-PI31, His-UBE1 and His-UBE2R1 were purified as follows: transformed BL21 cells were grown in LB (Luria Broth), 50 µg/ml carbenicillin until OD^{600} of 0.6, then induced with 300 mM IPTG (isopropyl β-D-1-thiogalactopyranoside) and expressed overnight at 15 °C. Cells were collected, lysed and protein purified using Ni^{2+} -nitriloacetic acid- Sepharose chromatography, followed by dialysis into 50 mM HEPES pH 7.5, 10% glycerol, 150 mM NaCl, 1 mM DTT).

2.2.15 **Covalent coupling of antibodies**

For the coupling of antibodies, protein G-sepharose and protein A-agarose beads were used. Protein G, isolated from Group G *Streptococci*, binds to the F_c region of IgG-class antibodies and has a high affinity for antibodies generated in many species, including sheep. Protein A, which originates from *Staphylococcus aureus*, also binds F_c region of IgG-class antibodies, particularly those generated in rabbit. Covalent coupling of antibodies was carried out using dimethyl pimelimidate (DMP), a homo-bifunctional imidoester that reacts with primary amine groups, as the cross-linker {Harlow, 2006 #718}. Protein A- or G-beads were washed in PBS followed by incubation of 1 µL or resin per 1 µg of antibody for 1-2 hrs at 4°C. Beads were then washed twice with PBS followed by three washes with 0.1 M sodium tetraborate pH 9.3. Beads were then mixed twice for 30 min in sodium tetraborate containing 20 mM DMP at room temperature followed by four washes with 50 mM glycine pH 2.5 to remove any non-covalently coupled antibody and two washes with 0.2 M Tris-HCl pH 8. Beads were mixed with 0.2 M Tris-HCl pH 8 at 4°C overnight to quench any residual DMP, before storage in PBS at 4°C.

2.2.16 **Anti-diglycine remnant antibody (K-ε-GG) Enrichment**

Cells were washed with PBS prior to harvesting and lysed at 4 degrees Celcius in denaturing conditions (8M Urea). Following lysis, cells were cen- trifuged at 20,000 x *g* for 15 min at 4°C to remove insoluble material. A total of 14 mg of protein lysates (7 mg of the SILAC light labled Fbxo7 wt MEFs and 7 mg of the SILAC heavy labled Fbxo7 R378G MEFs) were reduced with 5 mM dithiothreitol (DTT) for 45 min at room temperature. And subsequently carbamidomethylated using 10 mM iodoacetamide for 30 min at room temperature in the dark. Lysates were then diluted 4-fold to 2M Urea with 50 mM Tris-HCL, pH 7.5, and digested overnight at 37 degrees Celcius with sequencing grade trypsin (Promega) at an enzyme to substrate ratio of 1:50. Following digestion, samples were acidified with formic acid and desalted using 500mg tC18 Sep-Pak SPE catridge (Waters). C18 catriges were conditions with 5ml of 100% MeCN, followed by ollowed by 5 ml of 50% MeCN, 0.1% FA, and finally 20 ml of 0.1% trifluoroacetic acid (TFA). Sample was loaded onto the conditioned C18 cartridge, washed with 15 ml of 0.1% TFA, and eluted with 6

ml of 50% MeCN, 0.1% FA. Desalted samples were dried to completeness overnight in a Savant SC210A SpeedVac concentrator (Thermo Scientific). *Basic Reversed Phase (RP) Chromatography*—Off-line basic RP fractionation was completed using a custom-manufactured Zorbax 300 Extend-C18 column (9.4 □ 250 mm, 300 Å, 5 □m, Agilent) on an Agilent 1100 series HPLC system. Each sample was resuspended in 1.8 ml of basic RP solvent A (2% MeCN, 5 mM ammonium formate, pH 10), separated equally into two HPLC vials and injected succes- sively with solvent A at a flow rate of 3 ml/min. A 64-min basic RP LC method was utilized for off-line fractionation. The gradient consisted of an initial increase to 8% solvent B (1.1% B/min) (90% MeCN, 5 mM ammonium formate, pH 10) followed by a 38-min linear gradient (0.5% B/min) from 8% solvent B to 27% B and successive ramps to 31% B (1% B/min), 39% B (0.5% B/min), and 60% B (3% B/min). A flow rate of 3 ml/min was used for the entirety of the LC separation. Upon sample injection, 80 basic RP fractions were collected in a 96-well polypropylene round bottom plate (GE Healthcare). For K-□-GG peptide analysis, basic RP fractions were pooled in a non- contiguous manner into eight total fractions Fractions were dried to completeness. Dried peptide fractions were resuspended in 1.5 ml of IAP buffer and incubated with cross-linked anti-K-e-GG antibody beads for 1 h on a rotating unit at 4°C. Each basic RP fraction was incubated with 31 ug of antibody. Antibody beads were washed four times with 1 ml of ice-cold PBS. K-e-GG peptides were eluted by adding 2x 50 ul of 0.15% trifluoroacetic acetic (TFA) and cleaned by C18. Eluted peptides were dried to completeness prior to mass-spectrometry analysis. Also pre-IP fractions were collected and prepared for mass-spectrometry.

2.2.17 **Immunoprecipitation of proteins**

3 µL of covalently coupled antibody or for larger sample quantities 1 µL of antibody beads / 1 mg of lysate was mixed with the lysate for 1-4 hrs at 4°C on a rotating wheel. Beads were then washes twice with lysis buffer containing 0.5 M NaCl and twice with lysis buffer containing 0.15 M NaCl followed by 2 washes with buffer A. Reducing agent was omitted from the washes. To elute immunoprecipitates, beads were resuspended in

2x SDS sample buffer (or 2x NuPAGE LDS sample buffer for mass spectrometry) lacking reducing agent for 10 min prior to filtering through Spin-X columns to remove the antibody-bound beads. Reducing agent was added to the eluted samples and the samples were heated.

Endogenous FBXO7 immunoprecipitations from tissue lysates were precleared at least 3 times for 15 minutes with preimmune sheep Immunoglobulins (IgG) covalently coupled to G-sepharose beads.

2.2.18 **Resolution of protein samples via SDS-PAGE**

Sodium dodecyl sulphate polyacrylamide gel electrophoresis (SDS-PAGE) resolves proteins based on their apparent molecular weight. The anionic detergents SDS and lithium dodecyl sulphate (LDS) bind to proteins giving them a net negative charge that is proportional to the molecular mass of the protein. Consequently, the speed of migration of proteins through a PAGE matrix is a linear function of the logarithm of their molecular weight.

Resolving gels contained 375 mM Tris-HCl (pH 8.6), 0.1% SDS and 8-10% acrylamide. TEMED and ammonium persulphate (APS) were used to initiate polymerisation. Stacking gels contained 125 mM Tris HCl pH 6.8, 0.1% SDS, 4% acrylamide, TEMED and APS.

Samples were prepared either in 1x LDS sample buffer and 1x sample reducing agent (for use with pre-cast NuPAGE 4-12% Bis-Tris gels) or in 1x SDS sample buffer (for use with homemade gels) and heated at heated at 90°C for 5 min. 5-20 µg of lysate or 10-30 µL of immunoprecipitates were loaded per lane along with protein standards. Electrophoresis was carried out at 80 V until the protein markers started to resolve and then the voltage was increased to 160 – 180 V until the dye front reached the end of the resolving gel.

2.2.19 **Coomassie staining of polyacrylamide gels**

Polyacrylamide gels were stained in Instant Blue staining solution for 1-2 hrs and destained with MilliQ water.

2.2.20 **Transfer of proteins onto nitrocellulose membranes**

Gels were sandwiched between nylon sponges, Whatman 3 mm filter papers and nitrocellulose membrane all soaked in transfer buffer. The transfer cell was submerged in transfer buffer and transfer was carried out at at 750 mA for 1 hour.

2.2.21 **Immunoblotting**

After transfer, membranes were stained with Ponceau S and destained in distilled water in order to visualise the transferred proteins. Non-specific binding of antibodies was prevented by incubating the membranes with 5% (w/v) skimmed milk in TBST for 1 hour at room temperature. Membranes were then incubated with primary antibodies diluted in either 5% (w/v) skimmed milk or BSA in TBST at 4°C for 16 hrs. Membranes were next washed three times for 10 minutes with TBST. Horseradish peroxidase (HRP)-conjugated secondary antibodies diluted at 1:2500 in 5% (w/v) skimmed milk in TBST were incubated with the membranes for 1 hr at room temperature and the membranes were washed three more times with TBST. Membranes were incubated with the enhanced chemiluminescence (ECL) substrate and exposed to X-ray films for various lengths of time. Films were developed using a Konica automatic developer. Where indicated, signals were visualised using the Odyssey^{TM} Infrared Imaging System instead of ECL. The procedure was the same but the secondary antibodies were labelled with either IRD800 or Alexa680 dyes and the signal captured and quantified with an Odyssey Infrared Imaging System.

2.2.22 **Processing protein bands by in-gel digestion for mass spectrometry analysis**

To minimise contamination with proteins such as keratin, samples were handled in a laminar flow hood. Gels were cut into small pieces. The pieces were sequentially washed for 10 min in 0.5 mL water, 50% (v/v) acetonitrile, 0.1 M NH_4HCO_3 and 50% (v/v) acetonitrile/50 mM NH_4HCO_3. The last step was repeated until the pieces were colourless. Colourless gel pieces were incubated with 0.3 mL acetonitrile for 15 min at room temperature followed by drying in a Speed-Vac at 45°C. Dried gel pieces were incubated with 30 µL 25 mM Triethylammonium bicarbonate buffer containing 5 µg/mL trypsin at 30°C for 16 hrs on a shaking platform. Next an equal volume of acetonitrile

was added and the peptides obtained from the digestion were extracted for 15 min on a shaking platform. The supernatant was dried in a clean tube at 45°C using Speed-Vac. To extract further peptides, 100 µL of 50% (v/v) acetonitrile supplemented with 2.5% (v/v) formic acid was added to the gel pieces and incubated for 15 min at room temperature on a shaking platform. The supernatant was combined with the first dried peptide extract and dried using Speed-Vac. Dried peptides were stored at -20°C.

2.2.23 **Processing samples by solution digestion for mass spectrometry analysis**

Samples were prepared in mass-spectrometry compatible buffers (such as Rapigest) and Tris-HCL was added to 10 mM to ensure buffering at pH 7.5 followed by cysteine alkylation in 10 mM chloroacetamide at 20 degree Celcius in the dark for 30 min. Samples were diluted to 0.1% RapigestTM and digested with 1:50 w/w trypsin overnight at 37 degrees Celcius. Peptides were acidified with 1% TFA (trifluoroacetic acid) and incubated at 37 degrees Celcius for 1 hour before precipitating acid-cleaved RapigestTM by centrifugation at 17000 x g for 10 min. Peptides were purified on C18 MicroSpin Columns (the Nest Group) before mass-spectrometry analysis.

2.2.24 **Mass spectrometry**

Liquid chromatography–mass spectrometry (LC-MS) was performed by Dr. David Campbell, Mr. Robert Gourlay and Joby Varghese (MRC, College of Life Sciences, University of Dundee). Tryptic peptides were subjected to LC-MS/MS using a Proxeon EasynLC chromatography system coupled with a Thermo LTQ-Orbitrap Classic mass spectrometer. Results were searched against the SwissProt or IPI mouse databases using Mascot (www.matrixscience.com). Data analysis was performed using Online MassSpec Data Analysis Tool (http://www.proteinguru.com/MassSpec/OLMAT).

The mass-spectrometry analysis of the di-gly experiments was performed by Dr. Patrick Pedrioli and Dr. Kamila Chughtai (MRC, College of Life Sciences, University of Dundee). Mass spectra were acquired on a LTQ Oribitrap Velos mass spectrometer (Thermo Scientific) operating in a data-dependent mode. After conversion to mzXML the raw data were searched using Comet against the human, or mouse, protein databases. For

SILAC samples variable modification of lysine and arginine residues was also specified as well as Gly-Gly additions to lysines was searched for.

2.2.25 *In vitro* SCF complex formation and ubiquitinylation assays

Recombinant DAC-tagged FBXO7 co-purified with untagged SKP1 were incubated together with a 2 Molar excess of the various combinations of other SCF complex partners as well as PI31 at room temperature for 1 hour. The complex was then purified via DAC with ampicillin sepharose as described in 2.2.14 and otherwise treated like an immunoprecipitation as decribed in 2.2.17. For *in vitro* ubiquitinylation reactions wild-type or mutant FBXO7 – either R378G or R498X – were incubated together with the other SCF complex partners and His-PI31 in the presence of Flag-Ubiquitin (Boston Biochem), His-UBE1 and His_UBE2R1 in a reaction volume of 50ul (HEPES based, 2 mM ATP, 10 mM Magnesium acetate). Ubiquitinylation reactions were incubated at 30 degrees Celcius for 60 minutes and terminated by addition of SDS sample buffer. For all assays, reaction mixtures were resolved by SDS-PAGE and subjected to immunoblotting. In the case of the mitochondrial substrate assays, the ubiquitinylation reaction was heat terminated and intact mitochondria were pelleted by centrifugation. The mitochondrial pellet was washed 3 times before it was resuspended in 1% SDS buffer and subjected to sonication and benzonase treatment. Mitochondrial debris was removed by centrifugation and the supernatatnt was diluted to 0.1% SDS. This was then subjected to Flag immunoprecipitation and subsequent preparation for in solution tryptic digestion for mass-spectrometry analysis. If the reaction was not intended for mass-spectrometry analysis, the mitochondrial pellet was resolved in a small volume of HEPES buffer, benzonase was added, followed by sonication and addition of LDS buffer for resolution by SDS-PAGE and immunoblotting.

2.2.26 Generation of FBXO7 knock-in mouse model of the corresponding R378G mutation

A FBXO7 mouse model with constitutive knock-in of the R379G point mutation (corresponding to the human pathogenic R378G mutation) with optional conditional FBXO7 knock-out was generated using the Cre/LocP methodology(Nagy, 2000). The

R379G mutation was introduced into exon 7 and an additional silent mutation for the creation of a diagnostic restriction site. Exons 7 and 8 were flanked with 34-base pair DNA recognition sites (LoxP sites) and selection markers were inserted into intron 6 and 8 flanked by FRT (NeoR) and F3 (PuroR) sites, respectively. Homologous recombinant clones were isolated by using the double positive (Neomycin and Puromycin resistance) selection. The targeting vector was generated using BAC clones from the C57BL/6J RPCIB-731 BAC library and transfected into the TaconicArtemis C57BL/6N Tac ES cell line. The constitutive Knock- in-conditional Knock-out allele after Flp-mediated removal of the selection markers expressed the mutated R379G Fbxo7 protein. Heterozygous mice were shipped from TaconisArtemis to our animal unit and animals were bred to homozygosity.

Homozygeous R379G KI animals were subsequently crossed with mice expressing the Cre recombinase, leading to the recombination between the LoxP sequences and excision of the intervening DNA and either ablation of gene expression or at least expression of a truncated allele product.

2.2.27 **Extraction of DNA from ear / tail biopsies**

Ear notches were taken from mice at approximately 4 weeks of age by staff in the College of Life Sciences Transgenic Unit (University of Dundee) and DNA extractions carried out by the DNA service (University of Dundee). For confirmation of mouse genotypes, tail biopsies were taken. Biopsies were incubated with 500ul 1mg/ml Proteinase K in tail buffer at 65°C overnight. 167ul 6M NaCl was added to each tube and incubated on a rotating wheel for 5min at room temperature. This was followed by centrifugation at 13000rpm for 10 min and 500ul isopropanol was added to 500ul of the resulting supernatant and incubated on a rotating wheel for 1hr at room temperature. The mixture was centrifuged at 13000rpm for 25min, the pellet was washed with 1ml 70% ethanol and centrifuged for a further 10min. The pellet was left to air-dry, resuspended in 80ul water and stored at -20°C.

2.2.28 **Genotyping of mice via PCR**

PCR reactions were carried out in order to genotype mice, using purified DNA from biopsies. For FBXO7 R379G knock-in mice, a 20ul reaction contained: 5ul 10X Taq polymerase buffer, 1ul 10mM dNTPs (0.25mM final concentration), 2ul 25mM magnesium chloride (2.5mM final concentration), 1ul 50pmol/ul primer 1 (3874_35), 1ul 50pmol/ul primer 2 (3874_36), 0.2ul Taq polymerase, 37.8ul MilliQ water and 2ul template DNA. This reaction allowed detection of heterozygeous and homozygeous R379G KI as well as wildtype-alleles (Table 2-7). The size for the expected fragments was 210 basepairs (bp) for the wild-type and 329 bp for the KI alleles.

For genotyping FBXO7 mouse line after Cre recombination, a second PCR reaction was carried out and a 20ul reaction contained: 2ul 10X Taq polymerase buffer, 0.5ul 10mM dNTPs (0.25mM final concentration), 2ul 25mM 96 magnesium chloride (2.5mM final concentration), 0.5ul 50pmol/ul primer 1, 0.5ul 50pmol/ul primer 2, 0.25ul Taq polymerase, 11.75ul MilliQ water and 2ul template DNA. The PCR programme consisted of 5min at 95°C, 35 cycles of 30sec at 95°C, 30sec at 60°C and 1min at 72°C, followed by 10min at 72°C on a PTC- 200 Peltier Therma Cycler DNA engine. 5ul of DNA loading buffer was added to the PCR samples and these were run on a 1% agarose gel and visualized under a UV lamp. *In both cases P1 corresponded to sequences found in both alleles, P2 bound within the region excised following Cre recombination while P6 (Protor-1) and P4 (Protor-2) bound downstream of the excised region*. Therefore the first set of primer combinations allowed the identification of wild-type, floxed and knock-in mice. The second set of primer combination allowed the identification of the successful Cre-deletion recombination event. Mrs G. Fraser and Mrs E. Forsyth carried out the majority of the mouse genotyping for this project.

Primers	Sequence	Detection
3874_35	GTGGTGCAGGGAAACAAGC	Primer pair 35 + 36 detects heterozygous / homozygeous KI and wild-type alleles
3874_36	GCTGAATAACAATCTCACCATCC	

Table 2-7: Primers used for genotyping

2.2.29 **Mouse motor and behavioural phenotyping**

2.2.29.1.1 General phenotypic screen with the SHIRPA test battery

Before commencing the phenotypic analysis, animals were allowed to adapt to their new environment for at least 2 weeks – this applied to animals that had to be moved in between facilities before testing. All mice were then evaluated with a slightly modified SHIRPA test (SmithKline/Harwell/Imperial College/Royal Hospital/Phenotype Assessment). The SHIRPA primary screen contains 40 scores, and the testing protocol followed guidelines given on videotape as well as at the ENU Mutagenesis Programme web site (http://www.mgu.har.mrc.ac.uk/). The mice were first placed inside a perspex jar for 5 min and evaluated for body position (from flat to repeated leaping), movement (from immobile to extreme), respiration rate (from irregular to normal), body tremor (from absent to marked), and number of fecal boli. The jar was then lifted over an open-field made of perspex with four transparent walls (height: 18 cm) and a white opaque floor measuring 55 cm × 33 cm, separated by black line drawings into 121 cm2 squares (five rows and three columns) and the mice dropped in it. The following behaviors were recorded: transfer arousal (from prolonged freezing to manic-type behavior), eye opening (from open to completely closed), piloerection (none or coat on end), gait (from normal to incapacitated), pelvic elevation (from flattened to normal), tail position (from dragging to Straub type), and touch escape (from no response to vigorous attemps at escaping from being touched).

The mice were then lifted by the tail and assessed for the position at which struggling movements occurred (from tail to no struggle at all) as well as trunk curl (absent or present) and placing (absent, vibrissae, or visual) responses. After being restrained in a supine position, skin color (from blanched to red), lacrimation (absent or present), salivation (absent or present), and biting as well as Pinna (from absent to multiple flicks) and corneal (from absent to multiple blinks) reflexes were recorded. The air-righting reflex was then evaluated according to landing position (on all four paws, on side, on back or else failure to right even when placed on its back), followed by contact righting when placed inside a small plastic tube (absent or present). These observations were

completed by noting whether any sign of fear (none, freezes during transfer arousal), irritability (none, struggling during restraint), aggression (none or provoked biting), and vocalization (none or provoked while handling) arose for each mouse and its body weight. The main difference to the modified SHIRPA test battery was that we did not record acoustic startel and grip strength. Locomotor activity was also measured separately in a more elaborate fashion as described below.

2.2.29.1.2 Spontaneous locomotor activity

Mice were handled for a minimum of 3 days before the start of locomotor monitoring. Mice were placed in an open-topped transparent Perspex cube, 30 x 30 x 30 cm, for 3 daily sessions of 30 min each. The position of the mouse was monitored by an overhead camera connected to an HD recorder and a PC running Any-maze (details). A separate side-mounted camera recorded rearing behaviour. Total distance travelled (sub-divided into three 10-min sessions), distance travelled within cm of the box walls, distance travelled in the centre of the box (i.e. > 5 cm from the walls), and number of rears were analysed.

2.2.29.1.3 Gait analysis

Gait analysis was carried out in a narrow corridor, 45 cm long, approximately 5 cm wide, with 14-cm high walls. At the end of the corridor was a 'goal box' containing bedding and small pieces of breakfast cereal. Before the start of gait analysis, mice were placed into the goal box and allowed to explore the box and corridor for two 15-min sessions on successive days, in order to habituate them to the apparatus. Mice were also scruffed several times during this phase in order to habituate them to the restraint necessary for subsequent paint application. On the testing day, a strip of white paper was placed on the floor of the corridor. Poster paint was applied to the mouse's feet—red for the forepaws, and blue for the hind—and the mouse was released into the corridor and allowed to run towards the goal box. A run was considered acceptable if the mouse ran towards the goal box without stopping or changing direction. Three runs—i.e. three sets of paw prints—were collected for each mouse. For analysis, a single gait cycle from each run was selected based on the clarity of the paw prints. Three gait

parameters were calculated from the paw-print records—stride length, base width (front and hind), and overlap between front and hind feet. Stride length was defined as the distance between the centre of a given plantar from one footfall to the next; this was calculated separately for each foot, and the results were averaged. Base width was defined as the distance between the two front feet (front base width) and the two hind feet (hind base width) perpendicular to the direction of travel. Two front and hind base-width measurements were made for each run, corresponding to the first and second footfalls of the gait cycle, and these data were averaged. Overlap was calculated by measuring the distance between the centre of the front and hind plantars for each of the four pairs comprising the selected gait cycle; these measurements were then averaged.

2.2.29.1.4 Accelerating rotarod

On each testing day, a mouse was placed on each of 5 lanes of a rotarod (Model 47600, Ugo Basile, Italy), with the beam (diameter = 3 cm) rotating at a constant speed of 6 r.p.m. Each mouse occupied the same lane during each testing day, but lane occupancy was counterbalanced between subjects such that each lane was used by approximately the same number of wild type and homozygous mice across the series of runs carried out within each day. Once all lanes were occupied, the beam accelerated at a constant rate from 6 to 50 r.p.m. over a 300-s period. Latency to first lose grip on the beam was recorded. 'Loss of grip' included both falling from the beam and clinging to the rotating beam to avoid falling. Mice that fell from the beam within the first 20 s of the start of acceleration were placed back on. However, in these cases, the loss-of-grip latency recorded still corresponded to the first fall. If a mouse lost grip because of turning around on the beam, it was immediately placed back on the rotarod facing in the correct direction; these incidents were not counted in the analysis of latency to lose grip. Testing continued for a total of 4 days. All trials were recorded and latencies were analysed during video playback.

2.2.29.1.5 Fixed-speed rotarod

Fixed-speed rotarod testing was carried out in a single day. Mice were placed on the rotating beam, and latency to lose grip (defined as for the accelerating protocol) was recorded from the moment the mouse was released. Mice were tested at approximately 1-h intervals using progressively increasing rotational speeds—10, 20, 30 and 40 r.p.m. Mice that fell within the first 20 s were placed back on the beam, although the recorded latency still reflected the first loss of grip. Mice occupied the same lanes as during accelerating rotarod training. All trials were recorded and latencies were analysed during video playback.

2.2.29.1.6 Balance beam (or elevated bridge test)

The balance beam apparatus comprised a tapering aluminium beam, 1 m in length, inclined upwards at a 15-degree angle, and leading to an enclosed goal box, 40cm cm above the ground. Soft towels were placed underneath the beam to prevent injury in the event of a fall (although no falls occurred during the study). The beam tapered from a width of 1.2 cm at a 'start point', 15 cm from its lower end, to 0.5 cm at a 'finish point', 10-cm from the goal box. On the underside of the beam, 2 cm from its top surface, were ledges extending 1.5 cm from the edge of the beam on both sides. These ledges prevent falling in the event of a slip, and facilitate the identification of slips. The beam was brightly lit in order to encourage movement towards the dark goal box. Mice were first habituated to the goal box, filled with bedding and pieces of breakfast cereal, over two 15-min sessions on successive days. On the third day, mice were trained to run along the beam by placing them onto the beam at progressively greater distances from the goal box, until each mouse ran along the entire length of the beam without hesitation. On a subsequent testing day, mice were placed at the wide end of the beam and allowed to run towards the goal box while side-mounted cameras recorded their progress. This was repeated 8 times for each mouse, with runs separated by approximately 30 min. Video data were analysed off-line; the number of foot slips that occurred between the start and finish points was recorded for both left and right fore and hind limbs. A foot slip was recorded each time a paw lost grip on the upper surface of the beam, and made contact with the ledge below. Data from individual runs were only included if the mouse ran

along the top surface of the beam for its entire length; runs were discarded if the animal 'shuffled' along the beam for part of its length by using the ledge for support. Data from each two successive runs were averaged. Data from a mouse was discarded entirely unless at least one run in each of the 4 pairs was satisfactory.

2.2.30 **Lysis of mouse tissues**

Mouse tissues were rapidly excised, frozen in liquid nitrogen and stored at -80°C until use. Tissues were weighed and homogenised in a 10-fold excess of ice-cold lysis buffer (usually TRIS-CHAPS buffer unless otherwise stated). Lysates were clarified by centrifugation at 3,000 rpm for 15 min at 4°C and supernatants then further centrifuged at 18,000 ***g*** for 20 min at 4°C. Lysates that were intended for experiments involving mass-spectrometry analysis, lysates were also filtered (0.22um) and immediately prcessed without prior storage at -80°C. Otherwise, lysates were aliquoted, snap frozen and stored at -80°C.

2.2.31 **Mouse embryonic fibroblast (MEF) generation**

Female mice at 13 days gestation were culled, the uterine horn removed and embryos placed in PBS. Embryo heads were used to confirm the genotype by PCR (performed by Mrs G. Fraser). After removing internal organs embryos were chopped and incubated with trypsin at 37°C, 5% CO_2 for 5-10 min. Cells were centrifuged at 800 rpm for 5 min and resuspended in primary MEF media (Section 2.2.6). After 24 hrs, cells were trypsinised, resuspended in primary MEF media and filtered. These cells were designated as passage 1 (P1). MEFs were immortalised by continues passaging and were considered to be immortalised once the cells were proliferating at a rate similar to primary MEFs.

2.2.32 **Statistical analysis**

Statistical significance was assessed by one-way analysis of variance (ANOVA) followed by Tukey's multiple comparison tests using GraphPad Prism 5.0. All the experiments presented in this thesis were performed at least two or three times with similar results obtained on each occasion. Error bars indicate the standard deviation (SD) or standard error of the mean (SEM), as indicated in figure legends.

2.2.33 **Bioinformatics**

Sequence alignments were undertaken using Clustal Omega (Sievers et al., 2011) and the alignments were annotated using Jalview 2 (Waterhouse et al., 2009b).

3 SCF^{FBXO7} E3 ligase complex formation and screening for FBXO7 interactors in the stable overexpression system

3.1 Introduction

PD is the second most common neurodegenerative disorder after Alzheimer's disease, and progression of symptoms correlates with neurodegeneration in the nigrostriatal dopaminergic system. In fact, dopaminergic neuronal cell death and Lewy bodies are the neuropathological hallmark of PD although it is well known that neuronal degeneration is more widespread across the central and peripheral nervous system as reflected by the multitude and variety of clinical symptoms. Mitochondrial dysfunction and oxidative stress are believed to take a central role in the pathogenesis of PD. However, the identification of PD associated genes and the study of their cellular functions have sparked an interest in the ubiquitin proteasome system(Cook et al., 2012; Ebrahimi-Fakhari et al., 2012; Olanow and McNaught, 2006): Protein misfolding and dysfunctional protein clearance / aggregation – as seen in many neurodegenerative diseases - could be the result of disturbed quality control mechanisms and as such be critically involved in the cascade of events leading to neurodegeneration in PD. As a member of the F-box family, FBXO7 possesses the potential to act as the substrate recognizing subunit of a specific type of E3 ubiquitin ligases, and is as such well suited to play a crucial role in regulating protein quality control via the ubiquitin proteasomal system. Dysfunctional E3 ligase activity of the FBXO7 pathogenic mutants may therefore be the underlying cause of FBXO7 associated neurodegeneration. However, not all F-box proteins assemble into a Skp1-Cullin1-RBX1-F-box protein (SCF) complex or even if they do, do not necessarily function as E3 ubiquitin ligases(Skaar et al., 2009c). Therefore, the initial aim of my PhD thesis was to develop tools to study FBXO7 and then to establish whether the FBXO7 wild type protein and the pathogenic FBXO7 mutants - T22M, R378G and R498X – assemble into a SCF E3 ligase complex *in vivo*: First, I show that in a

stable overexpression system the wild-type FBXO7 protein does exists in a complex with SKP1, Cullin 1, RBX1. Second, I show that neither of the pathogenic mutants disrupts complex formation in a stable overexpression system. Furthermore, I demonstrate for the first time that the SCF^{FBXO7} complex is also formed at endogenous level in wild type brain *in vivo*; and that neither the R378G nor the R498X mutants disrupt endogenous complex formation *in vivo*. For the latter, I make use of a FBXO7 knock-in mouse model of the pathogenic R378G mutation (discussed in chapter 4) as well as patient derived, mutation specific immortalized cell lines (generously provided by Professor Henry Houlden, UCL).

3.2 Overexpression of FBXO7 wt / disease mutants and antibody validation

3.2.1 Stable overexpression of human FBXO7 wt and disease mutants

First, I stabily expressed the human FBXO7 wild-type as well as pathogenic disease mutants as N-terminal Flag-tagged constructs in Flp-In TRex HEK293 (Human Embryonic Kidney) cell lines. The Flp-In HEK293 cell line allows for integration and expression of constructs at a specific genomic location with subsequent doxycycline induced expression. The advantage of the Flp-In system is that equal gene expression is obtained in an isogenic cell pool. Stable cell lines expressing either Flag-tag alone or human N-terminal Flag-tagged wild-type FBXO7 or disease mutants (T22M, R378G, and R498X) were generated and induced for expression with 0.1μg/ml doxycycline for 18 hours (Figure 11).

3.2.2 Validation of DSTT - produced α human FBXO7 antibody

Two antibodies against the human FBXO7 - whole protein - antigen were raised by the DSTT (S916C and S038D), and all bleeds (1-3 for S916C and 1-4 for S038D) were tested for their recognition of over-expressed and endogenous FBXO7 in Flp-In TRex HEK293 whole cell lysates. Data is shown for the third bleeds (and fourth for S038D) only as these bleeds were chosen for carrying out future experiments. Both human FBXO7 antibodies successfully detect stable overexpressed FBXO7. However, the S038D

antibody also detects endogenous FBXO7 (uninduced panel), while the S916C antibody yields an additional unspecific signal at around 100 kDa. Usually, a DSTT antibody programme encompasses three bleeds; it is worth noting that carrying on for an additional fourth bleed in the case of the D038D antibody resulted in a significant improvement of its sensitivity (Figure 11).

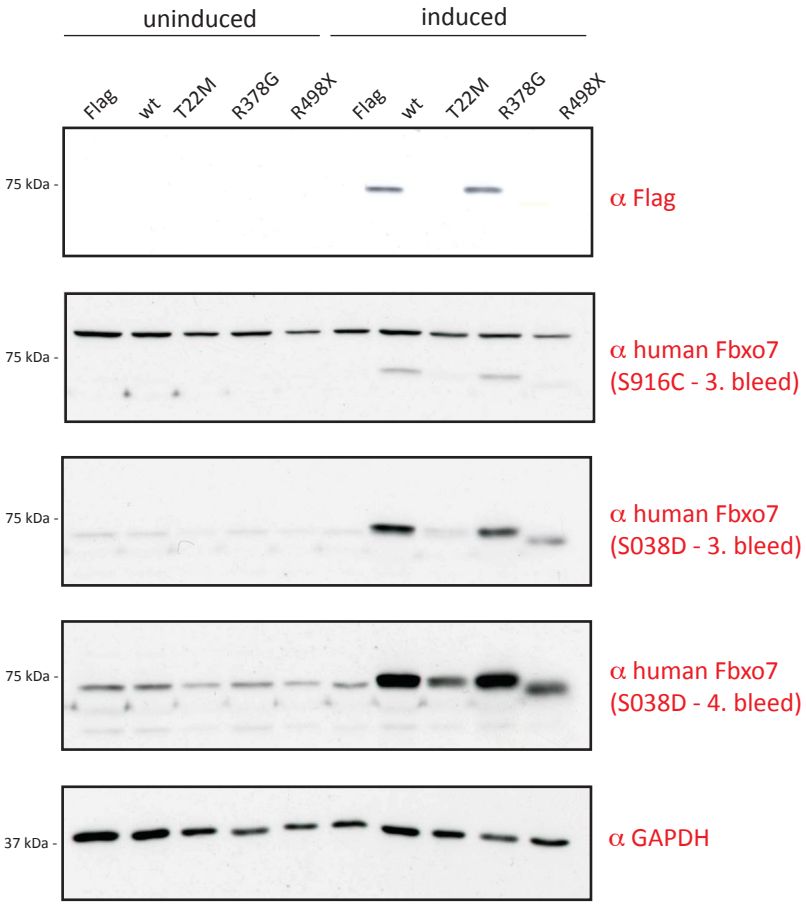

Figure 11: FBXO7 antibody testing in stable overexpression system of FBXO7 wt and pathogenic mutants

Flp-In TRex HEK 293 cells stably expressing either FLAG alone, human FBXO7 wild type N-terminal FLAG or any of the pathogenic mutants - T22M, R378G and R498X – each with a C-terminal FLAG were stimulated for protein expression with 0.1 ug/ml of doxycycline for 18 hours. Whole cell lysates were blotted for FLAG (Sigma), FBXO7 using 2 different DSTT produced anti - human FBXO7 antibodies (S916C 3. bleed, S038D 3. and 4.bleeds) and GAPDH as loading control. Antibody concentration for immunoblotting was 1ug/ml and exposure time was the same for all blots.

3.3 SCF^{FBXO7} complex formation in the stable overexpression system

Many E3 ubiquitin ligases are modular with a core scaffold and interchangeable substrate-targeting subunits, of which the SKP1-Cullin1-F-box protein (SCF) complexes are the best characterized. Cullin1 – as the scaffold of SCF complexes – brings the 2 functional entities of the complex in close proximity: its C-terminus binds the small RING protein RBX1, which directs the E2 enzyme to the E3 ligase complex, while its N-terminus binds the variable F-box protein via the small adaptor SKP1(Skaar et al., 2013). The specificity of the E3 ligase complex depends on the variable substrate recognizing subunit - the F-box protein -; and thus the core machinery can be used to ubiquitylate a myriad of different substrates. If the hypothesis is that the pathomechanism of FBXO7 mediated disease has anything to do with its potential role as a component of a SCF E3 ubiquitin ligase, it first needs to be established whether FBXO7 is able to form a complex with SLP1, Cullin1, and RBX1 and second whether this is also true for the pathogenic FBXO7 mutants.

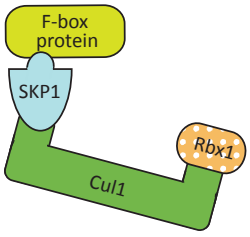

Figure 12: F-box proteins are the substrate recognizing subunit of SCF E3 ubiquitin ligase complexes

Cullin 1 (Cul1) serves as a scaffold bringing RBX1 at its carboxy-terminal end the substrate recognizing F-box protein via SKP1 to its amino-terminal end. Substrate specificity is hence dictated by the F-box protein; and the modular assembly of SCF complexes allows ubiquitinylation of many different substrates depending on which F-box protein participates.

3.3.1 FBXO7 assembles into the SCF^{FBXO7} complex and the pathogenic mutants do not disrupt complex formation

Three independent large scale Flag-pull-downs (about 30mg per condition) of stable expressing Flag-tagged Fbxo7-wildtype and disease mutants (T22M, R378G and R498X) with Flag-empty vector as a control have been performed. In order to analyse each immunoprecipitate (IP) for tryptic-peptide fingerprinting mass-spectrometry, 50% of each IP product was resolved by 4-12% Bis-Tris SDS-PAGE, gels were stained with colloidal Coomassie Blue and each lane was excise into same size fragments and prepared for mass-spectrometry. The remaining 50% of the IP product was retained for subsequent validation by immunoblotting.

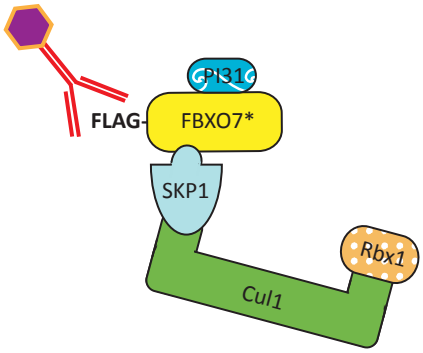

Flag-IP:
Bait: FLAG-FBXO7* (wt or mutant)
SCF complex: Cullin1, FBXO7, SKP1, RBX1 and potentially PI31

Figure 13: Illustration of FLAG-IP of FLAG-FBXO7 constructs for SCF complex identification

3.3.2 MS/MS identification of endogenous SCF complex partners in Flag-IPs of stable expressing Flag-Fbxo7 constructs

Peptide mass fingerprinting analysis was performed using OLMAT (http://www.proteinguru.com/MassSpec/OLMAT). The analysis workflow entailed subtracting all the proteins that were identified in the Flag-IP and therefore considered as unspecific interactors from the hit lists of the IPs from the Flag-FBXO7- wt and –mutants. Additionally, a generic list of well-known contaminants was removed from the result data; amongst them cytoskeletal and ribosomal protein(Trinkle-Mulcahy et al., 2008). In the first instance I was interested to see whether the individual subunits of the

SCF E3 ubiquitin ligase complex were amongst the proteomic hits: In case of the overexpressed Flag-tagged FBXO7 wild-type protein, FBXO7 as the bait as well as all the other complex partners – SKP1, Cullin1, Rbx1 - could be identified. This was also the case for the disease mutants FBXO7 R378G and R498X, but not for the T22M mutant. In the FBXO7 T22M, which constitutes to the compound heterozygeous mutations that have been identified in the Dutch family, RBX1 was not seen in any of the 3 replicates for the T22M mutant(Di Fonzo et al., 2009). RBX1 is not a direct binding partner of FBXO7, but binds indirectly via SKP1 and Cullin1. Hence, the probability of detecting RBX1 in the immunoprecipitate of FBXO7 is lower than that of SKP1, which is a direct binding partner and also Cullin1, which is a first degree indirect binding partner as reflected in the mascot score. Additionally, the proteasomal inhibitor PI31 was identified in all replicates of all conditions (wt and mutants). PI31 and FBXO7 have been shown to physically interact via their FP domains and this interaction is at least of functional significance in the drosophila melanogaster homologue of FBXO7(Bader et al., 2011; Kirk et al., 2008). PI31 was identified to interect with overexpressed FBXO7 wild-type as well as with all the disease mutants.

Replicate 1

Protein	MW (kDa)	WT	T22M	R378G	R498X
FBXO7	58.9	1632 (95, 43%)	1091 (71, 37%)	1403 (101, 37%)	1639 (110, 52%)
Cullin1	90.3	5900 (330, 65%)	3265 (178, 46%)	4146 (216, 55%)	3021 (178, 47%)
SKP1	18.8	1813 (81, 88%)	288 (29, 34%)	1412 (97, 66%)	925 (47, 52%)
RBX1	12.7	62 (5, 17%)	-	53 (6, 35%)	57 (5, 12%)
PI31	30	695 (84, 60%)	400 (52, 45%)	712 (72, 42%)	594 (68, 59%)

Replicate 2

Protein	MW (kDa)	WT	T22M	R378G	R498X
FBXO7	58.9	718 (44, 19%)	438 (26, 17%)	2793 (153, 47%)	512 (25, 20%)
Cullin1	90.3	2387 (117, 42%)	42 (2, 1%)	1634 (82, 33%)	2163 (121, 46%)
SKP1	18.8	1271 (73, 66%)	128 (7, 15%)	543 (41, 69%)	983 (71, 66%)
RBX1	12.7	-	-	20 (2, 12%)	-
PI31	30	718 (44, 19%)	313 (23, 30%)	648 (68, 45%)	199 (19, 13%)

Replicate 3

Protein	MW (kDa)	WT	T22M	R378G	R498X
FBXO7	58.9	3395 (211, 52%)	2030 (122, 40%)	2762 (164, 51%)	2368 (154, 47%(
Cullin1	90.3	8597 (409, 82%)	6042 (292, 70%)	6159 (273, 61%)	7930 (394, 80%)
SKP1	18.8	1920 (89, 80%)	2002 (88, 75%)	2179 (95, 80%)	2976 (140, 80%)
RBX1	12.7	60 (7, 17%)	-	23 (4, 12%)	48 (8, 12%)
PI31	30	1372 (157, 60%)	610 (54, 47%)	1352 (96, 61%)	1017 (79, 39%)

Table 3-1: Stable overexpressed FBXO7 wt as well as pathogenic mutants assemble into the SCF E3 ligase complex as identified by proteomics

The mascot score for each endogenous complex partner that immunoprecipitated with stable overexpressed Flag-Fbxo7 is shown for all 3 biological replicates. In brackets is the number of peptides and the sequence coverage in percent).

3.3.2.1 Validation of SCF complex formation by immunoblotting

Some of the remaining 50% of the IP products was used for 4-12% Bis-Tris SDS-PAGE and immunoblotting for the stable overexpressed FBXO7 constructs using α-Flag and α-human FBXO7 antibodies as well as for the endogenous complex partners and PI31. This shows that the wt as well as all of the 3 disease mutants in the stable overexpression system are able to physically bind to their endogenous SCF complex partners as well as PI31. While the interaction with RBX1, which does not directly interact with FBXO7, could not be detected in the immunoprecipitate of the T22M mutant by proteomics, immunoblotting is sensitive enough to show that RBX1 forms a complex with all Flag-FBXO7 constructs including the T22M mutant (Figure 14).

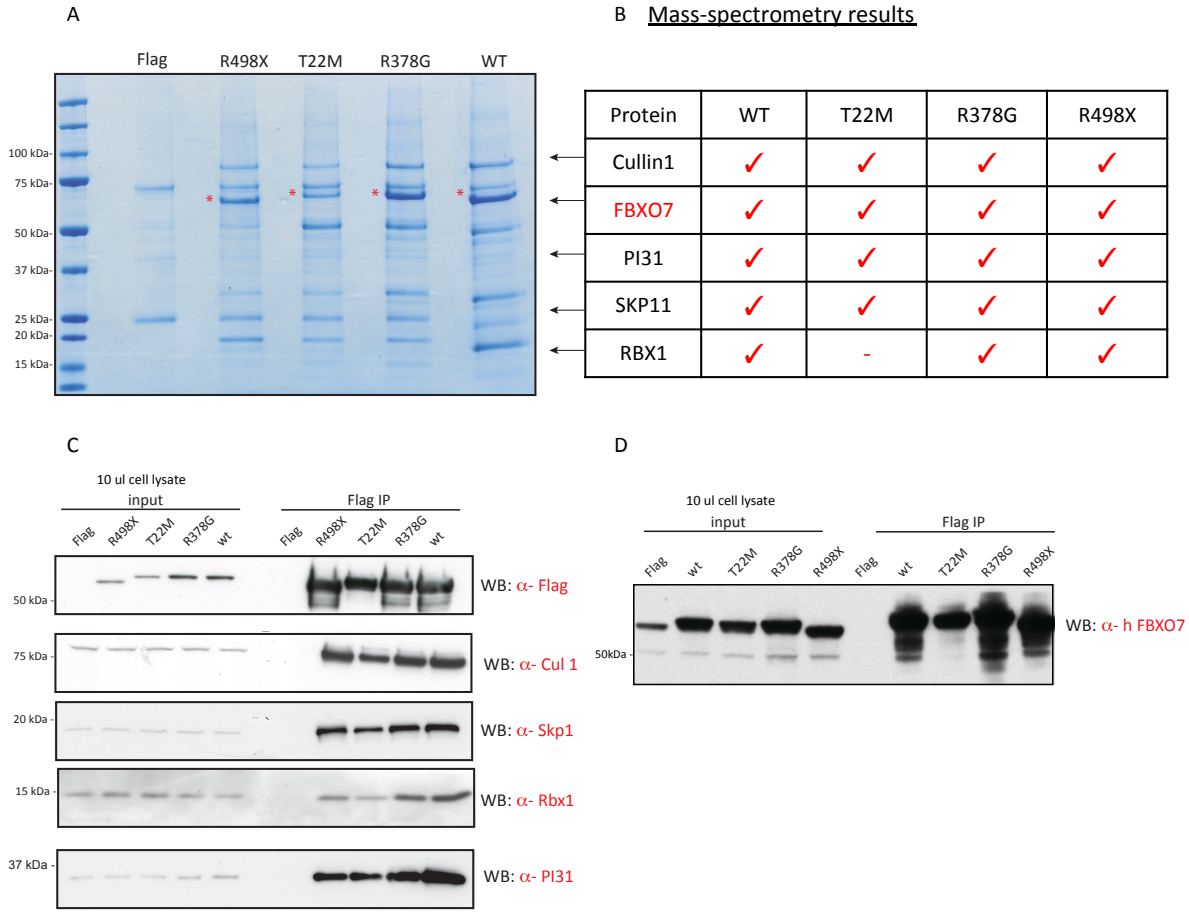

Figure 14: Stable overexpressed FBXO7 wt as well as pathogenic mutants assemble into the SCF E3 ligase complex as identified by immunoblotting

A: Representative Colloidal blue stained 4-12% Bis-Tris gel of 50% of the IP product of replicate 3 for in gel tryptic digestion for proteomic analysis.

B: Qualitative representation of results from all 3 replicates demonstrating that all endogenous SCF complex components as well as PI31 are present in the Flag-FBXO7 pull-downs of the wt as well as the disease mutants. The exception is RBX1, which could not be identified in any of the 3 IPs of the T22M mutant.

C: Flag immunoblotting of input lysates (10ug each) and 1% of the Flag-IP product for detection of the stable overexpressed Flag-Fbxo7 constructs. Immunoblotting for Cullin1, SKP1, RBX1, and PI31 shows that not only the wt, but also all of the pathogenic mutants assemble with all the other endogenously expressed SCF complex partners. Immunoblotting is able to detect RBX1 also in the Flag-IP of the T22M mutant.

D: Immunoblotting of input lysates (10ug) and 1% of the IP product for the human FBXO7 antigen.

3.4 Screening strategies for identifying FBXO7 interacting partners / SCF^{FBXO7} substrates by proteomics in the stable overexpression system

3.4.1 LC-MS/MS of Flag IPs of FBXO7 wt and disease mutants

The formation of the SCF^{FBXO7} complex is a prerequisite for any putative function of FBXO7 as part of an E3 ubiquitin ligase. The previous experiments (3.3) show that at least in the single, stable overexpression system FBXO7 wt as well as the disease mutants are able to form a complex with endogenous Cullin1, SKP1, RBX1 as well as PI31. The next question is whether it is possible to identify substrates of FBXO7 that interact with the SCF^{FBXO7} complex with sufficient affinity to be detectable by affinity-purification-mass-spectrometry. Furthermore, if this approach is able to identify possibly FBXO7 substrates, it would be interesting to investigate whether there are differences in binding partners between the wt and the disease mutants of FBXO7. To undertake this analysis, the mass-spectrometry data of the respective immunoprecipitations were analysed using proteinguru (www.proteinguru.com). Proteinguru facilitated the creation of a single excel spread sheet for each IP of all conditions - Flag-FBXO7 wt and the 3 disease mutants – and replicates (see 3.3.2). The data was then further analysed using BioVenn, a free web application for the comparison and visualization of biological lists using area-proportional Venn diagrams(Hulsen et al., 2008). This showed that there is a great degree of variation amongst the replicates for each condition in terms of number of proteins identified. Also, the number of proteins that were identified in all 3 set of experiments per condition was rather small: Only 28 proteins were identified in all 3 replicate experiments for the FBXO7 wt, 11 for the FBXO7 T22M, 35 for the FBXO7 R378G, and 21 for the FBXO7 498X mutants (Figure 15: Overlap of the proteomic datasets of the 3 replicate experiments per condition: FBXO7 wt, T22M, R378G, and R498X). Interestingly, the protein IDs that were shared amongst replicates mainly belonged to members of the proteasomal machinery, to the SCF^{FBXO7} complex as well as PI31. This was true for the FBXO7 wt as well as all 3 disease mutants.

A

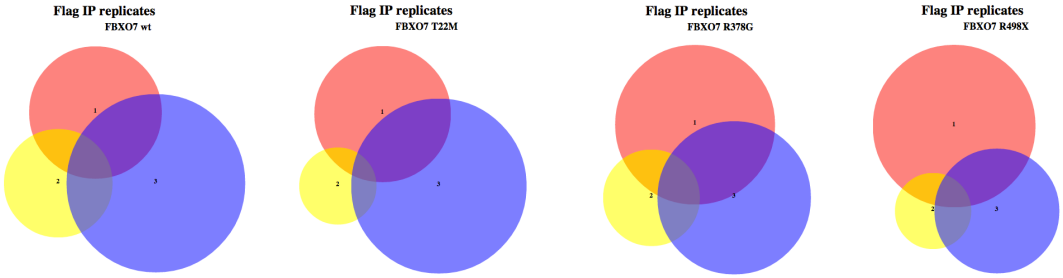

B

Replicate	FBXO7 wt	FBXO7 T22M	FBXO7 R378G	FBXO7 R498X
1	225	237	494	441
2	151	76	181	97
3	408	391	455	260
Overlap {1,2,3}	28	11	35	21

Figure 15: Overlap of the proteomic datasets of the 3 replicate experiments per condition: FBXO7 wt, T22M, R378G, and R498X

A: The Venn diagrams show the degree of variation amongst the 3 replicates per condition in terms of absolute number of identified proteins and the pool of protein IDs that were identified in all 3 experiments per condition. Each condition – wt and mutants – for each replicate were performed in parallel; replicate one is colour coded in red, replicate 2 in yeallow, and replicate 3 in blue.

B: The table indicates the number of proteins that were identified in each replicate experiment and the number of proteins that were identified in all 3 sets per condition.

FLAG-FBXO7 wt	FLAG-FBXO7 T22M	FLAG-FBXO7 R378G	FLAG-FBXO7 R498X
CUL1	CUL1	CUL1	CUL1
SKP1	FBXO7	TUBA8	FBXO7
FBXO7	GNB2L1	SKP1	SKP1
GNB2L1	IRS4	FBXO7	PSMF1
PSMF1	PSMF1	GNB2L1	PSMA7
PSMA7	SKP1	PSMF1	PSMA1
PSMC5	PRKDC	PSMA1	PSMB5
PSMA4	PSMB1	PSMD2	PSMC2
COPS4	PSMA3	PSMB5	PSMA2
PSMB5	PSMA2	PSMC5	PSMB3
PSMC1	ZBED4	PSMC2	PSMB1
PSMA3		PSMA7	PSMA5
PSMA1		PSMA6	PSMB2
PSMA6		COPS4	PSMC4
PSMC2		PSMB2	PSMB4
COPS5		PSMA2	PSMA3
IRS4		CTPS	ABCA5
PSMB2		PSMA3	SLX4
PSMA2		PSMB1	SNTN
PSMB4		PSMC6	ASPM
PSMA5		PSMB3	FBF1
PSMB1		PSMC1	
PSMG1		PSMC4	
PSMC4		ATAD3B	
SLX4		PSMB4	
ANXA5		COPS6	
MAGEB18		EEF1G	
H1FNT		PSMA5	
		PSMD8	
		SLX4	
		PSMD14	
		MAGEE1	
		KCNH5	
		ACE	
		PSMG2	

Table 3-2: Hits of the affinity-purification mass-spectrometry analysis of the Flag-FBXO7 wild-type and disease mutants, that were found in all 3 replicate experiments

The table shows the list of proteins that were identified in each of the 3 replicates for each condition – Flag-Fbxo7 wild-type, T22M, R378G and R498X ("Overlap (1,2,3)" in Venn diagram in Figure 15). Highlighted in red are FBXO7 as the bait, the other SCF complex partners (SKP1, Cul1, and RBX1) as well as PI31 (PSMF1). The latter as it has been reported to interact with FBXO7 before(Kirk et al., 2008).

3.4.2 **LC-MS/MS of Flag IPs of FBXO7 mutants deficient of forming SCF^{FBXO7} complex**

Identifying substrates of E3 ligases is notoriously difficult because of the transient and weak nature of this interaction. Several groups have designed general screening strategies for substrate identification, amongst them Yumimoto et al(Yumimoto et al., 2012). Here, they combine differential SILAC (**S**table **I**ncorporation of **A**minoacids in **C**ell culture) labelling with mutations within the F-Box domain that abolish SKP1 binding. The rational is that a substrate is specifically recognized and bound by the F-box protein as the substrate recognizing subunit of the SCF E3 ubiquitin ligase complex with subsequent ubiquitinylation and degradation by the proteasome resulting in decreased cellular expression levels of the particular substrate. In contrast, a F-box protein mutant deficient of SKP1 binding and hence SCF complex formation, is expected to retain its ability to recognize and bind its substrate, but in contrast to its wild type counterpart, not result in ubiquitylation, degradation and reduction in expression levels thereof (Figure 16). The relative difference in expression levels of proteins can then be exploited by SILAC based quantitative proteomics to identify putative substrates of a particular F-box protein of interest. Additionally, this approach is expected to stabilize the interaction between the mutant F-box protein and its substrates – which otherwise has been described as a “kiss and run” situation – and possibly make it more amenable for detection by mass-spectrometry of the immunoprecipitate even without employing SILAC.

The idea was then to apply this approach to FBXO7. However, rather than deleting the F-box domain of FBXO7 as a whole – with the caveat that deleting 46 AA might have structural implications for its interaction with either the complex or its substrates – I first intended to identify residues within the F-box domain of FBXO7 that were important for SKP1 binding and hence complex formation (see 3.4.2.1).

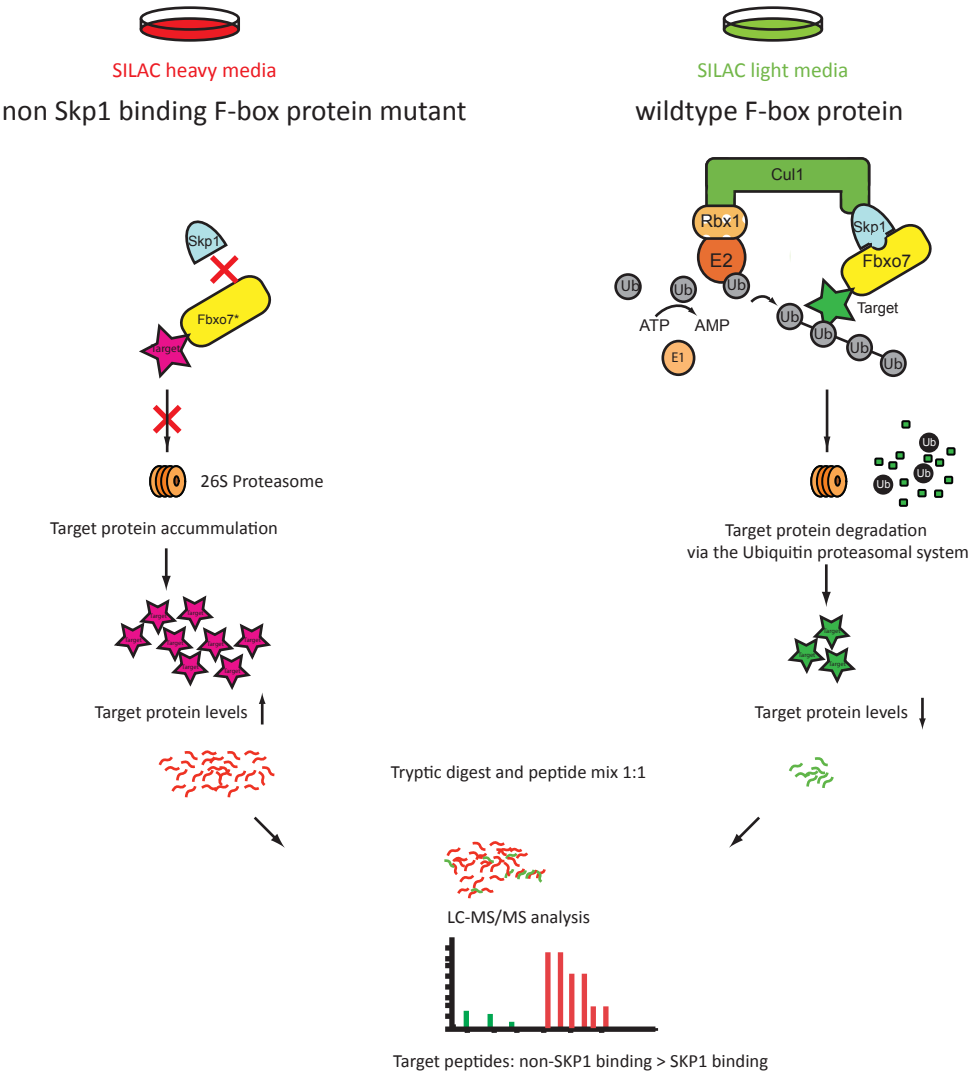

Figure 16: Strategy for F-box protein substrate screening by differential proteomics and use of non-SKP1 binding mutants

A substrate is specifically ubiquitylated and degraded upon recognition by the substrate recognizing F-box protein subunit of a particular ubiquitin ligase complex resulting in a decrease in its cellular protein expression levels (right side of illustration). In contrast, if the same F-box protein has a mutation in its F-box domain that abolishes SKP1 binding and hence complex formation, the expectation is that the same substrate is still being recognized and bound without being degraded. This would result in a relative increase in its cellular expression level (left side of the panel) as it is not degraded via the ubiquitin proteasomal system. This difference in expression level can be exploited in SILAC quantitative proteomics to identify putative SCF substrates.

3.4.2.1 Screening for FBXO7 residues important for SKP1 binding

The F-box domain in general is a degenerative motif consisting of about 40 AA residues, and for most F-box proteins it is not known which of these residues are mandatory for the interaction with SKP1(Skaar et al., 2009b). An exception is the F-box protein SKP2, as a crystal structure of the human SKP2 bound to SKP1 has been described(Schulman et al., 2000). Figure 17 shows an alignment of the F-box motif consensus sequence and SKP2, as well as all the amino acids that constitute the direct interface between the 2 proteins.

Figure 17: F-box domain residues of potential importance for SKP1 binding

Sequence alignment of the F-box motif consensus motif and the region around the F-box motif of the human F-box protein SKP2 (Q13309, AA 92-156). A red star denotes the AA residues of SKP2 that are in contact with SKP1 based on the crystal structure of the human SKP2 bound to SKP1 complex(Schulman et al., 2000).

This information was used as a template to design single Alanine point mutants of individual residues of the F-box domain of FBXO7 in order to determine the individual contribution of these residues for the interaction between FBXO7 and SKP1: In the first instance, the relevant part of the FBXO7 sequence was added to the SKP2 alignment and individual FBXO7 residues were picked for site directed mutagenesis of the Flag-FBXO7-wt template (Figure 18).

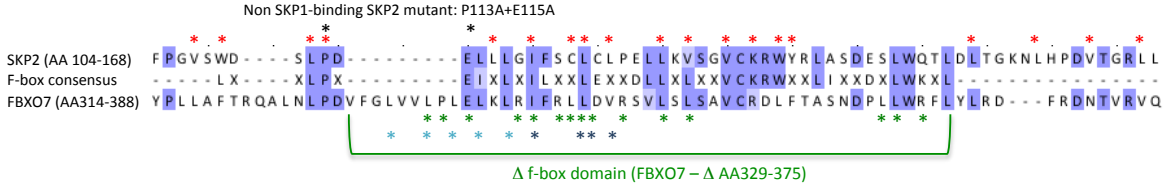

Figure 18: Stretegy of the Alanine screen to identify FBXO7 residues responsible for interacting with SKP1

Sequence alignment of the region around the F-box motif of FBXO7 (F-box motif: AA 329-375) and SKP2 (F-box motif: AA 94-140) as well as the consensus F-box motif. Red stars above the SKP2 sequence show

the AA residues of SKP2 that are in direct contact with SKP1 (as above in Figure 17); green stars directly under the FBXO7 sequence denote the residues for which single Alanine mutants of FBXO7 were tested and the blue stars in the second line underneath the FBXO7 sequence illustrate the residues that either as quadruple (dark blue) or quintuple (light blue) FBXO7 mutants have been shown to abolish SKP1 binding in the literature(Nelson and Laman, 2011). Additionally, a Δ f-box domain FBXO7 mutant, where all 46 AA of the presumed F-box domain of FBXO7 were deleted, was included in the screen. Also, a SKP2 double mutant unable to bind SKP1 has also been reported in the literature and is indicated with black stars(Yumimoto et al., 2012).

To test whether these single Alanine mutants were capable of SKP1 binding, each construct was transiently transfected into HEK293 cells, cells were lysed after 24 hours and subjected to a Flag-IP. The FLAG-IP products for each mutant were then subjected to immunoblotting for FLAG as well as SKP1 to demonstrate either unaffected or impaired / abolished SKP1 binding of the respective mutant. As shown in Figure 19, the FBXO7 wt construct served as a negative control as SKP1 binding was unaffected, whereas the Δ f-box domain FBXO7 mutant served as a positive control as SKP1 binding was completely abolished. None of the 15 single Alanine mutants within the F-box domain of FBXO7 were able to completely abolish SKP1 binding.

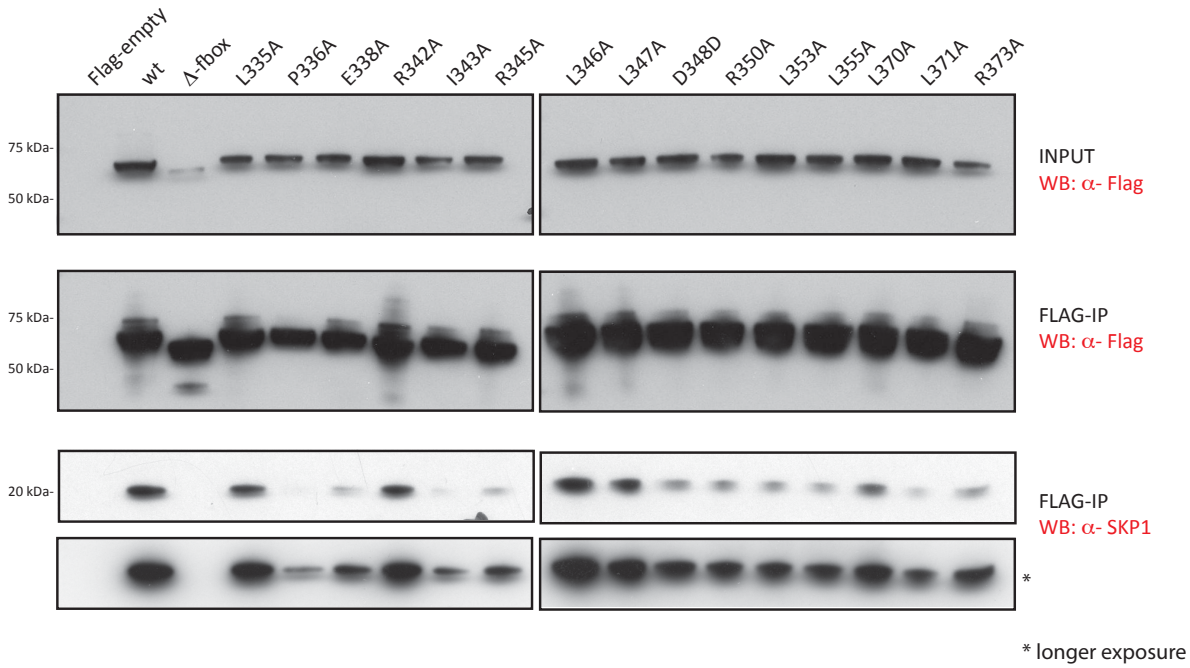

Figure 19: Alanine single mutant screen to identify SKP1 binding residues of FBXO7

Transient transfections of either Flag-empty vector or Flag-tagged FBXO7 wt (negative control: unaffected SKP1 binding), Δ f-box domain FBXO7 (positive control: abolished SKP1 binding) and 15 single Alanine mutants of F-box motif residues of FBXO7 (as indicated in Figure 18) into HEK293 cells were lysed after 24 hours and 1 mg of each lysate was subjected to FLAG immunoprecipitation for 2 hours. The reactions were then immunoblotted for FLAG (bait) and assayed for their ability to bind SKP1.

At the same time as these experiments were performed, a paper was published identifying 2 FBXO7 mutants in whom either simultaneous mutation of 4 or 5 FBXO7 residues resulted in abolished SKP1 binding(Nelson and Laman, 2011). We therefore included these mutants in our screen together with some of the single mutants that appeared to have had some effect on SKP1 binding as well as all the pathogenic disease mutants. Figure 20 shows that the quadruple (FLAG-FBXO7 - I343A+L346A+L347A+V349A) and quintuple FBXO7 mutants (FLAG-FBXO7 - L332A+L335A+L337A+L339A+L341A) were indeed incapable of SKP1 binding, whereas in comparison none of the single mutants or any of the disease mutants had a major effect on SKP1 binding.

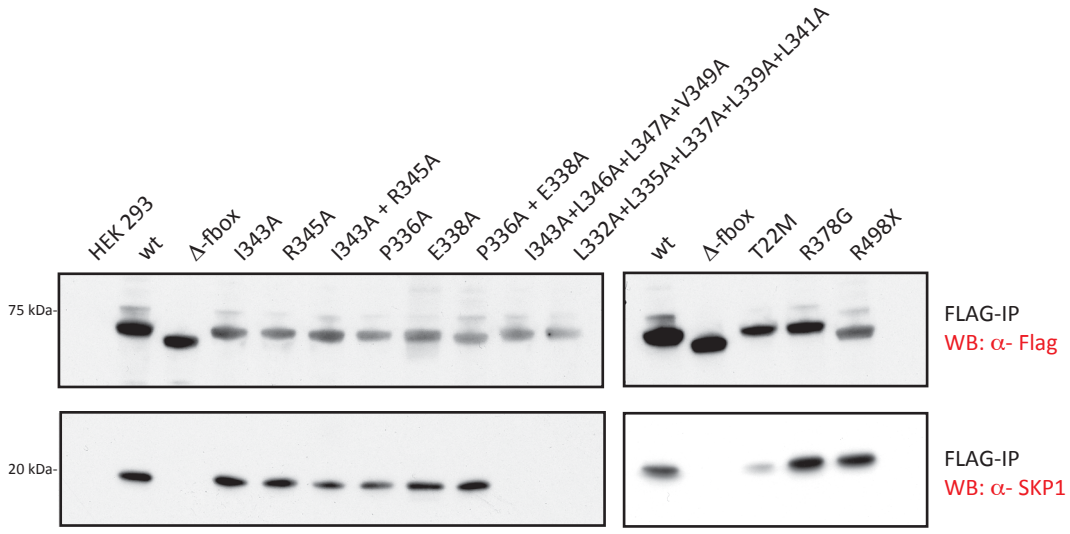

Figure 20: Confirmation of abolished SKP1 binding of previously reported FBXO7 mutants

FLAG immunoprecipitation of the wt, Δ f-box domain, pathogenic disease mutants, some of the previously shown (Figure 19) single mutants and the reported quadruple and quintuple FBXO7 mutants. FLAG-IPs were then assayed for their ability to bind SKP1 by immunoblotting of the IPs for SKP1.

As mentioned above (3.4.2), the intention was to utilize the non-SKP1 binding FBXO7 mutants in a proteomic screen to identify FBXO7 substrates. I was interested in identifying substrates of the FBXO7 wt protein, but in particular also in one of the pathogenic disease mutants: R378G FBXO7. This particular disease mutant is in immediate proximity of the F-box domain (AA 329-375), but experiments so far have demonstrated that it neither disrupts SKP1 binding (Figure 20) nor SCF^{FBXO7} complex formation (Figure 14). I therefore designed an additional non-SKP1 binding mutant – using the quadruple non-SKP1 binding mutant as a template (FLAG-FBXO7 - I343A+L346A+L347A+V349A (DU41285) – for the R378G disease mutant: FLAG-FBXO7 R378G plus I343A+L346A+L347A+V349A (DU41287). Figure 21 shows the result of the stable expression of these mutants – wt and R378G with intact SKP1 binding as well as wt (DU41285) and R378G (DU51287) with abolished SKP1 binding. As expected the non-SKP1 binding mutants – either wt or R378G background – are unable to bind SKP1 or any of the other SCF complex members (Cullin 1 and RBX1) while binding to PI31, which is facilitated via a different FBXO7 domain, is retained.

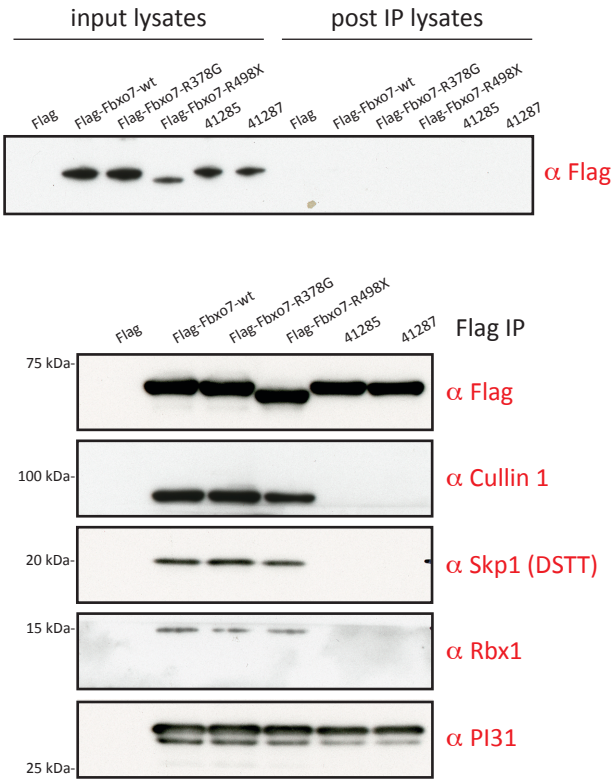

41285: Flag-FBXO7-wt (I343A, L346A, L347A, V349A)
41287: Flag-FBXO7-R378G (I343A, L346A, L347A,

Figure 21: Stable expressing non-SCF complex binding cell lines of the FBXO7 wt and pathogenic R378G mutant

Stable expressing Flp-In TRex HEK293 cell lines of Flag-tagged FBXO7 wt and the disease mutants R378G and R498X as well as FLAG-FBXO7 wt and R378G in the non-SKP1 binding background (FLAG-FBXO7-I343A+L346A+L347A+V349A) were subjected to FLAG-immunoprecipitation and assayed for their ability to bind the other members of the SCF complex as well as PI31. The top panel shows input lysates and complete depletion of the FLAG-FBXO7 constructs after the IP.

3.4.2.2 SILAC based quantitative proteomics of non-SKP1 binding FBXO7 mutants

As demonstrated in 3.4.2.1, stably expressing constructs of all FBXO7 mutants employed in this experiment were made and passaged at least 5 times in the respective SILAC medium to achieve >97% labelling efficacy for each condition (Table 3-3). After inducing construct expression with doxycycline for 18 hours, cells were harvested and Flag IPs were performed. Equal amounts of IP products were mixed and prepared for in solution tryptic digestion for mass-spectrometry analysis.

	LIGHT (K0,R0)	MEDIUM (K4, R6)	HEAVY (K8, R10)
1	Flag	wt	41285
2	Flag	wt	41284
3	Flag	R378G	41286
4	Flag	R378G	41287
5	Flag	wt	Δ F-box
6	Flag	41287	41285
7	Flag	R378G	Δ F-box

Table 3-3: Experimental setup and SILAC labelling conditions

Each experiment consisted of 3 conditions. Flag-empty vector was labelled with "light" SILAC medium (expected to bind "unspecific contaminants"), either the SKP1 - binding Flag-tagged FBXO7 wt or SKP1 – binding Flag-tagged FBXO7 R378G mutant were grown in "medium" SILAC media (in experiment 6, the non-SKP1 binding mutant of Flag-tagged FBXO7 R378G was also used in "medium" SILAC label) and the non-SKP1 binding mutants (either FLAG-FBXO7 wt - L332A+L335A+L337A+L339A+L341A (DU41284), FLAG-FBXO7 wt- I343A+L346A+L347A+V349A (DU41285), FLAG-FBXO7-R378G - L332A+L335A+L337A+L339A+L341A (DU41286), FLAG-FBXO7 R378G- I343A+L346A+L347A+V349A (DU41287), or FLAG- FBXO7 wt – Δ-F-box) were grown in "heavy" SILAC medium.

The proteomics raw data was then analysed using maxquant and the following questions were asked(Cox et al., 2009): Which proteins are more abundantly present (at least > 2.5 fold) in the non-SKP1 binding FBXO7 wt mutant (DU41284, DU41285 and Δ-F-box FBXO7 wt) than in the FBXO7 wt (Experiment 1, 2, and 5)? Which proteins are more abundantly present in the non-SKP1 binding R378G FBXO7 disease mutant compared to the SKP1-binding R378G FBXO7 mutants (DU41286 and DU41287) or FBXO7 wt – Δ-F-box (Experiment 3, 4, and 7)? And does a different subset of proteins bind more readily to the non-SKP1 binding R378G FBXO7 mutant in comparison to the non-SKP1 binding FBXO7 wt construct (Experiment 6)? Additionally, none of the SCF complex partners or any of the potential hits should be present in the FLAG-empty vector IP list. Table 3-4 illustrates the analysis paradigm.

RATIO	H/M
	Non-SKP1- binding FBXO7 (HEAVY) / SKP1- binding FBXO7 (MEDIUM)
FBXO7	↔
SKP1	↓
CULLIN1	↓
RBX1	↓
PI31	↔
putative substrates	↑↑

Table 3-4: Analysis paradigm of differential protein complexes associated with SKP1-binding and non-binding FBXO7 mutants

The expectation is that the non-SKP1 binding mutant is still able to recognize and bind its substrate, but without immediately releasing it for ubiquitylation and subsequent proteasomal degradation. The substrate should therefore be more abundantly present and detectable in the IP of non-SKP1 binding mutant than in the SKP1-binding and hence SCF E3 ligase complex forming counterpart. SILAC labelling of the different conditions allows mixing the samples at IP level before digestion and quantitatively assessing differences in protein complexes associating with the SKP1-binding and non-SKP1 binding conditions.

Coming now to the actual results: As expected, none of the SCF complex partners was present in any of the FLAG-empty vector IPs. FBXO7 should have been equally abundant in each set of experiments, but this was not the case as shown in

Table 3-5: The ratio for FBXO7 varied between 0.76 and 0.42 between the individual experiments. SKP1 was significantly less abundant in the non-SKP1 binding mutants (about factor 10) while PI31 was present in all experiments with a ratio of about 1. There were no other hits in any of the 7 experiments that fulfilled the criteria of being at least 2.5 fold more abundant in the non-SKP1 binding compared to the SCF complex binding FBXO7 mutants. Data is shown for one set of experiments. The same experiment was repeated twice without any difference in outcome: One time, lysates from the different SILAC conditions were mixed at lysate level rather than after performing the IP followed by in solution tryptic digestion for mass-spectrometry analysis and the other

Experiment	1	2	3	4	5	6	7
RATIO (H/L)	41285 (H) /wt (M)	41284 (H) /wt (M)	41287 (H) /R378G (M)	41287 (H) /R378G (M)	Δ F-box (H) /wt (M)	41287 (H) /41285(M)	Δ F-box (H) /R378G (M)
FBXO7	0.76	0.48	0.63	0.63	0.42	0.67	0.45
SKP1	0.08	0.09	0.06	0.06	0.06	0.55	0.05
CULLIN1	-	-	-	-	-	-	-
RBX1	-	-	0.64	0.64	-	-	0.74
PI31	1.05	0.82	1.03	1.03	1.07	1.07	1.04

time, the experiment was repeated exactly the same way as the experiment in 3.4.2.2 except that the samples were not prepared by in solution tryptic digestion for mass-spectrometry, but that a SDS PAGE electrophoresis was performed and bands were prepared for in-gel tryptic digestion for mass-spectrometry (data of the latter 2 experiments not shown).

Table 3-5: Results for SILAC based proteomics of SKP1-binding and non-SKP1 binding FBXO7 mutants

3.4.2.3 Non-SILAC based proteomics of non-SKP1 binding FBXO7 mutants

The non-SKP1 binding FBXO7 mutants may nonetheless represent a potentially powerful tool for identifying FBXO7 substrates. As mentioned before, the interaction between F-box proteins and their substrates is usually transient and possibly weak or at least weaker than the association between FBXO7 and the other SCF complex partners. As the non- SKP1 binding mutants are expected to be unimpaired in their ability to recognize and bind their targets without immediately passing them on to the proteasome, they may yield information about substrates in more straightforward conventional mass-spectrometry analysis of Flag-immunoprecipitation complexes without SILAC labelling.

In this experiment, I performed FLAG immunoprecipitations on 1.5mg of lysates from stable expressing FBXO7 constructs that had been induced overnight: Flag-empty vector, Flag-tagged FBXO7 wt and the disease mutant R378G and the non-SKP1 binding mutants FLAG-FBXO7 wt- I343A+L346A+L347A+V349A (DU41285), and FLAG-FBXO7 R378G-I343A+L346A+L347A+V349A (DU41287). Before harvesting the cells, cells were treated with chemical inhibitor of the NEDD8-E1, MLN4924 at a concentration of 3uM for 4 hours or DMSO as a control. By inhibiting the E1 activating enzyme of NEDD8, MLN4924 prevents the neddylation of cullins, thereby inactivating Cullin Ring E3 ligases / SCF E3 ligases resulting in accumulation of their substrates(Brownell et al., 2010; Soucy et al., 2009). The idea was that using MLN4924 might facilitate the identification of FBXO7 substrates as it prevents their degradation.

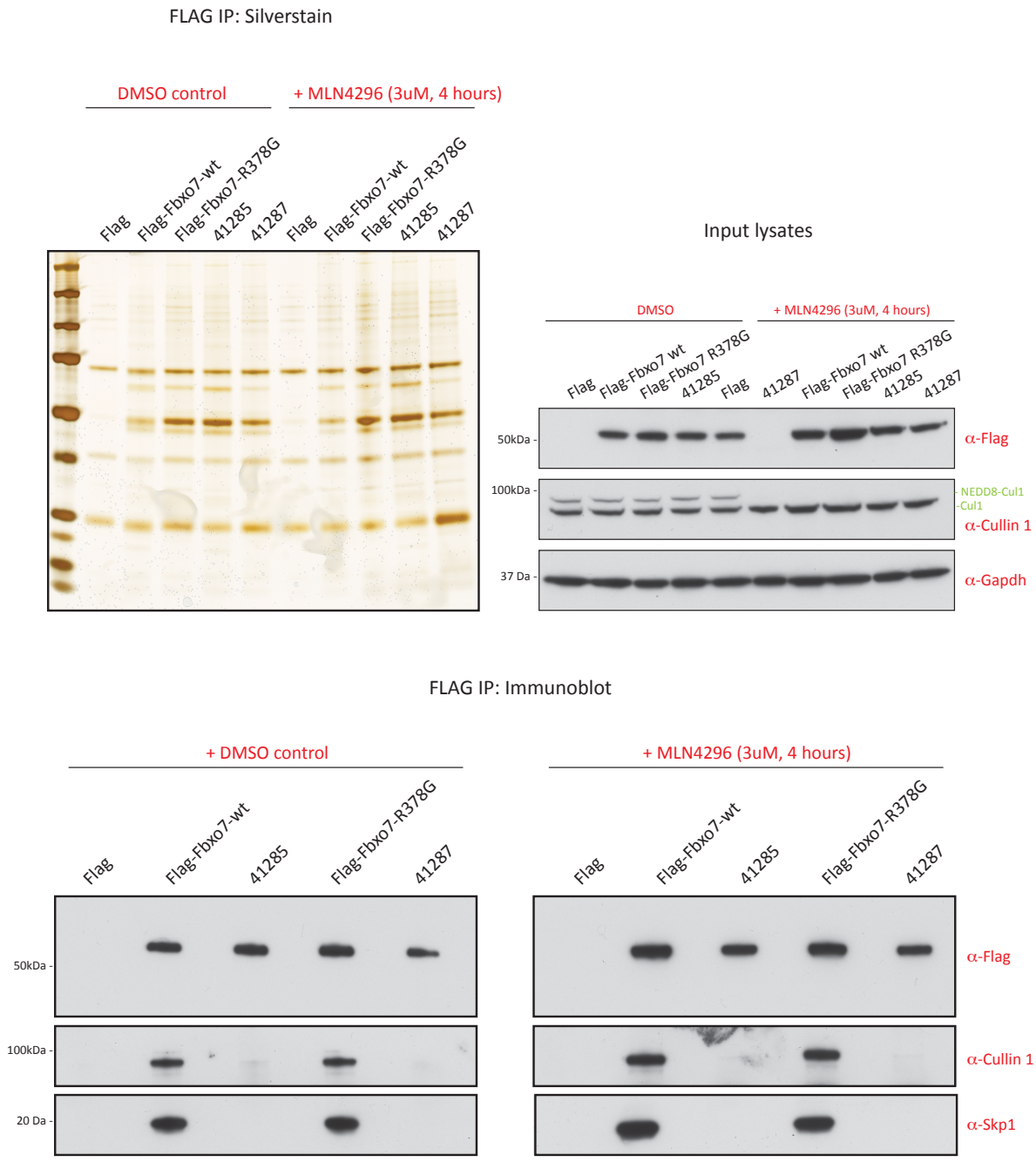

Figure 22: Control blots of FLAG-IPs of FBXO7 SKP1 binding and non-binding mutants for LC-MS/MS analysis

Silver stain of 5% of FLAG-IP products from 1.5mg lysates (top left) and immunoblot of input lysates (top right) of 10ug of input lysates for FLAG – demonstrating equal levels of doxycycline induced construct expression; Cullin 1 – showing the disappearance of the neddylated Cullin1 species upon treatment with MLN4924 as a control; and GAPDH as a loading control. The lower panel shows immunoblots of 10% of the FLAG-IP products for FLAG (bait) as well as SKP1 and Cullin1 to demonstrate that deneddylation of Cullin 1 does not disrupt SCF complex formation of the SKP1 binding constructs (Flag-FBXO7-wt and FLAG-

FBXO7-R378G) and to verify that the non-SKP1 binding mutants do not bind SKP1 nor Cullin1. The remaining 85% of the IP products were prepared for in-solution tryptic digestion for LC-MS/MS.

The data was analysed with proteinguru to compile the proteomic data from each condition into a single excel file. This data was then further processed using BioVenn to create the Venn diagrams in Figure 23: I wanted to know which proteins are exclusively amongst the proteins that associate with the non-SKP1 binding FBXO7 constructs – bind to the substrate recognizing F-box protein without being ubiquitylated for proteasomal degradation (yellow) - and at the same time did not overlap with any of the hits from the analysis of the FLAG-empty vector alone (blue). The latter were considered as unspecific contaminants. For the FBXO7 wt, this was the case for 62 proteins of 212 (29%) and for the FBXO7 R378G disease mutant, 44 proteins of 190 (23%). The MLN4924 treated datasets were used for cross-referencing protein IDs and can be found in the appendix.

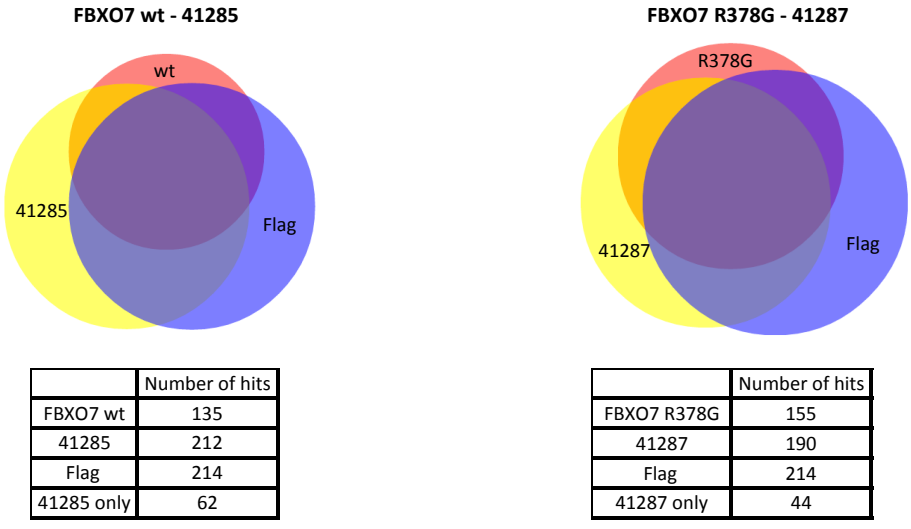

	Number of hits
FBXO7 wt	135
41285	212
Flag	214
41285 only	62

	Number of hits
FBXO7 R378G	155
41287	190
Flag	214
41287 only	44

Figure 23: Overlap of proteomic datasets of SKP1-binding and non-binding FBXO7 mutants for FBXO7 wt and the R378G disease mutants

The Venn diagrams show the overlap between the SKP1-binding (red) and non-SKP1 binding (yellow) FBXO7 constructs for the FBXO7 wt (FBXO7 wt – 41285) and the R378G disease mutant (FBXO7 R378G-41287). The corresponding tables underneath show the absolute number of identified proteins (duplicates removed) per condition and experiment. Additionally, the number of protein IDs that were exclusively found in the non-SKP1 binding constructs is shown.

To further narrow down the list of potential FBXO7 substrates, I cross-referenced the list of the proteins exclusively bound to the non-SKP1 binding proteins ("41285 only" for the FBXO7 wt construct and "41287 only" for the FBXO7 R378G mutant) against the list of proteins that were present in corresponding MLN4924 treated dataset and at the same time eliminating unspecific contaminants by excluding the hits from the FLAG-IPs. For the FBXO7 wt, this was the case for 9 proteins, and for the FBXO7 R378G mutant, 11 of 44 proteins. Amongst them were Keratins and cytoskeletal proteins that were considered unspecific. The protein IDs of the remaining hits (as long as $\geq$ 2 unique peptides were identified) is shown as well.

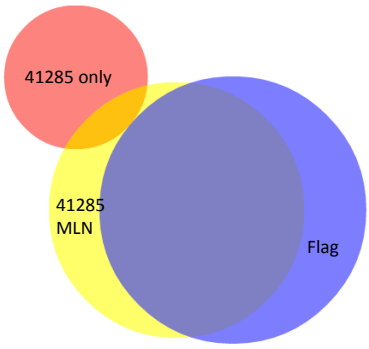

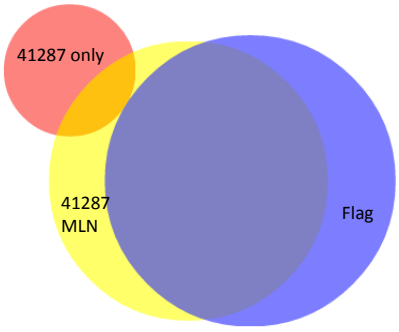

	Number of hits
41285 only	62
41285 MLN	196
Flag contaminants	214
Overlap (41285 only, 41285 MLN)	9

	Number of hits
41287 only	44
41287 MLN	197
Flag contaminants	214
Overlap (41287 only, 41287 MLN)	11

	MW	41285	41285 MLN
PCBP2	38.9	99 (5, 12%)	33 (4, 13%)
GEMIN8	28.9	54 (10, 16%)	22 (3, 3%)
ZNF618	106.6	32 (4, 1%)	26 (3, 1%)
CCT7	59.8	54 (5, 4%)	56 (5, 11%)

	MW	41287	41287 MLN
SNRPN	24.8	265 (16, 28%)	538 (29, 35%)

Figure 24: Summary of identified proteins that are associated with the non-SKP1 binding mutants of the FBXO7 wt and R3678G disease mutant.

The Venn diagrams show overlap between proteins that exclusively bound to the non-SKP1 binding mutant of the FBXO7 wt (41285) on the left and the same for the FBXO7 R378G disease mutant (41287) on the right that were also present in the corresponding MLN4924 treated dataset. The absolute number of protein hits for each dataset is shown in the table underneath. The corresponding protein IDs of the

"overlap group" is shown on the bottom left for the FBXO7 wt and on the bottom right for the FBXO7 R378G mutant with mascot scores and number of identified peptides and sequence coverage in brackets. Keratins, tubulins and any proteins with < 2 unique peptides amongst the overlap groups are not shown.

3.5 Yeast two - hybrid screen

In order to employ an alternative strategy to identify FBXO7 interactors, a yeast two-hybrid screen was performed using the full-length FBXO7 protein (Uniprot reference: Q9Y3I1) as bait. The screen done by Hybrigenics (http://www.hybrigenics.com). 145 million clones of an adult human brain library were screened and a total of 90 clones were obtained. Sequencing of the corresponding plasmids only yielded 2 proteins: SKP1 and PSFM1 (or PI31). For both proteins, the predicted biological score as an indicator for the reliability of the interaction was very high. Both proteins, SKP1 as well as PI31 are recognized interactors of FBXO7(Kirk et al., 2008; Skaar et al., 2009a). A table containing all the raw data and bioinformatics analysis of the yeast two-hybrid screen can be found in the appendix.

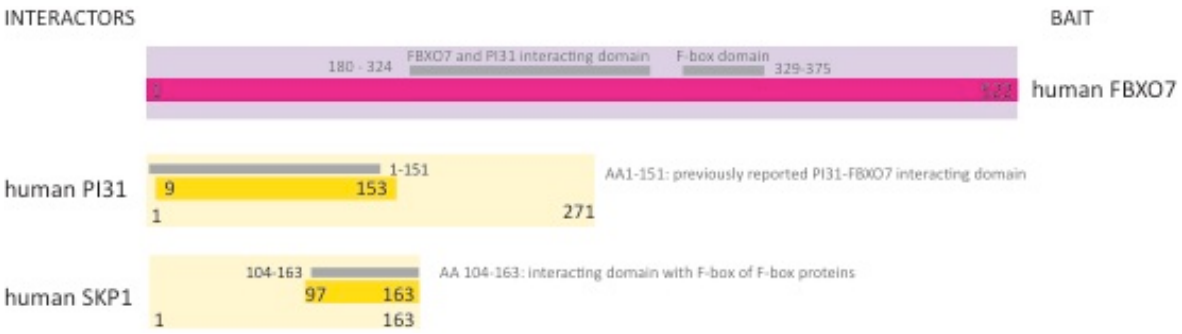

Figure 25: Results of the Yeast two-hybrid screen with full-length FBXO7 as bait and a human brain library as prey

90 positive clones out of 145 million clones of an adult human brain library were obtained and sequenced. These corresponding sequences could be mapped to 2 proteins: PI31 (Uniprot reference: Q92530) and SKP1 (Uniprot reference: P63208). The translucent boxes (pink for the bait and yellow for the identified interactors) indicate the full-length proteins; the opaque boxes indicate the size of the bait fragment (pink) and the amino acid sequence shared by all prey fragments matching the same reference protein (18 fragments for PI31 and 71 for SKP1). The grey boxes indicate previously identified interacting domains of bait as well as prey proteins.

3.6 Discussion

Little was known about FBXO7 at the time of embarking on my PhD project in December 2009: Mutations in the FBXO7 gene had been reported to co-segregate with an early onset Parkinsonian syndrome with pyramidal features in a single consanguineous family from Iran in 2008(Shojaee et al., 2008). FBXO7 as the disease causing gene was confirmed when two further 2 families – one from Italy and the other from the Netherlands – with a similar clinical syndrome associated with recessive FBXO7 mutations were reported in 2009(Di Fonzo et al., 2009). Since then, only a few more patients with FBXO7 mutations have been identified (as discussed in 1.3.2) and it can probably be assumed that mutations in the FBXO7 gene are not a major contributor to PD on a population-based level. Nonetheless, studying the molecular function of FBXO7 in health and disease and cross-referencing it with our existing knowledge about other monogenetic PD genes is expected to shed light onto pathways involved in PD and neurodegeneration.

FBXO7 belongs to the family of F-box proteins – a family that is characterized by the presence of an F-box domain, which mediates binding to the small protein SKP1(Skaar et al., 2009a). The interaction with SKP1 is necessary for linking the F-box protein as the variable module to the rest of the SCF E3 ubiquitin ligase complexFigure 7. However, not all F-box proteins assemble into E3 ligase complexes with Cullin1 and RBX1, demonstrating that the interaction with SKP1 is necessary, but not sufficient for complex formation(Skaar et al., 2009a). Additionally, SCF independent functions have been reported for some F-box proteins(Jonkers and Rep, 2009). FBXW8 is an example of an F-box protein that despite binding to SKP1, does not form a complex with Cullin 1, but rather unconventionally with Cullin 7 and RBX1(Litterman et al., 2011). The function of FBXL11 as either a histone demethylase or in complex with the H3K63 methylase NSD1 as a negative regulator of NF-κB is independent of SKP1 binding and hence SCF complex formation altogether(Du et al., 2013; Lu et al., 2010). There are also regulatory mechanisms of F-box protein function within the context of SCF E3 ligase activity that is brought about by SCF complex disruption: The F-box protein SKP2 forms a SCF^{SKP2} E3 ubiquitin ligase complex and has been found to be overexpressed in many human

cancers. On a transcriptional level, SKP2 gene expression is negatively regulated by Foxo3a. More recently, Foxo3a has been shown to also directly interact with SKP2 and thereby promoting SCF^{SKP2} complex disruption. This in turn leads to impaired SCF^{SKP2} E3 ubiquitin ligase activity and hence stabilization of p27, one of the physiological substrates of SKP2 dependent ubiquitinylation(Wu et al., 2013a). In analogy to F-box proteins, BTB proteins form Cullin-RING E3 ubiquitin ligase complexes with Cullin 3. The Gordon's hypertension syndrome is an example where human pathogenic mutations in components of the E3 ligase complex – either in the BTP protein KLHL3 or Cullin 3 – result in complex disruption or impaired binding to one of its substrates, WKN1(Ohta et al., 2013).

3.6.1 FBXO7 assembles into a SCF^{FBXO7} complex formation and the pathogenic disease mutants doe not disrupt SCF complex formation in the stable overexpression system

It was therefore one of my first incentives to find out whether FBXO7 does indeed assemble into a SCF^{FBXO7} E3 ligase complex together with SKP1, Cullin1 and RBX1; and whether the pathogenicity of the human disease mutants could possibly be associated with SCF complex disruption. In section 3.3, I show that the FBXO7 wt as well as all so far reported FBXO7 disease mutants – T22M, R378G, and R498X – readily form a complex with SKP1, Cullin1, and RBX1. This is demonstrated by tag-immunoprecipitation of the stable expressed Flag-tagged FBXO7 constructs and subsequent immunoblotting of the IP products for endogenous SKP1, Cullin1, and RBX1. One caveat for the conclusion that the disease mutants are equally apt to assemble into the SCF^{FBXO7} complex formation is that the Flp-InT-REx-HEK 293 host cell line itself expresses endogenous FBXO7 in addition to the stable overexpressed FBXO7 mutants (Figure 14). Dimerization of F-box proteins is a recognized phenomenon, although its effect on substrate recognition and ubiquitinylation *in vivo* is in the majority of cases unclear(Skaar et al., 2013). For FBX04 it has been shown that homodimerization is essential for SCF^{FBX04} ubiquitin E3 ligases activity towards its substrate TRF1(Li and Hao, 2010). FBXO7 has been shown to heterodimerize with PI31(Kirk et al., 2008). The authors also suggested that the FP domain, which facilitates heterodimerization with PI31 potentially allows the formation

of FBXO7 homodimers. If this is the case one might argue that the endogenous SCF complex partners of the stable overexpressed FBXO7 disease mutants do not directly interact with the mutant FBXO7 proteins, but that the interaction is rather indirect via dimerization between the mutant FBXO7 protein and the endogenous SCF^{FBXO7} complex from the Flp-InT-REx-293 host cell line. On the other hand, the same strategy – utilizing stable overexpression in Flp-InT-REx-HEK 293 cells – has allowed identifying non-SKP1 binding FBXO7 mutants. Figure 21 shows that despite the intact interaction between the mutant FBXO7 proteins and endogenous PI31, the interaction between the overexpressed non-SKP1 binding FBXO7 mutants and endogenous SKP1, Cullin1 as well as RBX1 is lost. This argues against dimerization between overexpressed FBXO7 disease mutants and endogenous FBXO7 from the Flp-InT-Rex HEK 293 cell line.

3.6.2 Interaction proteomics fails to identify robust SCFFBXO7 targets in the stable overexpression system

The preliminary evidence that the FBXO7 wt as well as disease mutants form a SCF^{FBXO7} complex supports the working hypothesis that FBXO7 functions as the substrate recognizing subunit of an E3 ubiquitin ligase enzyme and that the pathogenic mutations have different downstream effects on physiological FBXO7 ubiquitinylation targets. My next step was therefore to use affinity purification of the FLAG-FBXO7 constructs followed by mass-spectrometry and thereby identifying interacting proteins. Flag-empty vector Immunoprecipitations were used as a control to identify and subtract unspecifically binding background proteins from the pool of hits from the bait pull-downs. This approach has worked in principle to identify and confirm the core members of the SCF^{FBXO7} complex. Beyond that the success of identifying robust interacting partners that merit being considered as potential SCF^{FBXO7} has been disappointing. The variation between sample replicates was rather high, while the pool of proteins that were identified in all 3 biological replicates for each condition was rather small (Figure 15). In fact, amongst them were the bait - Flag-FBXO7 – and Cullin 1 and SKP1. RBX1 as the remainder of the SCF complex on the other hand was not present in any of the replicates of the FBXO7 T22M mutant, although it could readily be identified by immunoblotting of the same samples. Other proteins amongst the pool of replicated

interacting proteins were mainly proteasome associated proteins and components of the COP9 signalosome, which is a negative regulator of SCF E3 ligase activity by mediating the deneddylation of the Cullin subunit(Lyapina et al., 2001). The only other protein that was identified in each replicate and not in any of the control IPs was PI31. PI31 is a known interacting protein of FBXO7 and the interaction between the homologues of PI31 and FBXO7 has been suggested to be a regulatory mechanism for proteasomal activity in Drosophila(Bader et al., 2011; Kirk et al., 2008). PI31 was also the only other protein apart from SKP1 that was identified in the yeast two-hybrid screen (3.5).

In my opinion, there are several problems with the approach to identify FBXO7 interacting proteins by affinity purification of overexpressed tagged FBXO7 and subsequent mass-spectrometry: There is a rapid turnover of most degradative ubiquitinylation substrates, while the interaction between SCF E3 ubiquitin ligases - or more specifically the interaction between the F-box protein subunit of the SCF complex – and their respective substrate is typically rather weak and only transient. As a result, the protein levels of a particular substrate that is being ubiquitinylated for proteasomal degradation may be very low and stringent washing of the IP complexes during the procedure may additionally contribute to allowing the substrate to escape the threshold of detection by mass-spectrometry.

In fact, the identification of F-box protein substrates is a recognized challenge in the field, but over the last years novel proteomic approaches for the identification of SCF substrates and global pool of ubiquitinylated proteins and ubiquitinylation sites have been developed(Harper and Tan, 2012; Kim et al., 2011; Yen and Elledge, 2008; Yumimoto et al., 2012). The use of proteasomal inhibitors – either MG132 or Bortezomib – in a comparative IP-proteomics experiment that is performed in parallel with an untreated experiment aims to identify SCF substrates that are normally being degraded, but that are being stabilized with proteasomal inhibition. This approach has led to the discovery of new substrates of the F-box protein βTRCP2 and to identify the first substrate of the orphan F-box protein FBXO22(Harper and Tan, 2012). Employing

non-SKP1 binding overexpressed F-box protein mutants is another approach of proteomics based substrate trapping(Yumimoto et al., 2012). The non-SKP1 binding mutants do not assemble into a SCF E3 ubiquitin ligase complex, but retain their ability to recognize and bind substrates. As these substrates are subsequently not degraded by the proteasome, their relative abundance and therefore chance for detection by mass-spectrometry increases (Figure 16). This approach is referred to as "differential proteomics-based identification of ubiquitinylation substrates" in the SILAC mode or without SILAC labelling in the peptide counting mode. When SILAC labelling is employed, overexpressed wild-type F-box proteins are grown in different SILAC labelled media conditions. In the original experiments, little overlap was seen when the SILAC approach was compared with the peptide counting approach in HeLa cells for the well-characterized F-box proteins FBXW7, SKP2, and FBXL5(Yumimoto et al., 2012). A rapid exchange between differently labelled substrates present in the mixed lysates during the immunoprecipitation, and subsequent distortion of protein ratios has been suggested as an explanation(Harper and Tan, 2012). Nonetheless, as a proof of concept study this particular approach was able to confirm that the non-SKP1 binding F-box protein mutants did not bind the SCF E3 ligase component Cullin1 and that the some of the known substrates of the respective F-box proteins could be identified(Yumimoto et al., 2012).

In section 3.4.2, I am describing the experiments that I have undertaken to adopt the above described strategies for the identification of FBXO7 substrates. I have employed the substrate trapping IP-proteomic experiments for the FBXO7 wt as well as the disease mutant R378G – in both cases mutating 4 amino acid residues within the F-box domain to Alanine resulted in abolished SKP1 binding. Rather than deleting the entire F-box domain, these quadruple mutants were considered less likely to disturb the structure of FBXO7 as a whole as well as any potential substrate-binding domain. Stable expressing FBXO7 cell lines were preferred over transient expression given that recombinant protein expression levels can be adjusted more towards the endogenous level and because of better reproducibility in replicate experiments. Figure 21 demonstrates equal expression of all FBXO7 constructs as well as equal levels of the various constructs

after Flag-pull-down. Immunoblotting as well as the proteomics data validate that the non-SKP1 binding mutants do indeed not bind to the complex partners (Figure 21, Table 3-5). However, as shown in Table 3-5, the ratio for FBXO7 in each set of experiments - the SKP1 binding versus corresponding non-SKP1 binding FBXO7 construct – was not 1, which means that not equal amounts of each corresponding IP product was mixed resulting in a shift in the baseline of the differential ratio for all other identified proteins. Ultimately, no proteins with a ratio of $\geq$ 2.5 were identified in the tag-purified FBXO7 immunocomplexes.

In general, one of the advantage of differential SILAC proteomics is that differentially labelled samples are being combined early on during sample preparation – usually directly after cell lysis and determination of protein concentration – thereby minimizing the quantitative errors caused by handling different samples in parallel. In the context of trying to identify FBXO7 substrates, combining the different conditions at lysate level harbours the danger of introducing distorted outcome of protein ratios because of rapid exchange between differently labelled substrates present in the lysate mix during the immunoprecipitation process. Likewise, combining the different conditions after the IP introduces quantitative errors because of sample handling. I have therefore also performed individual non-SILAC based IP immunocomplex proteomics of the various FBXO7 constructs including the non-SKP1 binding mutants. These experiments were performed with and without treatment of cells with the Nedd8-E1 activating enzyme inhibitor MLN4924. While MG132 and Bortezomib are unspecific proteasomal inhibitors, MLN4924 specifically targets SCF complexes as Cullin neddylation is considered necessary for SCF complex activation blocking also the activity of the endogenous SCF^{FBXO7} complex(Wu et al., 2013b). As these last experiments were only performed recently, I have not taken any validation of the potential hits listed in Figure 24 forward. This decision was based on the fact that meanwhile I have shifted my focus on the endogenous system utilizing a FBXO7 knock-in (KI) mouse model of one of the human pathogenic FBXO7 mutations (R378G) for substrate identification rather than relying on the overexpression system. Also cross-referencing the list of potential hits from the Flp-In HEK293 overexpression system has not yielded any overlapping hits with those from

the endogenous system apart from the other SCF^{FBXO7} complex partners and PI31. The FBXO7 mouse model will be subject of the next chapter.

However, in view of designing a FBXO7 mouse model with knock-in of one of the human pathogenic mutations, it was important to establish whether the individual amino acid residues that are known to be associated with autosomal recessive FBXO7 disease in humans – T22M, R378G, and R498X – are conserved between the human and mouse species. Figure 26 shows that all 3 amino acid residues are identical between those 2 species. Next, I wanted to know whether it was possible to express each of the disease mutants either in the human or mouse FBXO7 background and that each mutant is indeed translated into a protein product. For the investigation of FBXO7 in the endogenous system, it was of great importance to have high quality antibodies against the FBXO7 antigen. Figure 11 and show that these antibodies are available and their ability to also pull-down FBXO7 immunocomplexes will be shown in the next chapter.

3.6.3 **Summary of result chapter 3**

In summary, my first result chapter shows that FBXO7 does assemble into the SCF^{FBXO7} E3 ubiquitin ligase complex and that this is true for the FBXO7 widtype protein as well as for all of the 3 known disease mutants - T22M, R378G and R498X. These findings suggest that SCF complex disruption is an unlikely mechanism by which the FBXO7 disease mutants exert their pathogenicity. The Alanine mutant screen of single residues within the F-box domain of FBXO7 gives some insight into the interaction between FBXO7 and SKP1: the employed single mutants in this study are on its own unable to abolish SKP1 binding, and based on what we know so far complete SCF complex disruption is only achieved by the simultaneous deletion of several residues ($\geq$ 4 amino acid residues). The non-SKP1 binding mutants also demonstrate that there is no dimerization between the endogenous $SCF^{FBXO7\ wt}$ E3 ubiquitin ligase complex and the overexpressed mutants. If this was the case one would have expected to see a signal for SKP1 in the immunoblot of the affinity purified Flag-immunocomplexes as Western blotting does not allow discrimination based on the source of SKP1 –either bound to endogenous or mutant FBXO7. Retained binding of the tag-immunocomplexes to PI31, which is mediated via

the FP-domain upstream of the F-box domain of FBXO7, shows that the mutations introduced in the non-SKP1 binding mutants does not cause disarray of the protein structure to such an extend that binding via other domains would be affected (Figure 21). Whether this allows any conclusion on towards whether FBXO7 (or $SCF^{FBXO7\ wt}$) forms homodimers is an open question.

4 Characterization of the *Fbxo7* mouse model with knock-in of the corresponding human disease mutant R378G mutation

4.1 Introduction

The identification of PARK genes provides a rational basis to model PD in cells or animals by genetic manipulation. Mice are amenable to genetic manipulation and share similar neuronal networks and disease-associated gene homologous with their human counterpart(Waterston et al., 2002). In comparison to other animal models, mice have a relatively long life span of about 2 years, which is an important aspect when studying neurodegenerative processes. Ideally, a genetic model of PD should recapitulate the characteristic neurodegeneration and pathological hallmarks of PD in an age dependent manner and also demonstrate correlates of the clinical motor and behavioural features(Dawson et al., 2010). Many different genetic mouse models of PD exist including conventional “transgenic models” where the animal constitutively overexpresses a foreign protein as well as the more refined approach where the overexpression of the aberrant gene product is under the control of an inducible on / off tetracycline promoter allowing temporal and spatial regulation (reviewed in (Lee et al., 2012)). Gene targeting strategies are based on homologous recombination events and either create knock-out models by deleting crucially important exons or introduce a premature stop codon to prevent expression of a functional protein product, or gene knock-in models that allow the discrete introduction of mutations(Capecchi, 1989). Viral models to introduce transgenes or facilitate gene knock-down are also being used(Lee et al., 2012).

4.2 Generation of the *Fbxo7* R379G KI mouse model

4.2.1 Rational for modelling the *Fbxo7* R378G mutation in a knock-in mouse model

The plan for my PhD project was to generate a knock-in mouse line modelling one of the human disease mutations in the FBXO7 gene. The knock-in gene approach allows studying the effect of one particular mutation in the endogenous system rather than using heterologous overexpression systems. On the one hand, I wanted to utilize the mouse for performing molecular and biochemical assays comparing the wild-type and knock-in genotype in the neuronal system and on the other hand for a phenotypic analysis to establish whether our mouse line could serve as a valid model of PD. Figure 26 shows a sequence alignment of the human and mouse FBXO7 homologous and that all 3 residues that are so far implicated in *FBXO7* mediated neurodegeneration - T22M, R378G, and R498X – are conserved between human and mouse species. I then wanted to assess expression levels and protein stability of the different Fbxo7 mutants in comparison to the wild-type protein as any impairment would render the respective mutant unsuitable for modelling in a KI mouse model. Figure 27 shows the stable expression in case of the human disease mutants and transient expression of the equivalent mouse constructs in HEK293 cells (each with C-terminal FLAG-tag) and suggests that the T22M mutant is expressed at relatively lower levels. This finding in combination with the fact that the T22M residue resides only in the N-terminal region of the longer isoform 1 while leaving the shorter isoforms of FBXO7 unaffected, was the rational for precluding the T22M mutation for modelling in a Fbxo7 KI mouse model. The choice was then between the nonsense R498X mutation, which introduces a premature stop codon resulting with truncation of the last 22 amino acid residues and the missense mutation R378G, which is located in juxtaposition downstream of the functionally important F-box domain of FBXO7. In general, introducing a missense mutation into a KI mouse model is generally considered more subtle than introducing a nonsense mutation. Nonsense mutations result in a truncated protein product, but also harbour the the risk of of medating nonsense-mediated mRNA decay, which would then have the same effect on protein level as a complete gene knock-out(Maquat, 2005). Therefore, our decision fell for modelling the missense R378G *FBXO7* human disease mutant. As

the mouse protein has an additional amino acid residue within in the FP domain of the FBXO7 protein, its amino acid sequence is one residue longer (523 instead of 522 residues). This also explains why the arginine at position 378 of the human FBXO7 protein corresponds to position 379 of the mouse protein. There is an overall identity between the mouse and human FBXO7 protein sequences of 73%. Figure 28 illustrates the percentage identities for different segments and domains of the 2 proteins, which is with 89% highest within the region of the F-box domain (residues 325 – 380). A multiple sequence alignment within the region of the F-box domain and around location of the disease mutant R378G of different species also shows there is a high degree of regional conservation and complete conservation of the arginine at position 378 of the human protein (Figure 29). Altogether the *R378G* FBXO7 disease mutant was considered a suitable candidate for modelling in an Fbxo7 knock-in mouse model at the endogenous locus.

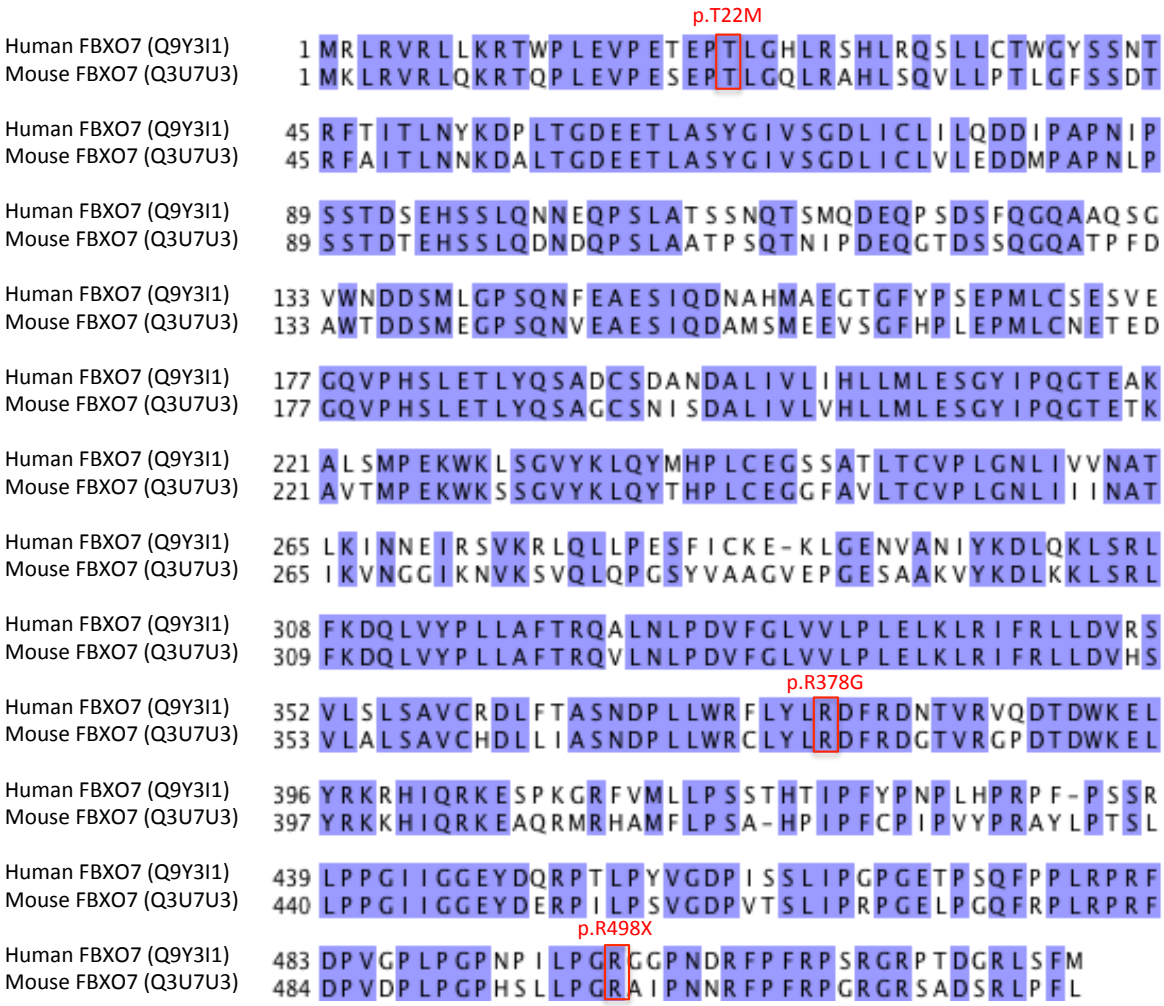

Figure 26: Sequence alignment of human and mouse FBXO7 proteins

Sequence alignment of the longer isoform 1 of human and mouse FBXO7 (Uniprot accession numbers: Q9Y3I1 for the human and Q3U7U3 for the mouse protein) were performed using the MUSCLE alignment program and annotated with the help of Jalview(Edgar, 2004; Waterhouse et al., 2009a). The red boxes indicate the location of the 3 pathogenic mutations and demonstrate that each of these residues is conserved between the human and mouse sequence. The Percentage ID using MUSCLE is 72.90% for the global alignment of the human and mouse FBXO7 proteins.

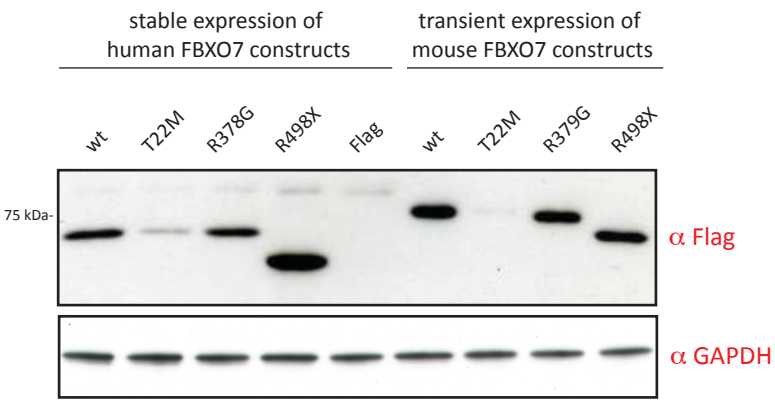

Figure 27: Expression of human and mouse Flag-tagged FBXO7 constructs in HEK293 cells

Either stable expressing FLAG alone, human wild type or human pathogenic mutants (T22M, R378G, and R498X) Flp-In TRex HEK293 (10ug each) or transient expressing mouse wild type and corresponding mutants (T22M, R379G, R498X) HEK293 (2ug) whole cell lysates were used for immunoblotting with Flag and GAPDH as a loading control. Expression of the stable constructs in Flp-In TRex HEK293 was induced with 0.1 ug/ml of doxycycline for 18 hours. The expression of the T22M FBXO7 mutant is impaired in comparison to the wt and the other mutants; a finding that is consistent between the human and the corresponding mouse construct despite 2 different expression systems.

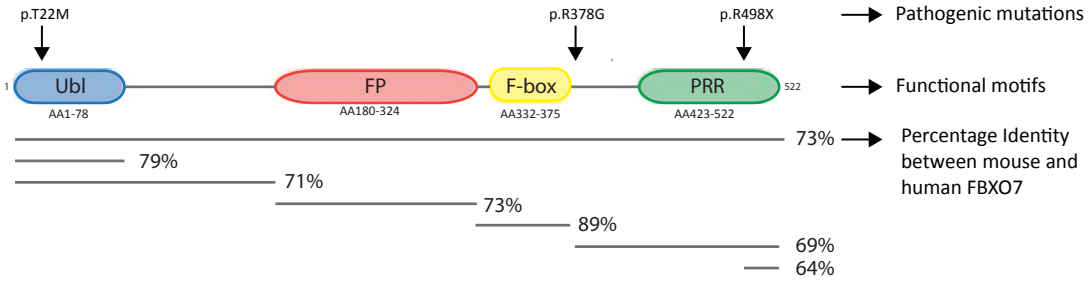

Figure 28: Percentage identity between human and mouse FBXO7 amino acid sequence

A pairwise alignment of the human (Q9Y3I1) and mouse (Q3U7U3) FBXO7 protein sequence (using MUSCLE(Edgar, 2004)) and calculation of pairwise percentage identity of functional domains and other segments as well as of the last 24 residues that are truncated in the R498X mutant results in the following: 73% overall identity, 79% identity between the UBL domain, 73% identify within the FP domain, 89% identity within the F-box domain and 69% identity within the unstructured C-terminal region of the protein (AA380-end). There is 64% identity between the last 24 residues of the human and mouse sequence.

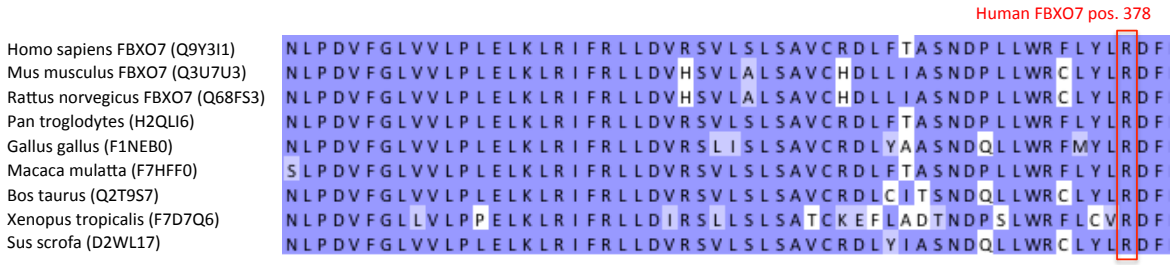

Figure 29: Multiple sequence alignments of FBXO7 homologues around the region of the human pathogenic mutation R378G

Sequence alignments using MUSCLE(Edgar, 2004) of FBXO7 homologues of different species (Uniprot ID in brackets) in the region of the F-box domain – shown are AA 318-380 of the human FBXO7 protein. The Arginine at position 378, which is one of the affected residues in FBXO7 associated disease where it is mutated to a glycine, is conserved across the different species. The R378G mutant is the particular mutation that was chosen for our FBXO7 knock-in mouse model (corresponding to R379G *Fbxo7* in the mouse genome).

4.2.2 The Fbxo7 R379G knock-in targeting strategy

The targeting strategy to insert the transition c>g in the first and g>c in the third position of the respective codon in exon 7 leading to the pathogenic missense mutation R379G as well as additional silent mutation to generate a diagnostic restriction site (BsaJI) was designed in collaboration with Taconis Artemis®, who also generated the mouse. Exons 7 and 8 were flanked by loxP (locus x-over P1) sites, while the selection markers flanked by FRT (NeoR) and F3 (PuroR) sites were inserted into intron 6 and intron 8, respectively. Homologous recombinant clones will be isolated by using double positive selection against Neomycine and Puromycine resistance to increase the efficacy of co-integration of both loxP sites and of the point mutations. The targeting vector was generated using Bacterial Artificial Chromosome (BAC) clones from the C57BL/6J RPCIB-731 BAC library and transfected into the Taconic Artemis C57BL/6N Tac ES cell line. Constitutive knock-in of the allele after Flp-mediated removal of the selection markers leads to the expression of the R379G mutated protein while the remaining loxP sites allow conditional deletion of exons 7 and 8 after site- and time-specific Cre-lox recombination(Metzger and Chambon, 2001). The deletion of exons 7 and 8 generates a frame-shift from exon 7 to

exon 9 introducing a premature stop codon. The outcome of whole body cre-recombinase mediated deletion of exon 7 and 8 will be discussed in 4.2.5.

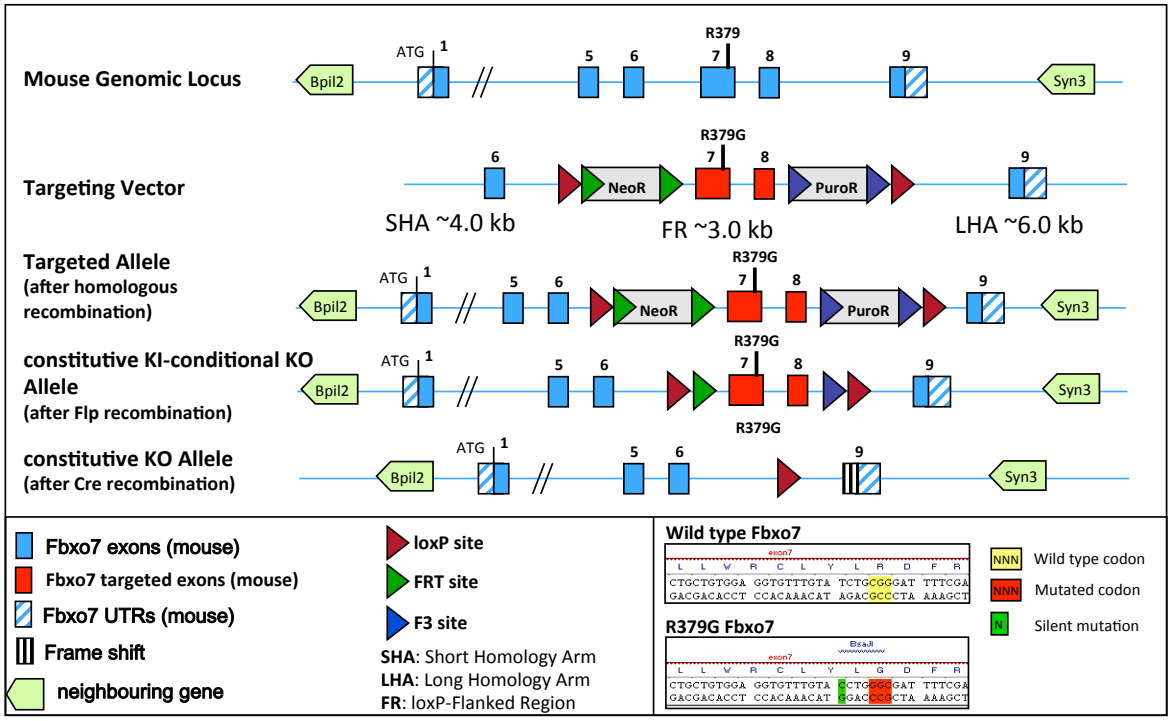

Figure 30: Targeting strategy of the *Fbxo7* constitutive Knock-in of R379G point mutation with optional conditional Knock-Out

Schematic illustration of the targeting strategy as explained in 4.2.2. The 2 genes in the neighbourhood of FBXO7 according to NCBI and Ensemble databases are Bpil2 (Entrez ID: 69754; ENSMUSG00000050108) is located approx. 33 kb upstream of the Fbxo7 exon 7 in a head-to-head orientation and Syn3 (Entrez ID: 27204; ENSMUSG00000059602) is located approx. 9 kb downstream of the Fbxo7 exon 8 in a tail-to-tail orientation.

4.2.3 DSTT α mouse FBXO7 antibody programme validation

In order to investigate the effect of the Fbxo7 R379G mutation in comparison to the wild-type protein in the endogenous neuronal system, a sensitive and specific antibody directed against FBXO7 is mandatory. Therefore, a DSTT antibody programme to raise a sheep polyclonal antibody against the full-length mouse FBXO7 protein was started. Figure 31 shows that this antibody detects the mouse as well as the human overexpressed Flag-tagged FBXO7 protein at least as good as the monoclonal mouse

antibody directed against the FLAG antigen (A). In (B) the ability of the DSTT antibody to not only detect, but also to immunoprecipitate endogenous FBXO7 protein from mouse tissue is demonstrated.

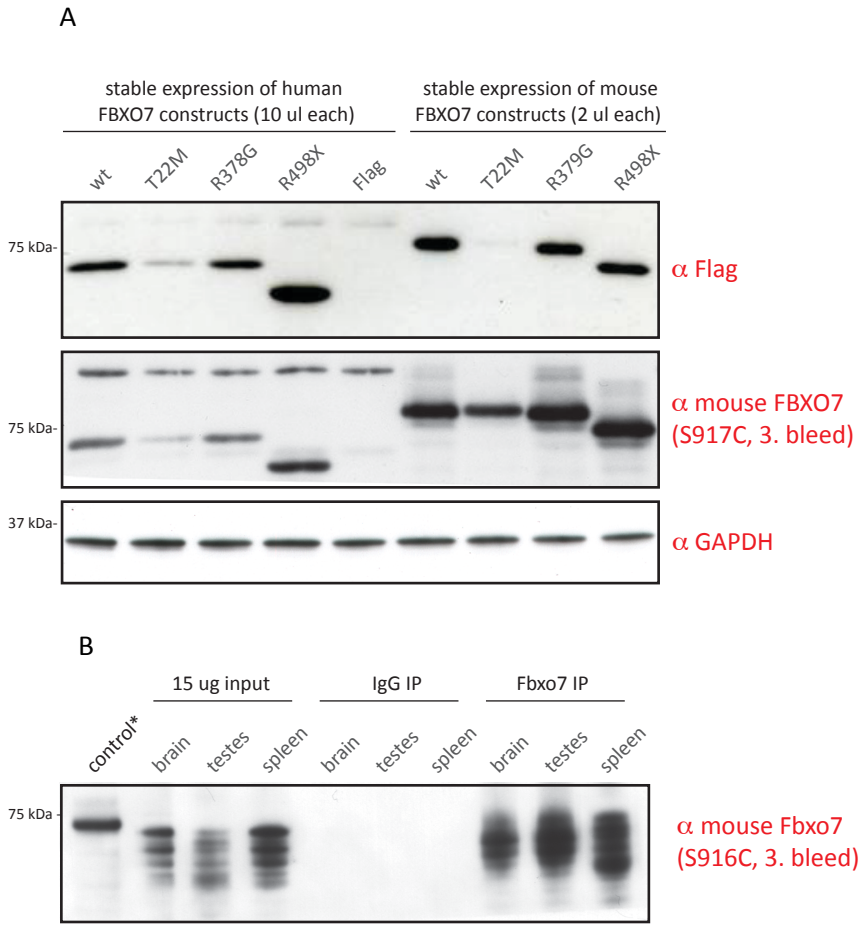

Figure 31: Validation of the α mouse FBXO7 antibody programme

A: HEK293 whole cell lysates *overexpressing* either human (stable, 10ug each) and mouse (transient, 2 ug each) Flag-tagged FBXO7 wt and disease mutants were immunoblotted for FLAG or the DSTT produced anti - mouse FBXO7 antibodies (S917C 3. bleed) and GAPDH as loading control. Antibody concentration for immunoblotting was 1ug/ml and exposure time was the same for all blots.

B: *Endogenous* FBXO7 immunoprecipitation (covalently coupled anti-mouse Fbxo7 antibody (S917D, 3. bleed) from 3 mg lysate of different wt mouse tissues. Covalently coupled preimmune sheep IgG served as a control IP. Immunoblotting for FBXO7 (S917D, 3. bleed) of 10ug of Flag-FBXO7 wt whole cell lysate and 10 ug of mouse brain, testes and spleen tissue lysates as well as 10% of the IP products of FBXO7 and control.

4.2.4 **R379G *Fbxo7* mouse line is viable and fertile**

The *R379G* Fbxo7 are viable and fertile in the heterozygeous and homozygous state. Both heterozygeous and homozygous carriers of the R379G point mutation cannot be discriminated from their wild-type littermates in respect to size, viability, breeding and home cage behaviour (4.3.1). Breeding heterozygeous males and females, the genotypes of the animals display a pattern of inheritance that best fits an autosomal recessive trait, normal gender distribution and litter size. Table 4-1 gives an overview of the genotype frequencies of offsprings from heterozygeous intercrosses. Male R379G Fbxo7 KI mice in the homozygous state are also able to propagate together with wild-type females (data not shown). Thus, R379G *Fbxo7* KI mice are viable and fertile.

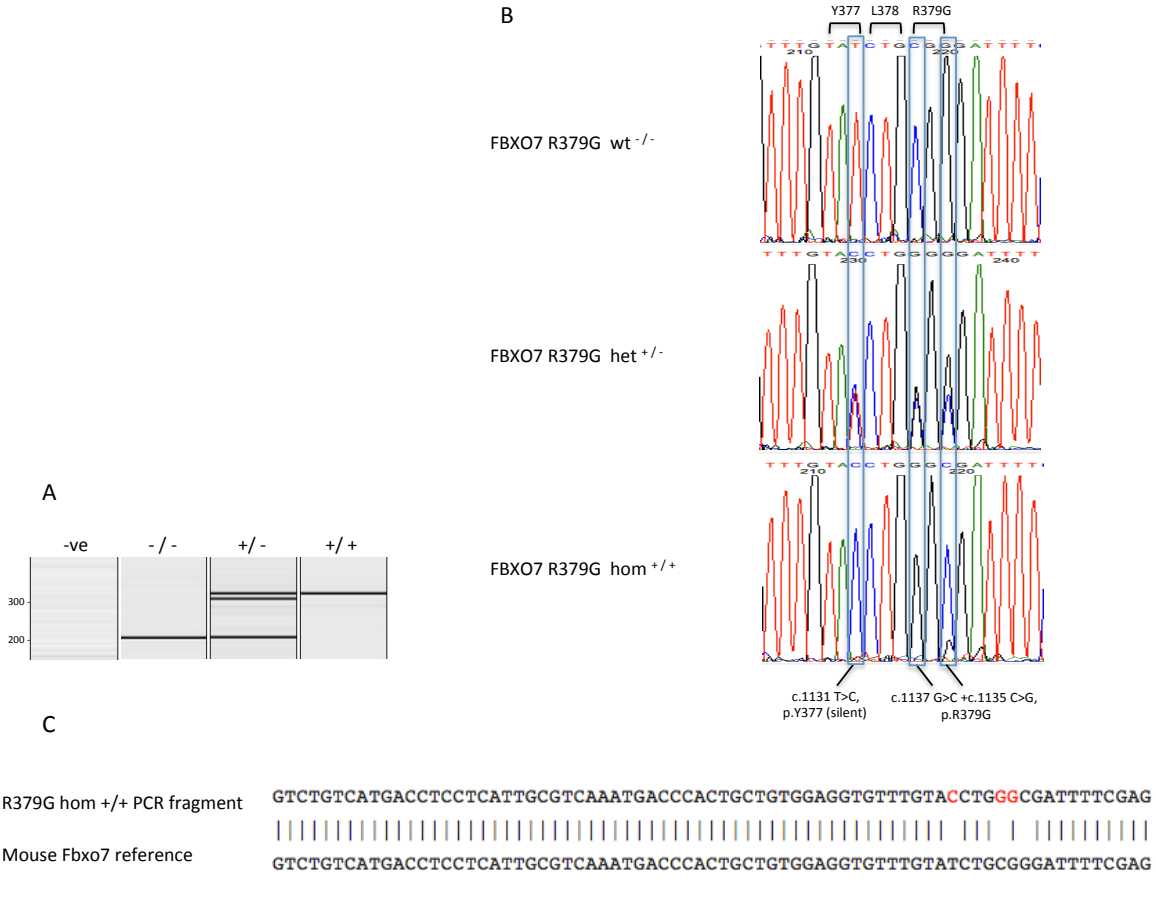

Figure 32: Verification of correct *Fbxo7* genotype by sequencing

A: PCR for mouse genotyping: A 210bp PCR product is present in the wild-type genotype (-/-), mice homozygous for the R379G mutation (+/+) give a 329 bp product and heterozygeous mice (+/-) result in a combination of the 2 fragments. (-ve = water control).

B: Sequencing traces for wt, het and hom *Fbxo7* R379G show the introduced silent and R379G knock-in mutations (blue boxes).

C: Sequence alignment of the Fbxo7 reference gene and the PCR amplified and sequenced homozygous Fbxo7 genotype of the Fbxo7 R379G KI mouse line confirming correct targeting of the endogenous locus.

Genotype	- / -	- / +	+ / +	Total	χ^2	p-value
Liveborn pups						
Fbxo7 R379G	30% (116)	50% (197)	20% (77)	390	4.3	> 0.1 and < 0.2

Table 4-1: Genotype frequencies of offsprings of *Fbxo7* R379G mouse line

Genotype frequencies for offspring at weaning derived from heterozygeous intercrosses are indicated. If a Chi square test is applied to compare the observed and expected genotype distribution of wild-type (+/+), heterozygeous (+/-) and homozygeous (-/-) R379G KI Fbxo7 alleles, the outcome is in keeping with an autosomal recessive pattern of inheritance rather than chance alone (p-value: > 0.1 and < 0.2).

4.2.5 C-terminal truncation of *Fbxo7* results in lethality

In a 2 step breeding strategy, homozygous *Fbxo7* R379G and heterozygeous whole body expressing Cre recombinase mice were crossed to derive conditional homozygous Cre-loxP mediated knock-out of exons 7 and 8 (Figure 33). While heterozygeous Cre-loxP mediated deletion of exons 7 and 8 was tolerated – animals are vital and fertile – homogenous animals are not: Of 81 animals, 16 pups died within 2 days of being born and no material for genotyping could be collected - the animals were presumably eaten by their mother. It is therefore not clear whether homozygous genotypes were amongst the dead / stillborn pups. Homogenous genotypes were, however, detected at embryonic stage E12.5 days: out of a total of 17 embryos, 6 embryos had a genotype corresponding to successful homozygous Cre-loxP mediated deletion of exons 7 and 8 (while 5 had a wt and 6 a wt/*Fbxo7* $^{\text{C-terminal trunc}}$ background) best fitting an autosomal recessive pattern of inheritance.

Genotype	- / -	- / +	+ / +	Total	χ^2	p-value
Liveborn pups						
Fbxo7 $^{del\ exons\ 7\ and\ 8}$	30% (25)	49% (40)	0% (0)	81	21.7	<0.001
Embryos E12.5						
Fbxo7 $^{del\ exons\ 7\ and\ 8}$	5	6	6	17	1.59	<0.5 and > 0.3

Table 4-2: Genotype frequencies of offsprings at weaning age and embryos derived from cre-loxP mediated deletion of exons 7 and 8 of the *Fbxo7* gene

No pubs with a homogenous Fbxo7 $^{del\ exons\ 7\ and\ 8}$ background were found to be alive at weaning age. 16 pubs were found dead aged between 1 and 2 days, but no material for genotyping could be collected as pubs were found eaten. This is not in keeping with the expected numbers of

4.2.6 FBXO7 expression in *Fbxo7* ^{R379G} and Fbxo7 $^{C\text{-terminal truncation}}$ MEFs

Murine embryonic fibroblast (MEF) cells were prepared from wild-type, heterozygeous and homozygous E12.5 littermates of the Fbxo7 R379G KI mouse lines as well as after Cre-loxP mediated deletion of exons 7 and 8 of *Fbxo7*. Each of the different cell lines was immortalized by serial passaging(Xu, 2005). Figure 33 shows the expression pattern of FBXO7 in the 2 different cell lines; in particular that deletion of exons 7 and 8 leads to a C-terminal truncated version of the FBXO7 protein, which is expected to end shortly before the start of the F-box domain. The expectation is that this mutant is unable to bind to SKP1 and hence is unable to form a SCF$^{FBXO7\text{-}C\text{-}terminal\ truncation}$ in the homozygous state. This us demonstrated in Figure 47.

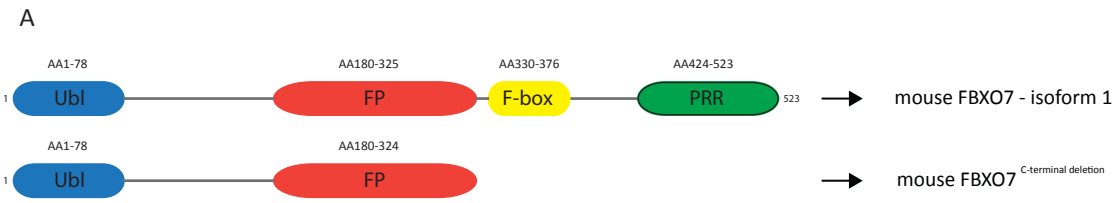

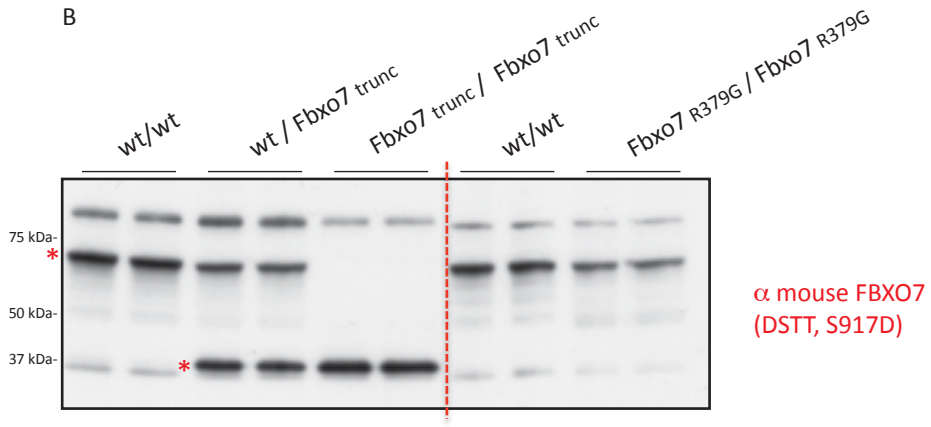

Figure 33: FBXO7 expression in Fbxo7 ^{R379G} and $^{C\text{-terminal truncation}}$ MEFs

A: Deletion of exons 7 and 8 is expected to yield a protein of a length of about 323 amino acid ending before the start of the F-box domain (35 kDa, computed molecular weight using the ProtParam tool by ExPASy (Wilkins et al., 1999)).

B: FBXO7 immunostaining of the various genotypes for the 2 different MEF cell lines are indicated above and run in duplicates. The red stars indicate the signal of the full-length FBXO7 wt and R379G proteins (upper star) and the signal for the shorter C-terminal truncated FBXO7 mutant (lower star).

4.2.7 Tissue expression analysis of FBXO7 in the *Fbxo7* R379G KI mouse model

Little is known about the tissue expression pattern of FBXO7 in general. I therefore analysed the distribution of FBXO7 protein expression by means of FBXO7 immunoreactivity in the wild-type animal and compared it to expression levels and distribution of the mutated FBXO7 protein product of the Fbxo7 R379G KI animal. Figure 34 shows that FBXO7 is widely expressed across a panel of different tissues (including brain, lung, liver, heart, kidney, and spleen). The expected molecular weight of the longer isoform 1 (Q3U7U3 – mouse FBXO7) of FBXO7 is 58kDa while the shorter isoform 2 (Q3UD93 - mouse FBXO7) is 49 kDa, but several more transcripts could potentially be expressed by alternative splicing(Di Fonzo et al., 2009). The FBXO7 immunoblotting signal yields several bands between the range of 50 – 75 kDa, and these may or may not represent different isoforms, degradation products or posttranslational modified forms of FBXO7.

With regards to the analysis of the Fbxo7 ^{R379G} mouse model, an important first step was to show that the mutant FBXO7 ^{R379G} protein is actually expressed in the homozygous state. Figure 34 and Figure 35 demonstrate that this is the case for animals aged 6 weeks and 6 months, albeit not at the same level as in the wild-type state. To investigate this further, I determined the expression levels of FBXO7 by quantitative immunoblotting in brain lysates of 3 age matched, littermate wt and homozygous Fbxo7^{R379G} KI animals at 10 months of age (using the Li-Cor Odyseey system). This analysis confirmed the initial observation that FBXO7 expression levels in brain lysates are reduced in the homozygous R379G KI state and showed that the reduction amounts to about 50%(Figure 36). This difference in expression levels was consistent across replicate experiments (data not shown) as well as different modes of detection; for example by differential quantitative proteomic using wt and homozygous Fbxo7 ^{R379G} MEFs or brain lysates (discussed in chapter 5.

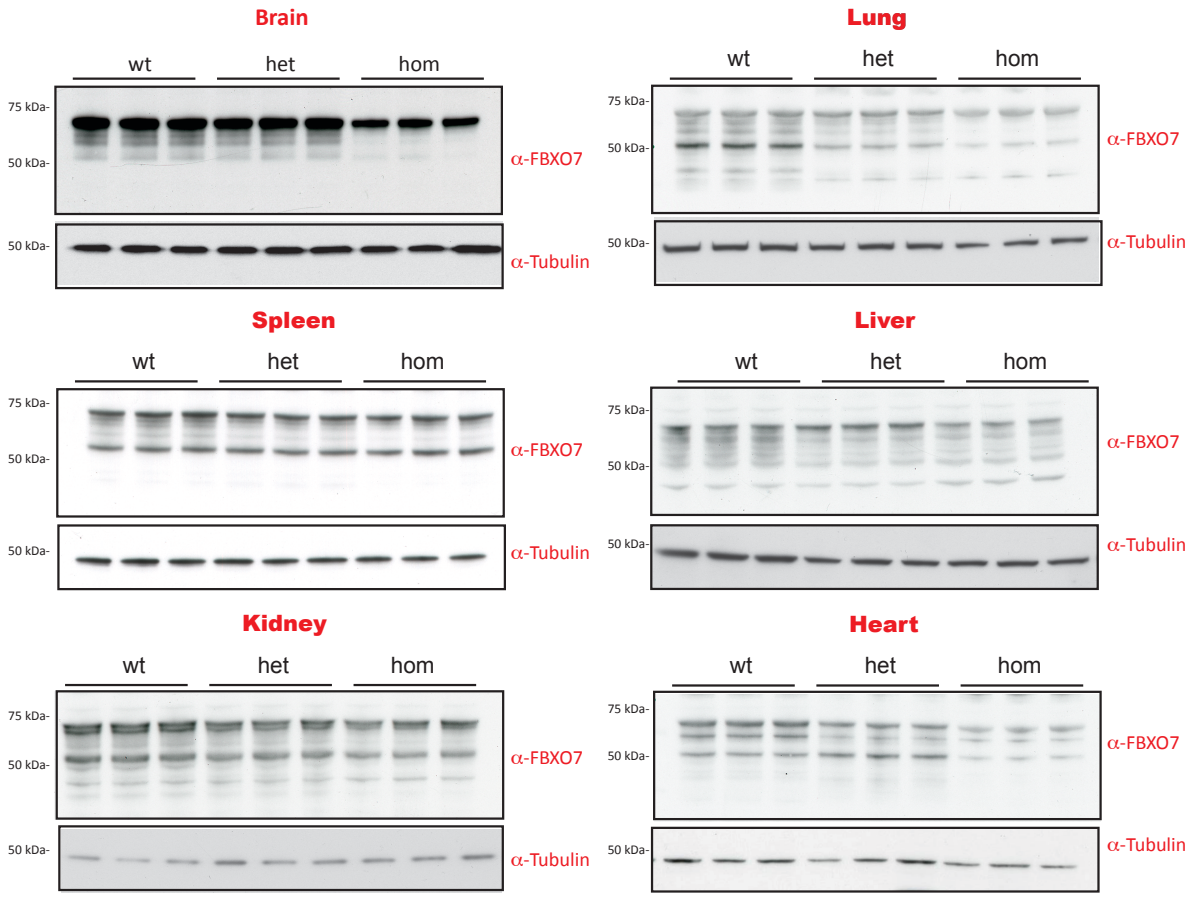

Figure 34: Expression analysis of FBXO7 in the Fbxo7 $^{R379G\ KI}$ mouse model at 10 months

Triplicate loading (10ug each, prepared in CHAPS lysis buffer) and immunostaining for FBXO7 of littermate wild-type (wt), heterozygeous (het) and homozygous (hom) Fbxo7 $^{R379G\ KI}$ mouse cell lysates across a panel of different tissues (Fbxo7 antibody: DSTT, S917D, 3rd bleed). Tubulin immunoblots are shown as a loading control.

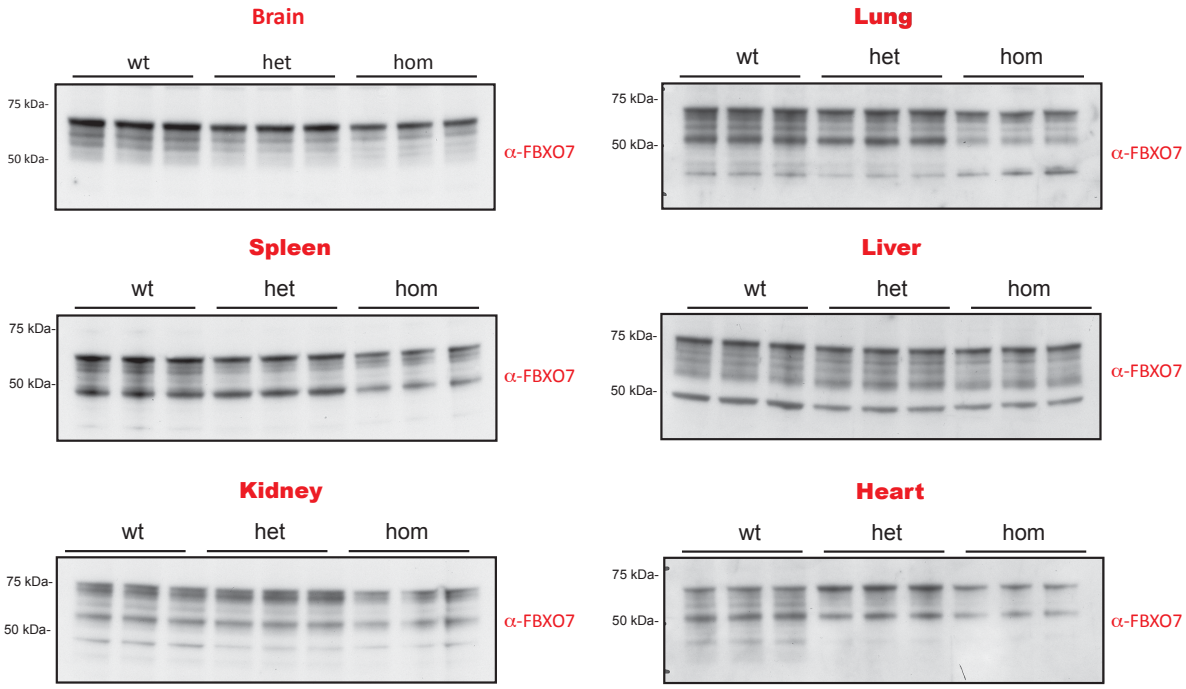

Figure 35: Expression analysis of FBXO7 in the Fbxo7 $^{R379G\ KI}$ mouse model at 6 weeks

Triplicate loading (10ug each, prepared in CHAPS lysis buffer) and immunostaining for FBXO7 of littermate wild-type (wt), heterozygeous (het) and homozygous (hom) Fbxo7 $^{R379G\ KI}$ mouse cell lysates across a panel of different tissues. Tubulin as a loading control is shown for brain. (mouse IDs: wt - 123206, het - 120703, hom - 120702, all females, DOB 27.09.2012, cull date 06.09.2012).

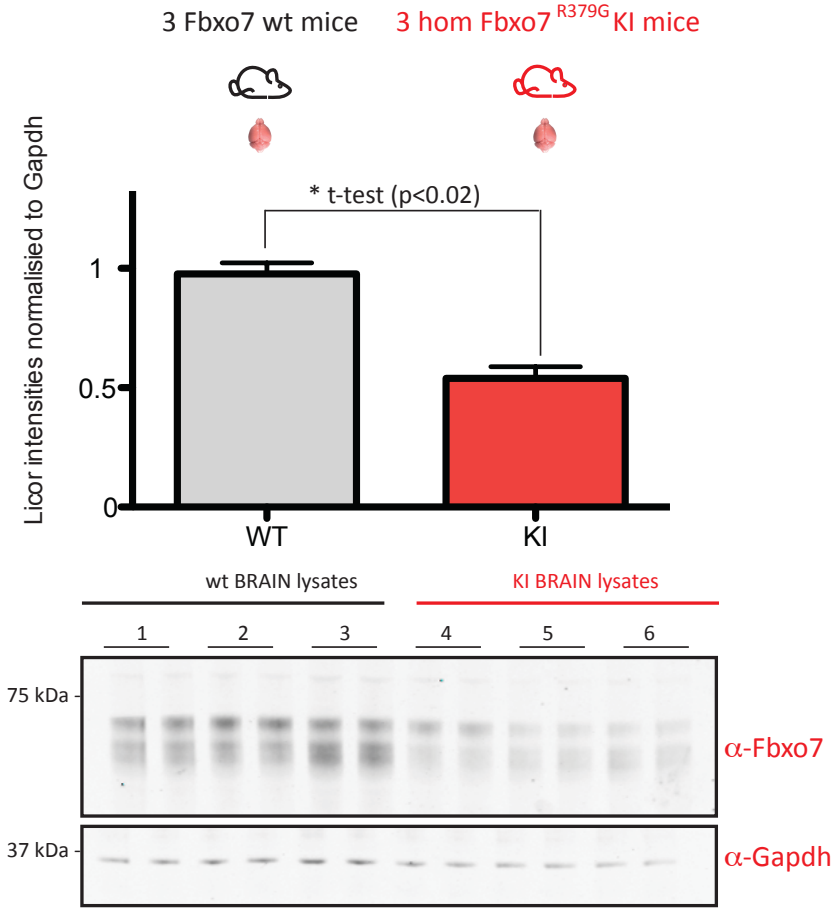

Figure 36: FBXO7 expression levels in the brain are reduced by half in the homozygous Fbxo7 ^{R379G} KI compared to the wild-type state at 10 months of age

Brain lysates were prepared from 3 wt (WT) and 3 homozygous FBXO7 ^{R379G} (KI) animals (littermate pairs) in Rapigest lysis buffer at the same time and each sample was loaded in duplicates for quantitative immunostaining with FBXO7 and Gapdh and simultaneous detection by the Li-Cor Odyseey system. Data is presented as relative FBXO7 levels over Gapdh levels ± SEM. FBXO7 wt levels were set to 1. Average age of each group (wt and KI) was 10.3 months. The difference in expression level by genotype was significant as analysed by a paired t-test.

4.2.8 *In vivo* SCF$^{Fbxo7\ wt}$ complex formation of the endogenous Fbxo7 wt protein

In Chapter 2, I have demonstrated that stable overexpressed FBXO7 - the wild-type protein as well as the pathogenic mutants (FBXO7 T22M, R378G, and R498G) - assembles together with endogenous SKP1, Cullin1 and RBX1 into a SCF^{FBXO7} E3 ubiquitin ligase complex. The next important question was whether I could reproduce this finding in the endogenous system. Figure 37 confirms that the SCF^{Fbxo7wt} E3 ligase complex does

indeed exist *in vivo*: Immunoblotting of the endogenous Fbxo7 immunoprecipitation products from different wild-type mouse tissues including brain lysates allows the detection of the other SCF complex partners.

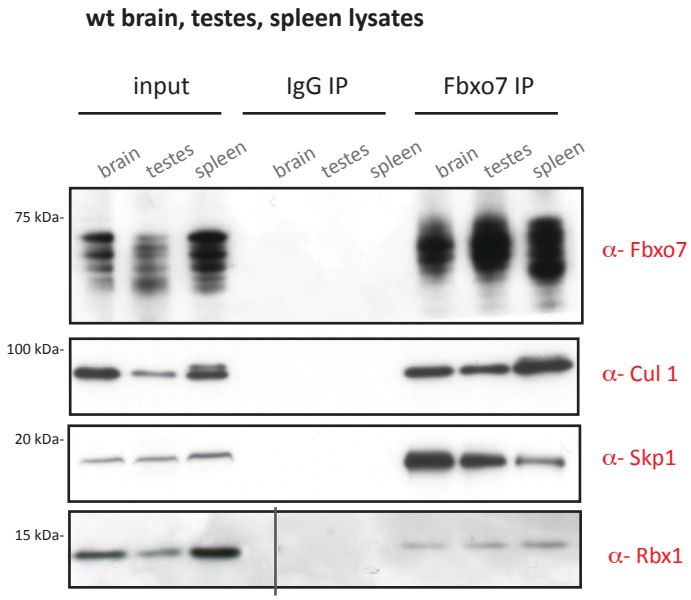

Figure 37: Endogenous SCF$^{Fbxo7\ wt}$ E3 ubiquitin ligase complex formation *in vivo*

Endogenous FBXO7 immunoprecipitation (covalently coupled anti-mouse Fbxo7 antibody (S917D, 3. bleed) from 3 mg lysate of different wt mouse tissues. Covalently coupled preimmune sheep IgG served as a control IP. Immunoblotting of 10% of the IP products for FBXO7 and the remainder for CULLIN1, SKP1 and RBX1 as well as 10ug of the respective input lysates demonstrates formation of the SCF^{FBXO7wt} complex *in vivo*.

4.2.9 *In vivo* SCF$^{Fbxo7\ R379G}$ complex formation of the endogenous Fbxo7 R379G mutant

I was then interested to see whether the SCF^{Fbxo7} E3 ligase complex formation was also possible in the homozygous R379G KI Fbxo7 mutant background. I therefore performed immunoprecipitations from wild-type and homozygous R379G KI *Fbxo7* brain lysates in parallel and subjected the pull-down products to immunoblotting for Cullin1, Skp1 and Rbx1. Figure 38 demonstrates that the other endogenous SCF complex partners cannot only be detected in the endogenous immunoprecipitate from wild-type, but also from homozygous Fbxo7 R379G KI mouse brain lysates. I have also performed large-scale

parallel Fbxo7 immunoprecipitations from wild-type and homozygous R379G KI brain lysates that were subjected to in gel tryptic digestion and subsequent proteomic fingerprint analysis. The proteomic analysis also confirms the identity of Cullin 1, Skp1, and RBX1 in the immunoprecipitate of both genotypes (Figure 39). Altogether, these findings suggest that the pathogenic R379G KI Fbxo7 mutant does not exert its pathogenicity by completely preventing association of Fbxo7 into the SCF E3 ubiquitin ligase complex.

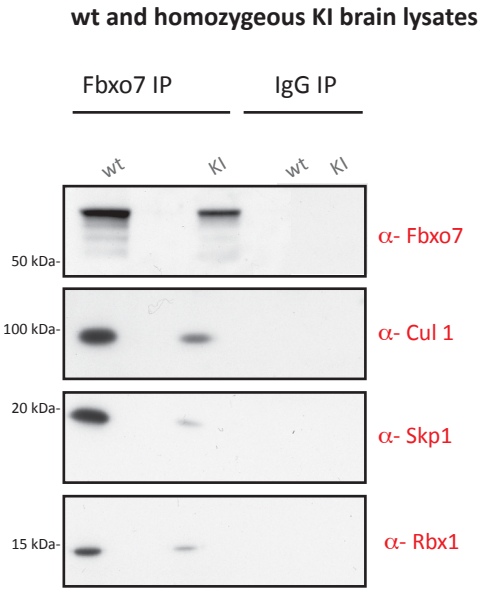

Figure 38: Endogenous SCF^{Fbxo7} complex formation of wild-type as well as homozygous R379G Fbxo7 derived brain lysates *in vivo*

Endogenous FBXO7 immunoprecipitation (covalently coupled anti-mouse Fbxo7 antibody (S917D, 3. bleed) from 3 mg lysate of wt and homozygous *Fbxo7* R379G brain lysates. Covalently coupled preimmune sheep IgG served as a control IP. Immunoblotting of 10% of the IP products for FBXO7 and the remainder for CULLIN1, SKP1 and RBX1 demonstrates formation of the SCF^{FBXO7} complex *in vivo* for both genotypes and that the Fbxo7 R379G mutant is equally capable of complex assembly *in vivo*.

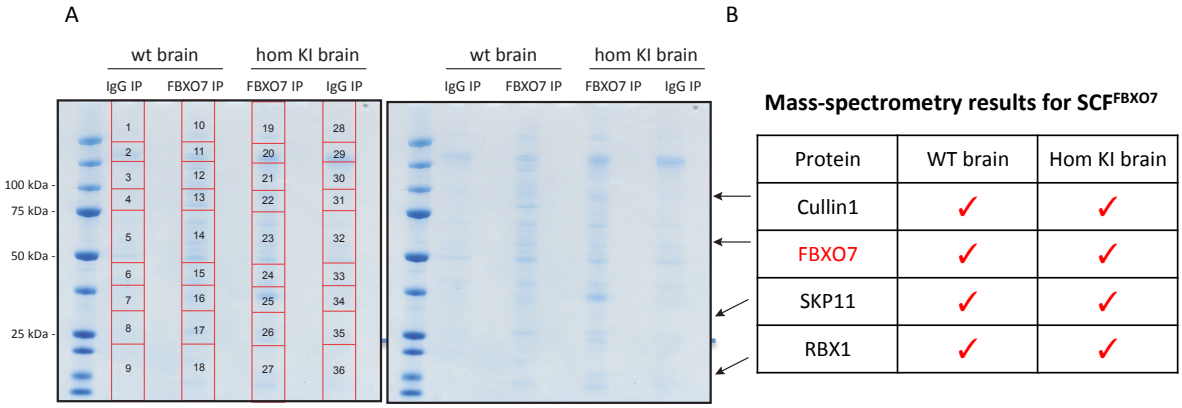

Figure 39: Identification of SCF^{FBXO7} complex by MS fingerprint analysis from wt and hom Fbxo7 R379G brain lysates

A: Representative Colloidal blue stained 4-12% Bis-Tris gel of 50% of the IP product for in gel tryptic digestion for proteomic analysis.

B: Qualitative representation of results from 3 replicates demonstrating that all endogenous SCF complex components as well as PI31 are present in the endogenous FBXO7 pull-downs from wt as well as homozygous R379G mouse brain lysates.

4.2.10 *In vivo* SCF$^{Fbxo7\ R378G}$ complex formation of patient derived heterozygeous and homozygous R378G *FBXO7* cell lines

Although this chapter is dedicated to the study of the R379G KI *Fbxo7* mouse model, I am including data derived from patient derived, mutation specific R378G *FBXO7* cell lines in this section. The finding that there is intact SCF^{Fbxo7} complex formation in the homozygous R379G KI Fbxo7 background of the mouse model is of significant importance and warrants follow up whether this is also the case in the corresponding human setting. I have therefore subjected whole cell lysates derived from immortalized, patient / carrier derived homozygous and heterozygeous R378G *FBXO7* fibroblasts to endogenous FBXO7 immunoprecipitation and immunoblotting of the SCF complex partners. These cell lines were kindly provided by Professor Henry Houlden from the Institute of Neurology, University College London. Figure 40 demonstrates that the human R378G FBXO7 mutant is equally able to assemble into the SCF$^{FBXO7\ R378G}$ complex and that the R379G *Fbxo7* KI mouse model faithfully recapitulates important biochemical properties of the corresponding human disease mutant. The human cell

lines cannot be used to address the second finding in the corresponding R379G Fbxo7 KI mouse model, which is the effect of the R379G mutant homozygosity on the reduction of Fbxo7 protein expression levels. I have demonstrated a consistent reduction of Fbxo7 protein levels in the homozygeous R379G genotype in comparison to wild-type littermate control animals. Although the expression level of the homozygeous R378G FBXO7 patient appears to be higher than that of the heterozygeous carrier, it needs to be noted that this is only data from 2 individuals. It would however be interesting to look at FBXO7 protein expression levels of more patients and carriers of FBXO7 R378G associated disease.

Human heterozygeous and homozygeous R378G FBXO7 fibroblasts

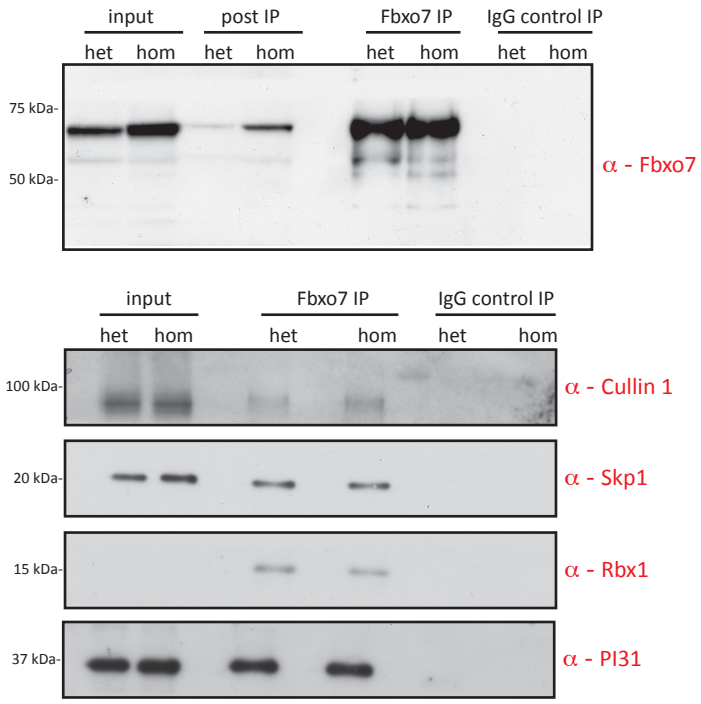

Figure 40: Endogenous SCF^{FBXO7} complex formation in patient derived, mutation specific R378G cell lines

Homozygous and heterozygeous immortalized fibroblasts derived from a patient with FBXO7 associated disease due to homozygosisty for the R378G *FBXO7* gene mutation and an unaffected family member with carrier status were subjected to endogenous FBXO7 immunoprecipitation (covalently coupled α human FBXO7 (S038D, 4th bleed) and preimmune sheep IgG as a control. 10 % of the IP product was used for

FBXO7 immunoblotting, the remaining 90% for immunoblotting of the other SCF complex members as well as PI31.

4.2.11 **Proteomic fingerprint analysis of endogenous FBXO7 IPs (wild-type mouse brain)**

Having demonstrated that the SCF^{FBXO7} E3 ubiquitin ligase complex exists *in vivo* the next step was to use proteomic fingerprint analysis to identify FBXO7 interacting partners in the immunoprecipitate of endogenous FBXO7 from mouse brain tissue lysates. The ultimate goal is to identify FBXO7 interacting partners that possibly function as SCF^{FBXO7} ubiquitylation substrates. As pointed out in previous sections, the limitation of this approach is that the interaction between FBXO7 and any putative substrates needs to be sufficiently strong to withstand the handling – in particular the washing procedures – of the immunoprecipitate. I have performed a total of 3 large scale biological replicates of endogenous FBXO7 pull-downs from wt and 2 replicates from homozygous FBXO7 R379G mouse brain tissue lysates using preimmune sheep Immunoglobulines as a control IP to identify unspecifically binding proteins. Figure 41 gives an overview of the overlap between the 3 replicates from wild-type brain. Presented are the numbers of proteins that were identified in each replicate after subtracting any proteins that were also found in any of the 3 preimmune IgG controls. Altogether, 42 proteins of these hits were found in all 3 endogenous FBXO7 pull-downs from wild-type brain reducing the chance of unspecificity. Amongst these 42 proteins were FBXO7 as the bait and CULLIN1 and SKP1 as SCF complex partners. RBX1 was not amongst the overlapping group as it was only detected in 2 of the 3 replicates. The overlapping list also contains 2 other proteins that have previously been reported to interact with FBXO7: Exportin 1 and PI31(Kirk et al., 2008; Nelson and Laman, 2011). With regards to the other proteins, there are 4 components of adaptor protein complexes involved in protein transport vesicles in different membrane traffic pathways (AP-1 and AP2 subunits). Huntingtin-interacting protein 1-related protein also relates to the function of (Rao et al., 2001) and is known to interact with AP-2. Then there are several members of the COP9 signalosome complex, which regulates the activity of SCF E3 ligase complexes; for

example by deneddylation of Cullins(Kato and Yoneda-Kato, 2009) and also proteasomal subunits. Arf-GAP is a GTPase-activating protein and isoform 1 is brain specific where it participates in the prevention of neuronal apoptosis by enhancing PI3 kinase activity(Xia et al., 2003). Liprin-α proteins may act as scaffolding molecules important for neuronal synapse maturation(Spangler and Hoogenraad, 2007). Additionally, 2 subunits of the Serine / threonine-protein phosphatase PP1 and the protein phosphatase 1 regulatory subunit 9B (Neurabine 2) as well as the calcium-binding protein nucleobindin, the sodium- and chloride dependent GAPA transporter 3 and the tubulin polymerization-promoting protein were found in all 3 wild-type replicates. Furthermore, 2 members of the reticulon family and 3 members of the RanBP2/RanGAP1*SUMO1/UBC9 E3 sumo ligase complex were found in all 3 FBXO7 pull-downs from wild-type brain.

Endogenous FBXO7 IP from wt brain (3 replicates):

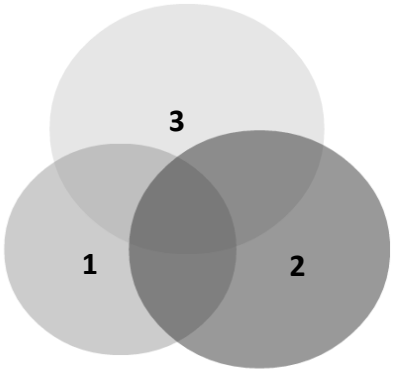

Replicate	Identified hits
1 (2011/05/11)	263
2 (2011/06/21)	188
3 (2012/05/31)	238
Overlap (1,2,3)	42

Figure 41: Venn diagram: Overlap between 3 endogenous FBXO7 IP from wt brain

Number of proteins found in each of the 3 endogenous FBXO7 IPs from wt brain after excluding any hits that were identified in any of the 3 preimmune IgG controls and the number of hits that were common to all 3 replicates.

Overlap (1,2,3)	MW (kDA)	1	2	3
F-box only protein 7	58	1517 (59, 31%)	1877 (66, 30%)	1024 (40, 28%)
Cullin-1*	90	6370 (337, 75%)	5185 (290, 72%)	390 (28, 25%
S-phase kinase-associated protein 1*	19	359 (12, 47%)	1063 (56, 82%)	1477 (56, 76%)
Proteasome inhibitor PI31 subunit*	30	22 (7, 18%)	108 (9, 25%)	110 (10, 18%)
COP9 signalosome complex subunit 4	46	113 (4, 7%)	207 (8, 13%)	242, (12, 19%)
COP9 signalosome complex subunit 3	48	58 (1, 3%)	81 (4, 4%)	109 (5, 11%)
COP9 signalosome complex subunit 6	36	44 (8, 23%)	31 (4, 4%)	71 (3, 9%)
COP9 signalosome complex subunit 4	46	113 (4, 7%)	207 (8, 13%)	242, (12, 19%)
COP9 signalosome complex subunit 5	38	143 (6, 12%)	48 (4, 12%)	43, (5, 11%)
Proteasome subunit alpha type-1	30	250 (19, 19%)	616 (44, 64%)	286 (21, 34%)
Proteasome subunit alpha type-5	27	110 (6, 22%)	556 (31, 56%)	370 (16, 37%)
Proteasome subunit alpha type-7	28	24 (2, 3%)	541 (25, 58%)	202 (13, 27%)
Proteasome subunit alpha type-6	28	177 (9, 21%)	494 (17, 42%)	275 (12, 24%)
Proteasome subunit alpha type-2	26	131 (5, 13%)	285 (21, 50%)	404 (21, 42%)
Proteasome subunit alpha type-3	28	148 (9, 21%)	368 (20, 33%)	178 (17, 30%)
Proteasome subunit alpha type-4	30	56 (3, 12%)	298 (12, 38%)	201 (13, 43%)
Proteasome subunit beta type-2	23	75 (2, 4%)	249 (17, 35%)	292 (18, 37%)
Proteasome subunit beta type-6	26	72 (6, 16%)	120 (3, 8%)	216 (5. 13%)
Proteasome subunit beta type-4	29	34 (3, 14%)	188 (14, 35%)	174 (14, 25%)
Proteasome subunit beta type-7	30	24 (2, 3%)	194 (23, 37%)	339 (20, 22%)
E3 SUMO-protein ligase RanBP2	345	3298 (228, 38%)	993 (60, 13%)	4922 (249, 55%)
Ran GTPase-activating protein 1	64	704 (34, 34%)	488 (20, 21%)	1274 (44, 40%)
GTP-binding nuclear protein Ran	25	183 (16, 31%)	160 (15, 31%)	87 (5, 11%)
Exportin-1*	123	1736 (108, 47%)	151 (19, 13%)	1119 (64, 38%)
Reticulon-1	84	45 (1, 1%)	402 (17, 21%)	193 (11, 5%)
Reticulon-4	127	590 (48, 14%)	90 (11, 10%)	1407 (79, 56%)
Neurabin-2	90	2300 (153, 58%)	1584 (83, 51%)	302 (21, 24%)
Liprin-alpha-3	117	2432 (147, 53%)	3821 (195, 58%)	4315 (181, 60%)
Liprin-alpha-2	144	67 (7, 1%)	62 (9, 4%)	133 (17, 7%)
AP-2 complex subunit alpha-1	109	485 (24, 9%)	1904 (97, 51%)	1199 (67, 40%)
AP-2 complex subunit alpha-2	105	357 916, 125)	1233 (76, 43%)	569 (31, 22%)
AP-1 complex subunit beta-1	105	88 (12, 9%)	568 (44, 30%)	964 (43, 36%)
AP-2 complex subunit mu	50	20 (5, 9%)	837 (39, 47%)	276 (21, 31%)
Formin-like protein 1	123	624 (53, 25%)	361 (36, 20%)	1694 (106, 43%)
Tubulin polymerization-promoting protein	24	1469 (102, 73%)	1415 (53, 52%)	298 (20, 33%)
Serine/threonine-protein phosphatase PP1-alpha catalytic subunit	38	838 (42, 43%)	610 (29, 44%)	29 (1, 3%)
Serine/threonine-protein phosphatase PP1-gamma catalytic subunit	38	642 (33, 41%)	523 (21, 36%)	73 (4, 11%)
Arf-GAP with GTPase, ANK repeat and PH domain-containing protein 3	99	458 (18, 10%)	31 (4, 2%)	66, (2, 1%)
Nucleobindin-2	50	363 (38, 23%)	229 (21, 28%)	355 (37, 45%)
BTB/POZ domain-containing protein KCTD3	89	230 (36, 31%)	157 (30, 23%)	299 (27, 37%)
Huntingtin-interacting protein 1-related protein	120	109 (13, 13%)	87 (10, 6%)	242 (21, 18%)
Protein enabled homolog	86	79 (11, 11%)	153 (15, 16%)	73 (5, 5%)
Sodium- and chloride-dependent GABA transporter 3	71	28 (2, 3%)	127 (2, 2%)	48 (1, 2%)

Table 4-3: Identity of the proteins found in all 3 replicate FBXO7 IPs from wild-type brain

Identities and molecular weight (in kDa) of the proteins that overlapped in all 3 endogenous FBXO7 pull-downs from wild-type brain after excluding any hits that were also present in the preimmune IgG controls. Shown are mascot scores of each protein as identified in the individual replicate with number of unique peptides and percentage of sequence coverage in brackets. SCF E3 ubiquitin ligase complex partners as well as previously reported Fbxo7 interacting partners are printed in bold and with a star. Proteins are grouped according to function / interacting complex partners.

4.2.12 **Proteomic fingerprint analysis of endogenous FBXO7 IPs (hom FBXO7^{R379G} brain)**

I was then interested in comparing the findings of the endogenous FBXO7 immunoprecipitations from wild-type to those from homozygous Fbxo7 R379G mouse brain lysates. Proteins that only associate with one genotype and not with the other may be interesting candidates for further analysis. I have therefore compiled the results of the 2 replicate pull-downs from homozygous Fbxo7 R379G KI brain lysates (which were done in parallel with wild-type experiments) and comparing them to the results of the wild-type experiments results in the following: a total of 50 proteins were identified in the wild-type background, whereas 42 proteins were identified in the homozygous R379G KI genotype. Amongst these hits were 29 proteins that were shared between the 2 genotypes and 21 proteins that could only be identified in the wild-type while 13 proteins could only be identified in the homozygous KI background.

Combined results of endogenous FBXO7 IP replicates from wt and homozygeous R379GKI brain lysates

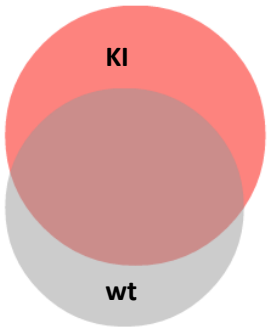

Replicate	Identified hits
WT hits TOTAL	50
KI hits TOTAL	42
WT hits ONLY	13
Ki hits ONLY	21
Overlap	29

Figure 42: Overlap between endogenous FBXO7 IP from wild-type and homogenous R379G KI brain lysates

The Venn diagram shows the overlap between proteomic hits for the endogenous FBXO7 IPs from wild-type and homozygous R379G KI brain lysates of 2 biological replicates. For each replicate littermate wt and hom KI mice were sacrificed and the whole experiment was done in parallel (date of experiments: 2011/12/15 and 2012/05/31). Mass-spectrometry raw data was processed using proteinguru (http://www.proteinguru.com/MassSpec/OLMAT) to exclude any hits that were identified in any of the preimmune IgG controls and to compile the data in single excel sheets. Venn diagram and overlapping lists were created using BioVenn(Hulsen et al., 2008).

Overlap (WT / KI)	WT ONLY	KI ONLY
F-box only protein 7	COP9 signalosome complex subunit 3	Rap guanine nucleotide exchange factor 2
Cullin-1	COP9 signalosome complex subunit 4	
S-phase kinase-associated protein 1	COP9 signalosome complex subunit 5	SH3-containing GRB2-like protein 3-interacting protein 1
	COP9 signalosome complex subunit 6	
Proteasome inhibitor PI31 subunit		60 kDa heat shock protein, mitochondrial
	GTP-binding nuclear protein Ran	
Proteasome subunit alpha type-1		V-type proton ATPase subunit E 1
Proteasome subunit alpha type-2	Proteasome subunit alpha type-4	
Proteasome subunit alpha type-3	Proteasome subunit alpha type-5	AP-2 complex subunit beta
Proteasome subunit beta type-4	Proteasome subunit alpha type-6	
Proteasome subunit beta type-6	Proteasome subunit alpha type-7	Nucleobindin-1
	Proteasome subunit beta type-2	
E3 SUMO-protein ligase RanBP2	Proteasome subunit beta type-7	Proteasome subunit beta type-3
Ran GTPase-activating protein 1		
Exportin-1*	Protein enabled homolog	V-type proton ATPase subunit C 1
Reticulon-1	Sodium- and chloride-dependent GABA transporter 3	Endonuclease domain-containing 1 protein
Reticulon-4		Myelin proteolipid protein
		Zinc transporter 3
Neurabin-2		Guanine nucleotide-binding protein G(o) subunit alpha
		Small ubiquitin-related modifier 1
Liprin-alpha-2		Serine/threonine-protein phosphatase 2A 65 kDa regulatory subunit A alpha isoform
Liprin-alpha-3		Receptor expression-enhancing protein 5
		Thromboxane-A synthase
AP-1 complex subunit beta-1		Transmembrane protein 26
AP-2 complex subunit alpha-1		Lymphoid-restricted membrane protein
AP-2 complex subunit alpha-2		Titin
AP-2 complex subunit mu		Polyadenylate-binding protein 1
		Protein FAM161A
Formin-like protein 1		
Tubulin polymerization-promoting protein		
Arf-GAP with GTPase, ANK repeat and PH domain-containing protein 3		
Nucleobindin-2		
BTB/POZ domain-containing protein KCTD3		
Huntingtin-interacting protein 1-related protein		
Serine/threonine-protein phosphatase PP1-alpha catalytic subunit		
Serine/threonine-protein phosphatase PP1-gamma catalytic subunit		

Table 4-4: List of proteins identified in endogenous FBXO7 IP experiments present either in both genotypes or wild-type and homozygous R379G alone

Amongst the proteins identified in both groups are FBXO7 as the bait and 2 other SCFFBXO7 E3 ubiquitin ligase complex members and the previously identified FBXO7 interactors Exportin-1 and PI31

4.2.13 **Validation of proteomic hits from endogenous brain FBXO7 IPs**

I employed different strategies in trying to validate the interaction between FBXO7 and its putative interactors: First, I wanted to see whether a putative interactor could be detected by direct immunoblotting of the endogenous FBXO7 immunoprecipitations from brain. I then tried to employ co-immunoprecipitating FBXO7 from brain using the putative interactor as bait. However, there are many factors that may preclude the detection of FBXO7 in the co-immunoprecipitate of any putative interactor / substrate: For example, it is well recognized that the interaction between a substrate and its respective F-box protein as the substrate-recognizing subunit of the SCF E3 ligase complex is stimulus-dependent – for instance many substrates need to be phosphorylated in order to be recognized by their respective F-box protein(Skaar et al., 2013). Immunoprecipitating the whole pool of a given substrate might dilute out the interaction with FBXO7. It may therefore be prudent not to automatically exclude proteins that do not co-immunoprecipitate FBXO7 from the list of potential FBXO7 substrates. Apart from immunoprecipitations, I also looked at expression levels of some of the proteins: If a protein is ubiquitylated for proteasomal degradation in an SCF^{FBXO7} manner, expression levels might increase upon proteasomal inhibition (MG132 inhibition) and also by inactivating SCF E3 ligase complexes by Cullin-deneddylation (MLN4924: Cullin deneddylator). For these experiments I have used MEF lysates, as they are amenable for manipulation with inhibitor treatments as well as brain lysates of wild-type and homozygous R379G KI animals to investigate whether there was genotype-dependent difference in expression levels.

4.2.13.1 Validation by immunoblotting - PI31 and Exportin 1

Amongst the list of proteomic hits are 2 proteins that have previously been identified as FBXO7 interactors: PI31 and Exportin 1. PI31 has been shown to physically interact with FBXO7 via an N-terminal FP domain that is present in both proteins by means of mutational analysis in cell culture and biophysical studies(Kirk et al., 2008). A functional implication for the 2 proteins as proteasomal regulators stems from genetic studies in Drosophila(Bader et al., 2011). FBXO7 has been shown to contain a functional nuclear

export sequence, which mediates binding to the nuclear export protein, EXPORTIN 1 (CRM1). As this nuclear export sequence is embedded in the F-box domain of FBXO7, SKP1 and Exportin 1 have been suggested to bind competitively. These studies were performed using N-terminal tagged FBXO7 constructs in U2OS cells(Nelson and Laman, 2011). Figure 43 and Figure 44 demonstrate that the interaction between FBXO7 and Exportin 1 as well as PI31 is also preserved in the endogenous system using neuronal material for the wild-type as well as the homozygous R379G genotype. Table 4-5 gives an overview of the proteomic data for each replicate IP per genotype.

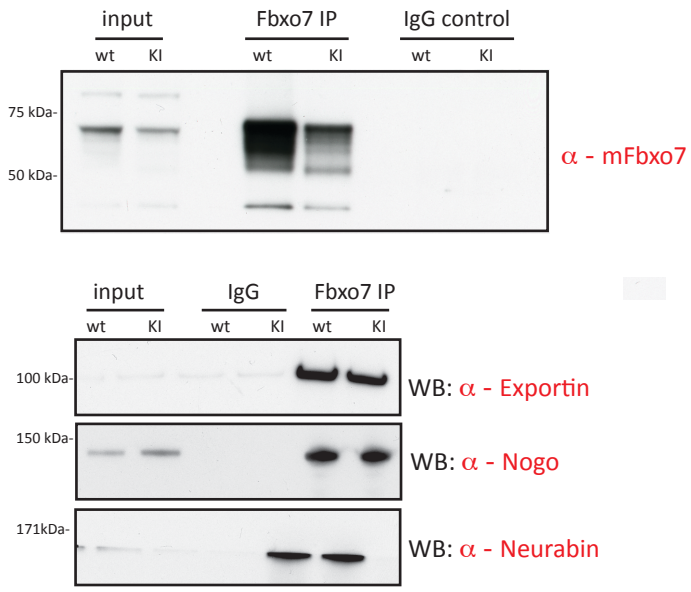

Figure 43: Detection of Exportin 1, Reticulon 4 and Neurabin 2 in endogenous FBXO7 IPs from brain by immunoblotting

Endogenous FBXO7 immunoprecipitation products from wild-type as well as homozygous R379G mouse brain lysates were blotted for FBXO7 along with Exportin 1, Nogo (brain specific isoform) and Neurabin 2. The control IP with preimmune sheep Immunoglobulin shows that the interactions are specific.

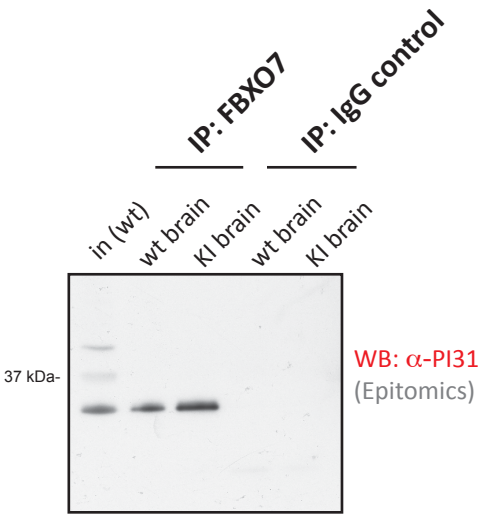

Figure 44: Detection of PI31 in endogenous FBXO7 IPs from brain by immunoblotting

Endogenous FBXO7 immunoprecipitation products from wild-type as well as homozygous R379G mouse brain lysates were blotted for PI31. The control IP with preimmune sheep Immunoglobulin shows that the interactions are specific.

	MW (kDa)	FBXO7 IP from wt brain		FBXO7 IP from KI brain	
PI31	30	1	22 (7, 18%)		
		2	108 (9, 25%)	1	56 (4, 11%)
		3	110 (10, 18%)	2	153 (9, 23%)
Exportin 1	124	1	1736 (108, 47%)		
		2	151 (19, 13%)	1	43 (8, 6%)
		3	1119 (64, 38%)	2	542 (38, 24%)

Table 4-5: Proteomic data for PI31 and Exportin 1 of each replicate IP

Molecular weight for each protein and mascot score with number of identified peptides and sequence coverage in brackets for each of the 3 replicate endogenous FBXO7 IPs from wild-type and the 2 replicates from homozygous R379G KI brain lysates. The candidate proteins were not present in any of the control IgG immunoprecipitations.

4.2.13.2 Validation by immunoblotting – E3 SUMO ligase RANBP2 / RanGap1*Sumo1 / Ubc9 complex

SUMOylation is yet another essential posttranslational modification essential for proper cellular physiological function, which in analogy to ubiquitylation involves a cascade of E1 activating enzyme (Aos1/Uba2), E2 conjugating enzyme Ubc9 and one of several known SUMO E3 ligases(Hay, 2013). RanBP2 is an important cellular protein involved in

nuclear transport and mitosis, but is also one of the few known proteins with SUMO E3 ligase activity(Pichler et al., 2002). It has recently been shown that the E3 SUMO ligase activity of RanBP2 depends on its assembly as a multisubunit complex consisting of SUMO1-modfied RanGAP1, RanBP2 and Ubc9(Werner et al., 2012)(Figure 45). An interesting observation is that all subunits of the RanBP2/ RanGAP1*Sumo1/Ubc9 complex are amongst the proteomic hits of the endogenous FBXO7 pull-downs from wild-type as well as homozygous R379G KI brain lysates. Table 4-6 gives an overview of the proteomic data for each replicate IP per genotype. RanBP2 is a very large protein (MW 345 kDa) and several commercial antibodies that I tested were unsuitable for detecting and immunoprecipitating endogenous RanBP2. A DSTT antibody program was therefore started (against AA2553-1838 of the human RANBP2 protein, NP_006258 - Figure 45), which successfully detects and immunoprecipitates endogenous human and mouse RanBP2 proteins (data not shown). Figure 46 and Figure 47 show that there were specific signals for RanGap1 and RanBP2 when the FBXO7 IP products from wild-type as well as homozygous R379G KI brain lysates were subjected to immunoblotting. Using the in the previous section (4.2.5) described homozygous Fbxo7$^{\text{C-terminal truncation}}$ MEFs as an endogenous means to show that the interaction between RanBP2 and the C-terminal truncated FBXO7 protein is either preserved or lost, I also subjected endogenous FBXO7 pull-downs from wild-type and homozygous Fbxo7$^{\text{C-terminal truncation}}$ MEFs to RanBP2 immunoblotting. As the Fbxo7$^{\text{C-terminal truncation}}$ protein lacks the F-box domain, SKP1 binding and SCF complex formation is lost as documented by the Cullin 1 immunoblot. Nevertheless, RanBP2 and appears to interact with the N-terminal half of FBXO7.

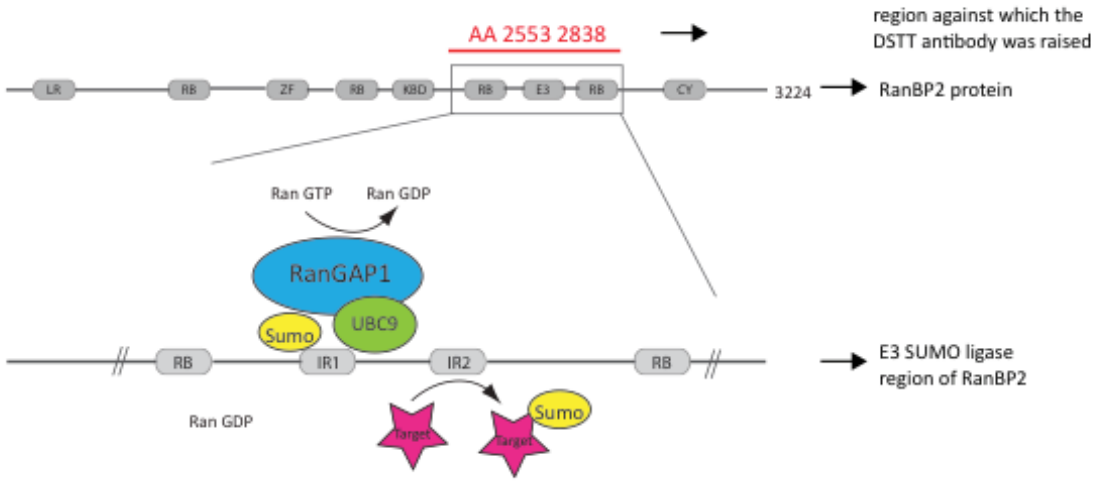

Figure 45: RanBP2 and sumoylated RanGAP1 forms the catalytically active E3 SUMO ligase

RanBP2 associated with sumoylated RanGAP1 and UBC9 to function as an E3 SUMO ligase localized at nuclear pore complexes. RanBP2 comprises a Leucin-rich domain (LR), several Zinc finger motifs (ZN), four Ran binding domains, several FG repeats (not shown), and a cyclophilin-like domain (Cy). The E3 ligase domain is situated between 2 Ran binding domains. IR1 and IR2 have been described as UBC9 binding sites. Our DSTT antibody programme was raised against the E3 ligase domain of RanBP2 indicated by red line (figure modified according to Figure 1 in (Werner et al., 2012)).

	MW (kDa)	FBXO7 IP from wt brain		FBXO7 IP from KI brain	
RanBP2	**345**	1	3298 (228, 38%)		
		2	993 (60, 13%)	1	68 (8, 1%)
		3	4922 (249, 55%)	2	3663 (198, 47%)
Ran GTPase-activating protein 1	**64**	1	704 (34, 34%)		
		2	448 (20, 21%)	1	308 (20, 19%)
		3	1274 (44, 40%)	2	1507 (48, 45%)
Sumo-conjugating enzyme Ubc9	**18**	1	39 (1, 8%)		
		2	/	1	32 (4, 27%)
		3	214 (11, 35%)	2	109 (5, 27%)

Table 4-6: Proteomic data for RANBP2 / RanGap1*Sumo1 / Ubc9 complex of each replicate IP

Molecular weight for each protein and mascot score with number of identified peptides and sequence coverage in brackets for each of the 3 replicate endogenous FBXO7 IPs from wild-type and the 2 replicates from homozygous R379G KI brain lysates. The candidate proteins were not present in any of the control IgG immunoprecipitations.

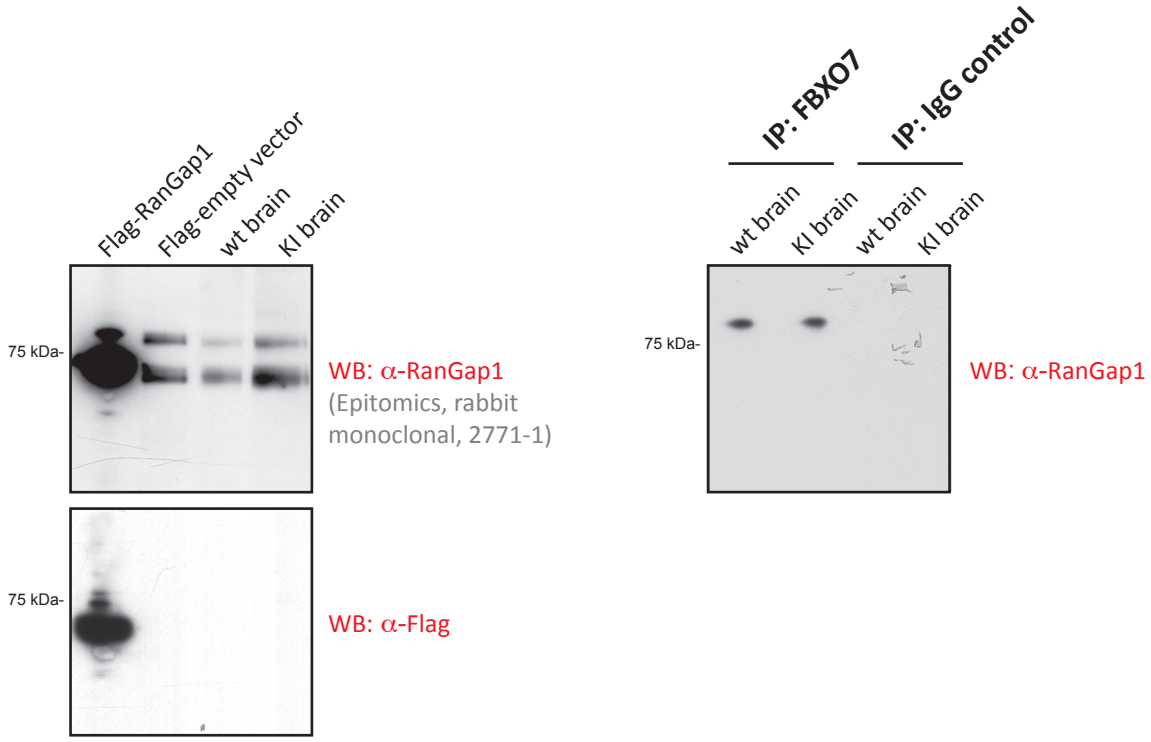

Figure 46: Detection of RanGAP1 in endogenous FBXO7 IPs from brain by immunoblotting

The immunoblots on the left hand side show lysates of transient overexpressed Flag-tagged RanGAP1, Flag-empty vector as well as wt and homozygous R379G KI brain lysates. RanGap1 has a molecular size of about 64 kDa, and is usually modified with SUMO1 reflected in the second slightly larger lane. The immunoblot on the right hand side shows that the SUMO-modified form of RanGAP1 can be detected in the FBXO7 IP products from both wt as well as homozygous R379G KI brain lysates, but not in the IgG control.

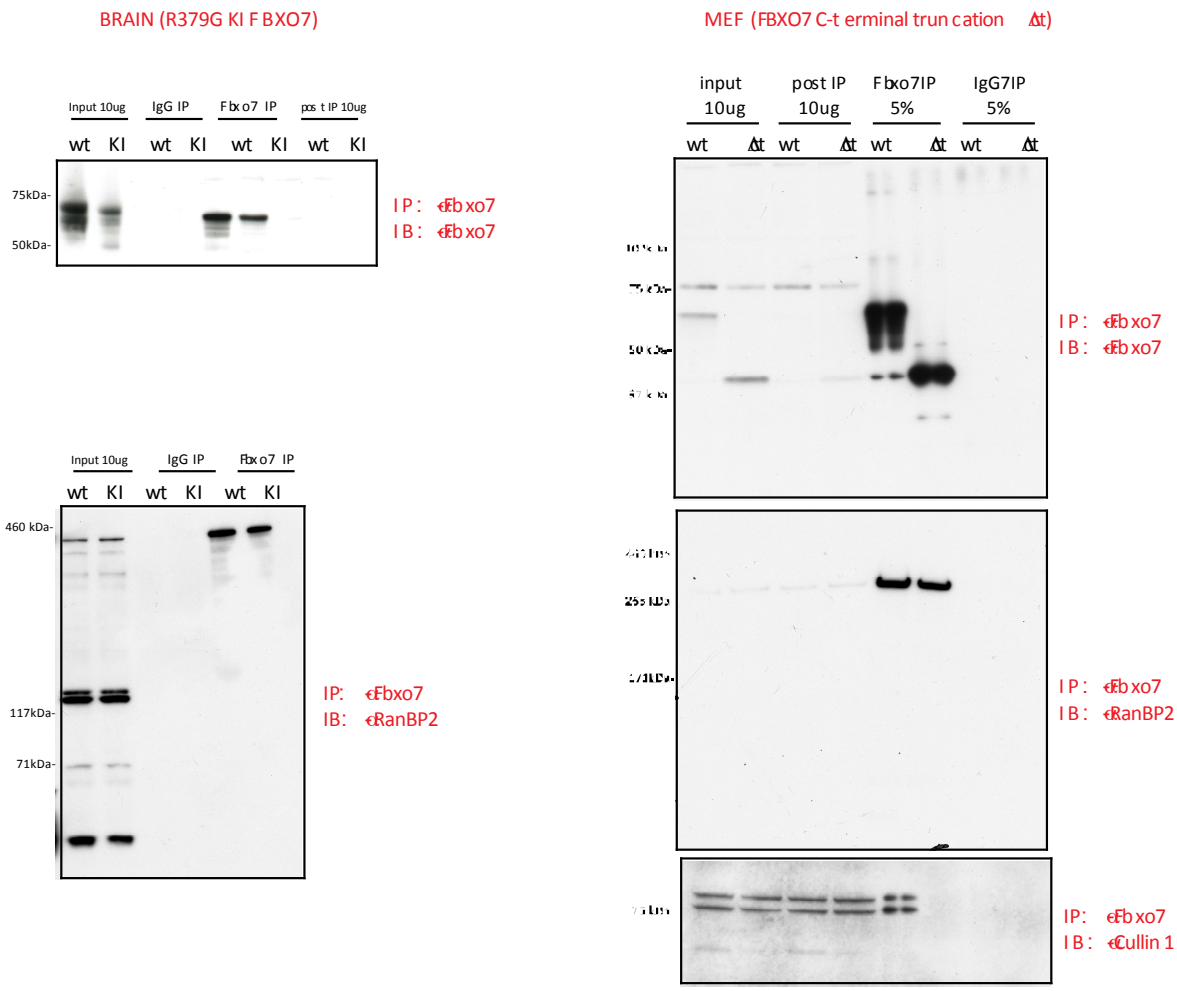

Figure 47: Detection of RanBP2 in endogenous FBXO7 IPs from brain by immunoblotting

A: R379G KI brain lysates: The top panel shows the FBXO7 immunoblot of input and post-IP lysates, FBXO7 immunoprecipitation products (5%) as well as appropriate controls for wt and homozygous R379G KI brain lysates. The lower panel shows input lysates and FBXO7 immunoprecipitation products and IgG controls immunoblotted for RanBP2: there is a specific signal for RanBP2 in the endogenous FBXO7 IP product from brain for both genotypes.

B: C-terminal truncation MEFs: Endogenous FBXO7 immunoprecipitations and controls were performed using wild-type and homozygous Fbxo7$^{C\text{-terminal truncation}}$ (C-terminal deletion starting immediately upstream of the start of the F-box domain- see 4.2.5) mouse embryonic fibroblast lysates. The Cullin 1 immunoblot serves as a control for SCF complex disruption; if the SKP1 binding domain is missing - as it is the case in the C-termninal truncation MEFs – SKP1 cannot interact with Fbxo7 for complex assembly. The immunoblot for RanBP2 shows that the interaction between FBXO7 and RanBP2 is still persevered if the C-terminal part of the FBXO7 protein is missing.

4.2.13.3 Fbxo7 is not a target of SUMOylation with Sumo1

Given that both the wild-type as well as the R379G KI Fbxo7 proteins associate with the RANBP2 / RanGap1*Sumo1 / Ubc9 E3 SUMO ligase complex, I wanted to explore whether Fbxo7 was possibly a SUMOylation target. I therefore used a 6His_SUMO overexpression protocol to test whether Fbxo7 was modified by SUMO1*(Tatham et al., 2009)*. 6His-SUMO1 stabily expressed in HeLa cells was purified from extracts using Nickel-affinity purification under denaturing conditions. This should allow the co-purification of any proteins that undergo posttranslational modification with SUMO. Figure 48 shows that neither Flag-FBXO7-wt nor the Flag-FBXO7-R378G mutant undergo SUMOylation *in vivo* under these conditions. As positive control serves Flag-RanGAP1, for which a band shift to the higher molecular SUMOylated form is marked with 2 red asterisks upon co-purification with 6 HIS-SUMO1.

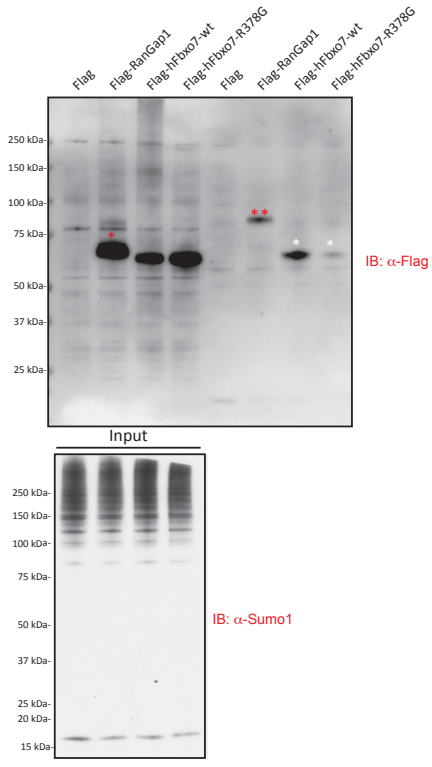

Figure 48: FLAG-FBXO7-wt and FLAG-FBXO7-R378G are not modified by SUMO1

Immunoblots from nickel-affinity purification from stable expressing 6His-SUMO1 HeLA cells transiently transfected either with Flag-empty vector, Flag-RanGAP1, Flag-FBXO7-wt or FLAG-FBXO7-R378G under denaturing condition. The top panel shows the Flag-immunoblot of the crude input lysates - demonstrating efficient expression of the Flag-constructs – and the nickel-affinity purifications on the

right hand side. The latter demonstrates the band shift of the higher molecular weight species of RanGAP1 in its SUMOylated state (**). This serves as a positive control. There is no band shift observed with FBO7. The lower panel shows the SUMO1 immunoblot of the crude input lysates. The high molecular weight smear corresponds to proteins modified by SUMO1.

4.2.14 **Validation by immunoblotting – Reticulon 4**

The Reticulon 4 gene gives rise to at least 3 isoforms of Nogo proteins, A, B, and C, which share a C-terminal homology domain of about 188 AA. Little is known about their physiological function, but they've been discovered and studied in the context of injury and repair of fibre tracts in the CNS(Schwab, 2010). DSTT antibodies against Nogo B are available allowing detection and immunoprecipitation of endogenous Nogo proteins from brain, and these were used for my validation of Reticulon 4. The longer Nogo isoform A and the shorter isoform B co-elute with endogenous Fbxo7 when immunoprecipitated from wild-type and KI mouse brain as shown by immunoblotting in Figure 49. I also immunoblotted the endogenous FBXO7 pull-downs from wild-type and homozygous $Fbxo7^{C\text{-terminal truncation}}$ MEFs for Nogo. Figure 50 shows that the N-terminal half of FBXO7 is sufficient to maintain the interaction with both Nogo isoforms (A and B). Table 4-7 gives an overview of the proteomic data for Reticulon 4 for each individual endogenous FBXO7 pull-down from brain. Reticulon 4 was not present in any of the controls.

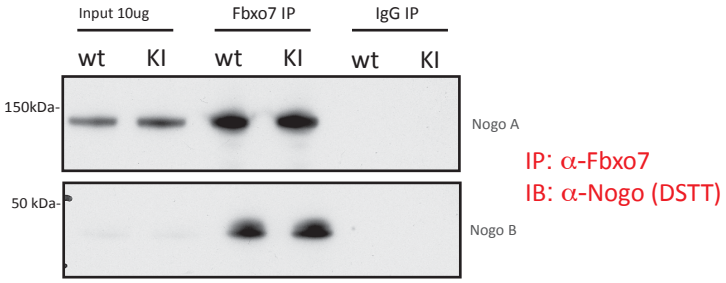

Figure 49: Detection of Nogo A and Nogo B (Reticulon 4) in endogenous FBXO7 IPs from brain by immunoblotting

The top panel shows that the brain specific Reticulon 4 isoform (Nogo A) can be detected in the FBXO7 IP products from both wt as well as homozygous R379G KI brain lysates, but not in the IgG control. The lower panel shows the equivalent for the shorter Nogo B.

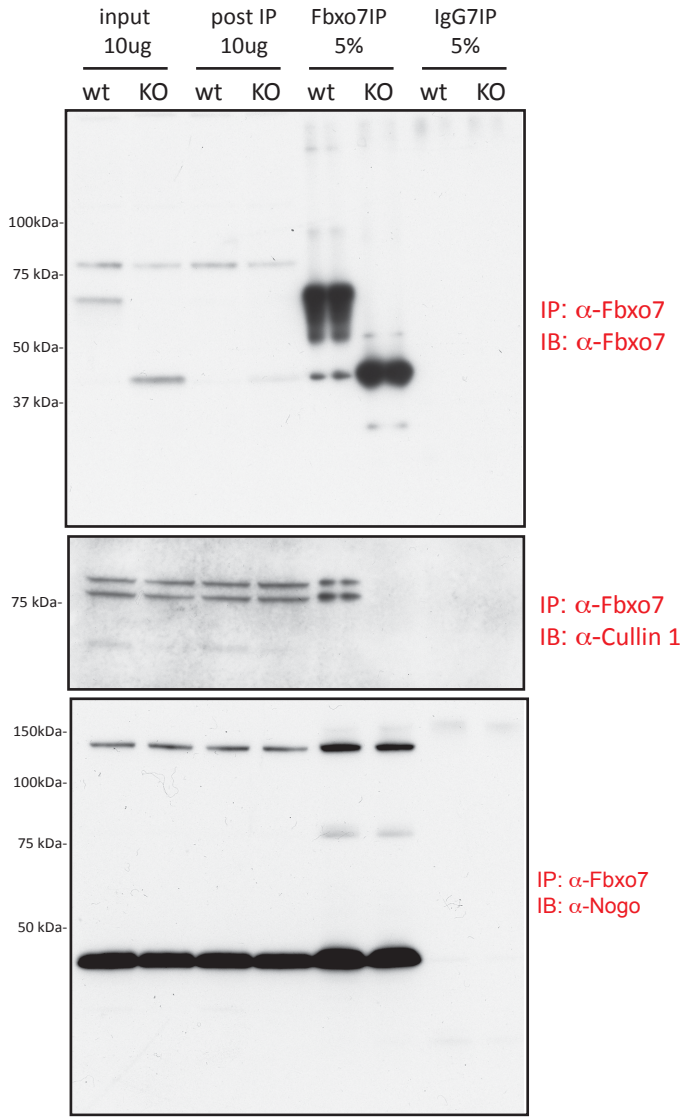

Figure 50: Detection of Nogo A and Nogo B (Reticulon 4) in endogenous FBXO7 IPs from MEFs by immunoblotting

Endogenous FBXO7 immunoprecipitations and controls were performed using wild-type and homozygous Fbxo7$^{C\text{-terminal truncation}}$ (C-terminal deletion starting immediately upstream of the start of the F-box domain- see 4.2.5) mouse embryonic fibroblast lysates. The Cullin 1 immunoblot confirms that in case of the C-terminal truncation MEFs complex formation is disrupted due to lack of the binding domain for SKP1. The immunoblot for Nogo shows that the interaction between FBXO7 and Nogo A / B is still persevered if the C-terminal part of the FBXO7 protein is missing.

	MW (kDa)	FBXO7 IP from wt brain		FBXO7 IP from KI brain	
Reticulon 4	**127**	1	1736 (108, 47%)		
		2	151 (19, 13%)	1	43 (8, 6%)
		3	1119 (64, 38%)	2	542 (38, 24%)

Table 4-7: Proteomic data for Reticulon 4 (Nogo) of each replicate IP

Molecular weight for each protein and mascot score with number of identified peptides and sequence coverage in brackets for each of the 3 replicate endogenous FBXO7 IPs from wild-type and the 2 replicates from homozygous R379G KI brain lysates. The candidate protein was not present in any of the control IgG immunoprecipitations.

4.2.15 **Validation by co-immunoprecipitation**

My efforts to validate the proteomic hits from the endogenous FBXO7 immunoprecipitations by co-immunoprecipitating FBXO7 vice versa have been laborious and inconsistent. I have been able to co-immunoprecipitate FBXO7 with large-scale (lysates from 1 mouse brain per immunoprecipitation (about 25mg)) pull-downs of RanBP2 as well as Nogo from brain lysates from both genotypes, but I have not been able to consistently reproduce these findings in repeat experiments. Additionally, I have performed endogenous Reticulon 4 / nogo as well as RanBP2 affinity purifications from brain lysates followed by protoeamic analysisPerforming mass-spectrometry fingerprint analysis: In these experiments Fbxo7 was not detected amongst the proteomic hits (data not shown).

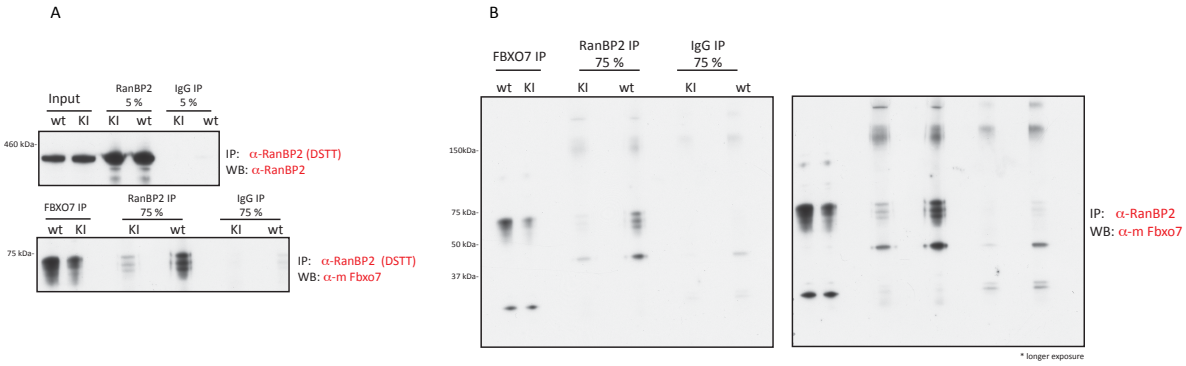

Figure 51: Co-immunoprecipitation of FBXO7 with RanBP2 from wt and homozygous R379G KI brain lysates

Large scale RanBP2 immunoprecipitation from about 25 mg (lysate from 1 animal per IP) of wild-type and homozygous R379G KI brain lysates allows the detection of FBXO7 as a co-eluting protein by

immunoblotting. The panels on the left hand side (A) show the immunoblot for RanBP2 as the bait with input lysates and the FBXO7 immunoblot of 75% of the RanBP2 IP and control for both genotypes. An FBXO7 pull-down from 1 mg of tissue served as a control for the correct size of FBXO7. The right hand side (B) shows the entire outline of the FBXO7 immunoblot for the RanBP2 IP with a shorter and a longer exposure time.

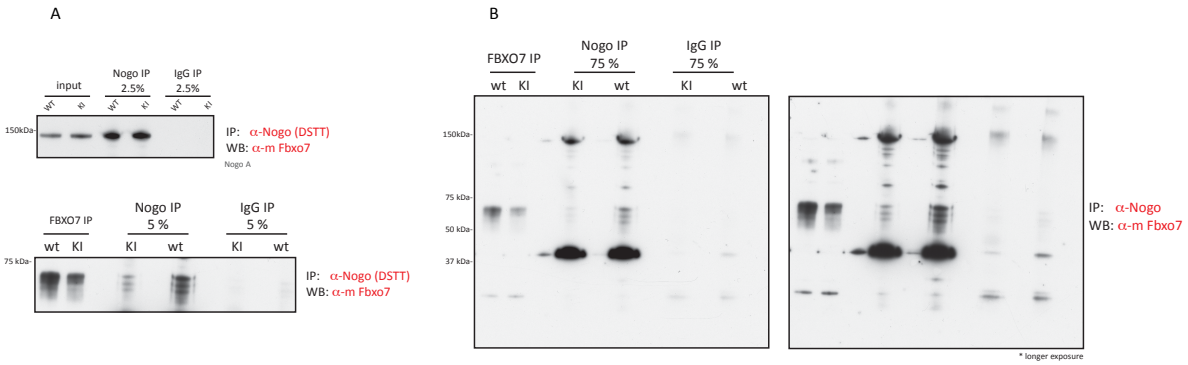

Figure 52: Co-immunoprecipitation of FBXO7 with Nogo from wt and homozygous R379G KI brain lysates

Large scale Nogo immunoprecipitation from about 25 mg (lysate from 1 animal per IP) of wild-type and homozygous R379G KI brain lysates allows the detection of FBXO7 as a co-eluting protein by immunoblotting. The panels on the left hand side (A) show the immunoblot for Nogo as the bait with input lysates and the FBXO7 immunoblot of 75% of the RanBP2 IP and control for both genotypes. An FBXO7 pull-down from 1 mg of tissue served as a control for the correct size of FBXO7. The right hand side (B) shows the entire outline of the FBXO7 immunoblot for the RanBP2 IP with a shorter and a longer exposure time.

4.2.16 Expression analysis of potential FBXO7 interactors in wt and homozygous R379G KI lysates

In this section I have used brain lysates from wild-type, heterozygeous and homozygous R379G KI animals for immunoblotting of FBXO7, SCF complex members and some of the putative FBXO7 interactors as identified by the endogenous FBXO7 immunoprecipitations. Figure 53 shows that there is no difference in RanBP2 expression levels between the wild-type and the homozygous R379G KI genotype (brain and MEF lysates). The same can be observed for Nogo A and Nogo B (Reticulon 4) as demonstrated by the LICOR quantification from wild-type, heterozygeous and

homozygous R379G KI brain lysates. I have then subjected brain lysates of all 3 genotypes to immunoblotting for FBXO7, GAPDH as a loading control, all other members of the SCF E3 ligase complex as well as PI31, Neurabin 2, Exportin 1, RanBP2, Nogo A and B. Although not amongst the list of putative FBXO7 interactors in my study, I have also included CIAP1 and HURP in the expression analysis as they are amongst the previously identified FBXO7 interactors in other studies(Chang et al., 2006; Hsu et al., 2004). RanGAP 1 could not be blotted for because the antibody was not suitable to work with these particular lysates (Figure 55). Overall, no striking differences in expression levels were seen for the candidates blotted for except for the robust hypomorphism of the homozygous R379G KI genotype.

I was then interested to see whether treatment with the MLN4294 compound – a Cullin deneddylating reagent which thereby also negatively regulates the activity of Cullin dependent SCF E3 ligases – had a genotype dependent effect on any the expression level of any of these proteins. For this experiment, I used not only littermate wild-type and homozygous R379G KI MEFs, but also littermate wild-type and homozygous $Fbxo7^{C\text{-}terminal\ truncation}$ MEFs. The latter lack the C-terminal half of the FBXO7 protein including the functionally important F-box domain. Figure 56 shows that there was mainly an effect on RanGAP1. RanGAP1 has an expected molecular weight of 64 kDa, but usually a second species at a higher molecular weight exists due to stable SUMOylation with SUMO1. The pool of not-SUMOylated RanGAP1 appears to be relatively lower in the $Fbxo7^{C\text{-}terminal\ truncation}$ as well as R379G KI genotype than in comparison with the wild-type.

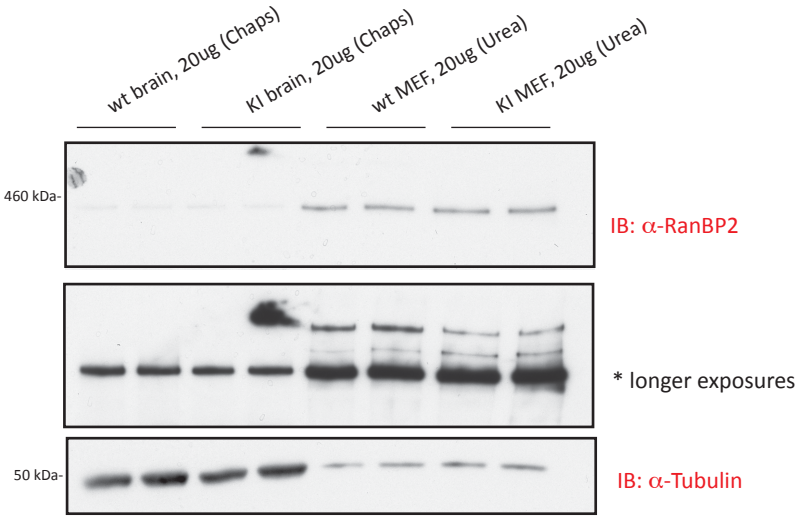

Figure 53: No difference in RanBP2 expression levels between wt and homozygous R379G KI brain and MEF lysates

RanBP2 expression levels in brain (lysed in CHAPS) and MEFs (lysed in Urea) do not show a difference between the wild-type and homozygous R379G KI genotype. The top panel shows a shorter and the middle panel a longer exposure time for the RanBP2 immunoblot. An immunoblot against tubulin serves as a control for equal loading.

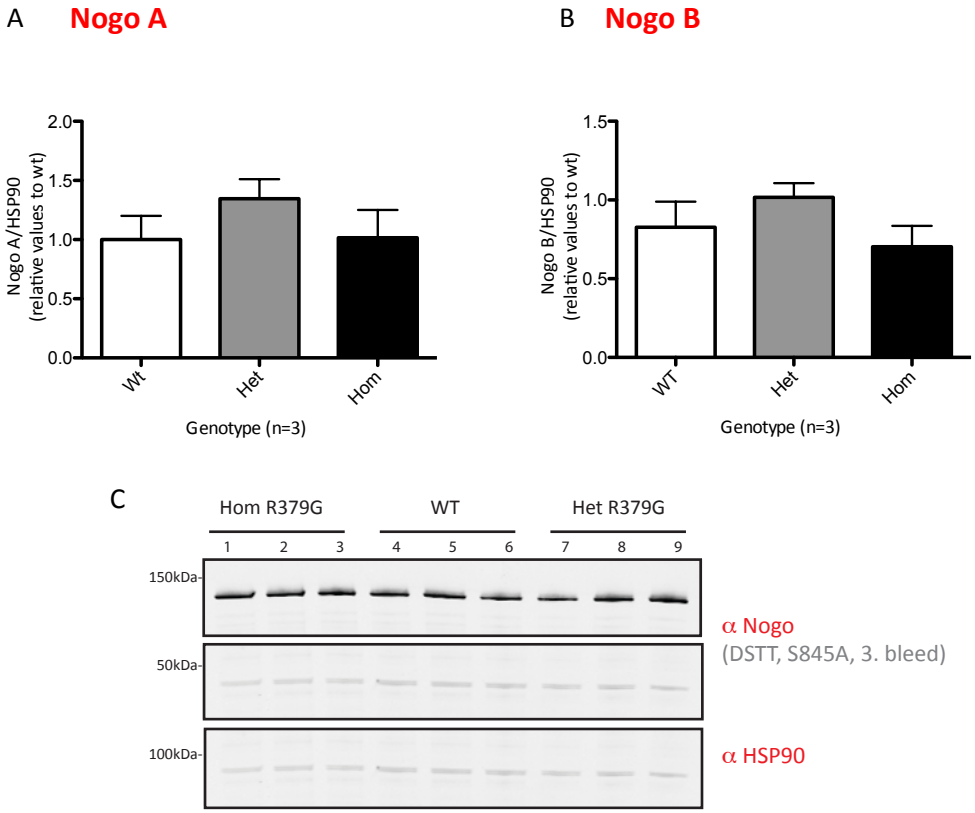

Figure 54: No difference in Nogo A and B expression levels between wt and homozygous R379G KI brain lysates

A: Li-Cor quantification of Nogo A and Nogo B in whole brain urea lysates from wild-type, heterozygeous and homozygous R379G KI animals at 10 months of age expressed as mean (with SEM) in relation to wild-type expression levels and standardized against HSP90. The difference between the heterozygeous and homozygous in comparison to the wild-type expression level was not significant (P> 0.05). B: Respective immunoblots that were used for LICOR quantification.

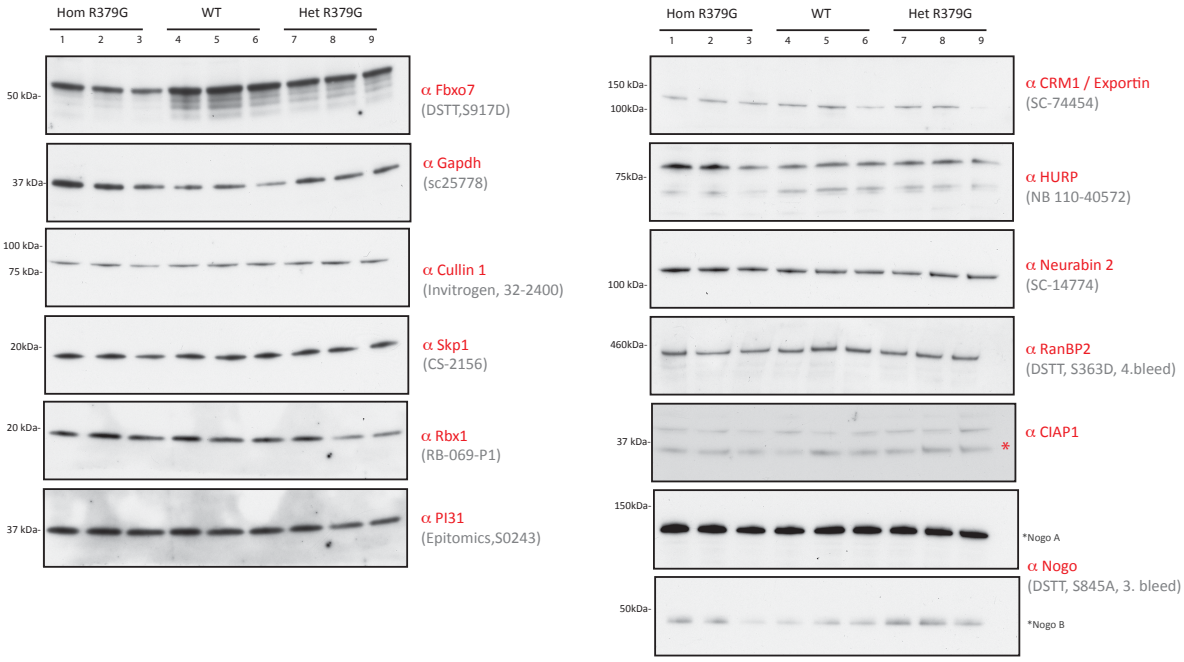

Figure 55: Expression analysis of potential interactors in brain lysates from wt, het and hom R379G KI animals

Rapigest brain lysates (15 ug each) from 3 animals of each genotype (wt, heterozygeous and homozygous R379G KI animals at 1 month of age) were subjected to immunoblotting for FBXO7, Gapdh as well as the other members of the SCF complex and putative interactors. There is no apparent difference in levels of any of the candidates except for FBXO7 itself.

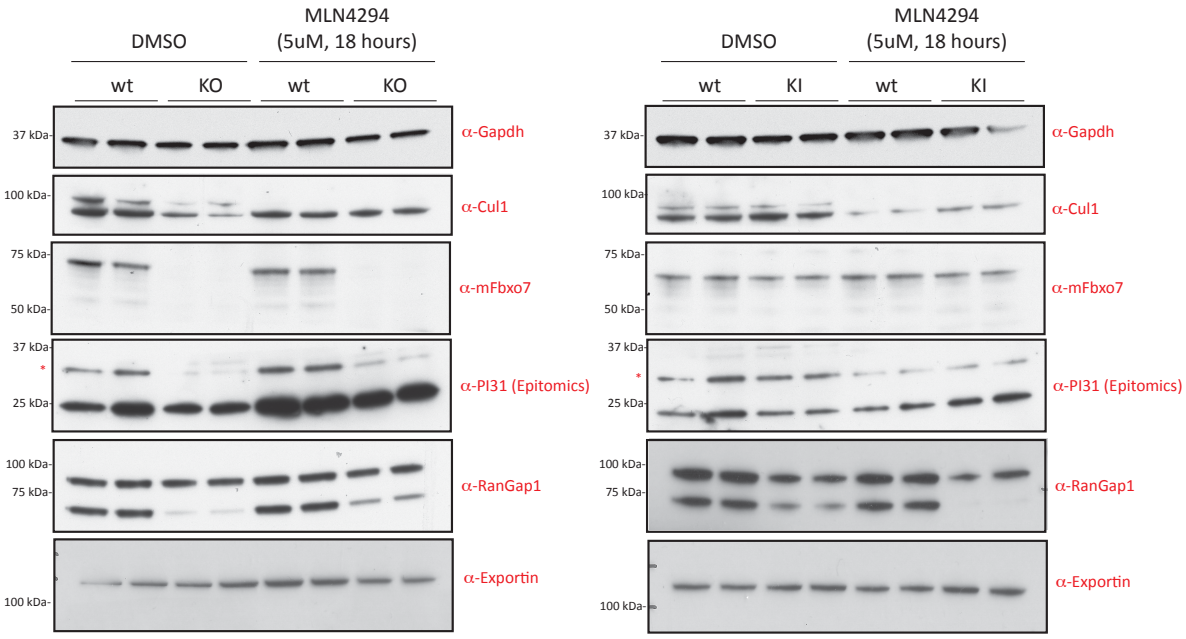

Figure 56: Expression levels of FBXO7 and putative interactors in MLN4926

Littermate wild-type and homozygous Fbxo7$^{C\text{-terminal truncation}}$ (KO) as well as littermate wt and homozygous R379G KI MEFs were treated for 18 hours with the neddylation 8 inhibitor MLN4924 at 5uM (MLN4924 inhibits Cullin 1 neddylation, thereby inhibiting Cullin dependent SCF E3 ligase activity) or DMSO control before cells were lyses under denaturing conditions in SDS. Duplicate loading of corresponding lysates were subjected to immunoblotting for FBXO7, GAPDH as a loading control, as well as PI31, RanGAP1 and Exportin1. The Cullin 1 blot demonstrates the disappearing band shift (neddylated form of Cullin 1) with MLN4296 treatment.

4.3 Behavioural phenotyping of the Fbxo7 ^{R379G} Knock-in mouse model

The aim was to perform a phenotypic analysis of the Fbxo7^{R379G} KI mouse model in comparison to wild-type littermates. A total of 35 animals were tested (13 wild-type and 22 homozygous KI animals) at a single time point at about 10 months of age. Amongst these animals were 12 gender-matched, littermate pairs of wild-type and homozygous KI animals (mean age of the littermate pairs was 307 days at the time of testing) derived from heterozygeous x heterozygeous breedings. An overview of all the general characteristics of the animals is given in 4.3.1. In section 4.3, the results of the 12 littermate pairs will be presented (unless otherwise stated) as they ensure a high degree

of comparability. The mouse behavioural phenotyping was performed with the help of Dr. Stephen Martin, manager of the behavioural neuroscience core facility at the University of Dundee (Ninewells Campus, NW). Dr. Martin supported me in performing the experiments, gathering the raw data and the analysis thereof. All mice were tested at around the same time, but the animals were housed in different facilities at 2 different sites. This was due to unforeseen problems with inter-facility transfer of animals due to differences in the facilities' "specific pathogen freeness". Post hoc it turned out that there was an unexpected and significant difference in body weight between animals house in one facility compared to the other – animals housed at the College of Life Sciences (CLS) were significantly heavier than those housed at the NW campus. The correlation between body weight and housing facility was greater than that seen for gender and genotype did not significantly influence the weight of the animals (**Table 4-8**). Figure 57 shows the bodyweight of each animal according to genotype and gender, and t-test analysis revelas that there is no significant difference in mean bodyweight between the 2 genotypes and gender. There is also no significant difference in mean body weight between the wild-type and homozygous R379G KI *Fbxo7* genotype when male and female animals are combined in the analysis (littermate pairs as well as all 35 animals; data not shown).

	Weight	Genotype	Gender	Housing facility
Genotype	0.00			
Gender	0.03	0.05		
Housing facility	0.51**	0.02	0.02	
Mean latency	0.46**	0.06	0.02	0.34**

Notes: correlation is significant at the 0.01 level (two-tailed)**; correlation is significant at the 0.05 level (two-tailed)*; correlation is not significant (no star).

Table 4-8: Correlation matrix of variables influencing body weight for all 35 animals

Pearson's correlation values (as r^2) between different variables for all 35 animals (21 male and 14 females; 13 wt and 22 homozygous R379G KI; 19 housed at NW and 16 housed at CLS). There is a significant correlation between body weight (in grams on day 1 of testing) not only for gender, but also for where the animals were housed. Genotype did not significantly affect body weight.

(Variables: mean latency to loose grip (days 1-4) (in seconds), genotype (wt=1, hom KI= -2), gender (male=1, female=-1), body weight on trial day 1 (in grams) and housing facility (Ninewells campus=1, College of Life Sciences=-1). Stars indicate the level of significance.

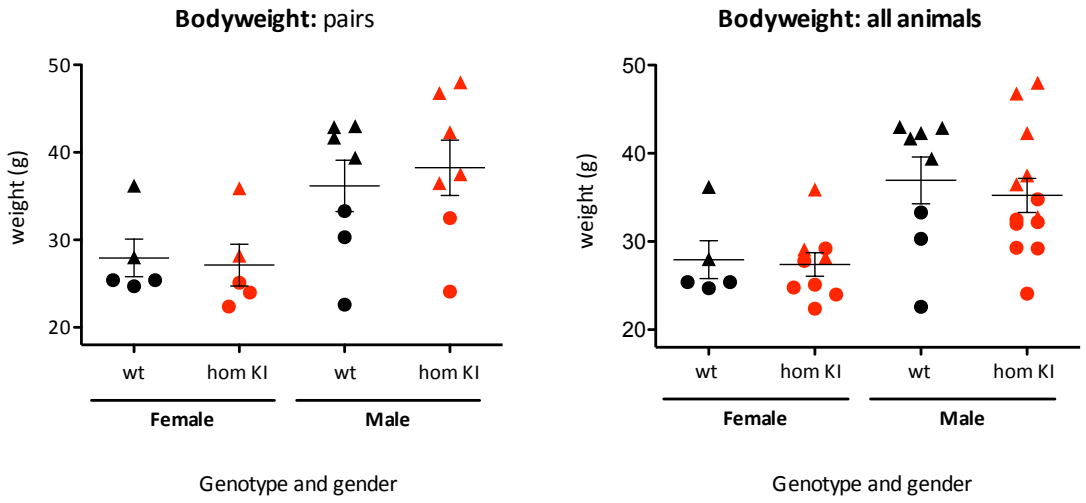

Figure 57: Dotblots of bodyweight in relation to gender and genotype

The panel on the left shows bodyweight of the littermate pairs in relation to gender and genotype while the panel on the right shows it for all 35 animals. Individual animals are represented either as triangular or round shape dependent on which facility they were housed in (triangular: College of Life Science; round: Ninewells site). The weight in grams corresponds to day 1 of testing (means and standard error of the mean are indicated by bars). T-test analysis confirms that the difference in mean weight between the 2 genotypes and per gender does not significantly differ. The graph also demonstrates that the animals housed at the CLS site tend to be heavier irrespective of genotype or gender.

4.3.1 General neurological screen of wild-type and Fbxo7^{R379G} KI mouse (SHIRPA)

All 35 mice underwent the SHIRPA test battery as an initial general neurological screen. The protocol involves a three stage screening procedure designed to mimic the human neurological and psychiatric diagnostic procedure(Masuya et al., 2005). Table 4-9 shows the results for the wild-type and homozygeous R379G Fbxo7 littermate pairs (n=12 pairs). There was a difference in coat appearance and transfer arousal. An untidy or

irregular coat can be an indication for an underlying illness if it is seen in combination with other features that are generally accepted as sick rodent signs (such as for example discharge from the eyes, hunched posture, skin lesions, reluctance to move, poor body condition)(Pettan-Brewer and Treuting, 2011). Other signs of an underlying illness were not seen in the homozygeous R379G *Fbxo7* KI mice and hence, the irregularities in coat appearance are unlikely a reflection of such. The difference in transfer arousal – with the homozygeous R379G *Fbxo7* KI mice demonstrating more often freezing – could potentially be a reflection of a difference in anxiety behaviour(Hafezparast et al., 2002). There was however no difference in the locomotor activity analysis between the 2 genotype (4.3.2), which would have corrobotorated a behavioural phenotype of the homozygeous R379G *Fbxo7* KI animals. Overall, the modified SHIRPA analysis of the littermate wild-type and homozygeous R379G KI *Fbxo7* mice did not show a consistent difference in their general phenotype.

			wt (n=12)	Hom KI (n=12)	p - value
1	Body weight (g)		32.33 ± 2.22	33.25 ± 2.58	n.s.
2	Body position	Inactive	0	0	
		Active	12	12	n.s.
		excessive active	0	0	
3	Tremor	Absent	12	12	n.s.
		Present	0	0	
4	Palpebral closure	Eyes open	12	12	n.s.
		Eyes closed	0	0	
5	Coat appearance	Tidy and well groomed	12	8	p<0.05
		Irregularities	0	4	
6	Whiskers	Absent	2	3	n.s.
		Present	10	9	
7	Lacrimation	Absent	12	12	n.s.
		Present	0	0	
8	Defecation	Absent	2	2	n.s.
		Present	10	10	
9	Transfer arousal	Extended freeze	0	2	p<0.05
		Brief freeze	1	3	
		Immediate movement	11	7	
10	Locomotor activity	see 1.3.1.2. for detailed analysis			n.s.
11	Gait	Fluid movement	12	11	n.s.
		Lack fluidity	0	1	n.s.
12	Tail elevation	Dragging	0	0	
		Horizontal extension	12	12	
		Elevated tail	0	0	
13	Touch escape	No response	0	3	n.s.
		Response to touch	12	9	
		Flees prior to touch	0	0	
14	Positional activity	Struggles when held by the tail			
		No struggle			
15	Skin colour	Blanched	0	0	n.s.
		Pink	12	12	
		Bright, deep red	0	0	
16	Trunk curl	Absen	0	0	n.s.
		Present	12	12	
17	Limb grasping	Absent	12	12	n.s.
		Present	0	0	
18	Pinna reflex	Present	12	12	n.s.
		Absent	0	0	
19	Corneal reflex	Present	12	12	n.s.
		Absent	0	0	
20	Righting reflex	Present	12	12	n.s.
		Absent	0	0	
21	Contact righting reflex	Present	12	11	n.s.
		Absent	0	1	
22	Evidence of biting	Present	0	1	n.s.
		Absent	12	11	
23	Vocalisation	None	11	12	n.s.
		Vocal	1	0	

Table 4-9: Results of the modified SHIRPA-analysis of the Fbxo7 wt and homozygeous R379G KI littermate pairs

Amongst the parameters tested, coat appearance and transfer arousal behaviour differed between the 2 genotypes. The homozygeous KI animals demonstrated more often localized patchy hair loss at the back. Irregularities in coat appearance can be an indication for an underlying illness if seen in combination with other features of generally accepted sick rodent signs (which was not the case here)(Pettan-Brewer and Treuting, 2011). The only difference in the arena was a difference in transfer arousal, where the homozygeous KI animals demonstrated more often freezing, which is a behaviour that can be influenced by expoloratory, emotional and arousal behaviour(Hafezparast et al., 2002).

4.3.2 **Testing of spontaneous locomotor activity**

The open-field test allows testing of spontaneous locomotor activity by observing and recording an animal's movement around an open area. Typically, a mouse will run to the walled edge and explore its surrounding while staying close to the wall as it fears novel and open spaces. As the animal habituates to its new surrounding, its anxiety usually diminishes and it will increasingly venture out to explore the centre of the arena. In addition to general locomotion, rearing is another variant of the search phase of exploratory behaviour in mice; it serves to provide head elevation to investigate more distant stimuli and is usually accompanied by undirected sniffing. This natural behaviour can be exploited in the open-field locomotor activity test to measure anxiety-like behaviour(Brooks and Dunnett, 2009). There was no difference in the total distance travelled, number of rears, or distance travelled in the periphery or centre of the arena between wild-type and homozygous Fbxo7^{R379G} KI mice: **Figure 58** shows the locomotor results for the littermate pairs (rearing not shown). There was also no difference seen when all 35 animals were taken into account (data not shown).

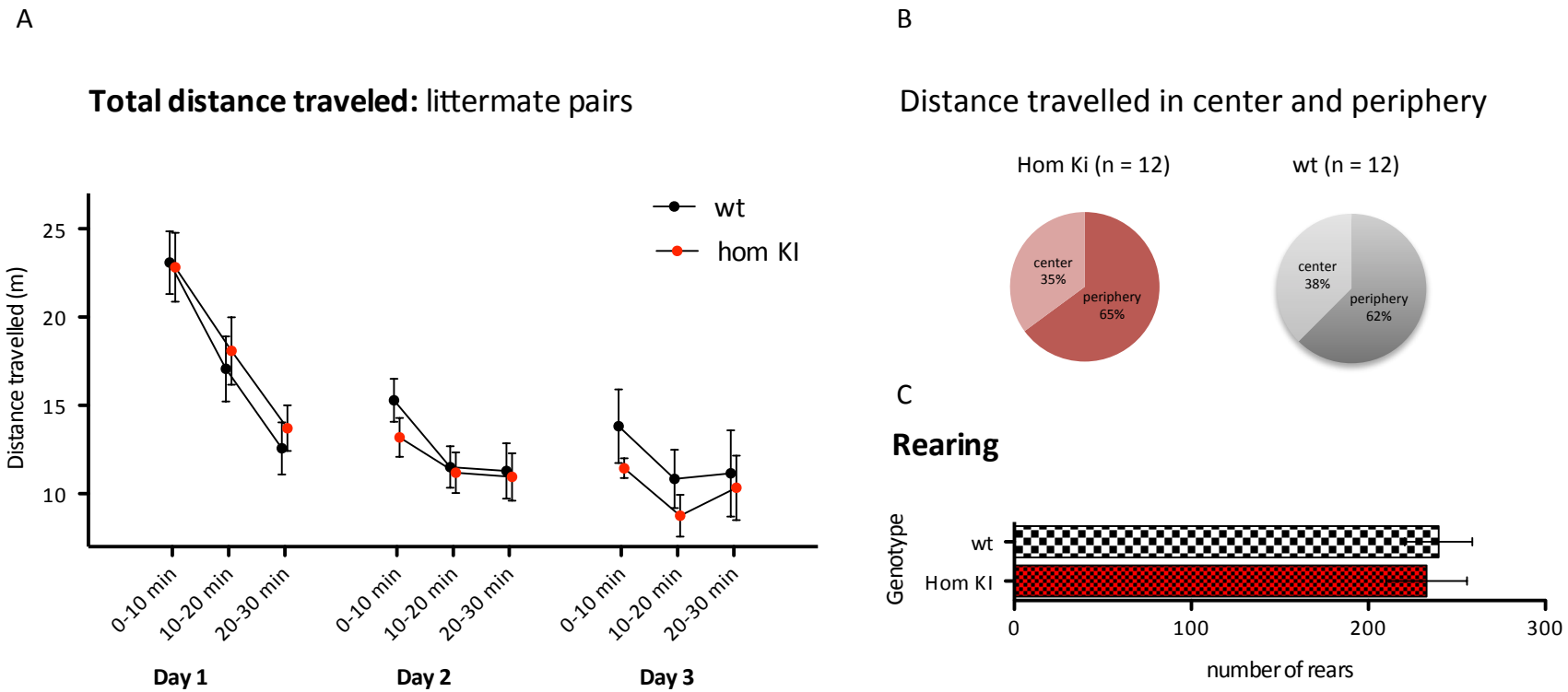

Figure 58: Open-field test for littermate pairs

A: Total distance travelled by each group (wt and hom KI) in each of the 3 daily sessions of 30 min subdivided into 10 min intervals (mean ± SEM). B: Percentage of the total distance that was travelled in the periphery versus the centre of the arena. C: Number of rears during all 3 sessions (mean ± SEM). The difference between the 2 genotypes was not significant for any of the parameters (paired t-test)

4.3.3 **Gait analysis**

Foot prints left on paper by a mouse walking down a narrow corridor whose fore and hind paws are dyed with different colours was used to analyse a range of gait parameters such as stride length, base width, and overlap between fore and hind paws. There was no difference in any of these parameters between the littermate pairs to suggest that the homozygous Fbxo7R379G KI mice had any problems with motor coordination and synchrony during normal walking (data not shown). The same was observed when all 35 animals were included in the analysis.

4.3.4 **Rotarod performance to assess motor coordination and balance**

The rotarod is a specifically designed instrument to assess neurological deficits in rodents(Dunham and Miya, 1957), and is one of the most commonly tests used to assess motor coordination and balance in mice. The mice are either tested on separate trials at a series of fixed speeds (fixed speed protocol) or during increasing revolutions of the rod in each trial (accelerating protocol) and their latency to fall down is measured. There are several recognized confounding factors of the rotarod test: 1) animals that don't perform and fall off as soon as they are placed on the rod – these can be excluded as outliers from the analysis. 2) animals may cling to the beam and rotate with it without falling off and 3) body weight of the animals - heavy mice perform worse than light mice(Brooks and Dunnett, 2009). In this study, all animals performed during the rotarod test to satisfaction and in addition to the latency to fall, also the latency to loose grip (the point when the animal clings and starts to rotate with the beam rather than to walk) was recorded. Results are presented as "latency to loose grip".

4.3.5 **Rotarod performance during the accelerating protocol**

There is a significant group difference in the overall rotarod performance during the accelerating protocol between the littermate wild-type and Fbxo7^{R379G} KI pairs at 10 months of age (Figure 59). Figure 60 demonstrates that the overall performance of the R379G KI Fbxo7 animals was significantly impaired in comparison to their wild-type littermate controls.

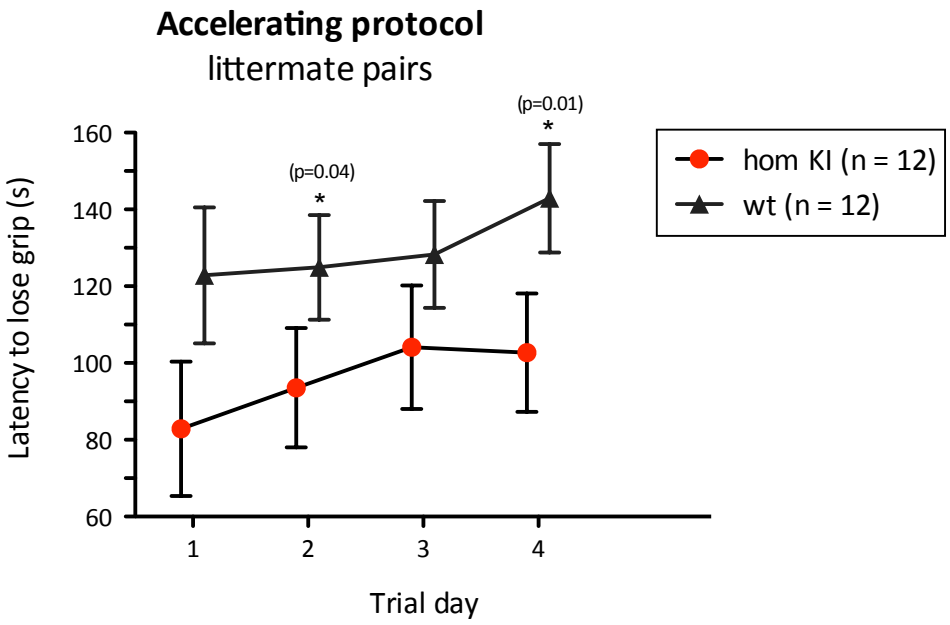

Figure 59: Impaired motor performance of the R379G KI Fbxo7 animals: Accelerating rotarod test

The graphs shows the mean latencies to loose grip of all 4 trial days for each group of littermate pairs of wt and homozygous R379G KI animals. A paired t-test demonstrates that the group difference between wt and mutant animals is significant on day 2 (p=0.04) and day 4 (p=0.01).

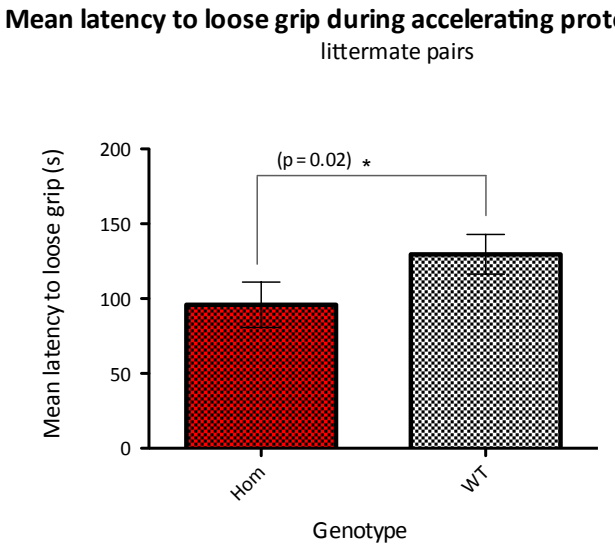

Figure 60: Significant group difference between wt and homozygous R379G KI animals across all 4 trial days during the accelerating protocol

The graph shows the mean latencies (raw data, not adjusted for weight of the animals) to loose grip of all 4 trial days for each group of littermate pairs of wt and homozygous R379G KI animals. A paired t-test demonstrates that the group difference between wt and mutant animals is significant (p=0.02).

The impact of body weight on the performance in the rotarod experiment has already been pointed out. Figure 61 shows the relationship between bodyweight and rotarod performance for all paired animals. The respective linear regression lines per genotype show that body weight affects rotarod performance likewise and irrespective of genotype.

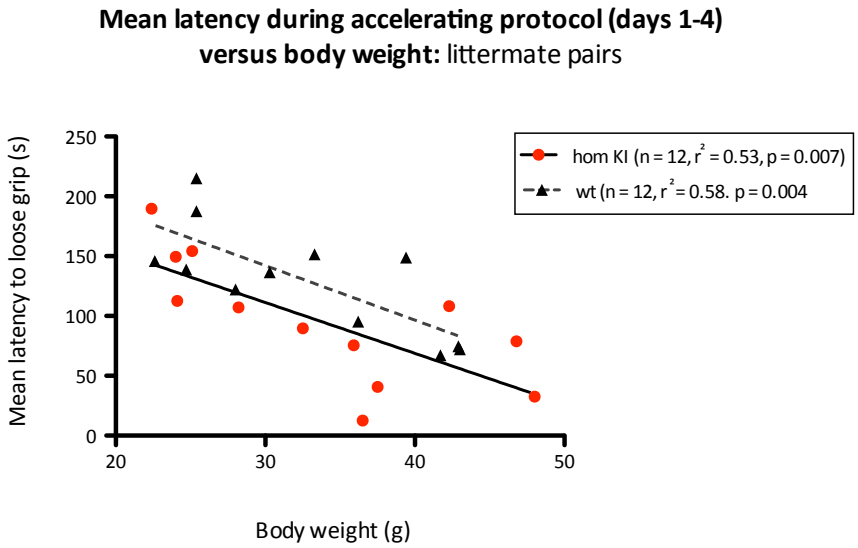

Figure 61: Mean latency during accelerating protocol (days 1-4) versus body weight

Body weight of the animals significantly affects their performance in the accelerating protocol of the rotarod test. Mean latency to lose grip of all 4 trial days for each animal is blotted against its body weight on trial day 1. The genotype of each animal is indicated as a red dot for homozygous R379G KI and as a black triangle for wt animals. The respective linear regression lines per genotype show that body weight affects rotarod performance likewise and irrespective of genotype. (Linear regression line for all paired animals irrespective of genotype: $r^2 = 0.51$, $p < 0.001$; line not shown in graph)

4.3.6 **Rotarod performance during the fixed speed protocol**

The fixed speed protocol provides separate data on each range of rotation speeds. There is a trend towards a better performance in the fixed speed protocol by the group of wild-type animals in comparison to their Fbxo7$^{R379G\ KI}$ littermates (Figure 62). This difference reaches statistical significance, when the difference in body

weight is being adjusted for by performing an analysis of covariance. The same can be observed when all 35 animals are being taken into account (data not shown).

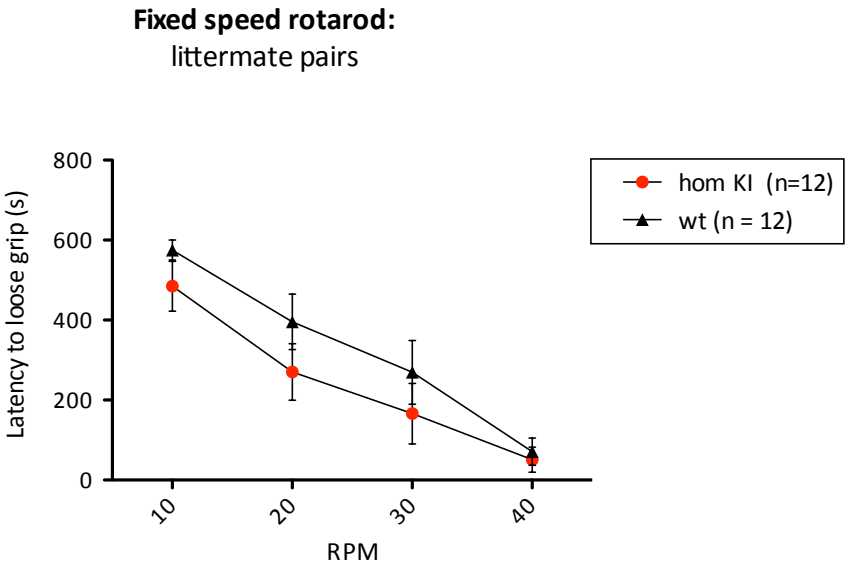

Figure 62: Fixed speed rotarod performance of littermate pairs

The mean latency to loose grip for each group (raw data, not adjusted for weight of the animals) is blotted for each trial of different rotational speeds used (data is expressed as mean ± S.E.M. either). The group difference between wt and homozygous R379G KI animals is not significant unless the difference in body weight is taken into account.

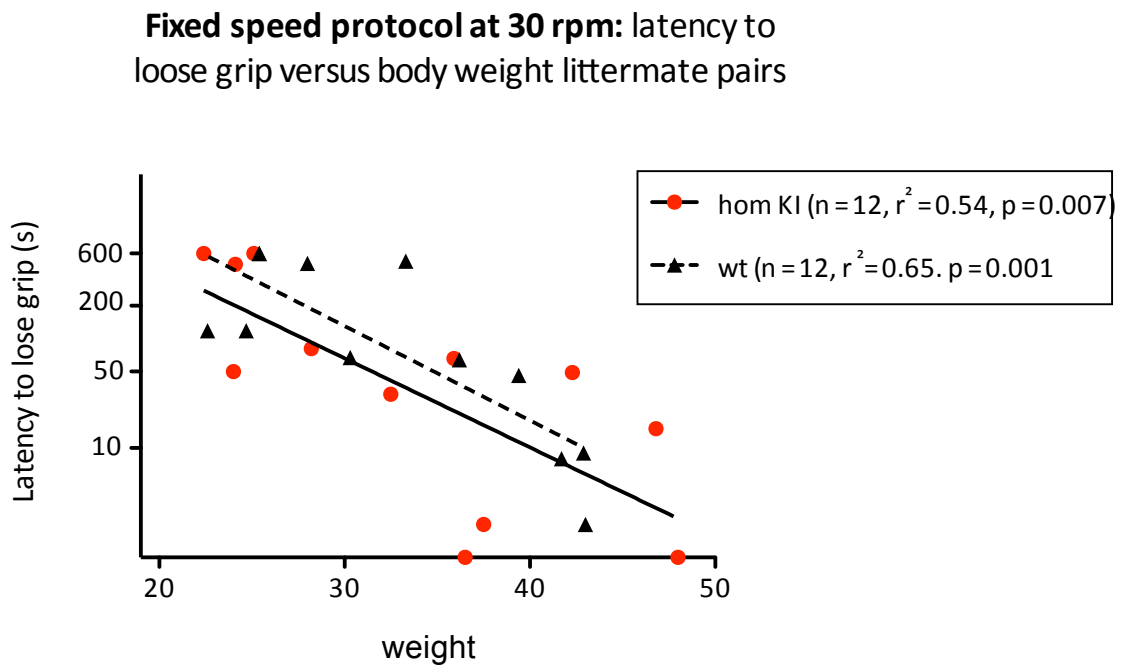

Figure 63: Relationship between bodyweight and fixed speed rotarod performance at 30rpm

Body weight of the individual animals is blotted against the latency to loose grip (Y scale as log10 of latency to loose grip in seconds) for the fixed speed rotarod performance at 30 rpm. Also shown are the respective regression lines for each genotype, demonstrating that the effect of body weight is the same on the performance for each genotype.

4.4 Discussion

My second result chapter is about the generation and characterization of the FBXO7 mouse model with knock-in of one of the human pathogenic mutations associated with early onset Pyramidal-Parkinsonism and my endeavour to identify endogenous FBXO7 interacting partners in the neuronal system. To focus my study on FBXO7 was particularly interesting because of several reasons: As a putative SCF E3 ubiquitin ligase component FBXO7 is likely to play a role in the ubiquitin proteasome system (UPS) and there is emerging evidence that the UPS plays an important role in the pathomechanism of Parkinson's disease and neurodegenerative processes in general(Cook et al., 2012; Dennissen et al., 2012; Ebrahimi-Fakhari et al., 2012). In comparison to the other genetic Parkinsonian syndromes for which animal models exist, *FBXO7* associated disease has a relatively complex clinical phenotype

(parkinsonism and pyramidal symptoms) with very early onset justifying the reasonable expectation that a FBXO7 animal model might recapitulate important aspects of the human phenotype. I have already explained in 4.2.1 why we chose to model the R378G mutation in the FBXO7 KI mouse model for my thesis: the particular residue is highly conserved as demonstrated in the sequence alignment of different FBXO7 homologues (Figure 29) and resides in very close proximity of the functionally important F-box domain of the FBXO7 protein. As the mouse homologue is one amino acid longer than the human one, the human R378G *FBXO7* mutation corresponds to R379G *Fbxo7* in the mouse. The R379G KI mouse model was commercially generated by Taconis Artemis® and in general, the *Fbxo7* R379G KI mouse line is viable and fertile.

The *Fbxo7* R379G KI mouse model was designed as a conditional model of cre-mediated deletion of exons 7 and 8, which should result in loss of function of the *Fbxo7* gene by deleting part of the F-box domain and by generating a frame shift from exon 6 to a premature stop codon in exon 9. Two observations were made: First, Cre-deletion of exons 7 and 8 of the *Fbxo7* gene (KO) did not yield any viable offspring in the homozygous state, while it was tolerated in the heterozygeous state. Second, the truncated mRNA product of the Cre-deletion KO allele was transcribed and translated resulting in the expression of a 323 AA long mutant protein, which in fact could be detected in the homozygous state in immortalized MEFs derived from embryo dissections at E 12.5 days. The truncated protein product lacks the C-terminal part of the Fbxo7 protein including the F-box domain. It is not clear from my study at which exact developmental stage from E12.5 onwards, the C-terminal truncation mutation exerts its lethal effect, as this would require staged dissections from E12.5 to the end of gestation ideally in combination with pathological evaluation of the embryos. This is clearly very interesting and will be followed up in future experiments. However, it could be speculated that the lethality of this particular mutant could be linked to the function of Fbxo7 as an SCF^{Fbxo7} E3 ubiquitin ligase given that the lack of the F-box domain prevents complex assembly. In fact, the C-terminal deletion MEF cell lines were used as an endogenous negative control for SCF complex formation and also as a cellular model for looking at expression levels of putative Fbxo7 interacting proteins.

4.4.1 **Availability of a sensitive and specific α mouse Fbxo7 antibody**

My specific aim was to study the function of Fbxo7 in the endogenous system rather than using heterologous overexpression. This necessitates the availability of a sensitive and specific antibody against Fbxo7. I show in section 4.2.3 that the in-house DSTT generated antibody which was raised against the whole mouse Fbxo7 protein, is able to detect and also immunoprecipitate endogenous Fbxo7. At least 2 FBXO7 isoforms are known to exist, but theoretically there could be more isoforms of different length depending on alternative splicing(Di Fonzo et al., 2009; Zhao et al., 2011). In the Fbxo7 tissue panel immunoblotting, I observe 2 main bands most likely corresponding to the longer isoform 1 (Uniprot Q3U7U3: 523AA, computed molecular weight using ProtParam tool by ExPASy(Wilkins et al., 1999): 58 kDa) and the shorter isoform 2 (Uniprot Q3UD93: 443 AA, computed molecular weight: 49 kDa) of the mouse Fbxo7 protein. There is a tissue-specific distribution pattern with the longer isoform 1 predominantly being present in brain, while for example both isoforms are present in an equal ratio in spleen and heart. Figure 33 also demonstrates the specificity of the Fbxo7 antibody: the Fbxo7 immunoblot of the truncated Fbxo7 protein in *Fbxo7* $^{\text{C-terminal trunk}}$ MEF lysates is devoid of any signals in the molecular weight range between > 37 kDa and 75kDa in the homozygous state (computed molecular weight of 35 kDa) while showing the signals for the larger isoform 1 and several smaller bands in the heterozygeous state. Additionally, the specificity of the antibody has been confirmed by proteomic fingerprinting as Fbxo7 of in-gel trypsin digested gel bands within the range of 50 – 75 kDa (as demonstrated in the proteomic data of the endogenous Fbxo7 immunoprecipitation experiments as shown in 4.2.11.).

4.4.2 **Reduced Fbxo7 protein levels in the homozygous Fbxo7 R379G mutant protein**

The next step was to look at the expression profile of the R379G knock-in insertion at the endogenous Fbxo7 locus by immunoblotting. Testing a panel of tissues derived from littermate wild-type, heterozygeous and homozygous R379G *Fbxo7* animals at 6 weeks as well as 6 months of age shows that Fbxo7 is widely expressed – at least in the tissues tested including brain, lung, spleen, liver, kidney, and heart. Additionally, it was evident that there was a consistent reduction in expression level of the Fbxo7

R379G mutant in the homozygous state. I quantified this difference for brain lysates derived from 3 littermate pairs of wild-type and homozygous R379G *Fbxo7* animals using the LI-COR system: In comparison to the wild-type Fbxo7 protein the expression of the homozygous R379G mutant is reduced by half (0.54). So far, brain tissue from patients with FBXO7 dependent disease has not become available for autopsy studies as yet. Recently, FBXO7 immunoreactivity was reported to be present in different regions of normal human brain samples, and the same pattern was observed in samples derived from patients with sporadic PD(Zhao et al., 2013). Furthermore, FBXO7 immunoreactivity was detected in α–synuclein-positive inclusion bodies, but not in tau-positive inclusions. With regards to the individual pathogenic mutations, the expression of the T22M *FBXO7* has been looked at in immortalized fibroblast cell lines from one heterozygeous carrier and 2 homozygous affected siblings in comparison to 3 unrelated controls. The T22M mutation only affects the longer isoform one, which was absent in the 2 homozygous patients and present in the healthy controls and decreased in the heterozygeous carrier in comparison to the controls. Immunoblotting of immortalized lymphoblast cell lines from one homozygous patient and 3 heterozygeous carriers of the R498X mutation as well as of one related and 3 unrelated healthy controls showed marked reduction of both bands for the mutation carriers and absent FBXO7 signals in the case of the homozygous patients(Zhao et al., 2011). This is the only available information on comparative expression levels between endogenous wild-type and 2 of the Fbxo7 disease mutants – T22M and R498X. No data is available on the expression of the FBXO7 R378G mutant. In the future, it would be critical to attempt to establish whether the R378G mutation in human patients reduces the expression of the FBXO7 protein and whether this is linked to the development of PD.

Given the lack of knowledge about the effect of the R378G *FBXO7* mutant on the protein levels of FBXO7 in humans, I can only speculate about the significance of the reduction on protein expression that I observe in the R379G KI *Fbxo7* mouse model: It could either be an artefact of the knock-in strategy or in fact recapitulate an intrinsic property of the R378/9G mutation. At least in the *in vitro* setting Skp1 has been suggested to stabilize the confirmation of F-box proteins, which in turn increases their expression levels(Yoshida et al., 2011). In an *in vitro* binding assay the

R378G FBXO7 mutant has been demonstrated to bind with lower affinity to Skp 1 than the wild-type FBXO7 protein(Nelson and Laman, 2011). If these observations were extrapolated into the *in vivo* system, the substitution of the basic, polar arginine with the neutral, non-polar glycine at residue 378 of the FBXO7 protein could result in a decrease in affinity to Skp1 and ultimately in a decrease in stability and hence expression level of the FBXO7 R378G mutant. If FBXO7 is indeed critical for protein quality control in the brain, reduced levels of FBXO7 in the brain could account for a threshold effect and thereby cause PD.

4.4.3 *In vivo* SCF^{Fbxo7} complex formation of the endogenous Fbxo7 wild-type protein

My thesis is centred around the hypothesis that Fbxo7 functions as the substrate recognizing subunit of a SCF E3 ubiquitin ligase complex and that the pathogenic effect of its human disease mutants is exerted by a perturbation thereof. A critical milestone was therefore to show that the wild-type Fbxo7 protein does in fact assemble into a SCF complex in the endogenous system. This is unequivocally demonstrated in sections 4.2.8 and 4.2.11: Immunoblotting of endogenous Fbxo7 immunoprecipitations from different mouse tissues – including brain - allows the detection of endogenous Cullin1, Skp1 and Rbx1. Furthermore, the identity of the SCF complex partners is also confirmed by proteomic fingerprinting of the endogenous Fbxo7 immunoprecipitation products from wild-type mouse brain lysates. This is the first time that the actual existence of the endogenous $SCF^{Fbxo7\text{-}wt}$ E3 ubiquitin ligase complex has been demonstrated.

4.4.4 *In vivo* SCF^{Fbxo7} complex formation of the endogenous Fbxo7 R379G mutant protein

The next important question was to establish whether the Fbxo7 R379G disease mutant was equally capable of SCF E3 ligase complex formation. I have already discussed in the previous chapter that SCF complex disruption could be a potential pathomechanistic effect of the human *FBXO7* disease mutants. Of all known pathogenic *FBXO7* mutants, the R378G mutant would have been the most likely candidate to disrupt SCF complex formation given the juxtaposition of the mutated amino acid residue to the functionally important F-box domain: The R378G mutation resides only 3 AA residues downstream of the F-box domain, which mediates binding

to the SCF complex via Skp1. Furthermore, *in vitro* data has already proposed that the R378G Fbxo7 mutant impairs SKP1 binding(Nelson and Laman, 2011). However, the corresponding R379G *Fbxo7* mouse mutant does not prevent Skp1 binding *in vivo*.

4.4.5 *In vivo* $SCF^{Fbxo7\text{-}R378G}$ complex formation of patient derived heterozygeous and homozygous R378G *FBXO7* cell lines

A very important finding is that SCF complex formation could also be reproduced in human derived, mutation specific fibroblast cell lines. Ultimately, the goal of my thesis is to gain insight into the physiological function of FBXO7 and the pathomechanism of the human disease mutants – in particular the R378G mutation. This section demonstrates that the R379G *Fbxo7* KI mouse model recapitulates an important biochemical property of the corresponding human mutation and serves as an additional step in the validation process of findings made in the R379G *Fbxo7* KI mouse model.

4.4.6 Identifying Fbxo7 interactors by means of proteomic fingerprint analysis of endogenous Fbxo7 immunoprecipitations from wild-type brain

A challenge in the field of SCF E3 ubiquitin ligases is the identification of substrates(Harper and Tan, 2012). The main problem is the transient and usually weak interaction between a substrate and its given E3 ligase, which is also the likely cause why the majority of substrates are potentially destined to escape the detection by the affinity-purification-mass-spectrometry approach (as discussed in the previous chapter). However, there are examples of partially retained substrate-ligase interactions after immunoprecipitation: β-TrCP was discovered to be the substrate-recognizing subunit of the E3 ligase that targets IκB for proteasomal degradation. Other examples include the ribonucleotide reductase M2 and CP110 as degradation targets of the F-box protein cyclin F(D'Angiolella et al., 2012; D'Angiolella et al., 2010). Most published reports investigate E3 ligase – substrate interactions in the tagged overexpression system. I have now adopted the affinity purification proteomics approach to the endogenous system; 3 large-scale replicates from wild-type brain have been performed and the combined list of proteins identified in the control experiments were subtracted from each set of hits identified in the endogenous Fbxo7 immunoprecipitation: of the 263 identified hits in replicate

1, 188 hits in replicate 2, and 238 hits in replicate 3, 42 proteins could be identified in every single set of experiments (Figure 39). Amongst these 42 proteins were FBXO7, Cullin 1 and Skp1 as the bait and members of the SCF E3 ligase complex (Rbx1 was not amongst the list of overlapping proteins as it was not identified in one of the 3 replicates). With regards to previously identified FBXO7 interactors, PI31 and Exportin 1 were also amongst this list. Otherwise the list contained multiple proteasomal subunits and several members of the COP9 signalosome complex, which is involved in regulating the activity of Cullin-dependent SCF E3 ligases (Kato and Yoneda-Kato, 2009; Lyapina et al., 2001). Altogether the association of Fbxo7 with the groups of aforementioned proteins supports the notion that Fbxo7 actually plays a role in the ubiquitin proteasome system and that the affinity purification – mass-spectrometry approach is well capable of reliably identifying the interaction between complex partners.

Amongst the remaining proteins in the list of overlapping hits that are present in all 3 endogenous Fbxo7 immunoprecipitations from brain, are 3 proteins that together function as an E3 SUMO ligase: RanBP2, RanGAP1*SUMO1 and Ubc9(Werner et al., 2012). RanBP2 in association with RanGAP1*SUMO1 / Ubc9 is one of the few known proteins or rather protein complexes with E3 SUMO ligase activity and the SUMOylation of RanGAP1 is not RanBP2-dependent, but rather a prerequisite for the association with it(Werner et al., 2012). RanBP2 is a large 357 kDa scaffolding protein involved in pleiotropic functions depending on context and respective binding partners: it is a component of the cytoplasmic filaments of the nuclear pore complex during interphase and after nuclear envelope breakdown is then present mainly in a soluble form, but occurs also attached to the kinethochor of the mitotic spindle(Joseph et al., 2002; Wu et al., 1995; Yokoyama et al., 1995). The fraction of RanBP2, RanGAP1*SUMO1 / Ubc9 that localizes to the kinetochore is dependent on the interaction with RanGTP and Exportin 1(Arnaoutov et al., 2005). Although RanGTP is not amongst the group of overlapping proteins, it was actually present in 2 of the 3 endogenous Fbxo7 immunoprecipitations from wild-type brain (replicate 1: mascot score – 160 (15 identified peptides and 31% sequence coverage; replicate 2: mascot score – 87 (11 identified peptides and 11% sequence coverage; molecular weight of Ran is 24 kDa). CRM1 is a nuclear transport receptor, which recognizes

proteins containing a leucine-rich nuclear export sequence in order to facilitate their nuclear export(Hutten and Kehlenbach, 2007). CRM1 has been described to interact with RanBP2 via its 8-fold zink finger motif (Figure 45)(Singh et al., 1999). The 2 known endogenous substrates of the RanBP2, RanGAP1*SUMO1 / Ubc9 E3 SUMO ligase comprise the Topoisomerase 2 α and Borealin; which both reside at the kinetochore / centromere(Dawlaty et al., 2008; Klein et al., 2009). Moreover, it has been shown that the localisation of Borealin to the centromere depends on CRM1(Knauer et al., 2006). CRM1 has also been suggested to be involved in the subcellular localization of FBXO7 via a functional leucin-rich recruitment motif localized near the N-terminal start of its F-box domain(Nelson and Laman, 2011). It is a matter of speculation whether Fbxo7 could actually be a target of RanBP2 mediated SUMOylation and be recruited to the complex by its interaction with CRM1. The detection of posttranslational modification with SUMO species *in vivo* can be difficult as usually only a small pool of a given protein is modified(Tatham et al., 2009). I have employed a dual-overexpression system to look into the possibility whether Fbxo7 could be sumoylated by SUMO1. While the positive control RanGAP1 demonstrates a band shift towards the higher-molecular weight species of its sumoylated form, no band shift is observed with either the wild-type or R378G mutant FBXO7. There are limitations to this approach and it is not possible to conclude that FBXO7 is not a SUMOylation target. All I can say is that I have not been able to gather further corroborating evidence for the SUMOylation of FBXO7 other than its physical association with the SUMOylation machinery.

I have also undertaken 2 large-scale endogenous Fbxo7 immunoprecipiations from homozygous R379G KI brain lysates in comparison to parallel immunoprecipitations from wild-type brain lysates. There was a remarkable overlap between the proteins that were identified in both wild-type as well as homozygous R379G KI *Fbxo7* experiments. Amongst the proteins identified for both genotypes were the bait, SCF complex partners Cullin 1, Skp1 as well as Exportin 1 and PI31. Amongst the other overlapping proteins were also RanBP2 and RanGAP1 as members of the RanBP2 E3 SUMO ligase, Reticulon 4, proteasomal subunits.

I have then undertaken further efforts to validate the affinity-purified proteomic hits. In the first instance I have demonstrated the ability to detect PI31, Exportin 1,

RanBP2, RanGAP1, Neurabin 2 as well as Nogo A and B (Reticulon 4) in the Fbxo7 immunoprecipitation products from both wild-type as well as homozygous R379G KI brain lysates. The gold standard for proving the validity of an interaction between 2 proteins is to show that they co-immunoprecipitate with each other. For this efficient antibodies directed against the proteins of interest are necessary that not only allow detection by immunoblotting, but also immunoprecipitation. For Reticulon 4 as well as RanBP2, in house DSTT generated antibodies are available. I have been able to detect Fbxo7 by co-immunoprecipitation with Reticulon 4 (Nogo B) as well as with RanBP2 as demonstrated in (Figure 51 and Figure 52). However, this was not a consistent finding in replicate experiments and only possible in large-scale experiments. I have been unable to identify Fbxo7 by mass-spectrometry in single immunoprecipitations of RanBP2 as well as Nogo B / Reticulon 4 from wild-type brain lysates. Unspecific cross-reactivity is a concern in the endogenous system, but the validation of each of the antibodies did not suggest that the α mouse Fbxo7 antibody detects either RanBP2 or Nogo A / B. Vice versa, there was no signal in keeping with the molecular size / pattern of Fbxo7 in the antibody validation for Nogo B (Reticulon 4) nor RanBP2 (data not shown). Overall, I have high confidence in the specificity of the α mouse Fbxo7 antibody used in this study given that it reliably detects Fbxo7 in complex with its SCF binding partners as well as other previously reported interacting proteins such as PI31 and Exportin 1. I can however not rule out that the Fbxo7 antibody itself impacts on the interaction between Fbxo7 and its substrates. An alternative explanation for why it is difficult to co-immunoprecipitate Fbxo7 with putative interacting partners is that Fbxo7 interacts with only a small pool of a posttranslationally modified form of the respective protein. The posttranslationally modification is then either reversed during the affinity purification or the interaction of the small pool of the modified protein with Fbxo7 is diluted below the threshold of detection.

In the end, there is one main difficulty in the evaluation of the significance of any detected interaction between Fbxo7 and other proteins: the lack of a functional read-out. The finding that FBXO7 actually assembles into a SCF^{FBXO7} E3 ubiquitin ligase complex *in vivo* has never been shown before and no *in vitro* or *in vivo* assay

exists that would allow monitoring the Fbxo7-dependent E3 ligase activity of the SCF^{FBXO7} complex against a pool of validated FBXO7 substrates.

4.4.7 Behavioural and motor phenotypic analysis of the R379G *Fbxo7* KI mouse model

The main reason for generating the R379G *Fbxo7* KI mouse line was to have sufficient neuronal material available for the biochemical study of the effect of one of the human pathogenic mutations at the endogenous Fbxo7 locus and to compare it with its wild-type counterpart. The behavioural and motor phenotypic analysis is only a small part of this study. Many PD mouse models have been developed over the last 3 decades, either based on neurotoxicity or genetic approaches. Prior to the identification of genetic factors for PD, neurotoxic models using compounds that produce reversible (for example reserpine) or irreversible (1-mehyl-1,2,3,6-tetrahydropiridine, 6-hydroxydopamine, paraquat, or rotenone) effects mainly on the basal ganglia were used(Tieu, 2011). In genetic PD mouse models overexpression is usually used the mimic the effect of autosomal dominant mutations as they are regarded as a "gain of function", while for modelling autosomal recessive genes – regarded to elicit their pathogenic effects via "loss of function' - either gene knock-out or knock-in of a particular pathogenic mutation is used(Lee et al., 2012). The expectation is that these mouse models can be utilized for gaining insight into disease mechanisms, but with the small molecules' therapeutic approach at the horizon that they could potentially be exploited for screening and testing new therapeutic compounds or the discovery of biomarkers. So far, therapies are mainly symptomatic rather than targeted at the actual disease process and a diagnosis of PD on clinical grounds is only possible when the disease process is already significantly advanced. Ideally, a PD mouse model should recapitulate the progressive key clinical and neuropathological hallmarks of PD. So far, none of the existing genetic models meets these criteria in full. Many different genetic mouse models exist for α-synuclein and LRRK2, the 2 autosomal dominant forms of genetic PD (reviewed in(Dawson et al., 2010; Lee et al., 2012)). With regards to autosomal recessive PD, several groups have generated constitutive PARKIN knock-out mice, which have failed to show any dopaminergic cell loss and only minimal motor phenotypes(Goldberg et al., 2003; Itier et al., 2003; Von Coelln et al., 2004). A viral

induced conditional PARKIN knock-out mouse model does show progressive dopaminergic cell loss 10 months after PARKIN deletion as well as accumulation of Parkin E3 ligase substrates and mitochondrial dysfunction(Shin et al., 2011). The PINK1 knock-out mouse models including one shRNA-mediated knock-down approach have also not resulted in significant nigrostriatal degenerative phenotypes, but also show mild mitochondrial abnormalities and subtle deficits in dopamine metabolism(Gispert et al., 2009; Kitada et al., 2007; Zhou et al., 2007). One of these PINK1 mouse models also showed a mild group difference in dopamine content in the striatum and reduces spontaneous voluntary activities of the genetically modified mice in comparison to the wild-type(Gispert et al., 2009).DJ-1 knock-out mice present with a similarly mild phenotype as the models for PINK1 and PARKIN(Chen et al., 2005; Goldberg et al., 2005). Even the triple knock-out of PINK1/PARKIN/DJ-1 fails to develop a nigrostriatal phenotype(Kitada et al., 2009). The assessment of the respective motor phenotypes of these mouse models is incongruent, making a direct comparison difficult. For the evaluation of the R379G *Fbxo7* KI mouse model I have restricted my analysis to one time-point at a mean age of 10 months. I first wanted to establish whether there was a group difference between the wild-type and R379G KI *Fbxo7* genotype at a later stage during the life span of the animals before embarking on a longitudinal study with repeated testing. The behavioural phenotyping in this study mainly focuses on motor function using rotarod and gait analysis. PD, however, also manifests with many non-motor features and these can equally be explored by a more behavioural phenotyping approach (reviewed in (Taylor et al., 2010)). The open field test used in this study to assess spontaneous locomotor activity can also reflect anxiety-like behaviours(George et al., 2008; Taylor et al., 2010). Overall, there was no group difference in the general neurological SHERPA screen, the open field spontaneous locomotor assessment or the gait analysis between the wild-type and homozygous R379G *Fbxo7* KI animals. It is recognized that body weight is a significant confounder of rotarod performance(Brooks and Dunnett, 2009). Gender significantly influenced body weight of the animals, but not genotype (Figure 57). Although the housing site – Ninwells or CLS campus – had an unexpected effect on body weight, this did not result in a bias of my analysis as paired animals were mainly housed at the same location. A very exciting fiding was that there was a difference in motor performance

as measured by the rotarod analsysis between the wild-type and the homozygeous R379G KI *FBbxo7* genotype: While there was a trend towards poorer performance of the R379G Fbxo7 KI littermate pairs in the fixed speed rotarod analysis, there was a significant impairement of the R379G KI animals in the accelerating rotarod analysis. The 2 operational rotarod approaches – accelerating speed versus fixed speed – have been suggested to be differentially sensitive to different aspects of motor function: While during the accelerating protocol, mice loose their grip due to the changing requirements of the accelerating rod, mice don't have to adjust their stepping pattern during the fixed-speed variant(Brooks and Dunnett, 2009; Monville et al., 2006). For the analysis of the Fbxo7 KI mosue model, the accelerating protocol is more sensitive to pick up a difference between the 2 genotypes.

Overall, the finding that there is a significant difference in rotarod performance between the wild-type and R379G *Fbxo7* KI animals is very encouraging. It warrants a longitudinal study across different time points and beyond the age of 10 months. The longitundinal study will help to clarify at which age the mutant animals devlop a motor eficit and whether this deficit is progressive over time. Furthermore, it will be crucial to correlate the deficit in motor performance with a neurodegenerative phenotype in immunopathological mouse brain studies. Littermate genotype-matched pairs have been sacrificed, subjected to whole body perfusion with a fixating reagent and brains have been harvested for further processing for immunohistochemistry. It has to be taken into account that no neuropathological study of human *FBXO7* dependent disease has been reported as yet.

4.4.8 **Summary of Chapter 4**

The second result chapter is dedicated to the characterization of the *Fbxo7* knock-in mouse model of one of the pathogenic *FBXO7* mutations (R378G in humans) and the endogenous study of Fbxo7 in brain comparing the wild-type to the homozygous Fbxo7 KI genotype. A first finding is that Fbxo7 is widely expressed in different tissues and that the *R379G* Fbxo7 KI mouse displays a hypomorphic expression pattern in the homozygous state. In brain lysates, the difference amounts to a reduction by half. If this is not an intrinsic artefact of the genetic mouse model, the reduction in protein levels of the pathogenic mutant could amount to a pathomechanistic threshold effect. A second important and novel finding is that

endogenous Fbxo7 assembles together with Cullin 1, Skp1, and Rbx1 to form the SCF^{Fbxo7} E3 ubiquitin ligase complex *in vivo*. The demonstration that the homozygous R379G Fbxo7 mutant is equally capable of SCF E3 ligase formation, a feature that is retained in human patient-derived homogenous R378G FBXO7 fibroblast cell lines. This allows the conclusion that the pathogenic R378G *FBXO7* mutant does not exert its pathogenicity via disruption of the SCF E3 ligase complex. Using endogenous Fbxo7 affinity purification in combination with mass-spectrometry has confirmed PI31 and Exportin 1 to not only interact with Fbxo7 in heterologous systems, but also on the endogenous level in brain samples of wild-type and homozygous R379G *Fbxo7* KI mice. I have identified potentially novel Fbxo7 interacting partners of which the RanBP2/ranGAP1*SUMO1/UBC9 E3 SUMO ligase complex is one of the most exciting findings. This warrants further exploration as it could be a further example of the crosstalk between the ubiquitylation and sumoylation system. Last but not least, the preliminary phenotype analysis of the R379G *Fbxo7* KI mouse line has revealed a significant motor deficit of the homozygous KI animals in comparison to the wild-type genotype. A neuropathological study to assess whether this deficit in motor performance correlates to a dopaminergic neuronal cell loss is still outstanding.

5 Quantitative proteomics comparing the proteome / ubiquitinome of the wild-type and R379G *Fbxo7* KI mouse and set up of an *in vitro* Fbxo7 dependent ubiquitylation assay

In this chapter, I am focusing on quantitative proteomics comparing either the whole proteome in mouse brain or the pool of ubiquitin modified proteins in MEF lysates between the wild-type and homozygous R379G *Fbxo7* KI genotype. The working hypothesis of my thesis is that FBXO7 functions as the substrate recognizing subunit of an SCF E3 ubiquitin ligase complex, and as such is involved in targeting proteins for degradation by the ubiquitin proteasome system. Quality control and regulation of abundance of such proteins may be crucial for neuronal health and perturbation thereof a first step towards FBXO7 dependent disease. Therefore, I was interested in looking at proteins whose abundance is either decreased or increased in whole brain

lysates dependent on the presence of the R379G Fbxo7 KI mutation in its homozygous state. Here, *ex vivo* stable isotope dimethyl labelling at peptide level was used to prepare the brain samples of the 2 genotypes for quantitative proteomics(Boersema et al., 2009). In another approach I set out to systematically identify differences in ubiquitylation targets in a site-specific manner using quantitative di-GLY capture proteomics(Kim et al., 2011; Wagner et al., 2011). Quantitative di-GLY capture proteomics combines *in vivo* SILAC labelling with antibody-based affinity enrichment of "di-GLY remnant motifs"- containing peptides prior to proteomic profiling of the wild-type in comparison to the homozygous R379G *Fbxo7* KI ubiquitinome in MEF lysates (Figure 65). This chapter also includes the set up of an *in vitro* FBXO7 ubiquitylation assay as the identification of putative FBXO7 substrates necessitates their validation with a functional read-out. A prerequisite was the recombinant expression of all the components of the SCF^{FBXO7} E3 ubiquitin ligase complex, which is not a trivial undertaking, and the *in vitro* SCF^{FBXO7} complex formation. Subsequently, I have successfully set up an assay to monitor FBXO7 free ubiquitin chain production and have made preliminary progress in assaying substrate ubiquitylation. I received significant help from the following people in the MRC Unit: Dr. Matthias Trost helped with the *ex vivo* dimethyl labelling of the brain samples for the whole proteome analysis in wild-type and homozygous R379G *Fbxo7* KI brain samples. Dr. Kamila Chughtai, a postdoctoral researcher in Dr. Patrick Pedriolis' laboratory supported me in the setting up and adopting the quantitative di-GLY capture protocol and performed the mass-spectrometry analysis. Dr. Axel Knebel and his team – Dr. Richard Ewan, Mr. Dan Fountaine, and Miss Clare Johnson – were critical for the production of the required recombinant proteins and helped me in the development of the *in vitro* FBXO7 assay.

5.1 Differential enrichment of the ubiquitylated proteome from SILAC labelled wt and homozygous R379G *Fbxo7* KI MEFs

My hypothesis throughout this thesis is that FBXO7 functions as the substrate recognizing subunit of an SCF^{FBXO7} complex and that the pathogenicity of the human disease mutants is linked to the FBXO7 – dependent function of the E3 ubiquitin

ligase activity of the SCF complex. I have therefore embarked on a differential “di-Glycine” capture experiment that aims to systematically identify Fbxo7-dependent ubiquitylation targets in a site-specific manner while comparing the wild-type with the homozygous R379G Fbxo7 KI genotype in SILAC labelled MEFs. The underlying principle of the “di-Glycine” capture experiment is that an antibody is available with specificity for the signature peptide (di-Glycin), which is left on an ubiquitylated protein after tryptic digestion; affinity purification with this antibody then allows enrichment of ubiquitylated species at peptide level(Kim et al., 2011; Wagner et al., 2011; Xu et al., 2010) (Figure 64).

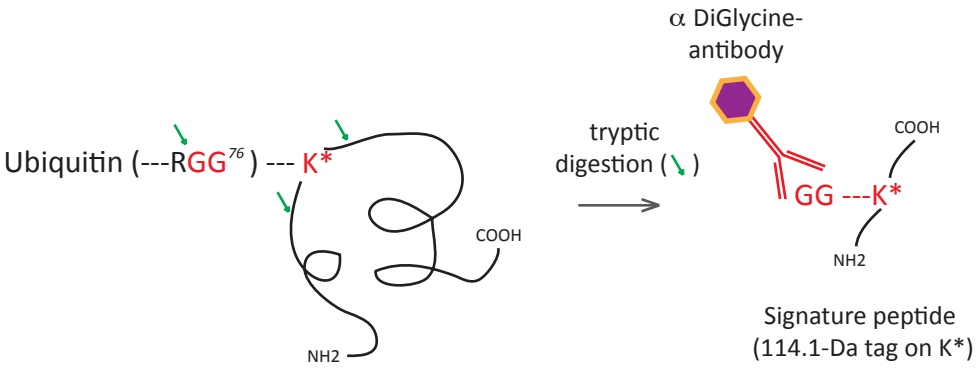

Figure 64: Principle of the Di-glycine enrichment of ubiquitylated species at peptide level

After tryptic digestion of an ubiquitin-modified protein, a di-Glycine remnant of Ubiquitin (signature) remains covalently attached to the lysine residue (K*) of the ubiquitinylated protein that is resistant to further tryptic digestion. The Di-glycine antibody is used for enriching ubiquitylated proteins at peptide level. The di-Glycin tag results in a 114.1 Da mass-shift of the ion fragment and forms the basis of site-specific detection of ubiquitylation.

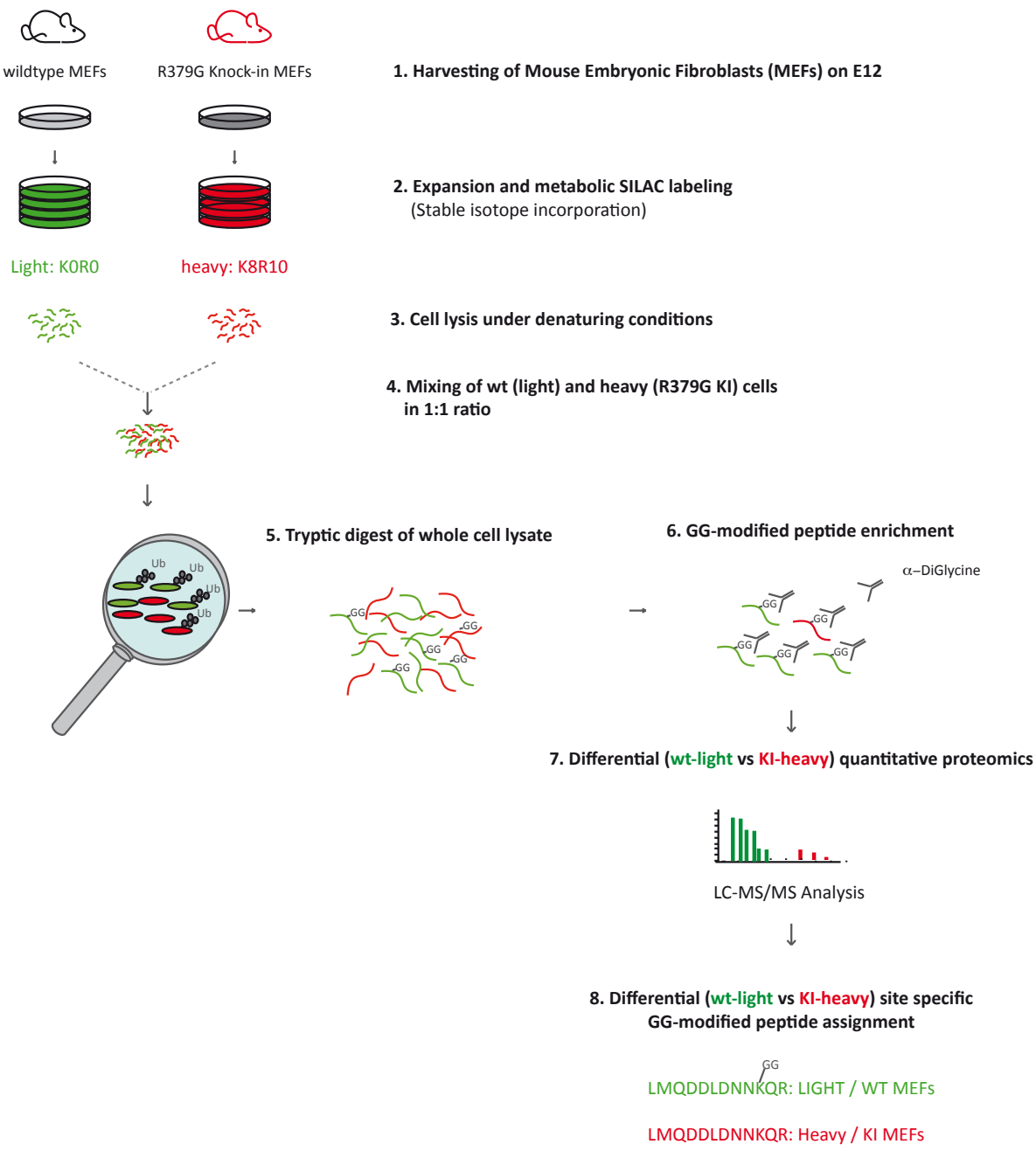

Figure 65: SILAC - base quantitative di-Glycine capture proteomics to compare the ubiquitinome of wt and hom R379G *Fbxo7* MEFs

Immortalized mouse embryonic fibroblasts derived from littermate wt and homozygous R379G Fbxo7 KI embryos (E12.5) were grown in differential SILAC media until full label incorporation was achieved (>98%). Cells were then harvested under denaturing conditions, mixed in a 1:1 ratio, and digested with trypsin prior to affinity purification of di-Glycin-peptides. The sample was then analysed by mass-spectrometry; while the differential SILAC labelling allowed determining the relative abundance of each peptide according to genotype, the intact di-glycine modification of the peptides yields the specific site reveals the specific site of the ubiquitin modification of the original protein. (Not shown are the various C-18 column clean up steps the basic reverse phase fractionation prior to the Di-Glycine-enrichment step).

The labelling efficacy for the homozygous R379G Fbxo7 KI MEF cell lines was determined as >98%, which is considered “complete” incorporation of the “heavy” stable isotopes Lysine and Arginine (K8, R10) (Figure 66). For a global comparison between the wild-type and homozygous R379G Fbxo7 KI MEFs, a small fraction of each sample was separately digested with trypsin and subjected to mass-spectrometry: The same number of proteins (about 2500) with an 80% overlap between the wild-type and homozygous R379G Fbxo7 KI MEFs was found (data not shown).

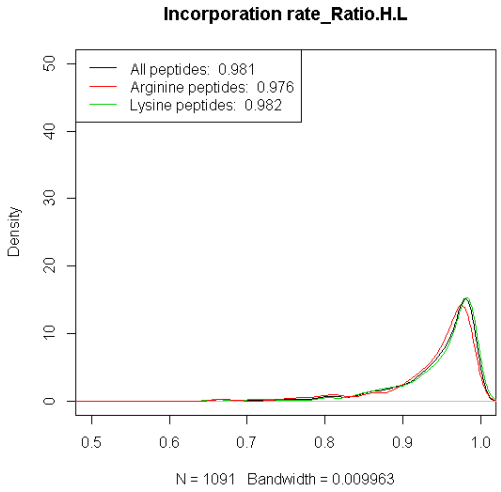

Figure 66: Labeling efficacy of the hom R379G Fbxo7 KI MEF cell line

The graph shows the incorporation rate of the “heavy” SILAC label for the hom R379G Fbxo7 KI MEF cell line (K8R10). Arginine and Lysine incorporation are blotted individually as well as together. The y-axis indicates the percentage of peptides labelled versus the percentage of label incorporation on the x-axis. Overall, there is an incorporation efficacy of >98%, which is considered “complete” labelling efficacy.

Two biological replicate experiments have been performed. Using the described workflow in Figure 65, 2060 unique endogenous ubiquitylation sites that were mapped to a single lysine with a localisation probability of over 0.9 in replicate 1 and 999 unique endogenous ubiquitylation sites were identified in replicate 2 (Figure 67). The differential SILAC –based proteomics allowed determining the relative abundance of these peptides depending on genotype – ion fragments originating

from wild-type MEFs ("light"/K0R0) had a relative lower mass than those derived from the heavy labelled homozygous R379G *Fbxo7* KI MEFs. Therefore, the following question could be asked: are there any ubiquitinylated peptides that are more abundant in either the wild-type or the homozygous R379G *Fbxo7* KI genotype – reflecting proteins that are ubiquitinylated in an *Fbxo7* genotype - dependent manner? Peptides were considered to be differentially ubiquitinylated if there was an at least 2 fold difference in their abundance between the 2 genotypes (expressed as an XPRESS ratio of either ≥ 2 or ≤ 0.5): Di-Glycine peptides that were at least 2-fold more abundant in the wild-type background and which are present in both replicate experiments are listed in Table 5-1 (XPRESS ratio ≥ 2). These peptides reflect proteins that are preferentially ubiquitinylated in the wild-type Fbxo7 genotype. Di-glycine peptides with were at least 2-fold more abundant in the homogenous R379G Fbxo7 KI genotype and which were identified in both replicate experiments are found in Table 5-2 (XPRESS ratio ≤ 0.5). These peptides reflect proteins that are preferentially ubiquitinylated in the R379G Fbxo7 KI *Fbxo7* genotype. Amongst the former group –preferential ubiquitinylation status in the *Fbxo7* wild-type background – were peptides that could be mapped to 3 closely related proteins: VDAC 1,2, and 3. Given that each of these 3 proteins was identified with several Di-glycine modified peptides that even had the highest Xpress ratios identified in this study, VDAC 1, 2 and 3 were considered to be potentially differential - ubiquitinylation targets of the Fbxo7 wild-type protein with high confidence.

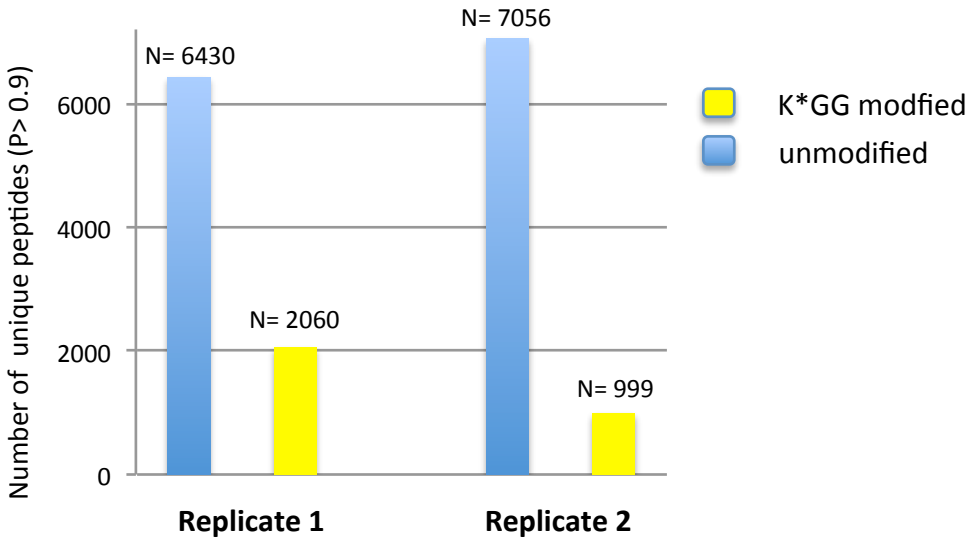

Figure 67: Enrichment efficacy of the DiGlycine affinity purification of replicates 1 and 2

In replicate 1, 6430 distinct peptides have been identified without the signature peptide (K*GG) indicative of ubiquitinylation at protein level. 2060 peptides were identified with a distinct site of K*GG modification(P>0.9, localization probability). In replicate 2, 7056 unmodified sites and 999 modified sites were identified. (Enrichment efficacy for replicate 1: 24%, for replicate 2: 12.4%)

Uniprot	Protein	Peptide	REPLICATE 1		REPLICATE 2	
			Probability	Ratio (wt-light / R379G KI - heavy)	Probability	Ratio (wt-light / R379G KI - heavy)
Q6P5G6	UBXN7	R.APIPQK[242.14]QEILVEPEPLFGAPK.R	1.00	1.9	0.99	2.17
Q6P5G6	UBXN7	R.APIPQK[242.14]QEILVEPEPLFGAPK.R	1.00	1.9	1.00	2.17
Q6P5G6	UBXN7	R.APIPQK[242.14]QEILVEPEPLFGAPK.R	1.00	1.9	1.00	2.09
Q6P5G6	UBXN7	R.APIPQK[242.14]QEILVEPEPLFGAPK.R	1.00	1.9	1.00	2.09
no entry	Peptidyl-prolyl cis-trans isomerase	R.VSFELFADK[250.15]VPK[136.11].T	1.00	2	1.00	2.03
Q3TKJ1	Bcat1 Uncharacterized protein	R.AK[242.14]DLIITPATVLK.E	0.93	2.26	0.94	5.15
Q5SV64	Myosin 10	R.Q[111.03]EEELQAK[242.14]DEELLK.V	1.00	2.37	1.00	2.03
Q5SV64	Myosin 10	R.Q[111.03]EEELQAK[242.14]DEELLK.V	1.00	2.37	1.00	2.03
Q91X82	Txnip protein	K.SFEVVFNDPEKVYGSGEK[242.14]VAGR.V	0.98	2.68	0.98	4.94
Q91X82	Txnip protein	K.SFEVVFNDPEKVYGSGEK[242.14]VAGR.V	0.98	2.68	1.00	4.93
Q91X82	Txnip protein	K.SFEVVFNDPEK[136.11]VYGSGEK[250.15]VAGR[166.11].V	0.97	2.7	0.99	5.05
Q91X82	Txnip protein	K.SFEVVFNDPEK[136.11]VYGSGEK[250.15]VAGR[166.11].V	0.97	2.7	0.91	5.05
Q91X82	Txnip protein	K.SFEVVFNDPEK[136.11]VYGSGEK[250.15]VAGR[166.11].V	1.00	2.7	0.99	5.05
Q91X82	Txnip protein	K.SFEVVFNDPEK[136.11]VYGSGEK[250.15]VAGR[166.11].V	1.00	2.7	0.91	5.05
Q5SV64	Myosin 10	R.Q[111.03]EEELQAK[242.14]DEELLK.V	1.00	3.23	1.00	2.03
Q5SV64	Myosin 10	R.Q[111.03]EEELQAK[242.14]DEELLK.V	1.00	3.23	1.00	2.03
O88543	Cops3	L.DVDMMDIC[160.03]K[242.14]ENGAYDAK.H	1.00	4.19	0.62	2.55
O88543	Cops3	L.DVDMMDIC[160.03]K[242.14]ENGAYDAK.H	1.00	4.19	0.62	2.55
P62984	Uba52	R.LIFAGK[250.15]QLEDGR[166.11].T	1.00	4.27	1.00	120.1
P62984	Uba52	R.LIFAGK[250.15]QLEDGR[166.11].T	1.00	10.04	1.00	120.1
Q60930	VDAC 2	K.SC[160.03]SGVEFSTSGSSNTDTGK[242.14]VSGTLETK.Y	0.95	11.54	0.64	5.5
Q60930	VDAC 2	K.SC[160.03]SGVEFSTSGSSNTDTGK[242.14]VSGTLETK.Y	0.99	11.54	0.64	5.5
Q60932-1	VDAC 1	K.TKSENGLEFTSSGSANTETTK[242.14]VNGSLETK.Y	0.98	12.48	0.73	3.73
Q60930	VDAC 2	K.SC[160.03]SGVEFSTSGSSNTDTGK[242.14]VSGTLETK.Y	0.98	15.4	0.64	5.5
Q60930	VDAC 2	K.SC[160.03]SGVEFSTSGSSNTDTGK[242.14]VSGTLETK.Y	0.99	15.66	0.64	5.5
Q60931	VDAC 3	K.SC[160.03]SGVEFSTSGHAYTDTGK[250.15]ASGNLETK[136.11].Y	NA	NA	0.71	2.04

Table 5-1: List of di-Glycine modified peptides that are preferentially ubiquitinylated in the Fbxo7 wild-type background (> 2-fold)

List of di-Glycine modified peptides that are more likely (≥2-fold difference in XPRESS ratio of wild-type (light) versus R379G KI (heavy) labled MEFs) ubiquitinylated in the *Fbxo7* wild-type genotype in MEFs in at least 1 of the 2 biological replicate experiments. The table list each of the identified peptides and corresponding protein name, Uniprot accession number, protein name, peptide sequence, as well as localization probability. The XPRESS ratio is a quantitation tool for MS/MS analysis.

Uniprot	Protein	Peptide	REPLICATE 1		REPLICATE 2	
			Probability	Ratio (wt-light / R379G KI - heavy)	Probability	Ratio (wt-light / R379G KI - heavy)
P26645	Myristoylated alanine-rich C-kinase	K.TAAK[250.15]GEATAER[166.11]PGEAAVASSPSK[136.11].A	0.94	0.5	1.00	0.26
Q91WG2-1	Isoform 2 of Rab GTPase-binding effector	K.DSISSYETQIAALK[250.15]QER[166.11].Q	1.00	0.5	1.00	0.33
Q91WG2-1	Isoform 2 of Rab GTPase-binding effector	K.DSISSYETQIAALK[250.15]QER[166.11].Q	1.00	0.5	1.00	0.33
Q91WG2-1	Isoform 2 of Rab GTPase-binding effector	K.DSISSYETQIAALK[242.14]QER.Q	1.00	0.5	1.00	0.35
Q91WG2-1	Isoform 2 of Rab GTPase-binding effector	K.DSISSYETQIAALK[242.14]QER.Q	1.00	0.5	1.00	0.35
Q91WG2-1	Isoform 2 of Rab GTPase-binding effector	K.DSISSYETQIAALK[242.14]QER.Q	1.00	0.5	1.00	0.35
Q91WG2-1	Isoform 2 of Rab GTPase-binding effector	K.DSISSYETQIAALK[242.14]QER.Q	1.00	0.5	1.00	0.35
Q91WG2-1	Isoform 2 of Rab GTPase-binding effector	K.DSISSYETQIAALK[250.15]QER[166.11].Q	1.00	0.5	1.00	0.35
Q91WG2-1	Isoform 2 of Rab GTPase-binding effector	K.DSISSYETQIAALK[250.15]QER[166.11].Q	1.00	0.5	0.98	0.35
Q91WG2-1	Isoform 2 of Rab GTPase-binding effector	K.DSISSYETQIAALK[250.15]QER[166.11].Q	1.00	0.5	1.00	0.35
Q91WG2-1	Isoform 2 of Rab GTPase-binding effector	K.DSISSYETQIAALK[250.15]QER[166.11].Q	1.00	0.5	0.98	0.35
Q64282	Interferon-induced protein with tetratricopeptide repeats 1	K.EAEALIQSEQLSK[250.15]R[166.11].S	1.00	0.48	1.00	0.22
P63024	Vesicle-associated membrane protein 3	R.DQK[242.14]LSELDDRADALQAGASQFETSAAK.L	0.99	0.48	1.00	0.41
P63024	Vesicle-associated membrane protein 3	R.DQK[242.14]LSELDDRADALQAGASQFETSAAK.L	0.99	0.48	1.00	0.41
P63024	Vesicle-associated membrane protein 3	R.DQK[242.14]LSELDDRADALQAGASQFETSAAK.L	1.00	0.47	1.00	0.41
P63024	Vesicle-associated membrane protein 3	R.DQK[242.14]LSELDDRADALQAGASQFETSAAK.L	1.00	0.47	1.00	0.41
P63024	Vesicle-associated membrane protein 3	R.DQK[242.14]LSELDDRADALQAGASQFETSAAK.L	1.00	0.47	1.00	0.41
P63024	Vesicle-associated membrane protein 3	R.DQK[242.14]LSELDDRADALQAGASQFETSAAK.L	1.00	0.47	1.00	0.41
P63024	Vesicle-associated membrane protein 3	R.DQK[250.15]LSELDDR[166.11]ADALQAGASQFETSAAK[136.11].L	1.00	0.47	1.00	0.42
P63024	Vesicle-associated membrane protein 3	R.DQK[250.15]LSELDDR[166.11]ADALQAGASQFETSAAK[136.11].L	1.00	0.47	1.00	0.42
P63024	Vesicle-associated membrane protein 3	R.DQK[250.15]LSELDDR[166.11]ADALQAGASQFETSAAK[136.11].L	1.00	0.47	1.00	0.42
P63024	Vesicle-associated membrane protein 3	R.DQK[250.15]LSELDDR[166.11]ADALQAGASQFETSAAK[136.11].L	1.00	0.47	1.00	0.42
Q9JKF1	Ras GTPase-activating-like protein	K.SLNIK[250.15]TDPVDIYK[136.11].S	0.95	0.44	0.99	0.1
Q9JKF1	Ras GTPase-activating-like protein	K.SLNIK[250.15]TDPVDIYK[136.11].S	0.95	0.44	1.00	0.13
Q9JKF1	Ras GTPase-activating-like protein	K.SLNIK[250.15]TDPVDIYK[136.11].S	0.97	0.35	0.99	0.1
Q9JKF1	Ras GTPase-activating-like protein	K.SLNIK[250.15]TDPVDIYK[136.11].S	0.97	0.35	1.00	0.13
Q9JKF1	Ras GTPase-activating-like protein	K.SLNIK[250.15]TDPVDIYK[136.11].S	0.98	0.29	0.99	0.1
Q9JKF1	Ras GTPase-activating-like protein	K.SLNIK[250.15]TDPVDIYK[136.11].S	0.98	0.29	1.00	0.13
Q63918	Serum deprivation-response protein	R.DNSQVNAVTVHTLLDK[250.15]L.V	1.00	0.21	1.00	0.24
Q63918	Serum deprivation-response protein	R.DNSQVNAVTVHTLLDK[250.15]L.V	0.95	0.21	1.00	0.24
P58774-1	Tropomyosin beta chain	R.C[143.00]K[250.15]QLEEEQQALQK[136.11].K	1.00	0.16	1.00	0.29
P58774-1	Tropomyosin beta chain	R.C[143.00]K[250.15]QLEEEQQALQK[136.11].K	1.00	0.16	1.00	0.29
P58774-1	Tropomyosin beta chain	R.C[143.00]K[250.15]QLEEEQQALQK[136.11].K	1.00	0.14	1.00	0.29
P58774-1	Tropomyosin beta chain	R.C[143.00]K[250.15]QLEEEQQALQK[136.11].K	1.00	0.14	1.00	0.29

Table 5-2: List of di-Glycine modified peptides that are preferentially ubiquitinylated in the Fbxo7 R379G KI background (> 2-fold)

List of di-Glycine modified peptides that are more likely (with a $\geq$ 2-fold difference) ubiquitinylated in the Fbxo7 R379G KI genotype in MEFs ($\leq$ 0.5 XPRESS ratio of wild-type (light) versus R379G KI (heavy) labled MEFs) in at least 1 of the 2 biological replicate experiments. The table list each of the identified peptides and corresponding protein name, Uniprot accession number, protein name, peptide sequence, as well as localization probability. The XPRESS ratio is a quantitation tool for MS/MS analysis

Uniprot Ref	Protein	Peptide	REPLICATE 1		REPLICATE 2		KGG site
			Probability	Ratio (wt-light / R379G KI - heavy)	Probability	Ratio (wt-light / R379G KI - heavy)	
Q60932	VDAC 1	K.TKSENGLEFTSSGSANTETTK[242.14]VNGSLETK.Y	0.97	12.48	0.96	3.73	**K66**
Q60930	VDAC 2	K.SC[160.03]SGVEFSTSGSSNTDTGK[242.14]VSGTLETK.Y	0.97	11.54	0.95	5.5	**K64**
Q60930	VDAC 2	K.SC[160.03]SGVEFSTSGSSNTDTGK[242.14]VSGTLETK.Y	1.00	11.54	0.95	5.5	**K64**
Q60930	VDAC 2	K.SC[160.03]SGVEFSTSGSSNTDTGK[242.14]VSGTLETK.Y	0.99	15.4	0.95	5.5	**K64**
Q60930	VDAC2	K.SC[160.03]SGVEFSTSGSSNTDTGK[242.14]VSGTLETK.Y	1.00	15.66	0.95	5.5	**K64**
Q60931	VDAC 3	K.SC[160.03]SGVEFSTSGHAYTDTGK[242.14]ASGNLETK.Y	1.00	5.71	1.00	1.88	**K53**
Q60932	VDAC 1	K.LTFDSSFSPNTGK[242.14]K.N	0.96	20.98			**K122**
Q60932	VDAC 1	K.LTFDSSFSPNTGK[242.14]K.N	0.99	20.98			**K122**
Q60930	VDAC 2	K.LTFDTTFSPNTGK[242.14]K.S	0.91	20.9			**K121**
Q60930	VDAC 2	K.LTFDTTFSPNTGK[242.14]K.S	0.99	20.9			**K121**
Q60930	VDAC 2	K.LTFDTTFSPNTGK[242.14]K.S	0.99	20.9			**K121**
Q60931	VDAC 3	K.LTLDTIFVPNTGKK[242.14].S	0.95	8.66			**K109**

Table 5-3: Differential site-specific K*GG modifications of VDAC 1, 2, and 3 in wild-type and R379G *Fbxo7* KI MEFs

List of all di-Glycine modified lysine peptides that mapped to either VDAC 1, 2, or 3 and had an Xpress ratio (Ratio wild-type (light) / R379G KI (heavy)) of over 2 in any of the 2 biological replicate experiments and a localization probability of > 0.9. Shown are Uniprot accession number, protein name, peptide sequence, and for each replicate probability, ions, and Xpress ratio as well as the specific modification site (as identified in the respective mouse VDAC protein).

5.1.1 **K*GG-specific ubiquitylation sites of VDAC 1, 2, and 3**

Table 5-3 shows the respective lysine residues of VDAC 1, 2 and 3 that were found to be preferentially ubiquitinylated in the *Fbxo7* wild-type genotype in MEFs with an Xpress ratio of > 2 in any of the 2 biological replicates and a localization probability of > 0.9. VDAC proteins are abundantly found in the outer mitochondrial membrane and form a pore that regulates the transport of metabolites between the cytoplasm and the mitochondria by switching between open and closed states(Mannella, 1982; Rostovtseva and Colombini, 1997; Zalman et al., 1980). They have also been suggested to interact with mitochondrial hexokinase isoforms and thereby play an important role in bioenergetics pathways(Fiek et al., 1982; Linden et al., 1982). To be an important component of the apoptotic machinery is yet another function that has been assigned to VDAC proteins(Shimizu et al., 1999). VDAC proteins are present in all eukaryotic cells and share conserved structural and functional features(Young et al., 2007). There are 3 VDAC proteins in mammals and Figure 68 shows the sequence alignment of the 3 proteins in mouse. The 3 VDAC proteins show a high degree of sequence conservation amongst each other (> 67%), and are highly conserved between mouse and human homologous (for VDAC 1, the percentage identity is 98.59%; for VDAC 2, it is 94.56%; and for VDAC 3, 98.23% as calculated by the pairwise alignment calculation feature in MUSCLE)(Edgar, 2004) (see Appendix for pairwise alignment of human and mouse VDAC1, 2, and 3).

Figure 68: Sequence alignment of all 3 VDAC proteins in mouse and indication of the ubiquitinylation sites that are differentially modified in an Fbxo7 dependent manner

The Sequence alignment of the mouse VDAC 1 (Uniprot accession number: Q60932), VDAC 2 (Q60903), and VDAC 3 (Q60931) were performed using MUSCLE and annotated with the help of Jalview(Edgar, 2004; Waterhouse et al., 2009a). The percentage ID using MUSCLE is 71.53% between VDAC 1 and VDAC 2; 67.49% between VDAC 1 and VDAC3; and 73.14% between VDAC 2 and VDAC 3. Indication of the differentially targeted ubiquitinylation sites of the wild-type versus R379G KI genotype in MEFs.

Recently, the three-dimensional structure of reconstructed recombinant human and mouse VDAC 1 proteins has been solved using nuclear magnetic resonance, X-ray crystallography, or a combination of the latter two techniques(Bayrhuber et al., 2008; Hiller et al., 2008; Ujwal et al., 2008): VDAC 1 features a 19-sheeted β-barrel with the first and last sheet being parallel and a helical region within the pore. The structures of the mouse and human homologous are almost identical in keeping with their high degree of conservation of 99% - they only differ by 4 amino acid residues. Based on modelling studies, the structures of VDAC 2 and 3 are considered also to be in keeping with a β-barrel structure(Ujwal et al., 2008).

A very interesting finding is that the various Di-Glycine sites that have unambiguously been identified in this study (Table 5-3) converge onto 2 lysine residues that are completely conserved between VDAC 1, 2, and 3: The first identified Di-Glycine site corresponds to K66 in VDAC 1, K65 in VDAC 2, and K53 in VDAC 3; and the second identified Di-Glycine site corresponds to K122 in VDAC 1, K121 in VDAC 2, and K109 in VDAC 3 (A in Figure 69). Furthermore, these sites are also conserved between the mouse and human homologous of VDAC 1, 2, and 3 and the corresponding residues for the 2 sites are listed in the table (C) of Figure 69. The availability of a three-dimensional structure of the mouse VDAC 1 protein allows mapping their positional orientation. Figure 69: C highlights that the 2 are not buried into any of the 19 transmembrane β-sheets, but is potentially accessible for being modified by ubiquitinylation in an *Fbxo7* wild-type dependent manner. There is an on-going debate as to whether the three-dimensional structures of the available mouse and human VDAC 1 proteins actually correspond to their native confirmation, as they fail to consolidate important functional data(Colombini, 2009). Figure 70 highlights the differences in folding pattern and residues buried in the transmembrane domains between the actually resolved NMR structure (A) and the predictions based on the wealth of functional data (B) for the human VDAC 1. The 2 corresponding D-glycine sites are in both scenarios not buried into the depths of the transmembrane domains. The discrepancies between the 2 models have been suggested to arise from the experimental procedure involving the recombinant expression and refolding in inclusion bodies: The particular refolding pattern on which the NMR structure is based on is preferential and alternative to the native state (discussed in(Colombini, 2009)). However, not only its native folding pattern, but also its orientation within the outer mitochondrial membrane is at debate: it is therefore not entirely clear which site of the β barrel faces the cytosol and which the inner mitochondrial membrane. The current understanding is that the C-terminal region of VDAC 1 faces the cytosol. It is therefore not entirely clear whether the 2 Di-Glycine modified lysine residues of VDAC 1 face the cytosol or towards the inner mitochondrial membrane.

In conclusion my differential enrichment of the ubiquitylated species in SILAC labelled wild-type and homozygous R379G *Fbxo7* KI MEFs clearly identifies 2 highly conserved lysine residues, which are conserved amongst VDAC 1, 2, and 3 in mouse as well as human homologous, to be preferentially ubiquitinylated in a *Fbxo7* wild-type background. This experiment looks at the ubiquitinylation landscape in an Fbxo7 genotype dependent manner in wild-type and homozygous R379G *Fbxo7* KI MEFs, but does not allow the conclusion that Fbxo7 is directly involved in the ubiquitinylation of the 3 VDAC proteins at the specified sites. A prerequisite would also be that the respective lysine residues are accessible to the SCF^{Fbxo7} E3 ubiquitin ligase complex.

A

B

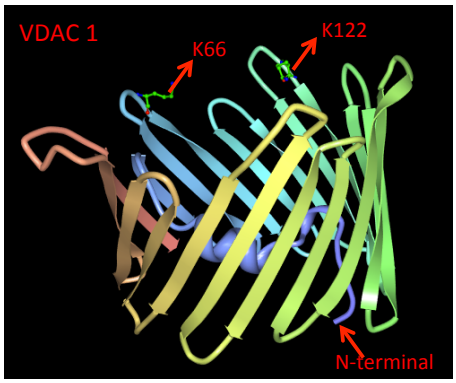

C

	1. K*GG	2. K*GG
Mouse VDAC 1 (Q60932)	**K66**	**K122**
Human VDAC 1 (P21796)	**K53**	**K109**
Mouse VDAC 2 (Q60930)	**K65**	**K121**
Human VDAC 2 (P45880)	**K64**	**K120**
Mouse VDAC 3 (Q60931)	**K53**	**K109**
Human VDAC 3 (Q9Y277)	**K53**	**K109**

Figure 69: The K*GG sites identified in this study are conserved across VDAC1, 2, and 3

A: Alignment of mouse sequences of VDAC 1,2 and 3 in the region of the identified K*RR sites shows that the individual sites identified converge onto 2 lysine residues that are completely conserved between the 3 proteins.

B: The K*GG sites identified in this study are highlighted in structure of the mouse VDAC 1 protein (image of PDB ID: 3EMN(Ujwal et al., 2008) created with Protein Workshop(Moreland et al., 2005)). They are located at the surface of the protein rather than buried into any of its transmembrane domains.

C: The 2 K*GG sites identified in this study are also conserved across the human and mouse homologous and the table lists the corresponding residues for mouse and human VDAC 1, 2, and 3 for the 2 sites.

Human VDAC 1 folding pattern

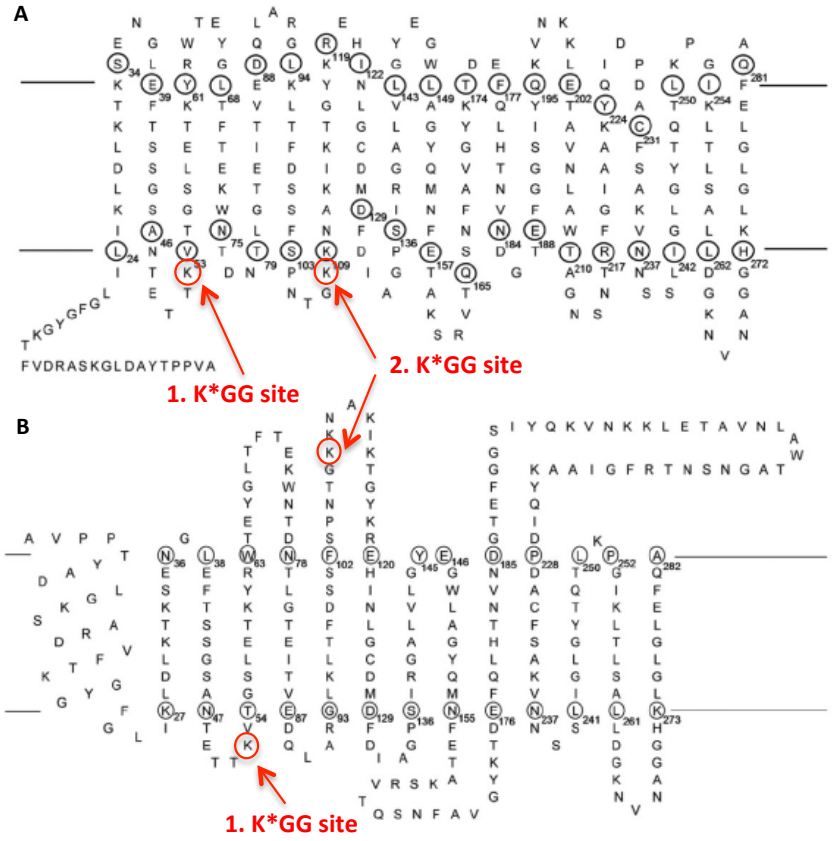

Figure 70: Differences in folding patterns of human VDAC 1 between NMR structure and predications from functional studies

Original figure from (Colombini, 2009) shows the differences in folding pattern between the human VDAC1 structures as determined my NMR (A) and the predictions based on functional studies (B). The corresponding lysine residues that have been identified to be preferentially ubiquitinylated by the Fbxo7 wild-type genotype in my study are highlighted in red. In either case the 2 sites are not buried inside the transmembrane spanning β-sheets of VDAC 1.

5.1.2 Predominantly cytosolic localization of endogenous FBXO7 in HEK293 cells

To gain inside into endogenous FBXO7 in human HEK293 cells localizes to the cytosolic or mitochondrial compartment, FlpIn TRex HEK293 cells stably expressing either FLAG-empty vector or human PINK1-wild-type-C-terminal FLAG were induced for protein expression using 0.1 ug/ml of doxycycline for 24 hours and treated either with the

mitochondrial decoupling agent CCCP (10uM) or DMSO as a control for 4 hours. It has been shown for PINK1 that mitochondrial membrane depolarization with CCCP at the given concentration leads to stabilization and activation of PINK1 in the mitochondria and subsequent phosphorylation of PARKIN at Serin 65(Kondapalli et al., 2012). I therefore decided to use the PINK1 translocation / stabilization as a positive control for efficient mitochondrial perturbation in my Fbxo7 localization experiment. Figure 71 shows that PINK1 – the full-length (63 kDa) as well as the cleaved form (53 kDa) - is present under basal conditions, and treatment with CCCP leads to a pronounced stabilization of full-length PINK1 in the mitochondrial fraction compared to treatment with DMSO. In contrast, endogenous FBXO7 was mainly identified in the cytosolic fraction irrespective of CCCP treatment or not. The stable expressing cell lines were kindly provided by Chandana Kondapalli, author of the above mentioned study. At least under conditions used in this experiments – especially duration of CCCP treatment of 4 hours – does not allow detection of endogenous FBXO7 in the mitochondrial fraction as is stable overexpressed PINK1. This would suggest that any SCF^{FBXO7} wt E3 ubiquitin ligase targets should be accessible from the cytosolic rather than the mitochondrial compartment.

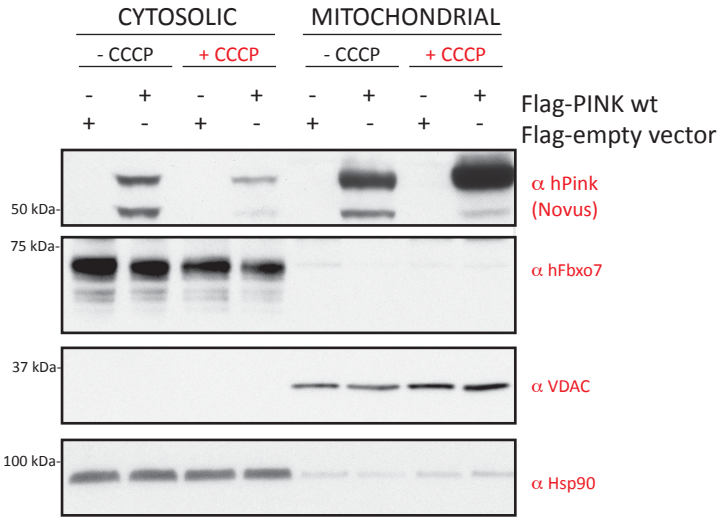

Figure 71: Endogenous FBXO7 in HEK293 localizes to the cytosolic compartment

Stable PINK1 wild-type-FLAG or FLAG-empty-vector expressing HEK293 cells were induced for protein expression (0.1 ug/ml for 24 hours) and stimulated with the mitochondrial decoupling reagent CCCP at 10uM for 4 hours. DMSO served as a negative control. Cytosolic and mitochondrial fractions were subjected to immunoblotting for PINK1 (positive control for efficient mitochondrial membrane depolarization with subsequent mitochondrial stabilization of PINK1) and FBXO7. VDAC and Hsp90 served as mitochondrial and cytosolic markers respectively.

5.2 Quantitative global proteomics to identify differences in expression levels across the whole proteome of wild-type and hom R379G *Fbxo7* KI brain lysates using *ex vivo* dimethyl labeling

The aim was to identify proteins whose expression levels significantly differ in whole brain tissue lysates dependent on the genotype of the animals. The expectation is then that the difference in expression level of any such protein reflects the altered SCF^{FBXO7} E3 ligase activity of the mutant Fbxo7 protein in comparison to the wild-type. In order to study and quantify the effect of the mutant Fbxo7 protein in the endogenous system in brain lysates, *ex vivo* chemical labeling was used(Boersema et al., 2009) (Figure 72): 3 littermate pairs of wild-type and homozygous R379G *Fbxo7* KI mouse brains with a mean age of 10 months were used. Individual brains were lysed in RapiGest buffer and equal amounts of each sample (200ug each) were digested with Trypsin. This was followed by stable isotope incorporation at peptide level using dimethyl labelling and subsequent multiplex quantitative proteomics(Boersema et al., 2009). The differential

dimethyl labelling permits us to distinguish peptides arising from either the wild-type ("light") or the homozygous R379G *Fbxo7* KI ("heavy") brain samples and the differential peptide abundance is then calculated as the ratio of extracted ion intensities between the 2 genotypes. Conventionally, a 1.5 ratio is applied as a threshold(Blagoev et al., 2004; Margolin et al., 2009). Figure 73 illustrates the important steps in this protocol: sample preparation and tryptic digestion, *ex vivo* differential labelling, mixing of the paired wild-type and homozygous R379G Fbxo7 KI brain samples at peptide level at a ration of 1:1 and multiplex quantitative proteomic analysis.

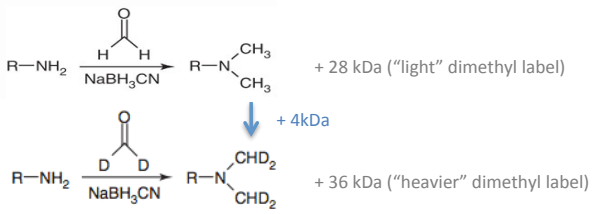

Figure 72: Principle of chemical dimethyl labelling at peptide level

After tryptic digestion, derived peptides of the different samples are labelled with isotopomeric dimethyl label: all primary amines in a peptide mixture are converted to dimethylamines to form monomethylamines. By using combinations of different isotopomeres of formaldehyde and cyanoborohydride, differential labelling can be obtained that differ in mass by a minimum of 4 kDa, which is the basis for differential detection by multiplex mass-spectrometry. (R: rest of the peptide that is being modified, only the 2 dimethyl labels that were used in this study are shown).

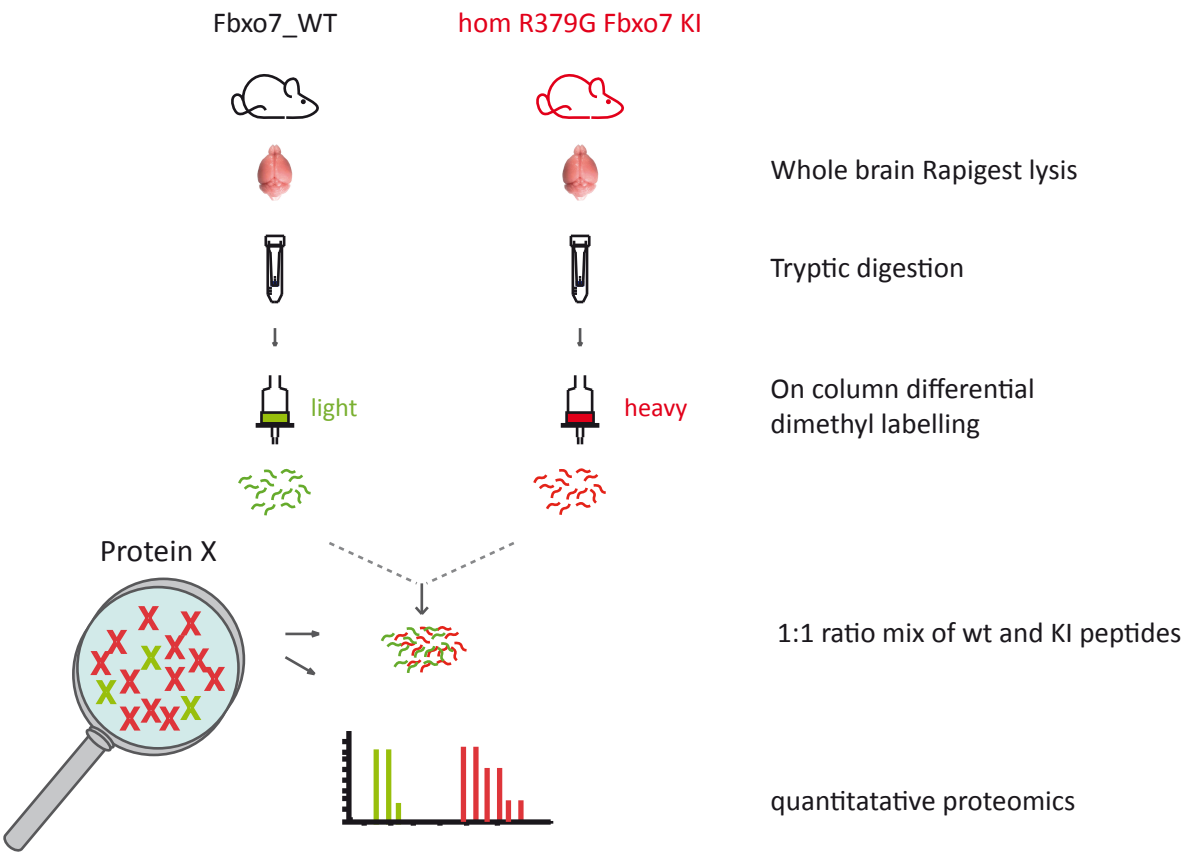

Figure 73: Schematics of *ex vivo* differential chemical labelling of wild-type and R379G *Fbxo7* KI brains for quantitative whole proteome analysis

The experiment was performed in parallel with 3 littermate pairs of wt and hom R379G *Fbxo7* KI animals with a mean age of 10 months. Brains were harvested and immediately homogenized in RapiGest lysis buffer. Protein concentration was determined and 200ug of each of the 6 samples was digested with Trypsin overnight at 37 degrees Celsius. Samples were then subjected to on column dimethyl labelling (light label for wild-type and intermediate label for hom KI samples) and subsequently peptides from littermate wt and hom Fbxo7 KI pairs were mixed at a 1:1 ratio. The samples were then analysed by multiplex quantitative proteomics. Protein X illustrates an example of a protein that is differentially targeted by the $SCF^{Fbxo7wt}$ E3 ligase complex for degradation by the ubiquitin proteasome system. Hence, its expression level is lower in the wt genotype its relative detection by mass-spectrometry lower.

In total, 6998 proteins were identified with at least 2 peptides. 107 of the 6998 proteins differed more than 1.5 fold in their expression levels, but only 15 changed reliably ($p < 0.05$) (Table 5-4: A), whereas the majority of proteins remained unchanged. The observed differences in expression amongst these 15 proteins ranged between 100

times higher to 11 times lower in the wild-type brain samples. I had previously determined that the expression level of Fbxo7 differ about 2-fold between the wild-type and homozygous R379G *Fbxo7* KI genotype by immunoblotting and Li-COR quantification (Figure 36). The same difference was observed in this experiment: Fbxo7 protein levels were reduced by half in the homozygous R379G *Fbxo7* KI genotype (p = 0.051) (Table 5-4:B). Fbxo7 therefore served as an internal quality control and the difference in expression levels was equivalent to that seen by immunoblotting.

A

Protein names	MW (kDa)	fold change (H/L)	Unique peptides	Sequence coverage [%]
Integrin beta;Integrin beta-5	90	**0.01**	4	9.7
Glycosyltransferase-like domain-containing protein 1	51	**0.13**	2	6.5
Latrophilin-2	167	**0.27**	7	6
60S ribosomal protein L36a	12	**0.41**	3	28.3
Sentrin-specific protease 7	116	**0.49**	5	8.4
Ras-specific guanine nucleotide-releasing factor RalGPS1	65	**0.57**	1	8.2
Protein SMG9	58	**1.51**	8	24.8
Protein sprouty homolog 2	35	**1.72**	2	9.5
Vascular endothelial growth factor receptor 1	150	**1.96**	7	6.8
Intraflagellar transport protein 20 homolog	15	**1.97**	2	17.4
Protein Pcdhb20	88	**2.37**	5	11.8
Protein KTI12 homolog	38	**3.37**	2	10
Glycosylphosphatidylinositol anchor attachment 1 protein	68	**6.60**	4	8.4
Neuroepithelial cell-transforming gene 1 protein	68	**9.85**	2	2.9
Neurogenic differentiation factor 2	41	**11.59**	3	11.7

B

Protein name	MW (kDa)	fold change (H/L)	Unique peptides	Sequence coverage [%]	p value
F-box only protein 7	59	0.514	4	13.2	0.051

Table 5-4: Differentially expressed hits across the proteome of dimethyl labelled wt (light) and hom R379G (heavy) Fbxo7 KI brain samples (3 biological replicates, ratio>1.5)

A: Of all 7000 proteins identified All differentially expressed proteins in wt and hom R379G Fbxo7 KI brain samples of 3 replicates with a ratio in expression levels as detected by quantitative proteomics of at least 1.5 and a p-value of less than 0.05. Proteins with an at least 2-fold excess in the wild-type genotype are highlighted in light green, whereas proteins with an at least 2-fold excess are highlighted in rose. B: Fbxo7 was found to differ between the 2 genotypes with a ratio of 0.5 (reduction by half in hom R379G KI compared to wt), but the p-value was 0.051, which is the reason why F-box 7 is not listed amongst the other proteins in A.

5.2.1 **Immunoblotting for candidate hits from the differential whole proteome experiment from wt and hom R379G *Fbxo7* KI brain**

In an effort to validate the hits from the differential whole proteome experiment I have used commercially available antibodies for immunoblotting. The antibodies were considered specific when they reliably detected a signal of the respective size and when they had been used in other publications. Figure 74 shows the immunoblot for Fbxo7 and Gapdh as loading control for duplicate whole brain lysates for the 3 littermate wild-type and homozygous R379G Fbxo7 KI pairs (corresponding to the 3 biological replicates used in the proteomic experiments). This shows that despite some variation there is a stronger signal for Fbxo7 in the wild-type compared to the homozygous R379G *Fbxo7* KI samples corresponding with the 2-fold higher abundance levels determined by the proteomic analysis. No clear pattern of differential expression between the 2 genotypes is seen for any of the other proteins that were subjected to immunoblotting: According to the proteomic analysis, the abundance of Integrin beta 5 is 100 times higher in the wild-type compared to the homozygous R379G *Fbxo7* KI, while the difference for Sentrin-sepcific protease 7 is 2-fold higher in the wild-type genotype. The same can be observed for proteins whose abundance has been measured to be higher in the homozygous R379F Fbxo7 KI brain samples: the expression for both neurogenic differention factor 2 and neuroepithelial cell-transforming gene protein 1 was measured to be about 10 times higher in the homozygous R379G KI genotype. Overall, the validation of the differential whole proteome analysis in the quest to identify genotype specific differences in wild-type and homozygous R379G KI Fbxo7 brain samples was not taken any further. I will explain in the discussion why we thought that lysates as complex as those from whole brain are not the most suitable material to study differences in protein expression between the Fbxo7 wildtype and mutant genotypes.

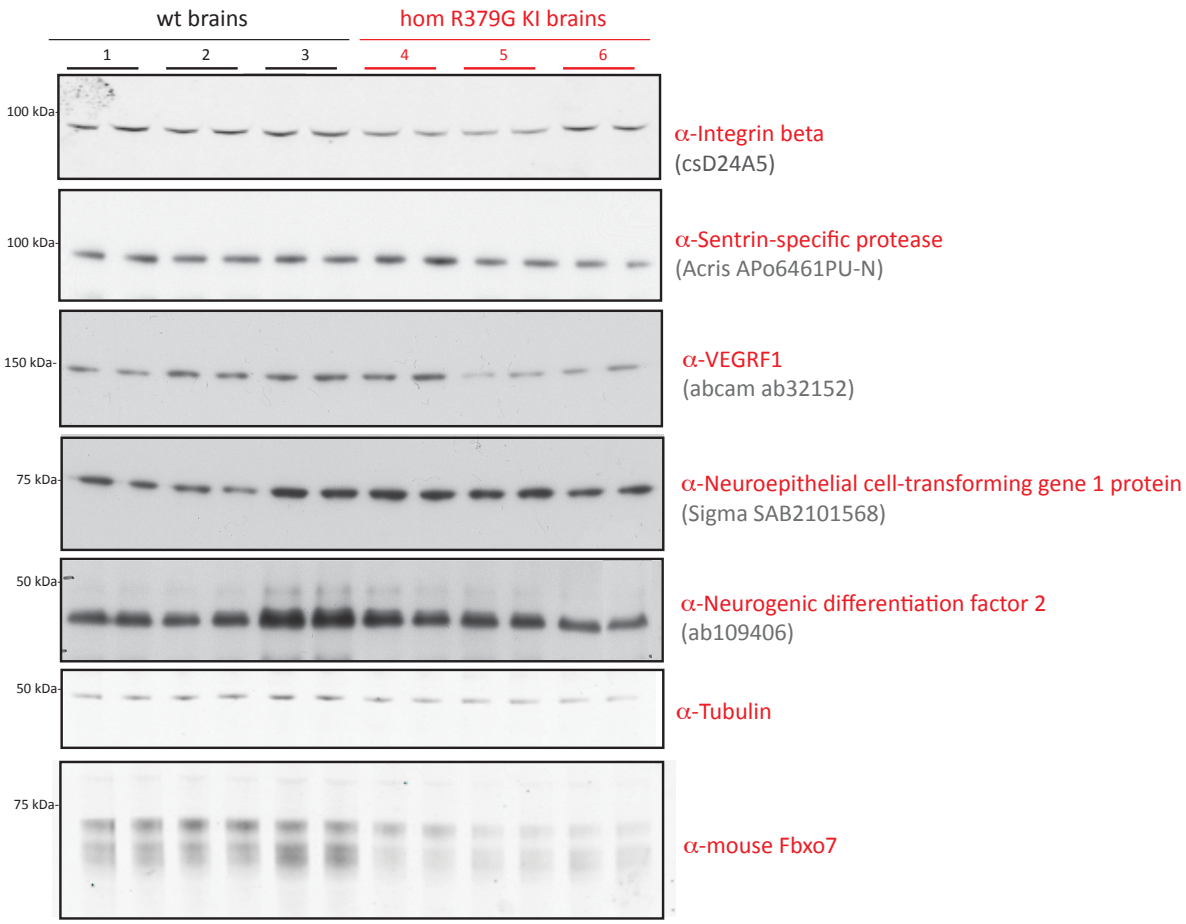

Figure 74: Immunoblotting of whole brain lysates from the 3 littermate pairs (wt and hom R379G Fbxo7 KI) used in the proteomic analysis

The same RapiGest whole brain samples from 3 littermate wt and hom R379G Fbxo7 KI pairs that were used for the proteomic analysis were subjected to immunoblotting (loading in duplicates, 15 ug each). According to the quantitative proteomic analysis Integrin beta 1 and Sentrin specific protease have a genotype-specific higher expression level in the wild-type, and neurogenic differention factor 2 and neuroepithelial cell-transforming gene protein 1 have a higher expression pattern in the hom R379G Fbxo7 KI, while VEGFR1 is equally expressed. Immunoblotting does not show a genotype specific difference in expression pattern for any of the proteins blotted for except for Fbxo7, but either no or a high intra-individual difference irrespective of genotype.

5.3 *In vitro* SCF^{FBXO7} complex formation

An important aspect in the validation of potential FBXO7 targets for SCF^{FBXO7} E3 ubiquitin ligase dependent degradation by the ubiquitin proteasome system is the availability of a functional read-out. I have therefore set out to establish conditions for

in vitro SCF^{FBXO7} E3 ubiquitin ligase assays to directly assess the impact of FBXO7 on any putative targets. The first important step was to express and purify high yields of all the components of the SCF^{FBXO7} complex: Cullin 1, SKP1, RBX1 and of course the wild-type and FBXO7 disease mutants. Cullin1 and RBX1 form the catalytical core of the complex in terms of being responsible for the recruitment of the E2 ubiquitin conjugating enzyme, while SKP1 functions an adaptor to link interchangeable F-box proteins via their SKP1-binding F-box domain to the Cullin1 / RBX1 core. It is then the F-box proteins that bring the substrate to the E3 ligase complex and thereby dictating substrate-specificity(Deshaies and Joazeiro, 2009). Figure 75 illustrates the complex and extensive interactions between the various SCF complex partners, which adopt an overall rigid structure(Schulman et al., 2000; Wu et al., 2003; Zheng et al., 2002).

5.3.1 Expression and purification strategy of the recombinant SCF^{FBXO7} complex components

Because of the overall rigid structure of the SCF complex, it has therefore been suggested that co-expression and co-purification of at least 2 subunits of the complex together yields soluble and functional components of the E3 ligase complex(Li et al., 2005). In this study, I used co-expressed insect cell expressed DAC-tagged Cullin1 / untagged RBX1 as well as His-tagged Cullin1 / untagged RBX1/ untagged SKP1 components as well as co-expressed DAC-tagged FBXO7 – either as wild-type, or disease mutants R378G and R498X - and untagged SKP1. The initial affinity purification selected for the DAC-tag in case of the Cullin and FBXO7 components. In case of the Cullin1 component, the purification step was followed by cleavage by the protease Tev to release and remove free DAC. Additionally, single expressed His-tagged PI31 was used. Figure 76 shows the final recombinant protein complex components and demonstrates good expression and purification of all recombinant proteins except for SKP1, when it co-expression and co-purified with the mutant R378G FBXO7: Subjecting serial dilutions of the FBXO7 wild-type / SKP1 complex components in comparison to the FBXO7 R379G mutant / SKP1 to immunoblotting for SKP1, clearly demonstrates that SKP1 is not as efficiently co-purified with the R378G mutant than with the FBXO7 wild-type. Re-sequencing of the original baculoviral constructs confirmed that both the untagged SKP1

and DAC-FBXO7 cassettes contained the correct sequences and that the mutant FBXO7 construct only differed by the correct insertion of the corresponding mutation. At least 3 separate expression and purification procedures of each of the 2 FBXO7 constructs yielded the same result: SKP1 was not as efficiently co-purified with the R378G FBXO7 mutant (Figure 77).

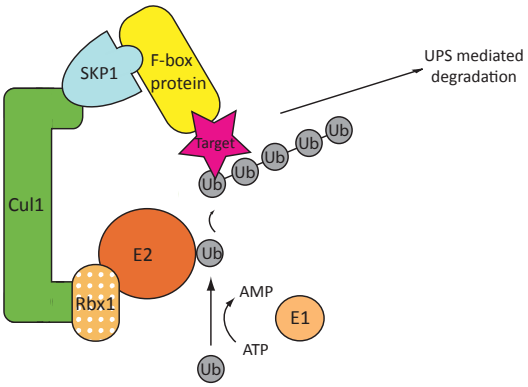

Figure 75: SCF E3 ubiquitin ligase complex and its relation to E1, E2 and potential targets

RBX1 binds to the C-terminus of Cullin 1 via its N-terminus and via its N-terminus to an E2 conjugating enzyme. Cullin 1 binds SKP1 via its N-terminus and SKP1 in turn acts as an adaptor for a multitude of different F-box proteins each with their own set of substrates. RBX1/Cullin1 catalyses then the transfer of ubiquitin from the E2 to the substrates.

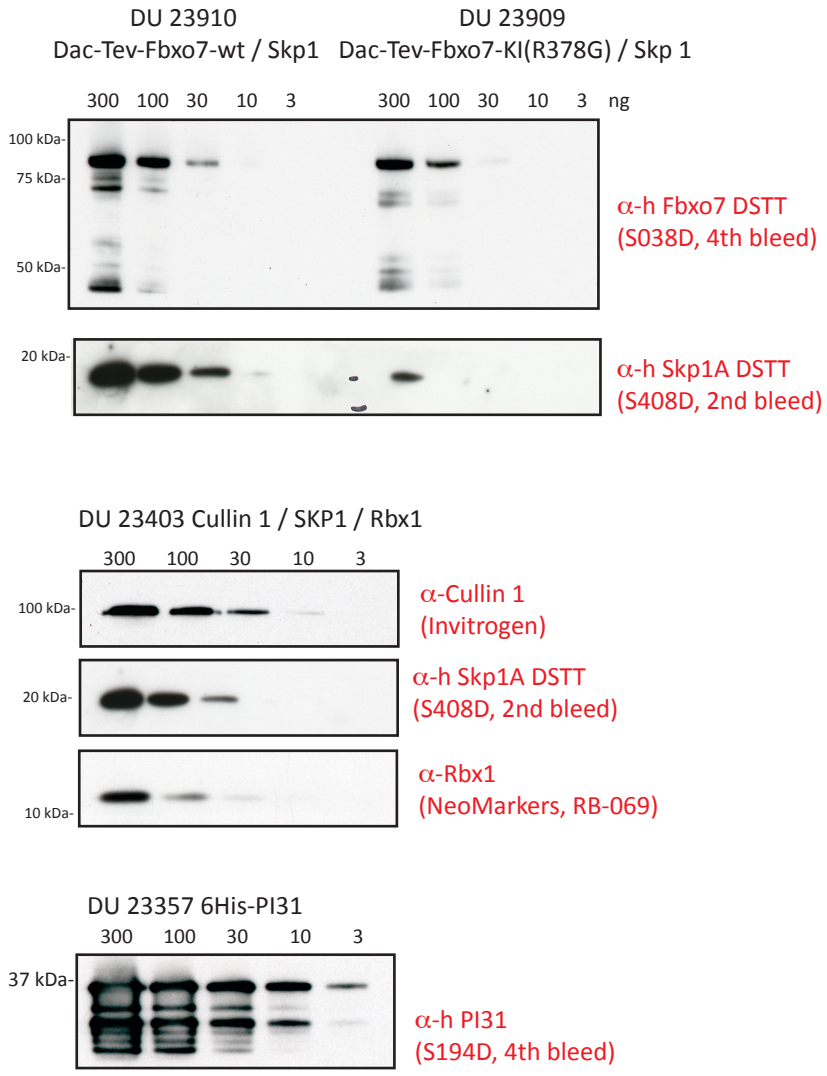

Figure 76: Expression of the components of the recombinant SCF^{FBXO7} complex components: co-expressed and purified Cullin 1 / Skp1 / Rbx1 and Fbxo7 / SKP1 as well as single expressed and purified His-PI31

Recombinant FBXO7-wild-type and Fbxo7-R379G mutant proteins were each co-expressed as full-length, DAC-tagged proteins together with untagged SKP1 in insect cells from a dual baculovirus vector and affinity purified for DAC. Full length PI31 was expressed with a 6His-tag and DAC-tagged, full-length Cullin 1 was co-expressed with untagged Rbx1 and untagged SKP1 followed by cleavage of the DAC-tag by the protease Tev. Serial dilutions (in ng) for each construct were prepared for immunoblotting with the respective antibodies.

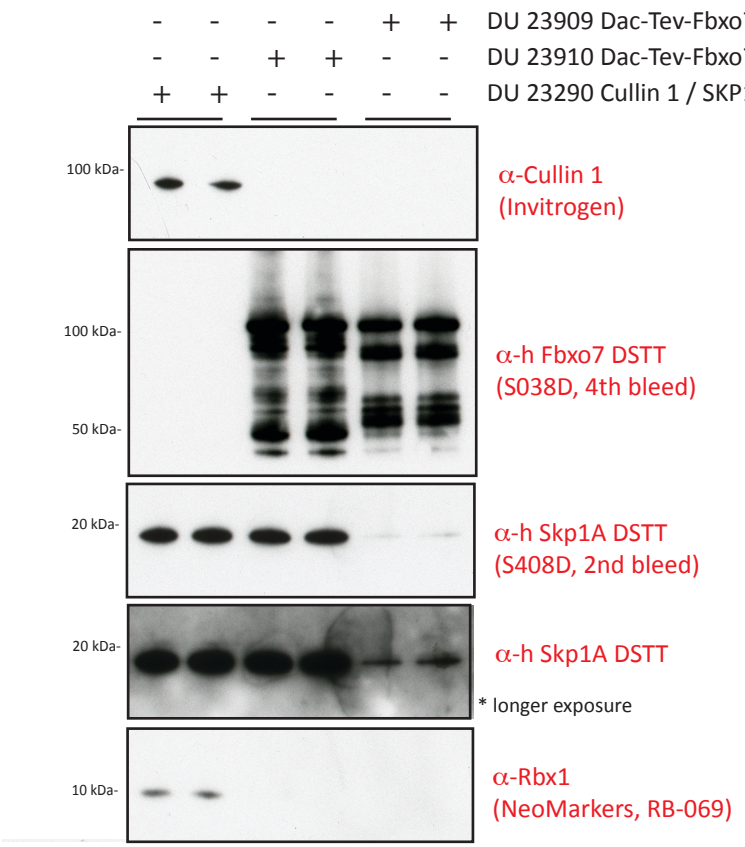

Figure 77: Re-expression and purification confirmed the consistently lower co-purification of SKP1 with the R378G FBXO7 mutant

A second and also third (data not shown) preparation of the DAC-FBXO7 wild-type and DAC-FBXO7 R378G mutant each co-expressed with untagged SKP1 shows consistently the lower abundance of SKP1 when it is co-purified with the FBXO7 R378G mutant. Also shown is a second preparation of the Cullin1 / SKP1 / RBX1 co-expression construct (duplicate loading, 150ng each, immunoblotting for the respective antibodies as shown).

5.3.2 Preparation of recombinant SCF^{FBXO7} E3 ubiquitin ligase complexes

After expressing each of the different components of the SCF complex for the wild-type as well as the R378G FBXO7 disease mutant, I moved on to prepare recombinant SCF E3 ubiquitin ligase complexes. Successful SCF complex formation is a prerequisite for functional E3 ligase activity for further assay development. In principle, the different components of the final complex should readily assemble upon mixing. As we suspected PI31 to be possibly part of the SCF^{FBXO7} complex, I included PI31 in the analysis and aim at tetrameric (SCF^{FBXO7}: Skp1 * Cullin 1 * Rbx 1 * Fbx07) as well as pentameric (SCF^{FBXO7}

plus PI31) complex formation. A molar ratio of 1:2:2 was used for DAC-FBXO7 (wild-type as well as R378G mutant) / SKP1 : Cullin1 / SKP1 / RBX1 : His-PI31. During initial pilot experiments I had used a Cullin1 construct from a dual expression vector co-expressing only RBX1 (data not shown), but because of the significantly lower abundance of SKP1 in the co-purification with the FBXO7 R378G mutant, I switched to using Cullin 1 expressed from a multi-baculoviral construct co-expressing RBX1 as well as SKP1. The SKP1 from the Cullin1 co-purification served as an alternative source of SKP1 in the FBXO7 R378G mutant complex formation experiment. After direct mixing of the individual complex components, DAC-affinity purification of the DAC-tagged FBXO7 component allowed successful separation of the complex from the excessive components that were not assembled into a complex with FBXO7. Figure 78 and Figure 79 show 2 replicate experiments of successful SCF^{FBXO7} and even pentameric SCF^{FBXO7} * PI31 complex formation for the FBXO7 wild-type construct. The same was not observed for the FBXO7 R378G disease mutant. The co-expression and co-purification of the FBXO7 R378G / Skp1 (5.3.1) had already pointed towards impaired binding of SKP1 to the FBXO7 R378G mutant. Despite compensating for the relatively lower abundance of SKP1 in the complex formation experiment with alternatively sourced SKP1 (from the Cullin1 / SKP1 / RBX1) construct, the FBXO7 R378G mutant was unable to form a $SCF^{FBXO7\ R378G}$ E3 ligase complex (Figure 80). To corroborate that it is actually the substitution of an Arginine by a Glycine in juxtaproximity to the F-box domain at position 378 of FBXO7 that is responsible for impaired SKP1 binding *in vitro*, I have also included another FBXO7 disease mutant: FBXO7 R498X. Figure 80: A shows the Coomassie gel picture of the purified FBXO7 wild-type / Skp1, FBXO7 R378G / Skp1 as well as FBXO7 R498X / Skp1 indicating that SKP1 fails to effectively co-purify with the DAC-affinity purification of DAC-tagged FBXO7, while it is effectively co-purified with the wild-type as well as the R498X FBXO7 mutant. Figure 80: B demonstrates the ability of the wild-type as well as the R498X FBXO7 mutant to form a SCF^{FBXO7} complex (with an without PI31), while the R378G FBXO7 disease mutant is not.

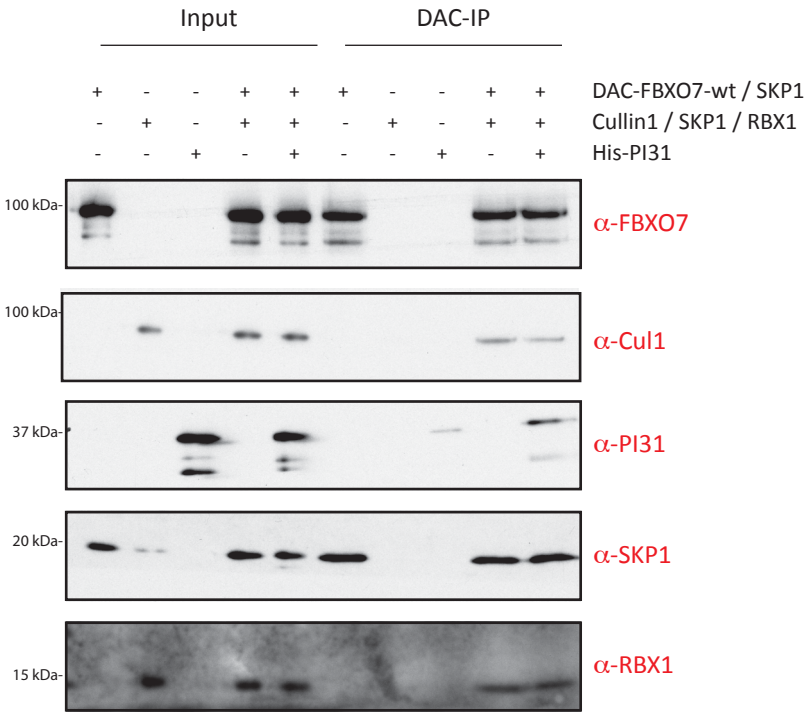

Figure 78: Successful recombinant SCF complex formation of the FBXO7 wild-type: Replicate 1

DAC-tagged FBXO7 wild-type / Skp1, untagged Cullin 1 / SKP1 / RBX1 and His-tagged PI31 were incubated alone or in all possible combinations with each other prior to affinity purification by DAC-tag binding to ampicillin sepharose. Co-eluting proteins were considered to be in a stable complex with the DAC-purified FBXO7. Shown are immunoblots for all components of input and DAC-purification. The DAC-pull-down of the individual components – when DAC-tagged FBXO7 is not present - serve as a control and shows that complex formation is not due to unspecific DAC-binding. The FBXO7 wild-type is able to form a tetrameric SCF^{FBXO7} complex as well as a pentameric SCF^{FBXO7} * PI31 complex.

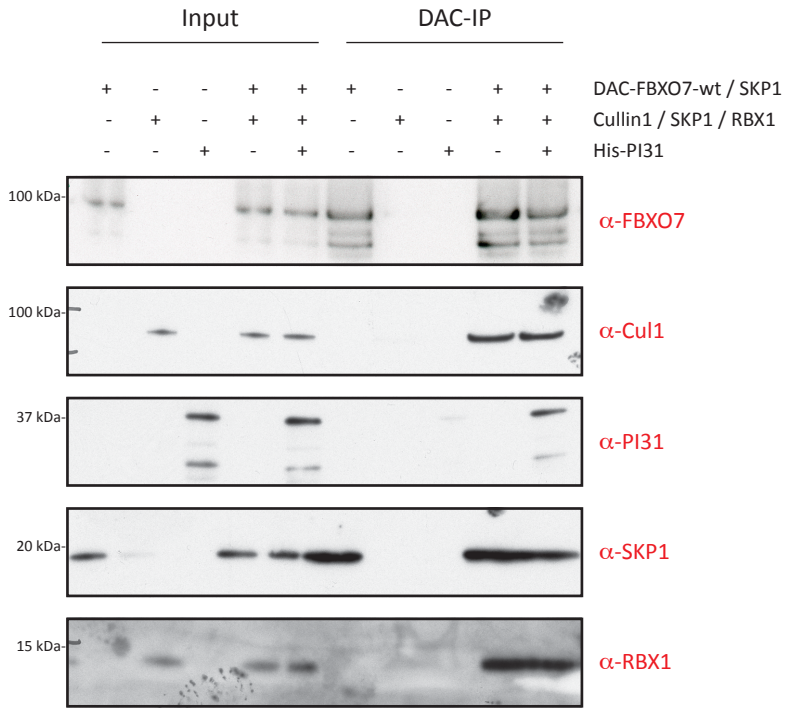

Figure 79: Successful recombinant SCF complex formation of the FBXO7 wild-type: Replicate 2

Biological replicate experiment: DAC-tagged FBXO7 wild-type / Skp1, untagged Cullin 1 / SKP1 / RBX1 and His-tagged PI31 were incubated alone or in all possible combinations with each other prior to affinity purification by DAC-tag binding to ampicillin sepharose. Co-eluting proteins were considered to be in a stable complex with the DAC-purified FBXO7. The FBXO7 wild-type is able to form a tetrameric SCF^{FBXO7} complex as well as a pentameric SCF^{FBXO7} * PI31 complex.

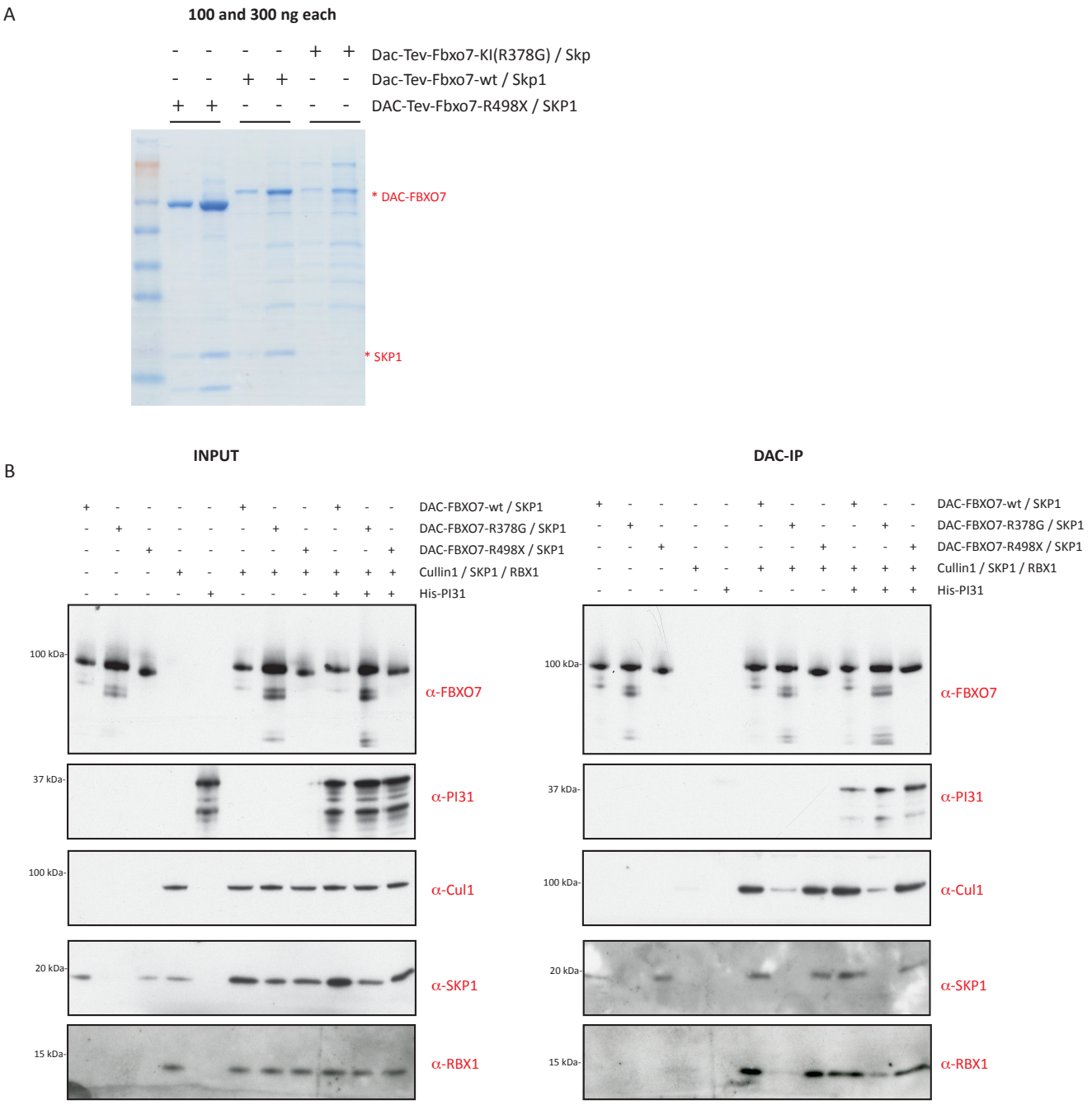

Figure 80: Inability of the R378G FBXO7 mutant to form a recombinant SCF^{FBXO7} R378G complex

A: Coomassie gel of the purified FBXO7 wild-type / SKP1, FBXO7 R378G / SKP1 and FBXO7 R498X / SKP1 demonstrated that SKP1 is ineffectively co-purified with the R378G mutant while it efficiently binds to the wild-type as well as the R498X FBXO7 mutant (loading of 100 and 300 ng for each construct).

B: Either DAC-tagged FBXO7 wild-type / Skp1 or the 2 DAC-tagged FBXO7 disease mutants (R378G and R498X) or untagged Cullin 1 / SKP1 / RBX1 and His-tagged PI31 were incubated alone or in all possible combinations with each other prior to affinity purification by DAC-tag binding to ampicillin sepharose. Co-

eluting proteins were considered to be in a stable complex with the DAC-purified FBXO7. The immunoblots for the input of all components of the complex is shown on the left, while the actual DAC-pull downs is shown on the right. The wild-type as well as the R498X FBXO7 disease mutant are both capable of tetrameric SCF^{FBXO7} complex as well as a pentameric SCF^{FBXO7} * PI31 complex. The R378G FBXO7 mutant is however unable to form a complex due to its inability to bind SKP1.

5.3.3 **Setting up a SCF^{FBXO7} E3 ligase activity assay *in vitro***

A sensitive means for assaying the potential activity of any SCF E3 ubiquitin ligase *in vitro* is to evaluate its capacity for free ubiquitin chain formation. For this I have used a modified protocol from (Lorick et al., 1999; Yang et al., 2005) and incubated DAC-FBXO7 / SKP1 as well as Cullin1 / SKP1 / RBX1 together with recombinantely expressed E1 activating enzyme Ube1 (DU32888), the E2 conjugating enzyme UBE2R1 and Ubiquitin (either Flag- or untagged) in the presence of Magnesium and ATP at 30 degrees for 45 minutes. The assay was terminated by the addition of SDS-loading buffer. I monitored the effect of the R378G and R498X mutants in comparison to the FBXO7 wild-type on the capacity of free ubiquitin chain formation as well as the presence or absence of PI31. Free ubiquitin chain formation was assessed by the absence or presence and intensity of high molecular weight species of ubiquitin upon immunoblotting. Figure 81 illustrates the ability of the FBXO7 wild-type constructs to form free ubiquitin chains in the presence of Cullin1, Skp1, Rbx1, E1 and E3 as well as Ubiquitin, magnesium and ATP. Although there is background free ubiquitin chain formation with either the E1 or E2 alone or a combination thereof, the FBXO7 wild-type construct is able to mount a significantly more intense response in terms of free chain formation above and beyond this background. To show that this increase in response is due to the specific effect of the addition of an F-box protein, I have also used recombinant β-TRCP (Fbxw1) as well as Fbxw7 (cdc4), both components of other well categorized $SCF^{F\text{-box protein}}$ complexes – as a positive control: the wild-type FBXO7 had the same capacity to form free ubiquitin chains as seen with β-TRCP and Fbxw7. The addition of albumin served as a negative control as it did not change the background level and equally, PI31 did not have an additional effect on the free ubiquitin chain formation either. Importantly, the R378G FBXO7 disease mutant was also not able to mount a free chain formation response

above and beyond the background and was comparable to that of E1*E2*Cullin1 / Skp1 / Rbx1 alone or in combination with either albumin or PI31. This outcome was anticipated due to the inability of the R378G FBXO7 mutant to bind to Skp1 and hence assemble into the $SCF^{FBXO7\ R378G}$ E3 ubiquitin ligase complex. Next, I wanted to compare the FBXO7 wild-type with the R378G and R498X disease mutants in terms of their effect on free ubiquitin chain formation and also explore the impact of adding PI31 to the complex. Figure 82 shows that the wild-type and FBXO7 R498X mutant are equally capable of free ubiquitin chain formation, while the FBXO7 R378G mutant is not. When PI31 is added to the individual complexes, the ability to form free ubiquitin chains of the SCF^{FBXO7} wt and $SCF^{FBXO7\ R498X}$ is impaired suggesting a negative regulatory role for PI31 in this particular *in vitro* set up.

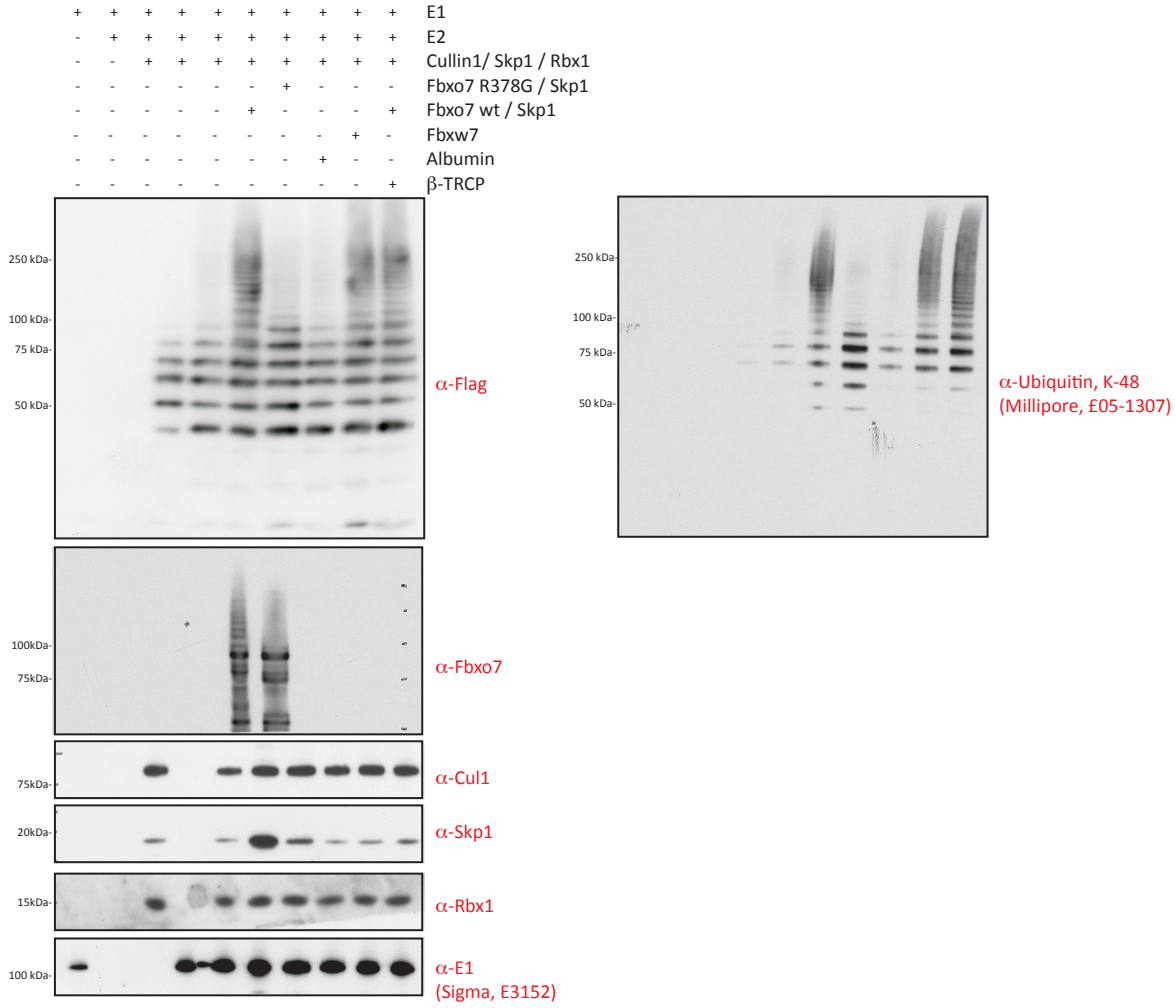

Figure 81: Free ubiquitin chain formation as functional read-out for SCF^{FBXO7} E3 ligase assay

0.5ug of either the wild-type or R378G mutant FBXO7 construct were added to the other ubiquitylation assay components (E1: human recombinant His-UBE1 expressed in insect cells (0.1ug), E2: human recombinant His-UBE2R1 expressed in E. coli (1ug); E3: human recombinant Cullin 1 / Skp1 / Rbx1 co-expressed in insect cells (0.5ug) and 0.5mM Flag-Ubiquitin). The reaction was initiated by adding ATP/$^{Mg2+}$at 30 degrees Celsius and terminated after 45 minutes by the addition of SDS-Page loading buffer. 1/10 of the reaction was then resolved by SDS-Page per immunoblot. Already the E1, E2 and Cullin / Rbx1 / Skp1 reaction without the Fbxo7 protein is able to generate free Ubiquitin chains as demonstrated in the Flag-immunoblot with a K48 specific linkage (K-48 immunoblot) as expected for the E2 enzyme used in this assay. However, the addition of the wild-type FBXO7 results in a significant increase in the generation of free ubiquitin changes ('autoubiquitylation') in comparison to the baseline chain formation by E1, E2 and Cullin1 / Rbx1 / Skp1 alone. In contrast, the R379G FBXO7 mutant is unable to mount an additional ubiquitinylation response – as one would expect given that the mutant Fbxo7 protein is unable to interact with Skp1. Two other F-box proteins – β–TRCP and FbxW7 – as well as albumin were used as positive controls.

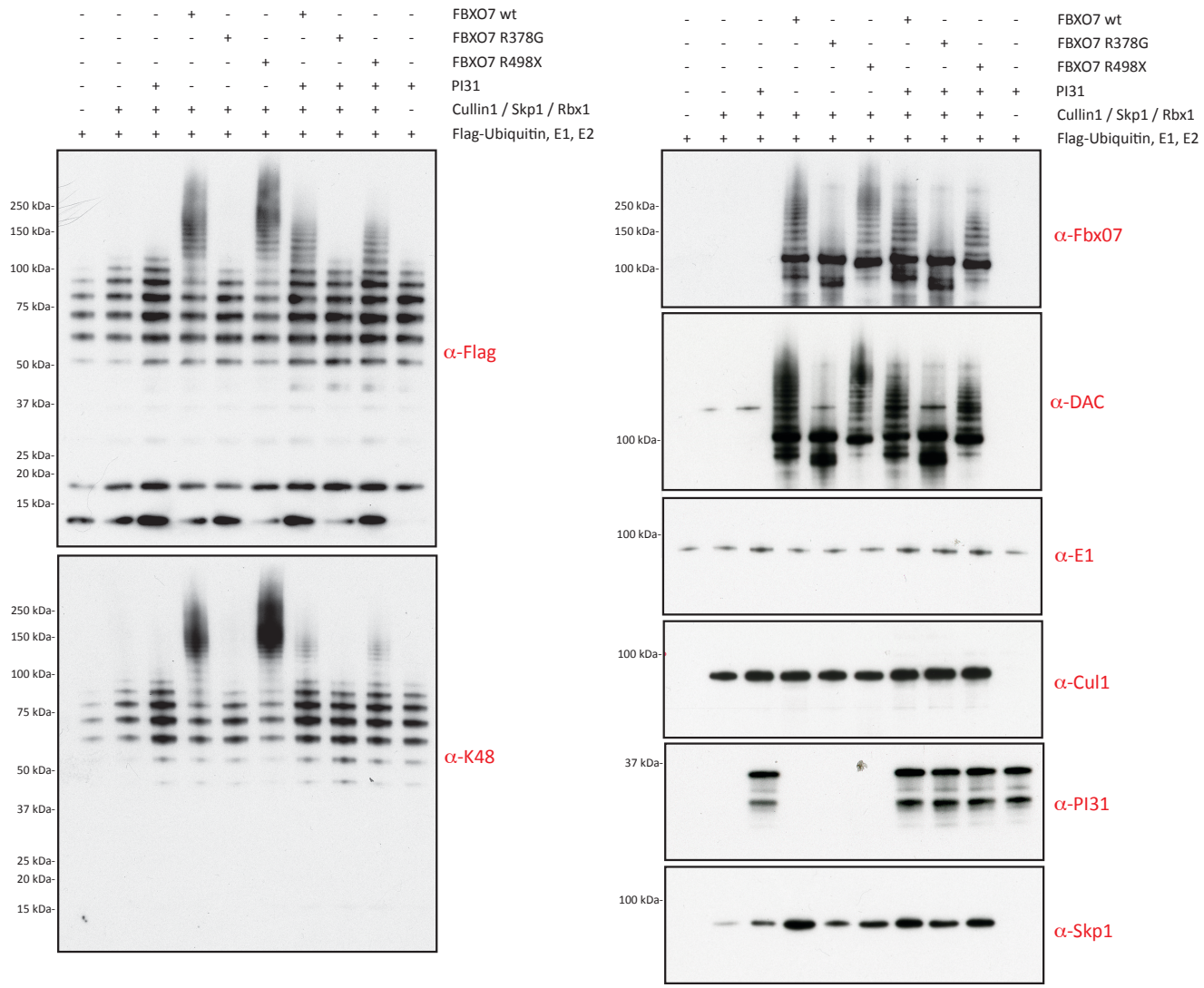

Figure 82: *In vitro* free ubiquitin chain formation assay of FBXO7 wt in comparison to the disease mutants R378G and R498X and the effect of PI31

Reaction set up as in Figure 81 for FBXO7 wild-type and the disease mutants R378G and R498X in the presence or absence of PI31 to assess free ubiquitin chain formation. Immunoblots for Flag and K48-linkage specific ubiquitin as the functional read-out and the individual components of the reaction except for the E2 (for which no antibody for immunoblotting was available). The inability of the R378G FBXO7 mutant to form free ubiquitin chains in vitro is most likely due to its impaired binding to Skp1 and the remainder of the SCF complex. The wild-type and R498X FBXO7 mutant are capable to form free ubiquitin chains, which is negatively impacted upon when PI31 is added.

5.3.4 **Failed reconstitution of the *in vitro* E3 ligase activity assay with endogenous SCF^{FBXO7} complexes**

My findings from the *in vitro* SCF^{FBXO7} complex formation and activity assay have unanimously demonstrated that the recombinantly expressed FBXO7 R378G mutant is incapable of efficiently binding to Skp1 and hence assembly into a functional $SCF^{FBXO7\ R378G}$ E3 ligase complex in the setting used in this thesis. This is in contrast to what I have observed in the *in vivo* system and on the endogenous level: I have previously shown that patient derived homozygous R378G *FBXO7* fibroblasts as well as brain lysates from homozygous R379G KI *Fbxo7* mice are readily able to form a $SCF^{FBXO7\ R378/9G}$ E3 ubiquitin ligase complex. Only one of mainy possibilities to explain and consolidate this discrepancy is to assume that the R378G mutation does indeed affect binding to Skp1, but that there are additional compensatory complex partners or conditions in the *in vivo* setting. I have therefore tried to reconstitute the *in vitro* E3 activity assay with endogenous SCF^{FBXO7} complexes that were immunoprecipitated from wild-type and homozygous R378G brain lysates using either preimmune IgG or G-sepharose alone as a negative control. However, as the expression level of the homozygous R379G Fbxo7 KI mutant is reduced by about half in comparison to the Fbxo7 wild-type protein, I have set up conditions to assure that about the same amount of SCF^{Fbxo7} immunocomplexes are being immunoprecipitate. Figure 83 shows that by using double the amount of homozygous R379G Fbxo7 KI lysates in comparison to the wild-type protein approximately equal amounts of Fbxo7 is being immunoprecipitated for each genotype and that the relative levels of the individual SCF complex partners do also not significantly differ – very much different from my *in vitro* findings.

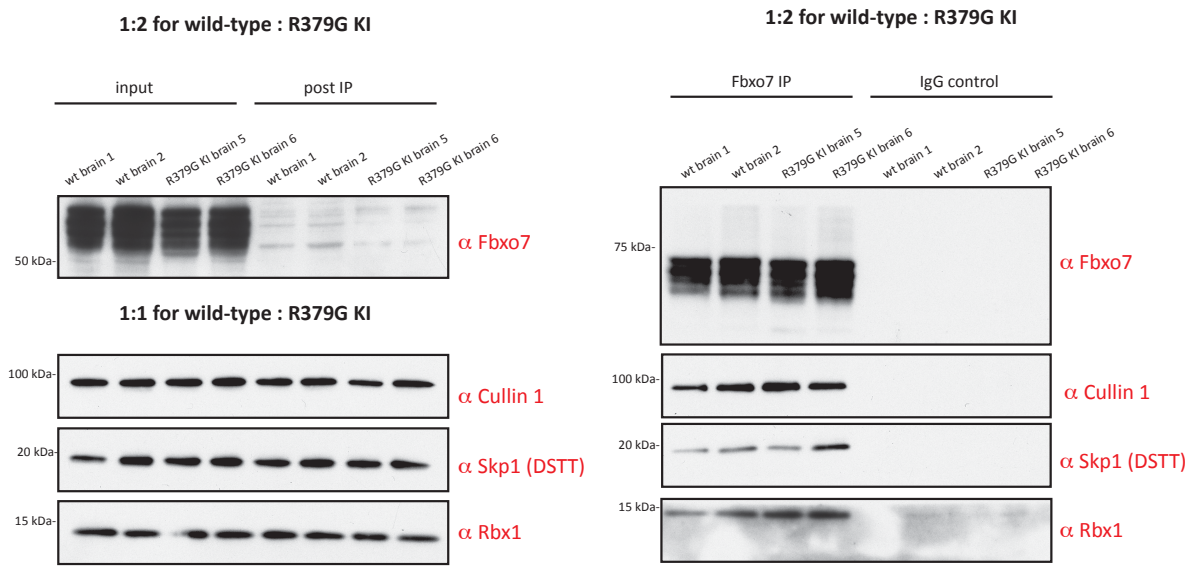

Figure 83: The relative stoichiometry of SCFFbxo7 complex partners does not significantly differ between wild-type and homozygous R379G *Fbxo7* KI brain lysates

Immunoprecipitation of endogenous Fbxo7 from double the amount of homozygous R379G *Fbxo7* KI brain lysates in comparison to wild-type Fbxo7 lysates (derived from 2 different genotypes for each genotype) shows that the relative stoichiometry of Fbxo7 from either wild-type or homozygous R379G Fbxo7 KI lysates and each of the other SCF complex partners – Cullin1, Skp1, and Rbx1 - is about the same. The immunoblots on the left hand side show input and post-IP lysates in a 1:2 ratio for the wild-type and homozygous R379G *Fbxo7* KI brain lysates and in a 1:1 ratio for the other SCF complex partners while the right hand side shows the immunoprecipitation products in a 1:2 ratio (wt : hom R379G *Fbxo7* KI).

I have then applied the 1:2 ratio for the reconstitution of the *in vitro* free ubiquitin chain assay with endogenous Fbxo7 immunoprecipitated SCF^{Fbxo7} complexes from wild-type and homozygous R379G *Fbxo7* KI brain lysates (Figure 84). Preimmune IgG immunoprecipitations as well as brain lysate incubations with G-sepharose alone were used as controls and show that there are sufficient contaminating molecules in the control experiments that mask any specific effect that might be due to the SCF^{Fbxo7} complex either in its wild-type or homozygous R379G form. I have subsequently tried to adjust the time of the duration of the assay from 30 over 20 to 10 minutes as well as subjecting the immunoprecipitation products to more stringent washing conditions prior to *in vitro* assay reconstitution without significant improvement of the signal to noise ratio (data not shown). This is certainly an important experiment that will need to be

optimized in the future, as it is one mean of combining and comparing *in vitro* with *in vivo* derived data.

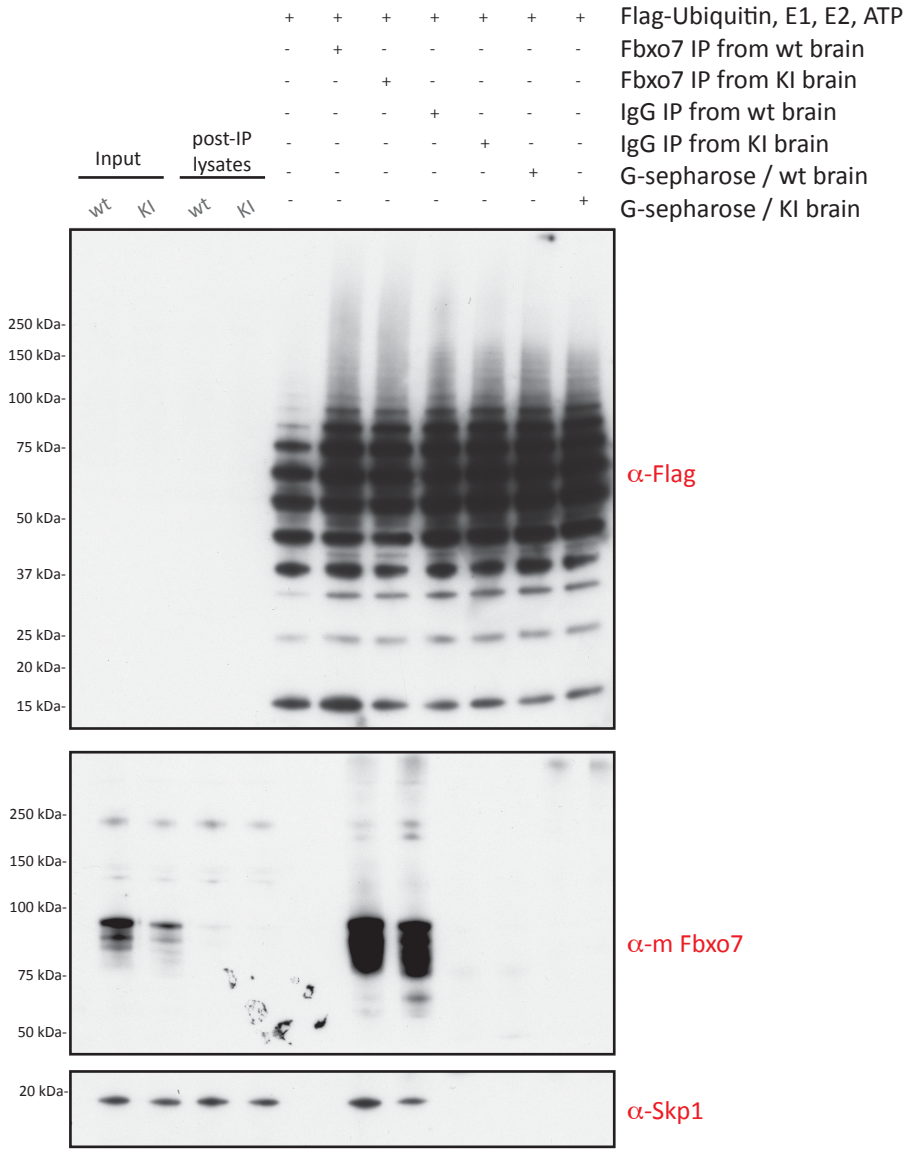

Figure 84: Failed reconstitution of *in vitro* assay with affinity purifications of endogenous SCF^{FBXO7} E3 ubiquitin ligase complexes

Endogenous Fbxo7 affinity purifications of endogenous SCF^{FBXO7} complexes from wild-type and homozygeous R379G *Fbxo7* KI brain lysates and controls - preimmune IgG IPs and G-sepharose only. To compensate for the reduced expression level of the homozygous R379G *Fbxo7* KI mutant, I used 1.3 mg of brain lysates from the wild-type and 2.6 mg of brain lysates from the mutant with the same amount of beads. The Fbxo7 immunoblot shows the reduced expression of the mutant Fbxo7 in the input lysate, while about equal amounts of Fbxo7 were found in the IP product. Post-immunoprecipitation lysates demonstrate complete depletion of Fbxo7. The G-sepharose and preimmune IgG serve as IP controls. The

Skp1 immunoblot confirms that the homozygous R379G Fbxo7 KI mutant is indeed capable of Skp1 binding and represents one of the SCF complex members. Equal amounts of immunoprecipitation reactions were washed with 4 x 1 ml of either 0.5M NaCl CHAPS lysis buffer and then washed once with reaction buffer prior to reconstituting the immunocomplexes attached to beads with reaction buffer. E1 and E2 enzymes, Flag-ubiquitin as well as ATP and Magnesium were added. The whole reaction was incubated at 30 degrees Celsius for 30 min before termination with LDS loading buffer. The Flag immunoblot shows that there was no difference between the FBXO7 wt, KI, and pre-immune complexes as well as even G-sephararose alone.

5.4 Preliminary data towards the validation of VDAC proteins as SCF^{FBXO7} ubiquitinylation targets

5.4.1 Immunoblotting of MEF and brain lysates for VDAC proteins with commercial VDAC antibodies

I have used different commercial antibodies for looking at VDAC expression levels in wild-type and homozygous R379G *Fbxo7* KI MEF whole cell lysates. In view of the complex structure of the VDAC proteins with multi-transmembrane spanning domains, I considered it important to be aware against which antigen the respective antibody was raised: The pan-VDAC antibody (source: polyclonal rabbit), which is supposed to recognize all 3 VDAC proteins, is raised against a synthetic peptide corresponding to the N-terminus of human VDAC 1. The VDAC 3 antibody (source: polyclonal rabbit) is raised against the N-terminal amino acid residues 73-122 of human VDAC 3, while the VDAC 1 antibody (source: polyclonal rat) is raised against a synthetic peptide corresponding to amino acid residue S104 of human VDAC 1. Except for the immunoblot with the VDAC 1 antibody, there was no difference in expression levels between the 2 genotypes (Figure 85). The immunoblot for the VDAC 1 antibody shows 2 bands for each lysate and although the upper band is slightly more intense in the wild-type *Fbxo7* lysates, it is not clear whether it corresponds to the unmodified or ubiquitin-modified form. I have since generated inducible stable expressing cell lines for VDAC 1 – C-terminal FLAG in FLP-in-TRex cells and also tested a further monoclonal VDAC antibody, which was raised in rabbit against a synthetic peptide corresponding to the N-terminus of human VDAC 1.

Figure 86 shows the immunoblot of induced and uninduced cytosolic as well as mitochondrial fractions of the VDAC 1- C-terminal FLAG HEK293 cell line and in the first line shows that the Flag-expressing VDAC 1 construct is exclusively found in the mitochondrial fraction suggesting that the C-terminal tag does not interfere with its correct subcellular localization. It also shows that the commercial monoclonal VDAC antibody is specific. I am intending to use the stable VDAC1-C-terminal FLAG cell line for preparing intact mitochondrial pellets as substrates in *in vitro* FBXO7 ubiquitinylation studies in the future.

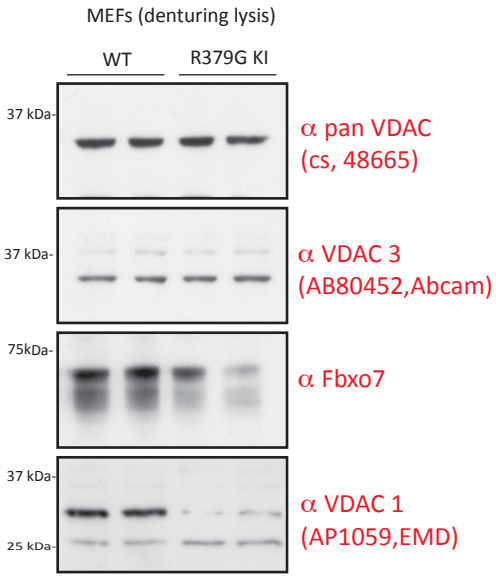

Figure 85: VDAC immunoblot of wt and hom R379G *Fbxo7* KI MEFS using commercial antibodies

Wt and hom R379G *Fbxo7* KI denaturing lysates (15 ug each) with duplicate loading was subjected to immunoblotting with 3 different commercial VDAC antibodies as well as Fbxo7. The immunoblot for the VDAC 1 antibody (AP1059, EMD) shows 2 bands for each lysate and although the upper band is slightly more intense in the wild-type *Fbxo7* lysates, it is not clear whether it corresponds to the unmodified or ubiquitin-modified form.

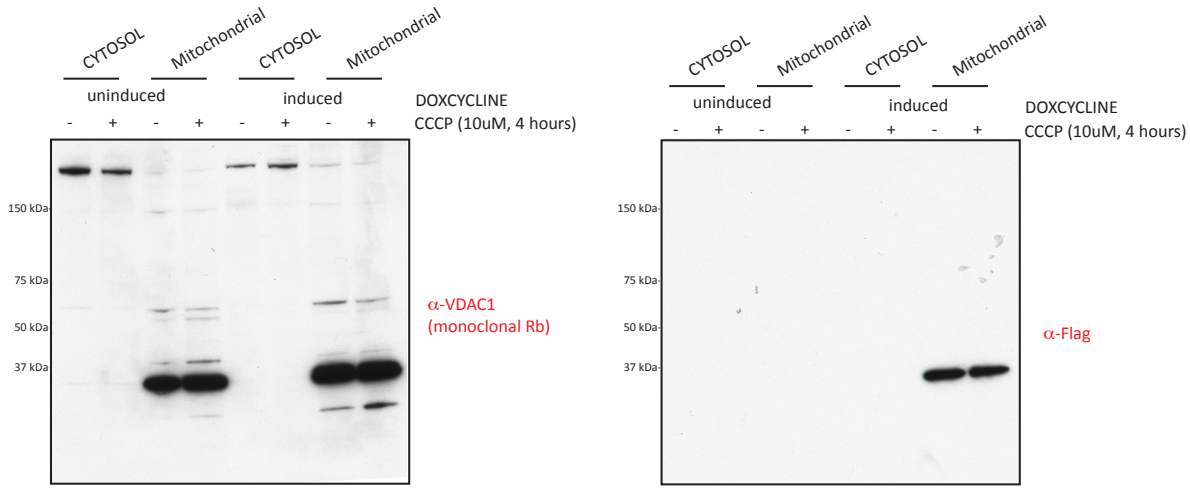

Figure 86: Generation of an inducible, stable expressing VDAC 1-C-terminal Flp-In T-REx HEK 293 cell

Stable expression of VDAC1-C-terminal FLAG was induced with 0.1ug/ml doxycycline for 18 hours prior to either treating them with 10uM CCCP or DMSO for 4 hours (as well as uninduced cells). Cells were then harvested and mitochondrial and cytosolic fractions prepared. Cytosolic and mitochondrial fractions were then subjected to immunoblotting for either FLAG or the monoclonal VDAC1 antibody. The Flag immunoblot shows that the stable construct is specifically expressed in the mitochondrial fraction; the VDAC1 antibody detects equivalent bands at the same molecular weight in both the uninduced as well as induced state suggesting that the antibody is specific.

5.4.2 Failed trial to detect endogenous VDAC proteins in a pool of ubiquitylated proteins using tandem-ubiquitin binding entities

Immunoblotting for several VDAC antibodies did not allow unequivocal identification of the ubiquitinylated form of the VDAC proteins in wild-type and homozygous R379G *Fbxo7* KI MEFs. In an alternative strategy to identify and compare ubiquitinylated forms of VDAC between the 2 genotypes *in vivo*, I have employed tandem-repeated ubiquitin-binding entities (TUBEs) that are based on ubiquitin-associated domains to purify poly-ubiquitinylated proteins from wild-type and homozygous R379G *Fbxo7* KI brain lysates(Hjerpe et al., 2009; Hjerpe and Rodriguez, 2008). In order to determine whether TUBEs could be used to capture endogenously ubiquitinylated VDAC proteins, I have subjected the TUBEs pull downs to immunoblotting for VDAC. Figure 87 shows that polyubiquitinylated species are efficiently pulled down by TUBEs, but that no higher

molecular weight species of VDAC's – that would suggest their posttranslational modification with polyubiquitin – is being captured by this approach.

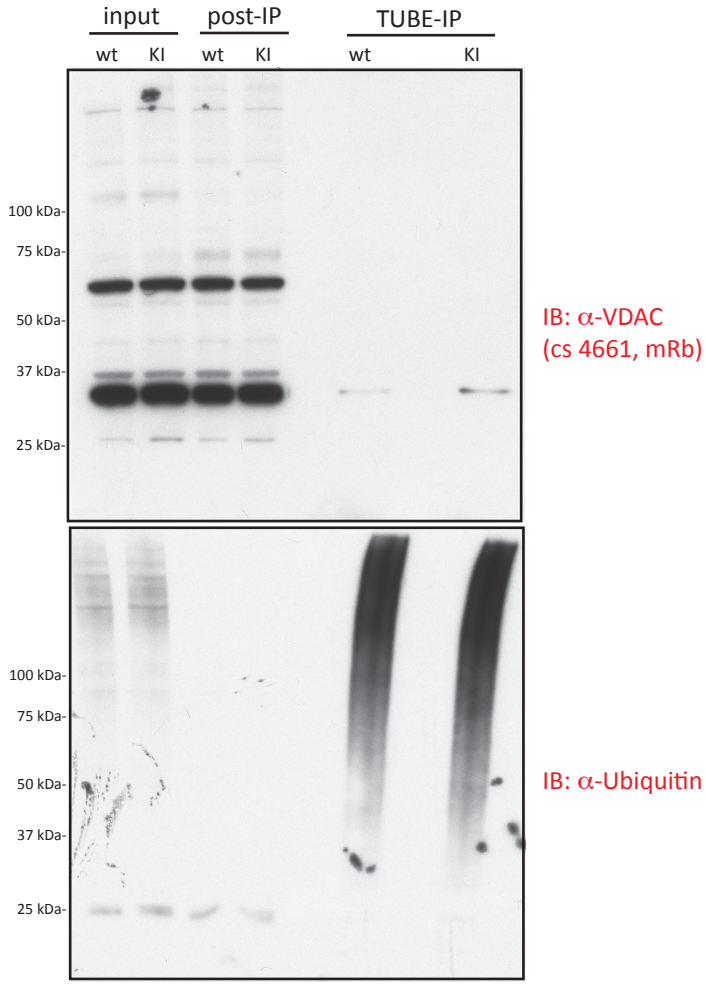

Figure 87: No VDAC proteins are detected in the TUBEs pull-down of endogenous polyubiquitinylated species from wt and hom R379G *Fbxo7* brain lysates

10 mg 1% triton X lysates from wt and hom R379G *Fbxo7* brains were prepared and subjected to covalently coupled TUBEs to G-sepharose. The immunoblots show 15 ug of each input and post-TUBEs IP lysates as well as 5% of the IP product for the Ubiquitin and 30% for the VDAC blot. While the Ubiquitin blot shows efficient enrichment of ubiquitinylated species from endogenous brain lysates, no higher molecular weight species of VDAC proteins are detected.

5.4.3 *In vitro* Fbxo7 ubiquitinylation assay with mitochondrial pellet as substrate

Having set up the *in vitro* SCF^{FBXO7} autoubiquitinylation assay, my next aim was to demonstrate *in vitro* SCF^{FBXO7} - dependent VDAC ubiquitinylation. We are currently in the

process of expressing recombinant VDAC proteins reconstituted in detergent micelles in analogy to the protocol that allowed solving the β-barrel structure of VDAC1. In the meantime, I have used freshly prepared intact mitochondria from HEK293 cells as a substrate. In the first instance, I have tried to determine the *in vitro* ubiquitinylation of VDAC proteins by immunoblotting of the direct product of the *in vitro* assay as well as after a FLAG-purification to enrich for any FLAG-ubiquitin modified mitochondrial proteins. The final FLAG-purification step was also introduced to prepare the respective samples for mass-spectrometry analysis. The expectation is that if an endogenous outer mitochondrial membrane protein – those proteins (such as VDACs) that are accessible to ubiquitin modification when intact mitochondrial pellets are being used in this experiment – is *in vitro* ubiquitinylated in a SCF^{FBXO7} dependent manner, higher molecular weight FLAG-ubiquitinylated species of that particular protein could either be detected by direct immunoblotting or subsequently by proteomic analysis of the FLAG-purification. Figure 88 shows the immunoblot of the FLAG and VDAC immunoblots of the in vitro ubiquitinylation reaction before and after the subsequent FLAG-purification step: The VDAC immunoblot confirms that endogenous VDAC proteins were indeed present in the intact mitochondrial pellet that was used as a substrate, but without being able to demonstrate a discernable difference dependent on the absence or presence of an F-box protein in the assay. I had used the FBXO7 wild-type as well as the R379G mutant, but also the F-box protein βTRCP as a control. The VDAC immunoblot also demonstrates that the FLAG-pull-down failed to enrich for any potential VDAC protein. Interestingly, the FLAG-immunoblot shows a differential pattern of higher molecular weight species – possibly corresponding to *in vitro* ubiquitinylated mitochondrial membrane proteins – for the $SCF^{FBXO7\ wt}$ and $SCF^{-\beta TRCP}$ dependent *in vitro* ubiquitinylation reactions. Exactly these higher molecular weight species of FLAG-ubiquitin / FLAG-ubiquitin modified proteins were actually purified by the FLAG-pull-down. Some of the FLAG-purified in vitro assay was also prepared and analysed by mass-spectrometry. As expected, VDAC proteins were not amongst the identified hits – given the absent VDAC signal in the corresponding immunoblot.

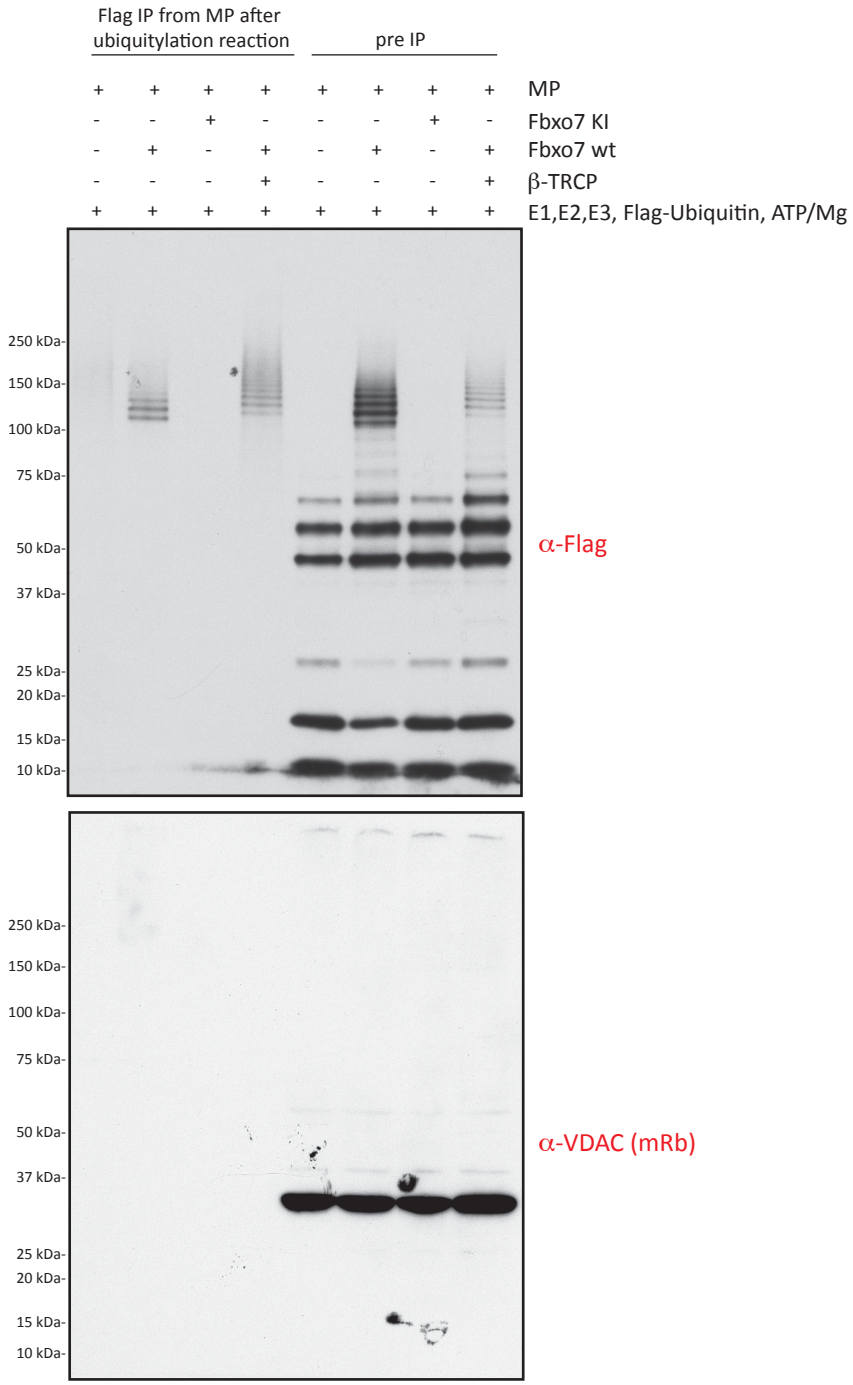

Figure 88: *In vitro* FBXO7 ubiquitinylation assay with intact mitochondria as substrates

Intact mitochondria prepared from HEK293 cells were used as a substrate for an *in vitro* $SCF^{F\text{-box protein}}$ E3 ubiquitinylation with either FBXO7 wild-type, R378G or β-TRCP. The reaction was heat-inactivated and 2%SDS was used for mitochondrial pellet lysis and sonication. Some material was retained for immunoblotting (right hand side on immunoblots: pre-IP), but most of it was used for a FLAG-IP to immunoprecipitate any Flag-ubiquintylated mitochondrial proteins. The FLAG immunoblot shows the in vitro ubiquitinylation reaction products for each of the different F-box proteins and (E1, E2 and E3 (=

Cullin1 / RBX1 / SKP1) as a control as well as the product of the FLAG-immunoprecipitation of the *in vitro* ubiquitinylation product. The FLAG-immunoblot shows a differential pattern of higher molecular weight species – possibly corresponding to *in vitro* ubiquitinylated mitochondrial membrane proteins – for the $SCF^{FBXO7\ wt}$ and $SCF^{\beta\text{-}TRCP}$ dependent *in vitro* ubiquitinylation reactions, but no difference between the control (E1,2,3 and MP alone) and the R378G FBXO7 as expected. The VDAC immunoblot failed to pick up a signal in the IP samples and shows the same signal for all input / post assay samples.

I have subsequently worked towards optimizing the assay and post-assay purification of potential FLAG-ubiquitinylated species mainly by using different mitochondrial pellet lysis conditions post- in vitro assay and adjusting the FLAG-pull-down procedure. Additionally, I have used intact mitochondrial pellets from HEK293 cells that were either treated with CCCP or DMSO control. This was to see whether mitochondrial depolarization was a requirement for subsequent SCF^{FBXO7} dependent *in vitro* ubiquitinylation. Figure 89 shows the FLAG immunoblot of the *in vitro* ubiquitinylation assay with intact mitochondria from HEK293 cells - that were either CCCP stimulated or not - as a substrate and in the presence or absence of recombinant wild-type FBXO7. The majority of the FLAG-purified assay product was prepared for in-gel tryptic digestion and subsequent mass-spectrometry analysis. It has to be noted that the proteomic identification of Di-glycine peptides is unable to differentiate whether the modification was an *in vivo* residual one or a result of the SCF^{FBXO7} dependent *in vitro* reaction. The aim of the proteomic analysis was to detect VDAC peptides with a di-Glycine signature in only those reactions where recombinant FBXO7 was present. Figure 89 shows the Flag-immunoblot the pre-immunoprecipitation / post in vitro ubiquitinylation samples and the FLAG immunoprecipitations of the controls (without FBXO7, but with mitochondrial pellets either treated or untreated with CCCP) and the FBXO7 in vitro ubiquitinylation reactions with mitochondrial pellets from either untreated or CCCP treated intact mitochondrial preparations. The FLAG-enrichment aimed to purify FLAG-ubiquitin modified mitochondrial proteins. Separating the individual samples on a gel by SDS page allowed to eliminate all free FLAG-tagged ubiquitin by excluding the corresponding molecular weight bands from the analysis.

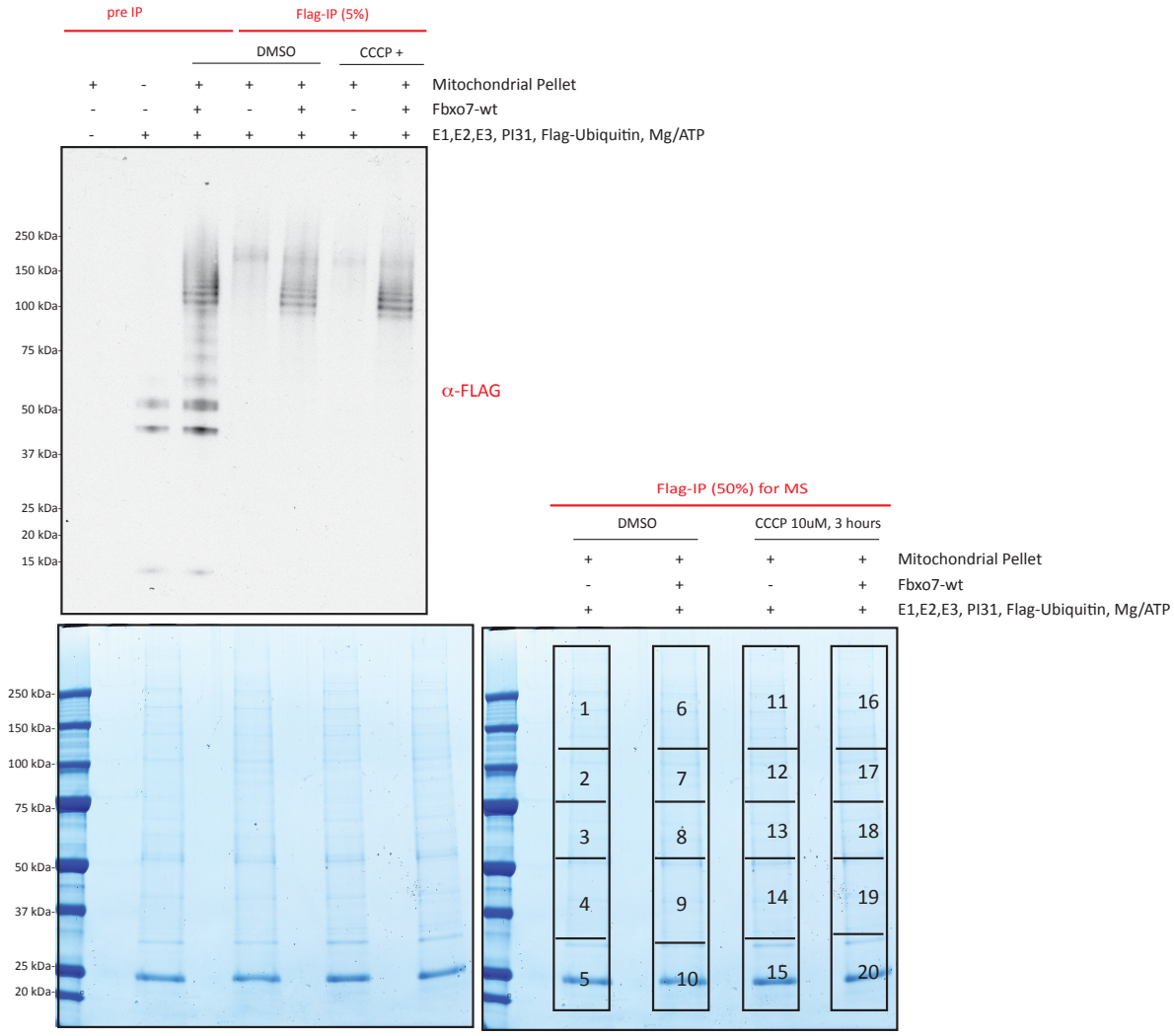

Figure 89: *In vitro* FBXO7 ubiquitinylation assay with intact mitochondria from untreated and CCCP treated HEK293 cells as substrates

Intact mitochondria prepared from HEK293 cells either untreated or CCCP treated (3 hours, 10uM) were used as substrates for an *in vitro* $SCF^{FBXO7\ wt}$ E3 ubiquitinylation reaction. The reaction was heat-inactivated and 2% SDS was used for mitochondrial pellet lysis and sonication. Upper panel: Some material was retained for post *in vitro* assay / pre FLAG-IP imput (left-hand side) and post-FLAG IP (right-hand side) immunoblotting with FLAG. Lower panels: Most of the FLAG-IP product (95%) was used for Coomassie staining of a SDS PAGE resolution (4-12%) for subsequent in gel-tryptic digestion for mass-spectrometry analysis. Individual gel pieces as processed are indicated on the right.

Figure 90 shows a qualitative schematic of the proteomic analysis of the FLAG immunoprecipitation of the *in vitro* ubiquitinylation assay. It shows that I am successfully immunoprecipitating VDAC proteins with a FLAG tag possibly suggesting that they Flag-ubiquitin modified in the course of the in vitro ubiquitinylation reaction. Alternatively, they could bind unspecifically to FLAG. However, VDAC proteins were also found in gel pieces corresponding to a higher molecular weight than that of unmodified VDACs. These could potentially represent posttranslationally modified VDAC species. No VDAC peptide carrying the Di-glycine signature of a peptide that is ubiquitinylated at protein level. Without enrichment, the detection of Di-Glycine peptides is difficult. These experiments are overall encouraging, but need to be repeated and scaled up to allow simultaneous immunoblotting for VDAC as well. An alternative strategy to the post assay FLAG immunoprecipitation would be to perform a Di-Glycine enrichment step prior to the proteomic analysis. Certainly a plethora of different experiments could be done and these will be addressed in the discussion.

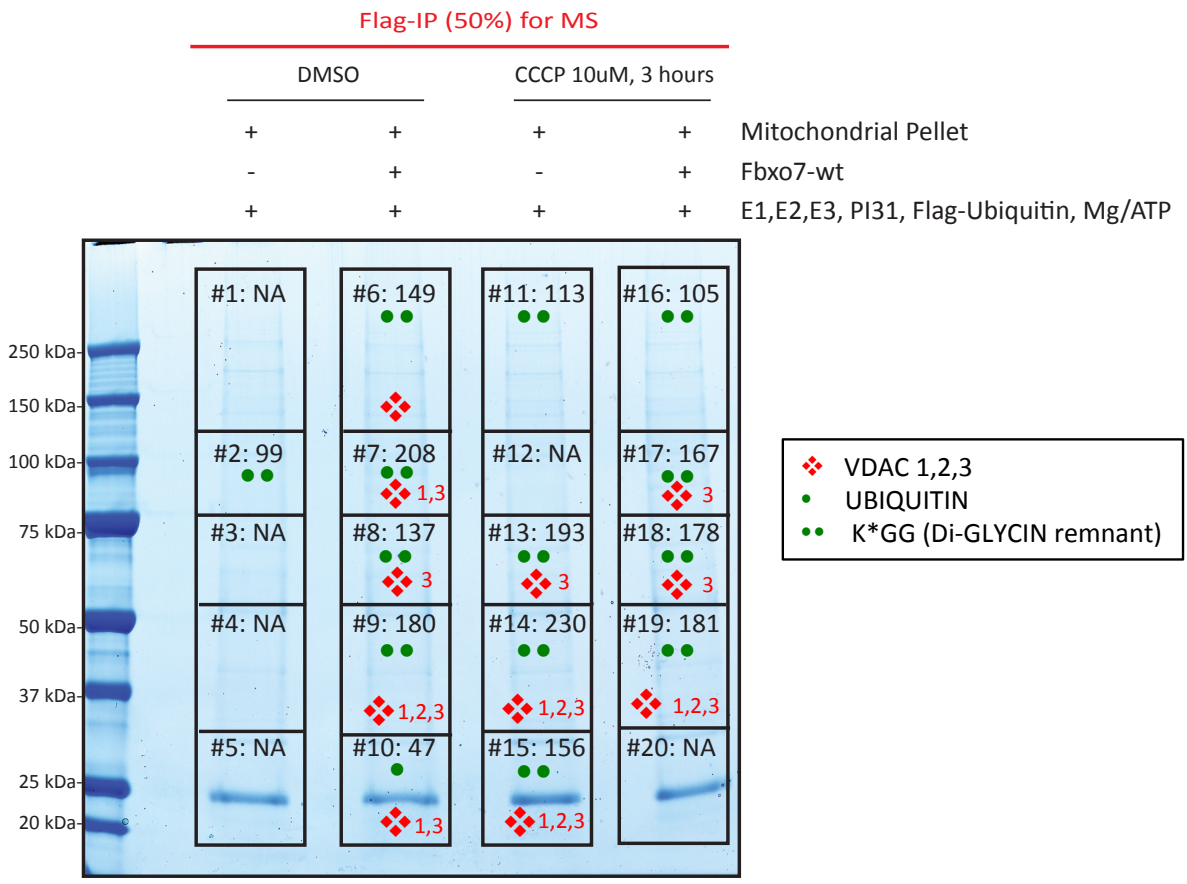

Figure 90: Proteomic analysis of the mitochondrial pellet substrate assay for SCF^{FBXO7}

Schematic representation of proteomic analysis with respect to the identification of VDAC proteins, Di-Glycine peptides and ubiquitin for each gel piece from Figure 89. NA: Some of the samples have not yet been analysis or were unsuitable for analysis. VDAC proteins have a molecular weight of about 30 kDa.

5.5 Discussion

In this last result chapter I am making use of the homozygous R379G *Fbxo7* KI mouse to explore the Fbxo7-dependent proteome as well as ubiquitinome by quantitative proteomics in the endogenous system. While I had used proteomics in the previous 2 results chapters for mapping protein interactions, the aim is now to look at differential post-translational modification states ("ubiquitinome") as well as comparative expression proteomics ("whole proteome") between the wild-type and homozygous R379G *Fbxo7* KI genotypes. Last but not least, I am also focusing on setting up an *in vitro*

SCF^{FBXO7} ubiquitinylation assay as a functional read-out for the FBXO7-dependent SCF E3 ligase activity.

5.5.1 Differential enrichment of the ubiquitylated proteome from SILAC labelled wt and homozygous R379G *Fbxo7* KI MEFs

Quantitative ubiquitin remnant profiling combines SILAC labelling with an enrichment step for Di-Glycine modified peptides prior to differential proteomic analysis. I was interested in using this approach to identify Di-Glycine modification sites that are altered as a consequence of the difference between the wild-type and homozygous R379G KI genotype in MEFs. MEFs were used in this study, as they are amenable to *in vivo* differential labelling by SILAC, while Di-Glycine enrichment was used as the difference in mass-shift between a modified and unmodified peptide allows unequivocal insight into its ubiquitinylation status at a specific site. So far, more than 20000 unique ubiquitinylation sites have been reported using Di-glycine affinity proteomics(Emanuele et al., 2011; Kim et al., 2011; Wagner et al., 2011; Xu et al., 2010). Still, many already known ubiquitinylation targets have not been identified in any of these studies. It has been suggested that this reflects their overall low abundance on protein level(Harper and Tan, 2012). Another reason is the incomplete depletion of all di-Glycine peptides by the Di-Glycine antibody. Efforts have been undertaken to increase the in-depths coverage of the ubiquitinome as well as the efficiency of depletion by the Di-Glycine antibody and mainly included optimizing the ratio of peptide input and antibody used, Di-Glycine antibody cross-linking, and basic reversed phase chromatography prior to fractionated Di-Glycine enrichment and proteomic analysis(Udeshi et al., 2012; Udeshi et al., 2013). In my experiment I have incorporated these aforementioned technical refinements. I have completed 2 biological replicate experiments identifying 2060 unique ubiquitinylation sites in the first and 999 in the second experiment. How does this compare to studies published in the literature? Prior to using the Di-Glycine enrichment strategy, the reported number of ubiquitinylation sites in large-scale studies was around 110 sites in yeast and up to 100 sites in human cell lines(Denis et al., 2007; Meierhofer et al., 2008; Peng et al., 2003; Tan et al., 2008; Vasilescu et al., 2005). In the original Di-Glycine enrichment report, 374 unique di-glycine modified lysine sites were

identified in 236 ubiquitinylated proteins from HEK293 cells(Xu et al., 2010). Another Di-Glycine enrichment study identified 753 unique sites in 471 proteins from HEK293 and U2OS osteosarcoma cell lines(Danielsen et al., 2011). Although the number of identified sites has in very recent times risen from more than 5000 and even up to 20000 sites, this could only be achieved by using either large amount of input material, the completion of many experimental replicates (>4) and also the use of proteasomal inhibition(Emanuele et al., 2011; Kim et al., 2011; Udeshi et al., 2012; Wagner et al., 2011). 20000 non-redundant sites have been detected in the combined analysis from replicates of 5 different mouse tissues, but only a few thousand sites were identified in each individual tissue sample with significant variations in the numbers depending on the respective tissue(Wagner et al., 2011). Proteasomal inhibition can result in an increase in the number of identified sites several folds, but the majority of these sites appear in a protein-synthesis dependent manner and might represent a perturbation bias rather than true endogenous ubiquitinylation events(Harper and Tan, 2012; Kim et al., 2011; Wagner et al., 2011). This is the context in which my experiment needs to be seen: Given that my study encompasses 2 biological replicates and no proteasomal inhibition, I consider the number of identified sites to be average to above average. However, the implication of a less than complete in-depth coverage of the global ubiquitinome automatically means that any differentially modified sites in a protein with relatively low expression levels will be missed.

Quantitative Di-Glycine capture has been used in the setting of identifying substrates of the PD disease gene PARKIN in response to mitochondrial depolarization(Sarraf et al., 2013). PARKIN is a RING-HECT hybrid E3 ubiquitin ligase and mutations in PARKIN are the most frequent cause of familial early onset Parkinsonism(Singleton et al., 2013; Wenzel et al., 2011). It has been shown that the activity of PARKIN is regulated by an interaction between its N-terminal UBL domain and its C-terminal, which results in autoinhibition of the E3 ligase activity of PARKIN(Chaugule et al., 2011). Is, however, a highly conserved residue within the UBL domain of PARKIN phosphorylated by the protein product of yet another PD associated gene – PINK1 – a conformational change occurs resulting in PARKIN activation(Burchell et al., 2012; Kondapalli et al., 2012). These

observations have been made *in vitro* and require conditions of mitochondrial stress. PARKIN activation is also accompanied by its recruitment to the outer mitochondrial membrane, where most of the so far identified ubiquitinylation substrates of PARKIN reside(Chan et al., 2011; Glauser et al., 2011; Narendra et al., 2012; Narendra et al., 2010; Wang et al., 2011). The aforementioned quantitative Di-Glycine capture experiment aimed to identify the PARKIN-dependent ubiquitinome in a site-specific manner and in response to mitochondrial stress(Sarraf et al., 2013). In this study, HCT116 and HeLa cells with and without overexpression of tagged-PARKIN as well as untransfected SH-SY5 neuronal cells were used in a total of 73 proteomic control and quantitative Di-Glycine capture experiments. In some experiments proteasomal inhibition was used. In total, 4772 non-redundant ubiquitinylation sites in 1654 proteins were identified. The rational of the experiment is that overexpressing PARKIN in combination with mitochondrial stress – a condition that has been shown to activate the E3 ligase activity of PARKIN – yields an increase in the likelihood of detecting signal-dependent (PARKIN-dependent) and mechanistically relevant ubiquitinylation events. Additionally, tag affinity purification mass-spectrometry was used to identify interacting partners of overexpressed PARKIN. Overall, this study has led to the discovery of many new ubiquitinylation targets as well as interacting partners of PARKIN including proteins involved in metabolism, mitochondrial fusion and trafficking, autophagy, and the proteasome / ubiquitin receptors and also mitochondrial pore proteins – namely VDAC proteins(Sarraf et al., 2013). VDAC proteins were identified to interact with overexpressed PARKIN in response to mitochondrial stress and also to be ubiquitinylated at the following sites: VDAC 1 (K53, 109, and 274); VDAC 2 (K135 and 300); and VDAC3 (K53, 109, 163, 266, 274).

In contrast, my experiment aims to identify specific ubiquitinylation sites / targets that differ between the wild-type SCF^{Fbxo7} and the R379G mutant $SCF^{Fbxo7\ R379G}$ complex. Rather than using tagged overexpression in different tumour cell lines, I am using material derived from littermate wild-type and homozygous R379G *Fbxo7* KI embryos, which allows me to observe differences in the ubiquitinylation status of target proteins on the endogenous level. I have also not used mitochondrial stress in order to avoid

potential artefacts. Amongst the differentially ubiquitinylated proteins in my study are also all 3 VDAC isoforms: For each VDAC protein, several different peptides carrying the unequivocal Di-Glycine remnant signature of site-specific ubiquitinylation at protein level have been identified. The peptides in Table 5-3 show all Di-Glycine remnant peptides for which an Xpress ratio of > 2 has been identified suggesting that the particular peptide was x-fold more often identified in the SILAC light-labelled wild-type than in the SILAC heavy labelled homozygous R379G *Fbxo7* KI MEFs. In fact some of the specific ubiquitinylation sites have been identified to be more than 20-fold more often in case of the wild-type background (for VDAC 1: K122). Interestingly, all unique sites converge onto exactly 2 lysine residues that are conserved between VDAC 1, 2, and 3 as well as between the mouse and human homologues (Figure 69). Additionally, differential ubiquitinylation of VDAC proteins was robustly demonstrated across the 2 biological replicates. This is very unlikely due to an artefact; the protein concentration of the input lysates for both genotypes had been carefully quantified and differential proteomic analysis of the digested wild-type and homozygous R379G *Fbxo7* KI peptide mix prior to the Di-Glycine enrichment step confirmed that there was no significant difference in the abundance for VDAC 1,2, and 3 between the 2 genotypes. The fact that the identified ubiquitinylation sites are in all likelihood facing the cytosolic compartment rather than towards the inner mitochondrial membrane or being buried within the many transmembrane domains of VDAC 1,2, and 3 corroborates the validity of the experiments with regards to the VDAC proteins (Figure 69). Furthermore, the in my experiment as differentially modified VDAC sites have been reported before as endogenous ubiquitinylation sites for both human and mouse homologous(Chen et al., 2014): In the one study that identified as many as 20000 endogenous ubiquitinylation sites in different mouse tissues, the authors were also particularly interested in the divergent pattern of ubiquitinylation sites depending on tissue type(Wagner et al., 2011). This allowed cross-referencing whether the 2 conserved and differentially ubiquitinylated VDAC sites identified in my experiment in MEFs had also been identified in brain: While the first ubiquitinylation site in my experiment (VDAC 1: K66; VDAC 2: K64; VDAC 3: K53) was only detected for VDAC 1 in mouse brain samples, the second

conserved ubiquitinylation site was found in all 3 VDAC proteins in brain. Overall, I have high confidence for having identified 2 conserved lysine residues in all 3 VDAC proteins that are not only functional ubiquitinylation sites *in vivo*, but also highly suggestive of being instrumental in the difference between wild-type and homozygous R379G *Fbxo7* KI and the pathogenicity of the latter.

Of course, my findings only allow the conclusion that VDAC 1, 2, and 3 are differential ubiquitinylated dependent on the *Fbxo7* wild-type or R379G mutant genotype in MEFs. The set up of my experiment does not all the conclusion that VDAC proteins are actually direct ubiquitinylation targets of Fbxo7. So which E3 ligases have been implemented in the ubiquitinylation of VDAC proteins in general? So far, only PARKIN has been put forward to be involved in VDAC ubiquitinylation: As mentioned before, PARKIN overexpression in combination with mitochondrial stress leads to increased ubiquitinylation of all 3 VDAC proteins at specific sites in HeLa and HCT116 cells(Sarraf et al., 2013). Overexpression of functional PARKIN in neuronal (inducible SH-SY5SY cells) as well as non-neuronal cell types in combination with mitochondrial stress has been shown to result in the identification of higher molecular weight species of VDAC 1 while overexpression of several different pathogenic PARKIN mutants fail to do so(Geisler et al., 2010).

It is intriguing that 3 different autosomal recessive PARK gene products – wild-type PARKIN(Sarraf et al., 2013), functional PINK / PARKIN(Geisler et al., 2010) as well as wild-type FBXO7 (my study) - have all been implicated in the ubiquitinylation of VDAC proteins, while another recent study suggests that PINK1, PARKIN and FBXO7 not only physically interact, but also map to the same pathway converging on the mitochondria and possibly mitophagy (degradation of mitochondria by the autophagy system). It is therefore highly desirable to set up *in vitro* ubiquitinylation experiments with FBXO7 as well as PARKIN to demonstrate which of the 2 E3 ligases is directly involved in VDAC ubiquitinylation.

5.5.2 Quantitative global proteomics to identify differences in expression levels across the whole proteome of wild-type and hom R379G *Fbxo7* KI brain lysates

There is uncertainty about the number of proteins that constitute the mammalian proteome. One general approach is to apply the one-gene-one protein rule, and accordingly the human (as well as mouse) proteome comprises about 20000 proteins(Clamp et al., 2007; Cox and Mann, 2011). Up to 10000 non-redundant proteins have been identified in a single human cell line and about 8000 proteins have been found in the whole mouse proteome(Cox and Mann, 2011; Wang et al., 2006). In our study, we identified a total of just under 7000 proteins in RapiGest brain lysates of 3 biological replicate pairs of wild-type and homozygous R379G *Fbxo7* KI animals. Of these 7000 proteins, less than 1.5% (107 proteins) changed their expression levels by more than 1.5, and this number was further diminished to 0.2% (15 proteins) if only those proteins were included whose expression level changed reliably (p value of less than 0.5). The total number of proteins identified in this study is significantly smaller than the expected number based on the one-gene-one protein rule, but comparable to what has been published in the literature(Wang et al., 2006). In contrast, the number of proteins whose expression level differed reliably dependent on either the wild-type or R379G *Fbxo7* KI genotype was negligibly small. In fact, the rate of false positive discovery, which conventionally is in the magnitude of 1%, is significantly higher(Higdon et al., 2011; Y, 1995). Subsequent immunoblotting indeed failed to validate any of the as differentially expressed hits by the proteomic analysis and a p-value of < 0.5. For example, Integrin-β5 and Neurogenic differentiation factor 2 are each at the end of the magnitude spectrum of differential expression between the wild-type and homozygous R379G *Fbxo7* KI genotypes: While the proteomic analysis of Integrin-β5 determined it to be 100-fold more abundant in the wild-type background, the expression level of the latter was measured to be 11 times higher in the homozygous R379G *Fbxo7* KI background. Immunoblotting for the 2 proteins reveals greater inter-individual differences than any discernable difference based on genotype. I have aimed to validate as mainly of the 15 proteins that were identified in this study as long as commercial antibodies were available, the change in expression level was more than 2-fold and if

more than 2 peptides were identified by the proteomic analysis. Although this precluded some of the potential hits from being validated – such as Glycosyltransferase-like domain containing protein 1, Lactrophilin-2, 60s ribosomal protein L36a, Protein Pcdhb 20, Protein KTI22 homolog, and Glycosylphosphatidylinositol anchor attachment 1 protein – I decided to conclude the experiment at this stage. This was based on the negative validation of the proteins that I actually examined – amongst them the 2 proteins that were accordingly differently expressed either 10 or 100 – fold, but also because I consider this approach retrospectively not as the most suitable for many reasons: Ultimately, it is not clear as yet whether FBXO7 functions as an E3 ligase component with an effect on the proteasome and whether the disease mutants – in particular the one for which I have the R379G *Fbxo7* KI mouse model – differ from the wild-type only in their substrate specificity / incompatibility. Even if a difference in substrate specificity was the underlying pathomechanism of the FBXO7 disease mutants, a differential ubiquitinylation activity upon substrate proteins, does not necessary affect total protein expression levels. In fact, it is usually only a small pool of a particular protein that is being post-transnationally modified by ubiquitin. Another argument against this approach is the high complexity of the mammalian brain in contrast to for example a single cell line. It could also be that FBXO7 might exert its specific function in one particular part of the brain – for example within the basal ganglia – and any possible effect on protein expression levels in this particular region is being diluted out by analysing whole brain lysates rather than specific compartments or regions of functional neuronal networks. There are many publications that address the various different strategies for the identification of SCF substrates by the means of proteomics, but employing a difference in protein abundance on the endogenous level to identify substrates that differ between the wild-type and a mutant form of an F-box protein or any other SCF component is not amongst them(Harper and Tan, 2012; Vertegaal, 2011). In terms of using a genetic approach in combination with global protein expression / stability levels as a read-out, there is only one successful and established approach: Global Protein Stability (GPS) profiling(Yen and Elledge, 2008; Yen et al., 2008). GPS is based on a dual fluorescence reporter system that uses fluorescence-activated cell

sorting with DNA microarray deconvolution to detect changes in protein expression levels in live cells, but is far from my aim which is studying the effect of a particular F-box protein mutation on the endogenous level *in vivo*. To conclude, the depth and coverage of this experiment in terms of total proteome, the low number of proteins with a differential expression pattern between the 2 genotypes – which was in fact lower than the accepted number of false positives in any given proteomic experiment, the complexity of the sample, and possibly a false hypothesis that the Fbxo7-dependent ubiquitinylation of a potential substrate automatically results in a reduction in protein expression level thereof. The problem of inter-individual differences between the individual animals could possibly have been overcome by pooling brain tissue from animals of the same genotypes together prior to tissue lysis and analysis and could be considered in future experiments.

5.5.3 **Steps towards establishing an in vitro FBXO7 dependent ubiquitinylation assay**

A big step towards setting up functional in vitro FBXO7 assays was the recombinant expression of the various SCF^{FBXO7} complex components. The original protocol was developed for the biochemical and structural analysis of recombinant SCF^{SKP2} and SCF^{TRCP1}_{β} complexes(Li et al., 2005). Recombinant baculovirus production in insect cells allows efficient production, while the use of a dual or multi-expression baculoviral vector allows protein-protein interactions between direct binding partners and subsequent intermolecular hydrophobic packing to occur. Initially, we focused on the recombinant expression of the FBXO7 wild-type and the R378G KI disease mutant, which forms the basis of the R379G *Fbxo7* KI mouse model in my thesis. It emerged early on that despite co-expression of untagged SKP1 and the DAC-tagged R378G FBXO7 mutant the interaction between the 2 proteins was impaired. As SKP1 is co-purified with its respectively co-expressed FBXO7 binding partner via DAC-tag purification, significantly lower amounts of SKP1 were repeatedly co-purified with the R378G mutant in comparison to the wild-type FBXO7 protein (Figure 78). Re-sequencing of baculoviral expression cassette excluded simple cloning mistakes as the underlying cause. It was therefore decided to also include the only other homozygous FBXO7 mutation – R498X – into the analysis for comparison. Figure 80 (A) shows that the truncating R498X mutant

was indeed capable of SKP1 binding. My conclusion is that the failure of the R378G mutant to efficiently bind SKP1 is an intrinsic property of this particular mutant protein and possibly explained by the close proximity of the mutated residue to the SKP1-binding F-box domain of FBXO7. In fact, this is an observation that was already made in a different recombinant expression system: Bi-cistronic expression vectors expressing recombinant GST-tagged FBXO7 wild-type as well as the R378G mutant together with SKP1 demonstrated impaired SKP1 binding of the R378G mutant.

The next step was to demonstrate that all components of the SCF^{FBXO7} complex – individually or co-expressed were in principle able to assemble into a SCF complex. As the functional association between FBXO7 and PI31 is not as yet clarified and PI31 could potentially be a regulatory component of the SCF^{FBXO7} complex as is the case in Drosophila melanogaster, I investigated tetrameric (without PI31) and pentameric (with PI31) SCF complex formation. 5.3.2 shows that DAC-purification of the SCFFBXO7 complex with and without PI31 is successfully achieved in the FBXO7 wild-type as well as R498X mutant setting, while not possible in case of the R378G FBXO7 mutant. It was therefore also no surprise that the R378G mutant was incapable of mounting an ubiquitin free chain formation response in the SCFFBXO7 E3 ligase activity assays (5.3.3). Based on these *in vitro* findings alone it could have been easy to speculate that the pathogenicity of the R378G FBXO7 disease mutant is explained by its inability to assemble into a functional $SCF^{FBXO7\ R378G}$ E3 ubiquitin ligase complex. This is of course not the case given my contradicting *in vivo* findings: the human R378G FBXO7 mutant as well as its mouse R379G homologue are very well capable to SCF^{FBXO7} complex formation as convincingly shown in the overexpression systemFigure 14, as well as in the endogenous human and mouse system in Figure 38 and Figure 40. One of my seminal findings in the R379G Fbxo7 KI mouse has been that the expression level of the homozygous mutant protein is significantly lower it is for the wild-type Fbxo7 protein (Figure 36 and Figure 34). I am demonstrating in Figure 83 that the relative ability of SKP1 biding of the mutant in comparison to the wild-type protein is about the same. In the *in vivo* system additional SCF^{FBXO7} binding / complex partners might compensate for the perturbed SKP1 binding ability of the R378/9G FBXO7 mutant. One possibility of

following this up is to perform a size exclusion chromatography of the *in vivo* affinity purified SCF^{FBXO7} wild-type and R379G mutant complex in comparison to the *in vitro* complex and possibly subsequent mass-spectrometry analysis of the relevant *in vivo* fractions.

The most important application of the *in vitro* SCF^{FBXO7} E3 ligase assay will be to validate potential FBXO7 ubiquitinylation substrates – such as HURP, cIAP1 and TRAF2 as well as to differentiate between physical interacting partners and ubiquitinylation targets as identified in my affinity purification mass-spectrometry experiments(Chang et al., 2006; Kirk et al., 2008; Kuiken et al., 2012). So far, we are in the process of recombinant expression and purification of some of my potential ubiquitinylation targets (for example Reticulon B). Another crucial implication of the *in vitro* FBXO7 assay is the validation of VDAC proteins.

5.5.4 Preliminary data towards the validation of VDAC proteins as SCF^{FBXO7} ubiquitinylation targets

One of the most exciting findings during my PhD has been the identification of VDAC proteins as differential ubiquitinylation targets of endogenous FBXO7 wild-type and homozygous R379G MEFs. Of course, I will not be able to demonstrate a difference in ubiquitinylation efficiency between the FBXO7 wild-type and R378G mutant towards VDACs as the R378G mutant does not assemble into a SCF complex *in vitro* in the first place. However, I would potentially be able to demonstrate that VDACs are direct ubiquitinylation targets of FBXO7 and shed light on at least the question of whether it is FBXO7 or PARKIN that is responsible for VDAC ubiquitinylation. As these results are very recent, we are still developing tools for the adequate assessment and study of VDAC proteins: *in house* DSTT-production of VDAC 1,2 and 3 antibodies and recombinant production and micellar refolding of VDAC proteins. I am currently performing experiments with intact mitochondrial preparations with and without CCCP stimulation as substrates in the SCF*FBXO7* in vitro assays. Due to the lack of efficient and sensitive VDAC antibodies I have developed SCF^{FBXO7} *in vitro* substrate assays with intact mitochondria and FLAG-tagged ubiquitin in combination with denaturing post-assay lysis

and FLAF affinity purification mass-spectrometry. Preliminary data shows the identification peptides mapping to VDAC as well as ubiquitin proteins as well as Di-Glycine remnant peptides suggestive of ubiquitinylation events. I will have to scale up and refine the procedure in order to reliably detect in vitro FBXO7 dependent ubiquitinylation events of VDAC proteins in situ in the outer mitochondrial membrane of intact mitochondria. This could involve differential Di-Glycine affinity purification mass-spectrometry: for example using intact mitochondrial preparations from "heavy" isotope (K8R10) labelled HEK293 cells in combination with Di-Glycine enrichment after the in vitro SCF^{FBXO7} assay (using "light" labelled ubiquitin), I would be able to unequivocally identify site-specific ubiquitinylation events of VDAC or other mitochondrial membrane proteins as dependent on the FBXO7 *in vitro* assay. Until reliable VCDA antibodies are available I am also planning to perform *in vitro* FBXO7 assays using the inducible, stable expressing VDAC 1-C-terminal FLAG Flp-In T-REx HEK 293 cell (in combination with untagged ubiquitin) and use FLAG immunoblotting of the assay product for higher molecular weight species as a functional read out. Figure 86 shows that the VDAC 1-C-terminal FLAG is actually expressed in the mitochondria and hence suitable for this kind of assay.

5.5.5 **Summary of chapter 5**

In summary, this chapter has focused on trying to dissect the differences between the wild-type and the homozygous R379G *Fbxo7* KI mutant by comparing protein expression levels across the entire proteome as well as differences in the site-specific modification of the entire ubiquitinome. Caveats as in any other comparable proteomic studies are the incomplete sequencing depth of the proteome and incomplete capture of the ubiquitinome. While I discovered no discernable difference in terms of protein expression / abundance in as many as 7000 proteins between the wild-type and homozygous R379G Fbxo7 KI genotype in mouse brain lysates, I have made a significant discovery by identifying 2 conserved ubiquitinylation sites in each of the 3 VDAC proteins that are preferentially ubiquitinylated in the *Fbxo7* wild-type in comparison to the homozygous R379G genotype in MEFs using SILAC based Fbxo7-dependent Di-Glycine capture proteomics. One of the big advantages of my study is that they have

been performed in the endogenous system either with differential *ex-vivo* chemical labelling of mouse brain lysates or *in vivo* SILAC labelling of MEF lysates. I have used the in the previous chapter characterized *Fbxo7* mouse model with knock-in of the corresponding R378G FBXO7 disease mutants at the endogenous locus for these experiments. Furthermore, I have set up functional assays for monitoring the FBXO7 dependent SCF E3 ligase activity *in vitro.* The compromised SKP1 binding of the R378G FBXO7 mutant explains why it is unable to form a tetrameric or even pentameric complex with Cullin1, SKP1, RBX1 and PI31, which is a necessary prerequisite for any functional enzymatic activity. In contrast, the only other so far described homozygous FBXO7 disease mutant is able of $SCF^{FBXO7\ R498X}$ E3 ligase complex formation and as a read out for functional activity also capable of free ubiquitin chain formation. At least *in vitro*, this would suggest a different pathogenic mechanism for the truncating R498X disease mutant in comparison to the R378G mutant. The substrate-binding region of F-box proteins has often been described to reside in their C-terminal domains; hence binding of a physiological FBXO7 substrate could be impaired in the R498X disease mutant as it is devoid of the C-terminal 22 amino acids(Ho et al., 2006; Jin et al., 2004; Skaar et al., 2013). In contradiction to my *in vitro* findings, I have unequivocally demonstrated that the human R378G FBXO7 and corresponding mouse R379G Fbxo7 mutant proteins are able to assemble into the SCF^{FBXO7} E3 ubiquitin ligase complex. I am proposing that there additional binding / interacting partners or co-factors that compensate the impaired binding between this particular mutant and SKP1. Given the juxtaposition of the mutated R378G / R379G residue and the F-box domain of FBXO7 compromised binding is likely. Usually binding of 2 proteins – such as for example FBXO7 and SKP1 – strengthens their intermolecular hydrophobic packing and hence stability which might explain, why I observe reduced Fbxo7 expression levels in the homozygous R379G *Fbxo7* KI mouse. It would be interesting to examine and compare FBXO7 expression levels in human brain or other tissue between the wild-type and R378G disease mutant. If a reduction in expression level of the R378G mutant in its homozygous compared to the wild-type state could be reproduced in humans, it could be argued that not a difference in actual ubiquitinylation targets but a threshold effect of the R378G FBXO7 disease

mutant is the basis for its pathogenicity. Nevertheless, FBXO7 is an important player in genes and proteins that map into signalling pathways involved in Parkinson' disease associated neurodegeneration. There are only a handful of patients worldwide affected by FBXO7 associated disease, but unravelling the signalling pathway of FBXO7 and further exploring its entanglement with PINK, PARKIN and VDAC proteins as well as other PARK genes is an exciting avenue for appreciating the relevance of FBXO7 in the bigger picture of neurodegeneration. In the end, it is about identifying new, targeted means for developing causal treatment for patients with Parkinson's Disease.

6 Summary of all result chapters and outlook

My first result chapter shows that FBXO7 does assemble into the SCF^{FBXO7} E3 ubiquitin ligase complex and that this is true for the FBXO7 widtype protein as well as for all of the 3 known diease mutants - T22M, R378G and R498X. These findings suggest that SCF complex disruption is an unlikely mechanism by which the FBXO7 disease mutants exert their pathogenicity. The Alanine mutant screen of single residues within the F-box domain of FBXO7 gives some insight into the interaction between FBXO7 and SKP1: the employed single mutants in this study are on its own unable to abolish SKP1 binding, and based on what we know so far complete SCF complex disruption is only achieved by the simultaneous deletion of several residues ($\geq$ 4 amino acid residues). The non-SKP1 binding mutants also demonstrate that there is no dimerization between the endogenous $SCF^{FBXO7\ wt}$ E3 ubiquitin ligase complex and the overexpressed mutants. If this was the case one would have expected to see a signal for SKP1 in the immunoblot of the affinity purified Flag-immunocomplexes as Western blotting does not allow discrimination based on the source of SKP1 –either bound to endogenous or mutant FBXO7. Retained binding of the tag-immunocomplexes to PI31, which is mediated via the FP-domain upstream of the F-box domain of FBXO7, shows that the mutations introduced in the non-SKP1 binding mutants does not cause disarray of the protein structure to such an extend that binding via other domains would be affected (Figure

21). Whether this allows any conclusion on towards whether FBXO7 (or $SCF^{FBXO7\ wt}$) forms homodimers is an open question.

The second result chapter is dedicated to the characterization of the *Fbxo7* knock-in mouse model of one of the pathogenic *FBXO7* mutations (R378G in humans) and the endogenous study of Fbxo7 in brain comparing the wild-type to the homozygous Fbxo7 KI genotype. A first finding is that Fbxo7 is widely expressed in different tissues and that the *R379G* Fbxo7 KI mouse displays a hypomorphic expression pattern in the homozygous state. In brain lysates, the difference amounts to a reduction by half. If this is not an intrinsic artefact of the genetic mouse model, the reduction in protein levels of the pathogenic mutant could amount to a pathomechanistic threshold effect. A second important and novel finding is that endogenous Fbxo7 assembles together with Cullin 1, Skp1, and Rbx1 to form the SCF^{Fbxo7} E3 ubiquitin ligase complex *in vivo*. The demonstration that the homozygous R379G Fbxo7 mutant is equally capable of SCF E3 ligase formation, a feature that is retained in human patient-derived homogenous R378G FBXO7 fibroblast cell lines. This allows the conclusion that the pathogenic R378G *FBXO7* mutant does not exert its pathogenicity via disruption of the SCF E3 ligase complex. Using endogenous Fbxo7 affinity purification in combination with mass-spectrometry has confirmed PI31 and Exportin 1 to not only interact with Fbxo7 in heterologous systems, but also on the endogenous level in brain samples of wild-type and homozygous R379G *Fbxo7* KI mice. I have identified potentially novel Fbxo7 interacting partners of which the RanBP2/ranGAP1*SUMO1/UBC9 E3 SUMO ligase complex is one of the most exciting findings. This warrants further exploration as it could be a further example of the crosstalk between the ubiquitylation and sumoylation system. Last but not least, the preliminary phenotype analysis of the R379G *Fbxo7* KI mouse line has revealed a significant motor deficit of the homozygous KI animals in comparison to the wild-type genotype. A neuropathological study to assess whether this deficit in motor performance correlates to a dopaminergic neuronal cell loss is still outstanding.

The last result chapter focuses on trying to dissect the differences between the wild-type and the homozygous R379G *Fbxo7* KI mutant by comparing protein expression levels across the entire proteome as well as differences in the site-specific modification of the entire ubiquitinome. Caveats as in any other comparable proteomic studies are the incomplete sequencing depth of the proteome and incomplete capture of the ubiquitinome. While I discovered no discernable difference in terms of protein expression / abundance in as many as 7000 proteins between the wild-type and homozygous R379G Fbxo7 KI genotype in mouse brain lysates, I have made a significant discovery by identifying 2 conserved ubiquitinylation sites in each of the 3 VDAC proteins that are preferentially ubiquitinylated in the *Fbxo7* wild-type in comparison to the homozygous R379G genotype in MEFs using SILAC based Fbxo7-dependent Di-Glycine capture proteomics. One of the big advantages of my study is that they have been performed in the endogenous system either with differential *ex-vivo* chemical labelling of mouse brain lysates or *in vivo* SILAC labelling of MEF lysates. I have used the in the previous chapter characterized *Fbxo7* mouse model with knock-in of the corresponding R378G FBXO7 disease mutants at the endogenous locus for these experiments. Furthermore, I have set up functional assays for monitoring the FBXO7 dependent SCF E3 ligase activity *in vitro.* The compromised SKP1 binding of the R378G FBXO7 mutant explains why it is unable to form a tetrameric or even pentameric complex with Cullin1, SKP1, RBX1 and PI31, which is a necessary prerequisite for any functional enzymatic activity. In contrast, the only other so far described homozygous FBXO7 disease mutant is able of $SCF^{FBXO7\ R498X}$ E3 ligase complex formation and as a read out for functional activity also capable of free ubiquitin chain formation. At least *in vitro*, this would suggest a different pathogenic mechanism for the truncating R498X disease mutant in comparison to the R378G mutant. The substrate-binding region of F-box proteins has often been described to reside in their C-terminal domains; hence binding of a physiological FBXO7 substrate could be impaired in the R498X disease mutant as it is devoid of the C-terminal 22 amino acids(Ho et al., 2006; Jin et al., 2004; Skaar et al., 2013). In contradiction to my *in vitro* findings, I have unequivocally demonstrated that the human R378G FBXO7 and corresponding mouse R379G Fbxo7 mutant proteins are

able to assemble into the SCF^{FBXO7} E3 ubiquitin ligase complex. I am proposing that there are additional binding / interacting partners or co-factors that compensate the impaired binding between this particular mutant and SKP1. Given the juxtaposition of the mutated R378G / R379G residue and the F-box domain of FBXO7 compromised binding is likely. Usually binding of 2 proteins – such as for example FBXO7 and SKP1 – strengthens their intermolecular hydrophobic packing and hence stability which might explain, why I observe reduced Fbxo7 expression levels in the homozygous R379G *Fbxo7* KI mouse. It would be interesting to examine and compare FBXO7 expression levels in human brain or other tissue between the wild-type and R378G disease mutant. If a reduction in expression level of the R378G mutant in its homozygous compared to the wild-type state could be reproduced in humans, it could be argued that not a difference in actual ubiquitinylation targets but a threshold effect of the R378G FBXO7 disease mutant is the basis for its pathogenicity. Nevertheless, FBXO7 is an important player in genes and proteins that map into signalling pathways involved in Parkinson' disease associated neurodegeneration. There are only a handful of patients worldwide affected by FBXO7 associated disease, but unravelling the signalling pathway of FBXO7 and further exploring its entanglement with PINK, PARKIN and VDAC proteins as well as other PARK genes is an exciting avenue for appreciating the relevance of FBXO7 in the bigger picture of neurodegeneration. In the end, it is about identifying new, targeted means for developing causal treatment for patients with Parkinson's Disease.

In conclusion, my PhD work has mainly focused on the E3 ligase dependent function of FBXO7 as the substrate recognizing subunit of the SCF^{FBXO7} E3 ubiquitin ligase and its potential role in protein quality control in the central nervous system. However, it is well known that F-box proteins also have SCF independent functions and this also appears to apply to FBXO7 as reviewed in (Nelson et al., 2013). It is important to keep the possible SCF independent roles of FBXO7 in mind when putting the findings of my PhD work into context of what is known about FBXO7. For example, it is very exciting that 2 conserved lysine residues of the outer mitochondrial membrane proteins VDAC 1, 2 and 3 are differentially ubiquitinylated in an FBXO7 genotype dependent manner. Based on my results so far it is not possible to say whether VDAC proteins are direct ubiquitinylation

substrates of FBXO7 or whether the preferential ubiquitinylation of these proteins in the FBXO7 wildtype-dependent background is a result of other regulatory factors. Factors that might influence the ubiquitinylation efficacy of VDAC proteins could be the reported interaction between FBXO7 and for example PINK1 or PARKIN(Burchell et al., 2013)(Figure 91). This and some of he other findings discussed in my PhD thesis are very exciting avenues for further exploration.

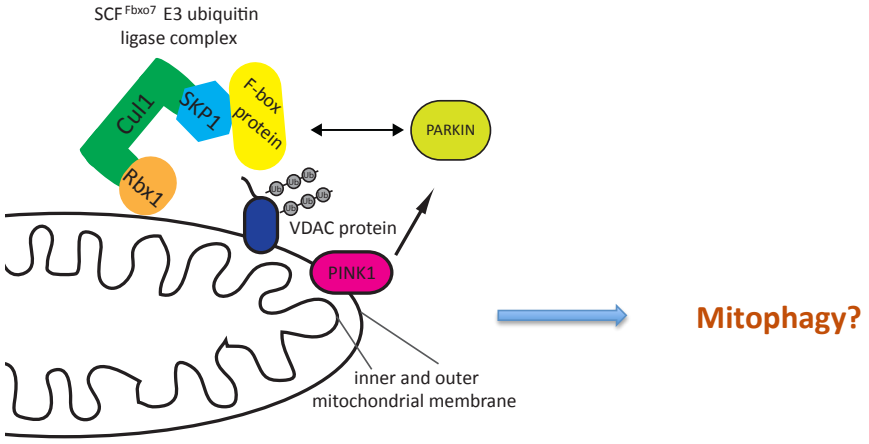

Figure 91: Proposed model of how FBXO7, PINK1 and PARKIN could interact

The PD disease gene products FBXO7, PARKIN and PINK1 have been suggested to interact with each other and could potentially function to maintain mitochondrial integrity. Impaired mitochondrial integrity is a recognized pathomechanism of PD associated neurodegeneration in general and the outer mitochondrial membrane proteins VDAC 1,2 and 3 have been suggested to play a central role in this. It may therefore be that VDAC proteins are direct ubiquitinylation targets of FBXO7 or alternatively, that their ubiquitinylation status is dependent on the interplay between FBXO7, PINK1 and PARKIN in an SCF^{FBXO7} independent fashion. All this is a very exciting avenue for further exploration.

IX REFERENCES

Anderson, P.C., and Daggett, V. (2008). Molecular basis for the structural instability of human DJ-1 induced by the L166P mutation associated with Parkinson's disease. Biochemistry *47*, 9380-9393.

Andersson, S., Davis, D.L., Dahlback, H., Jornvall, H., and Russell, D.W. (1989). CLONING, STRUCTURE, AND EXPRESSION OF THE MITOCHONDRIAL CYTOCHROME-P-450 STEROL 26-HYDROXYLASE, A BILE-ACID BIOSYNTHETIC ENZYME. J Biol Chem *264*.

Arnaoutov, A., Azuma, Y., Ribbeck, K., Joseph, J., Boyarchuk, Y., Karpova, T., McNally, J., and Dasso, M. (2005). Crm1 is a mitotic effector of Ran-GTP in somatic cells. Nat Cell Biol *7*, 626-632.

Bader, M., Benjamin, S., Wapinski, O.L., Smith, D.M., Goldberg, A.L., and Steller, H. (2011). A conserved F box regulatory complex controls proteasome activity in Drosophila. Cell *145*, 371-382.

Bayrhuber, M., Meins, T., Habeck, M., Becker, S., Giller, K., Villinger, S., Vonrhein, C., Griesinger, C., Zweckstetter, M., and Zeth, K. (2008). Structure of the human voltage-dependent anion channel. Proc Natl Acad Sci U S A *105*, 15370-15375.

Behrens, M.I., Bruggemann, N., Chana, P., Venegas, P., Kagi, M., Parrao, T., Orellana, P., Garrido, C., Rojas, C.V., Hauke, J.*, et al.* (2010). Clinical spectrum of Kufor-Rakeb syndrome in the Chilean kindred with ATP13A2 mutations. Movement disorders : official journal of the Movement Disorder Society *25*, 1929-1937.

Bertler, A., and Rosengren, E. (1959). Occurrence and distribution of dopamine in brain and other tissues. Experientia *15*, 10-11.

Bhatia, I.M.D.C.D.M.S.A.S.K.P. (2012). Marsden's Book of Movement Disorders, 1 edn (Oxford University Press).

Bignell, G.R., Warren, W., Seal, S., Takahashi, M., Rapley, E., Barfoot, R., Green, H., Brown, C., Biggs, P.J., Lakhani, S.R.*, et al.* (2000). Identification of the familial cylindromatosis tumour-suppressor gene. Nature genetics *25*, 160-165.

Bilguvar, K., Tyagi, N.K., Ozkara, C., Tuysuz, B., Bakircioglu, M., Choi, M., Delil, S., Caglayan, A.O., Baranoski, J.F., Erturk, O.*, et al.* (2013). Recessive loss of function of the neuronal ubiquitin hydrolase UCHL1 leads to early-onset progressive neurodegeneration. Proc Natl Acad Sci U S A *110*, 3489-3494.

Blagoev, B., Ong, S.E., Kratchmarova, I., and Mann, M. (2004). Temporal analysis of phosphotyrosine-dependent signaling networks by quantitative proteomics. Nat Biotechnol *22*, 1139-1145.

Boersema, P.J., Raijmakers, R., Lemeer, S., Mohammed, S., and Heck, A.J. (2009). Multiplex peptide stable isotope dimethyl labeling for quantitative proteomics. Nat Protoc *4*, 484-494.

Brooks, S.P., and Dunnett, S.B. (2009). Tests to assess motor phenotype in mice: a user's guide. Nat Rev Neurosci *10*, 519-529.

Brownell, J.E., Sintchak, M.D., Gavin, J.M., Liao, H., Bruzzese, F.J., Bump, N.J., Soucy, T.A., Milhollen, M.A., Yang, X., Burkhardt, A.L*., et al.* (2010). Substrate-assisted inhibition of ubiquitin-like protein-activating enzymes: the NEDD8 E1 inhibitor MLN4924 forms a NEDD8-AMP mimetic in situ. Mol Cell *37*, 102-111.

Budny, B., Badura-Stronka, M., Materna-Kiryluk, A., Tzschach, A., Raynaud, M., Latos-Bielenska, A., and Ropers, H.H. (2010). Novel missense mutations in the ubiquitination-related gene UBE2A cause a recognizable X-linked mental retardation syndrome. Clinical genetics *77*, 541-551.

Burchell, L., Chaugule, V.K., and Walden, H. (2012). Small, N-terminal tags activate Parkin E3 ubiquitin ligase activity by disrupting its autoinhibited conformation. PLoS One *7*, e34748.

Burchell, V.S., Nelson, D.E., Sanchez-Martinez, A., Delgado-Camprubi, M., Ivatt, R.M., Pogson, J.H., Randle, S.J., Wray, S., Lewis, P.A., Houlden, H*., et al.* (2013). The Parkinson's disease-linked proteins Fbxo7 and Parkin interact to mediate mitophagy. Nature neuroscience *16*, 1257-1265.

Capecchi, M.R. (1989). Altering the genome by homologous recombination. Science *244*, 1288-1292.

Cenciarelli, C., Chiaur, D.S., Guardavaccaro, D., Parks, W., Vidal, M., and Pagano, M. (1999). Identification of a family of human F-box proteins. Current biology : CB *9*, 1177-1179.

Chan, N.C., Salazar, A.M., Pham, A.H., Sweredoski, M.J., Kolawa, N.J., Graham, R.L., Hess, S., and Chan, D.C. (2011). Broad activation of the ubiquitin-proteasome system by Parkin is critical for mitophagy. Hum Mol Genet *20*, 1726-1737.

Chang, Y.F., Cheng, C.M., Chang, L.K., Jong, Y.J., and Yuo, C.Y. (2006). The F-box protein Fbxo7 interacts with human inhibitor of apoptosis protein cIAP1 and promotes cIAP1 ubiquitination. Biochem Biophys Res Commun *342*, 1022-1026.

Chartier-Harlin, M.C., Kachergus, J., Roumier, C., Mouroux, V., Douay, X., Lincoln, S., Levecque, C., Larvor, L., Andrieux, J., Hulihan, M*., et al.* (2004). Alpha-synuclein locus duplication as a cause of familial Parkinson's disease. Lancet *364*, 1167-1169.

Chau, V., Tobias, J.W., Bachmair, A., Marriott, D., Ecker, D.J., Gonda, D.K., and Varshavsky, A. (1989). A multiubiquitin chain is confined to specific lysine in a targeted short-lived protein. Science *243*, 1576-1583.

Chaugule, V.K., Burchell, L., Barber, K.R., Sidhu, A., Leslie, S.J., Shaw, G.S., and Walden, H. (2011). Autoregulation of Parkin activity through its ubiquitin-like domain. Embo J *30*, 2853-2867.

Chen, L., Cagniard, B., Mathews, T., Jones, S., Koh, H.C., Ding, Y., Carvey, P.M., Ling, Z., Kang, U.J., and Zhuang, X. (2005). Age-dependent motor deficits and dopaminergic dysfunction in DJ-1 null mice. J Biol Chem *280*, 21418-21426.

Chen, T., Zhou, T., He, B., Yu, H., Guo, X., Song, X., and Sha, J. (2014). mUbiSiDa: A Comprehensive Database for Protein Ubiquitination Sites in Mammals. PLoS One *9*, e85744.

Chen, Y., and Dorn, G.W., 2nd (2013). PINK1-phosphorylated mitofusin 2 is a Parkin receptor for culling damaged mitochondria. Science *340*, 471-475.

Christensen, D.E., Brzovic, P.S., and Klevit, R.E. (2007). E2-BRCA1 RING interactions dictate synthesis of mono- or specific polyubiquitin chain linkages. Nature structural & molecular biology *14*, 941-948.

Ciechanover, A. (2005). Intracellular protein degradation: from a vague idea, through the lysosome and the ubiquitin-proteasome system, and onto human diseases and drug targeting (Nobel lecture). Angewandte Chemie *44*, 5944-5967.

Clamp, M., Fry, B., Kamal, M., Xie, X., Cuff, J., Lin, M.F., Kellis, M., Lindblad-Toh, K., and Lander, E.S. (2007). Distinguishing protein-coding and noncoding genes in the human genome. Proc Natl Acad Sci U S A *104*, 19428-19433.

Cohen, P., and Tcherpakov, M. (2010). Will the ubiquitin system furnish as many drug targets as protein kinases? Cell *143*, 686-693.

Colombini, M. (2009). The published 3D structure of the VDAC channel: native or not? Trends Biochem Sci *34*, 382-389.

Cook, C., Stetler, C., and Petrucelli, L. (2012). Disruption of protein quality control in Parkinson's disease. Cold Spring Harb Perspect Med *2*, a009423.

Cox, J., and Mann, M. (2011). Quantitative, high-resolution proteomics for data-driven systems biology. Annu Rev Biochem *80*, 273-299.

Cox, J., Matic, I., Hilger, M., Nagaraj, N., Selbach, M., Olsen, J.V., and Mann, M. (2009). A practical guide to the MaxQuant computational platform for SILAC-based quantitative proteomics. Nat Protoc *4*, 698-705.

D'Angiolella, V., Donato, V., Forrester, F.M., Jeong, Y.T., Pellacani, C., Kudo, Y., Saraf, A., Florens, L., Washburn, M.P., and Pagano, M. (2012). Cyclin F-mediated degradation of ribonucleotide reductase M2 controls genome integrity and DNA repair. Cell *149*, 1023-1034.

D'Angiolella, V., Donato, V., Vijayakumar, S., Saraf, A., Florens, L., Washburn, M.P., Dynlacht, B., and Pagano, M. (2010). SCF(Cyclin F) controls centrosome homeostasis and mitotic fidelity through CP110 degradation. Nature *466*, 138-142.

Danielsen, J.M., Sylvestersen, K.B., Bekker-Jensen, S., Szklarczyk, D., Poulsen, J.W., Horn, H., Jensen, L.J., Mailand, N., and Nielsen, M.L. (2011). Mass spectrometric analysis of lysine ubiquitylation reveals promiscuity at site level. Mol Cell Proteomics *10*, M110 003590.

Dawlaty, M.M., Malureanu, L., Jeganathan, K.B., Kao, E., Sustmann, C., Tahk, S., Shuai, K., Grosschedl, R., and van Deursen, J.M. (2008). Resolution of sister centromeres requires RanBP2-mediated SUMOylation of topoisomerase IIalpha. Cell *133*, 103-115.

Dawson, T.M., Ko, H.S., and Dawson, V.L. (2010). Genetic animal models of Parkinson's disease. Neuron *66*, 646-661.

de Lau, L.M., and Breteler, M.M. (2006). Epidemiology of Parkinson's disease. Lancet Neurol *5*, 525-535.

Denis, N.J., Vasilescu, J., Lambert, J.P., Smith, J.C., and Figeys, D. (2007). Tryptic digestion of ubiquitin standards reveals an improved strategy for identifying ubiquitinated proteins by mass spectrometry. Proteomics *7*, 868-874.

Dennissen, F.J., Kholod, N., and van Leeuwen, F.W. (2012). The ubiquitin proteasome system in neurodegenerative diseases: culprit, accomplice or victim? Prog Neurobiol *96*, 190-207.

Deribe, Y.L., Pawson, T., and Dikic, I. (2010). Post-translational modifications in signal integration. Nature structural & molecular biology *17*, 666-672.

Deshaies, R.J., and Joazeiro, C.A. (2009). RING domain E3 ubiquitin ligases. Annu Rev Biochem *78*, 399-434.

Di Fonzo, A., Dekker, M.C., Montagna, P., Baruzzi, A., Yonova, E.H., Correia Guedes, L., Szczerbinska, A., Zhao, T., Dubbel-Hulsman, L.O., Wouters, C.H.*, et al.* (2009). FBXO7 mutations cause autosomal recessive, early-onset parkinsonian-pyramidal syndrome. Neurology *72*, 240-245.

Di Fonzo, A., Tassorelli, C., De Mari, M., Chien, H.F., Ferreira, J., Rohe, C.F., Riboldazzi, G., Antonini, A., Albani, G., Mauro, A.*, et al.* (2006). Comprehensive analysis of the LRRK2 gene in sixty families with Parkinson's disease. European journal of human genetics : EJHG *14*, 322-331.

Ding, H., Xu, Y., Chen, Q., Dai, H., Tang, Y., Wu, J., and Shi, Y. (2005). Solution structure of human SUMO-3 C47S and its binding surface for Ubc9. Biochemistry *44*, 2790-2799.

Doherty, K.M., and Hardy, J. (2013). Parkin disease and the Lewy body conundrum. Movement disorders : official journal of the Movement Disorder Society *28*, 702-704.

Dorsey, E.R., Constantinescu, R., Thompson, J.P., Biglan, K.M., Holloway, R.G., Kieburtz, K., Marshall, F.J., Ravina, B.M., Schifitto, G., Siderowf, A.*, et al.* (2007). Projected number of people with Parkinson disease in the most populous nations, 2005 through 2030. Neurology *68*, 384-386.

Du, J., Ma, Y., Ma, P., Wang, S., and Fan, Z. (2013). Demethylation of epiregulin gene by histone demethylase FBXL11 and BCL6 corepressor inhibits osteo/dentinogenic differentiation. Stem Cells *31*, 126-136.

Dunham, N.W., and Miya, T.S. (1957). A note on a simple apparatus for detecting neurological deficit in rats and mice. J Am Pharm Assoc Am Pharm Assoc (Baltim) *46*, 208-209.

Durocher, Y., Perret, S., and Kamen, A. (2002). High-level and high-throughput recombinant protein production by transient transfection of suspension-growing human 293-EBNA1 cells. Nucleic Acids Research *30*.

Duvoisin, R.C. (1996). Recent advances in the genetics of Parkinson's disease. Advances in neurology *69*, 33-40.

Ebrahimi-Fakhari, D., Wahlster, L., and McLean, P.J. (2012). Protein degradation pathways in Parkinson's disease: curse or blessing. Acta neuropathologica *124*, 153-172.

Edgar, R.C. (2004). MUSCLE: multiple sequence alignment with high accuracy and high throughput. Nucleic acids research *32*, 1792-1797.

Emanuele, M.J., Elia, A.E., Xu, Q., Thoma, C.R., Izhar, L., Leng, Y., Guo, A., Chen, Y.N., Rush, J., Hsu, P.W.*, et al.* (2011). Global identification of modular cullin-RING ligase substrates. Cell *147*, 459-474.

Farrer, M., Chan, P., Chen, R., Tan, L., Lincoln, S., Hernandez, D., Forno, L., Gwinn-Hardy, K., Petrucelli, L., Hussey, J.*, et al.* (2001). Lewy bodies and parkinsonism in families with parkin mutations. Annals of neurology *50*, 293-300.

Fiek, C., Benz, R., Roos, N., and Brdiczka, D. (1982). Evidence for identity between the hexokinase-binding protein and the mitochondrial porin in the outer membrane of rat liver mitochondria. Biochim Biophys Acta *688*, 429-440.

Flick, K., Raasi, S., Zhang, H., Yen, J.L., and Kaiser, P. (2006). A ubiquitin-interacting motif protects polyubiquitinated Met4 from degradation by the 26S proteasome. Nat Cell Biol *8*, 509-515.

Froyen, G., Corbett, M., Vandewalle, J., Jarvela, I., Lawrence, O., Meldrum, C., Bauters, M., Govaerts, K., Vandeleur, L., Van Esch, H.*, et al.* (2008). Submicroscopic duplications of the hydroxysteroid dehydrogenase HSD17B10 and the E3 ubiquitin ligase HUWE1 are associated with mental retardation. American journal of human genetics *82*, 432-443.

Geisler, S., Holmstrom, K.M., Skujat, D., Fiesel, F.C., Rothfuss, O.C., Kahle, P.J., and Springer, W. (2010). PINK1/Parkin-mediated mitophagy is dependent on VDAC1 and p62/SQSTM1. Nat Cell Biol *12*, 119-131.

George, S., van den Buuse, M., San Mok, S., Masters, C.L., Li, Q.X., and Culvenor, J.G. (2008). Alpha-synuclein transgenic mice exhibit reduced anxiety-like behaviour. Exp Neurol *210*, 788-792.

Gispert, S., Ricciardi, F., Kurz, A., Azizov, M., Hoepken, H.H., Becker, D., Voos, W., Leuner, K., Muller, W.E., Kudin, A.P.*, et al.* (2009). Parkinson phenotype in aged PINK1-deficient mice is accompanied by progressive mitochondrial dysfunction in absence of neurodegeneration. PLoS One *4*, e5777.

Glauser, L., Sonnay, S., Stafa, K., and Moore, D.J. (2011). Parkin promotes the ubiquitination and degradation of the mitochondrial fusion factor mitofusin 1. J Neurochem *118*, 636-645.

Goldberg, M.S., Fleming, S.M., Palacino, J.J., Cepeda, C., Lam, H.A., Bhatnagar, A., Meloni, E.G., Wu, N., Ackerson, L.C., Klapstein, G.J.*, et al.* (2003). Parkin-deficient mice exhibit nigrostriatal deficits but not loss of dopaminergic neurons. J Biol Chem *278*, 43628-43635.

Goldberg, M.S., Pisani, A., Haburcak, M., Vortherms, T.A., Kitada, T., Costa, C., Tong, Y., Martella, G., Tscherter, A., Martins, A.*, et al.* (2005). Nigrostriatal dopaminergic deficits and hypokinesia caused by inactivation of the familial Parkinsonism-linked gene DJ-1. Neuron *45*, 489-496.

Gomez-Garre, P., Jesus, S., Carrillo, F., Caceres-Redondo, M.T., Huertas-Fernandez, I., Bernal-Bernal, I., Bonilla-Toribio, M., Vargas-Gonzalez, L., Carballo, M., and Mir, P. (2013). Systematic mutational analysis of FBXO7 in a Parkinson's disease population from southern Spain. Neurobiology of aging.

Grabbe, C., and Dikic, I. (2009). Functional roles of ubiquitin-like domain (ULD) and ubiquitin-binding domain (UBD) containing proteins. Chemical reviews *109*, 1481-1494.

Greenfield, J.G., and Bosanquet, F.D. (1953). The brain-stem lesions in Parkinsonism. Journal of neurology, neurosurgery, and psychiatry *16*, 213-226.

Gwinn-Hardy, K., Singleton, A., O'Suilleabhain, P., Boss, M., Nicholl, D., Adam, A., Hussey, J., Critchley, P., Hardy, J., and Farrer, M. (2001). Spinocerebellar ataxia type 3 phenotypically resembling parkinson disease in a black family. Archives of neurology *58*, 296-299.

Hafezparast, M., Ahmad-Annuar, A., Wood, N.W., Tabrizi, S.J., and Fisher, E.M. (2002). Mouse models for neurological disease. Lancet Neurol *1*, 215-224.

Haglund, K., Di Fiore, P.P., and Dikic, I. (2003a). Distinct monoubiquitin signals in receptor endocytosis. Trends Biochem Sci *28*, 598-603.

Haglund, K., Sigismund, S., Polo, S., Szymkiewicz, I., Di Fiore, P.P., and Dikic, I. (2003b). Multiple monoubiquitination of RTKs is sufficient for their endocytosis and degradation. Nat Cell Biol *5*, 461-466.

Hardy, J., Cai, H., Cookson, M.R., Gwinn-Hardy, K., and Singleton, A. (2006). Genetics of Parkinson's disease and parkinsonism. Annals of neurology *60*, 389-398.

Harlalka, G.V., Baple, E.L., Cross, H., Kuhnle, S., Cubillos-Rojas, M., Matentzoglu, K., Patton, M.A., Wagner, K., Coblentz, R., Ford, D.L*., et al.* (2013). Mutation of HERC2 causes developmental delay with Angelman-like features. Journal of medical genetics *50*, 65-73.

Harper, J.W., and Tan, M.K. (2012). Understanding cullin-RING E3 biology through proteomics-based substrate identification. Mol Cell Proteomics *11*, 1541-1550.

Hassler (1937). Zur Pathologie der Paralysis agitains und postenzephalitischen Parkinsonismus. J Psychol Neurol, 387-476.

Hattori, N., Shimura, H., Kubo, S., Kitada, T., Wang, M., Asakawa, S., Minashima, S., Shimizu, N., Suzuki, T., Tanaka, K*., et al.* (2000). Autosomal recessive juvenile parkinsonism: a key to understanding nigral degeneration in sporadic Parkinson's disease. Neuropathology : official journal of the Japanese Society of Neuropathology *20 Suppl*, S85-90.

Hay, R.T. (2013). Decoding the SUMO signal. Biochem Soc Trans *41*, 463-473.

Hermand, D. (2006). F-box proteins: more than baits for the SCF? Cell division *1*, 30.

Hershko, A. (2005). The ubiquitin system for protein degradation and some of its roles in the control of the cell-division cycle (Nobel lecture). Angewandte Chemie *44*, 5932-5943.

Hershko, A., and Ciechanover, A. (1998). The ubiquitin system. Annu Rev Biochem *67*, 425-479.

Higdon, R., Reiter, L., Hather, G., Haynes, W., Kolker, N., Stewart, E., Bauman, A.T., Picotti, P., Schmidt, A., van Belle, G*., et al.* (2011). IPM: An integrated protein model for false discovery rate estimation and identification in high-throughput proteomics. J Proteomics *75*, 116-121.

Hiller, S., Garces, R.G., Malia, T.J., Orekhov, V.Y., Colombini, M., and Wagner, G. (2008). Solution structure of the integral human membrane protein VDAC-1 in detergent micelles. Science *321*, 1206-1210.

Hjerpe, R., Aillet, F., Lopitz-Otsoa, F., Lang, V., England, P., and Rodriguez, M.S. (2009). Efficient protection and isolation of ubiquitylated proteins using tandem ubiquitin-binding entities. EMBO Rep *10*, 1250-1258.

Hjerpe, R., and Rodriguez, M.S. (2008). Efficient approaches for characterizing ubiquitinated proteins. Biochem Soc Trans *36*, 823-827.

Ho, M.S., Tsai, P.I., and Chien, C.T. (2006). F-box proteins: the key to protein degradation. Journal of biomedical science *13*, 181-191.

Hsu, J.M., Lee, Y.C., Yu, C.T., and Huang, C.Y. (2004). Fbx7 functions in the SCF complex regulating Cdk1-cyclin B-phosphorylated hepatoma up-regulated protein (HURP) proteolysis by a proline-rich region. J Biol Chem *279*, 32592-32602.

Hulsen, T., de Vlieg, J., and Alkema, W. (2008). BioVenn - a web application for the comparison and visualization of biological lists using area-proportional Venn diagrams. BMC genomics *9*, 488.

Hurley, J.H., Lee, S., and Prag, G. (2006). Ubiquitin-binding domains. Biochem J *399*, 361-372.

Hutten, S., and Kehlenbach, R.H. (2007). CRM1-mediated nuclear export: to the pore and beyond. Trends Cell Biol *17*, 193-201.

Inoue, H., Nojima, H., and Okayama, H. (1990). HIGH-EFFICIENCY TRANSFORMATION OF ESCHERICHIA-COLI WITH PLASMIDS. Gene *96*.

Itier, J.M., Ibanez, P., Mena, M.A., Abbas, N., Cohen-Salmon, C., Bohme, G.A., Laville, M., Pratt, J., Corti, O., Pradier, L.*, et al.* (2003). Parkin gene inactivation alters behaviour and dopamine neurotransmission in the mouse. Hum Mol Genet *12*, 2277-2291.

Jellinger, K.A. (2003). Neuropathological spectrum of synucleinopathies. Movement disorders : official journal of the Movement Disorder Society *18 Suppl 6*, S2-12.

Jin, J., Cardozo, T., Lovering, R.C., Elledge, S.J., Pagano, M., and Harper, J.W. (2004). Systematic analysis and nomenclature of mammalian F-box proteins. Genes & development *18*, 2573-2580.

Jonkers, W., and Rep, M. (2009). Lessons from fungal F-box proteins. Eukaryotic cell *8*, 677-695.

Joseph, J., Tan, S.H., Karpova, T.S., McNally, J.G., and Dasso, M. (2002). SUMO-1 targets RanGAP1 to kinetochores and mitotic spindles. J Cell Biol *156*, 595-602.

Kato, J.Y., and Yoneda-Kato, N. (2009). Mammalian COP9 signalosome. Genes Cells *14*, 1209-1225.

Kawaguchi, Y., Okamoto, T., Taniwaki, M., Aizawa, M., Inoue, M., Katayama, S., Kawakami, H., Nakamura, S., Nishimura, M., Akiguchi, I.*, et al.* (1994). CAG expansions in a novel gene for Machado-Joseph disease at chromosome 14q32.1. Nature genetics *8*, 221-228.

Kessler, B.M. (2013). Ubiquitin - omics reveals novel networks and associations with human disease. Current opinion in chemical biology *17*, 59-65.

Kim, W., Bennett, E.J., Huttlin, E.L., Guo, A., Li, J., Possemato, A., Sowa, M.E., Rad, R., Rush, J., Comb, M.J*., et al.* (2011). Systematic and quantitative assessment of the ubiquitin-modified proteome. Mol Cell *44*, 325-340.

Kirk, R., Laman, H., Knowles, P.P., Murray-Rust, J., Lomonosov, M., Meziane el, K., and McDonald, N.Q. (2008). Structure of a conserved dimerization domain within the F-box protein Fbxo7 and the PI31 proteasome inhibitor. J Biol Chem *283*, 22325-22335.

Kirkin, V., and Dikic, I. (2011). Ubiquitin networks in cancer. Current opinion in genetics & development *21*, 21-28.

Kitada, T., Asakawa, S., Hattori, N., Matsumine, H., Yamamura, Y., Minoshima, S., Yokochi, M., Mizuno, Y., and Shimizu, N. (1998). Mutations in the parkin gene cause autosomal recessive juvenile parkinsonism. Nature *392*, 605-608.

Kitada, T., Pisani, A., Porter, D.R., Yamaguchi, H., Tscherter, A., Martella, G., Bonsi, P., Zhang, C., Pothos, E.N., and Shen, J. (2007). Impaired dopamine release and synaptic plasticity in the striatum of PINK1-deficient mice. Proc Natl Acad Sci U S A *104*, 11441-11446.

Kitada, T., Tong, Y., Gautier, C.A., and Shen, J. (2009). Absence of nigral degeneration in aged parkin/DJ-1/PINK1 triple knockout mice. J Neurochem *111*, 696-702.

Klein, C., and Westenberger, A. (2012). Genetics of Parkinson's disease. Cold Spring Harb Perspect Med *2*, a008888.

Klein, U.R., Haindl, M., Nigg, E.A., and Muller, S. (2009). RanBP2 and SENP3 function in a mitotic SUMO2/3 conjugation-deconjugation cycle on Borealin. Mol Biol Cell *20*, 410-418.

Knauer, S.K., Bier, C., Habtemichael, N., and Stauber, R.H. (2006). The Survivin-Crm1 interaction is essential for chromosomal passenger complex localization and function. EMBO Rep *7*, 1259-1265.

Komander, D. (2009). The emerging complexity of protein ubiquitination. Biochem Soc Trans *37*, 937-953.

Komander, D., and Rape, M. (2012). The ubiquitin code. Annu Rev Biochem *81*, 203-229.

Kondapalli, C., Kazlauskaite, A., Zhang, N., Woodroof, H.I., Campbell, D.G., Gourlay, R., Burchell, L., Walden, H., Macartney, T.J., Deak, M*., et al.* (2012). PINK1 is activated by mitochondrial membrane potential depolarization and stimulates Parkin E3 ligase activity by phosphorylating Serine 65. Open Biol *2*, 120080.

Kuiken, H.J., Egan, D.A., Laman, H., Bernards, R., Beijersbergen, R.L., and Dirac, A.M. (2012). Identification of F-box only protein 7 as a negative regulator of NF-kappaB signalling. Journal of cellular and molecular medicine *16*, 2140-2149.

Laman, H. (2006). Fbxo7 gets proactive with cyclin D/cdk6. Cell cycle *5*, 279-282.

Laman, H., Funes, J.M., Ye, H., Henderson, S., Galinanes-Garcia, L., Hara, E., Knowles, P., McDonald, N., and Boshoff, C. (2005). Transforming activity of Fbxo7 is mediated specifically through regulation of cyclin D/cdk6. Embo J *24*, 3104-3116.

Latif, F., Tory, K., Gnarra, J., Yao, M., Duh, F.M., Orcutt, M.L., Stackhouse, T., Kuzmin, I., Modi, W., Geil, L.*, et al.* (1993). Identification of the von Hippel-Lindau disease tumor suppressor gene. Science *260*, 1317-1320.

Lee, Y., Dawson, V.L., and Dawson, T.M. (2012). Animal models of Parkinson's disease: vertebrate genetics. Cold Spring Harb Perspect Med *2*.

Leroy, E., Boyer, R., Auburger, G., Leube, B., Ulm, G., Mezey, E., Harta, G., Brownstein, M.J., Jonnalagada, S., Chernova, T.*, et al.* (1998). The ubiquitin pathway in Parkinson's disease. Nature *395*, 451-452.

Lewy, F. (1912). In Handbuch der Neurologie, M. Lewandowsky, ed. (Berlin: Springer), pp. 920-933.

Li, T., Pavletich, N.P., Schulman, B.A., and Zheng, N. (2005). High-level expression and purification of recombinant SCF ubiquitin ligases. Methods Enzymol *398*, 125-142.

Li, W., Bengtson, M.H., Ulbrich, A., Matsuda, A., Reddy, V.A., Orth, A., Chanda, S.K., Batalov, S., and Joazeiro, C.A. (2008). Genome-wide and functional annotation of human E3 ubiquitin ligases identifies MULAN, a mitochondrial E3 that regulates the organelle's dynamics and signaling. PLoS One *3*, e1487.

Li, Y., and Hao, B. (2010). Structural basis of dimerization-dependent ubiquitination by the SCF(Fbx4) ubiquitin ligase. J Biol Chem *285*, 13896-13906.

Lin, C.H., Chen, M.L., Lai, T.T., Tai, C.H., and Wu, R.M. (2013). Mutational analysis of FBXO7 gene in Parkinson's disease in a Taiwanese population. Neurobiology of aging *34*, 1713 e1711-1714.

Linden, M., Gellerfors, P., and Nelson, B.D. (1982). Pore protein and the hexokinase-binding protein from the outer membrane of rat liver mitochondria are identical. FEBS Lett *141*, 189-192.

Lipkowitz, S., and Weissman, A.M. (2011). RINGs of good and evil: RING finger ubiquitin ligases at the crossroads of tumour suppression and oncogenesis. Nature reviews Cancer *11*, 629-643.

Litterman, N., Ikeuchi, Y., Gallardo, G., O'Connell, B.C., Sowa, M.E., Gygi, S.P., Harper, J.W., and Bonni, A. (2011). An OBSL1-Cul7Fbxw8 ubiquitin ligase signaling mechanism regulates Golgi morphology and dendrite patterning. PLoS Biol *9*, e1001060.

Lorick, K.L., Jensen, J.P., Fang, S., Ong, A.M., Hatakeyama, S., and Weissman, A.M. (1999). RING fingers mediate ubiquitin-conjugating enzyme (E2)-dependent ubiquitination. Proc Natl Acad Sci U S A *96*, 11364-11369.

Lu, T., Jackson, M.W., Wang, B., Yang, M., Chance, M.R., Miyagi, M., Gudkov, A.V., and Stark, G.R. (2010). Regulation of NF-kappaB by NSD1/FBXL11-dependent reversible lysine methylation of p65. Proc Natl Acad Sci U S A *107*, 46-51.

Lucking, C.B., Durr, A., Bonifati, V., Vaughan, J., De Michele, G., Gasser, T., Harhangi, B.S., Meco, G., Denefle, P., Wood, N.W*., et al.* (2000). Association between early-onset Parkinson's disease and mutations in the parkin gene. The New England journal of medicine *342*, 1560-1567.

Luo, L.Z., Xu, Q., Guo, J.F., Wang, L., Shi, C.H., Wei, J.H., Long, Z.G., Pan, Q., Tang, B.S., Xia, K*., et al.* (2010). FBXO7 gene mutations may be rare in Chinese early-onset Parkinsonism patients. Neuroscience letters *482*, 86-89.

Lyapina, S., Cope, G., Shevchenko, A., Serino, G., Tsuge, T., Zhou, C., Wolf, D.A., Wei, N., and Deshaies, R.J. (2001). Promotion of NEDD-CUL1 conjugate cleavage by COP9 signalosome. Science *292*, 1382-1385.

Malzac, P., Webber, H., Moncla, A., Graham, J.M., Kukolich, M., Williams, C., Pagon, R.A., Ramsdell, L.A., Kishino, T., and Wagstaff, J. (1998). Mutation analysis of UBE3A in Angelman syndrome patients. American journal of human genetics *62*, 1353-1360.

Mannella, C.A. (1982). Structure of the outer mitochondrial membrane: ordered arrays of porelike subunits in outer-membrane fractions from Neurospora crassa mitochondria. J Cell Biol *94*, 680-687.

Maquat, L.E. (2005). Nonsense-mediated mRNA decay in mammals. J Cell Sci *118*, 1773-1776.

Margolin, A.A., Ong, S.E., Schenone, M., Gould, R., Schreiber, S.L., Carr, S.A., and Golub, T.R. (2009). Empirical Bayes analysis of quantitative proteomics experiments. PLoS One *4*, e7454.

Marygold, S.J., Leyland, P.C., Seal, R.L., Goodman, J.L., Thurmond, J., Strelets, V.B., and Wilson, R.J. (2013). FlyBase: improvements to the bibliography. Nucleic acids research *41*, D751-757.

Massano, J., and Bhatia, K.P. (2012). Clinical approach to Parkinson's disease: features, diagnosis, and principles of management. Cold Spring Harb Perspect Med *2*, a008870.

Masuya, H., Inoue, M., Wada, Y., Shimizu, A., Nagano, J., Kawai, A., Inoue, A., Kagami, T., Hirayama, T., Yamaga, A*., et al.* (2005). Implementation of the modified-SHIRPA protocol for screening of dominant phenotypes in a large-scale ENU mutagenesis program. Mamm Genome *16*, 829-837.

Meierhofer, D., Wang, X., Huang, L., and Kaiser, P. (2008). Quantitative analysis of global ubiquitination in HeLa cells by mass spectrometry. J Proteome Res *7*, 4566-4576.

Metzger, D., and Chambon, P. (2001). Site- and time-specific gene targeting in the mouse. Methods *24*, 71-80.

Metzger, M.B., Hristova, V.A., and Weissman, A.M. (2012). HECT and RING finger families of E3 ubiquitin ligases at a glance. J Cell Sci *125*, 531-537.

Moldovan, G.L., and D'Andrea, A.D. (2009). How the fanconi anemia pathway guards the genome. Annual review of genetics *43*, 223-249.

Monville, C., Torres, E.M., and Dunnett, S.B. (2006). Comparison of incremental and accelerating protocols of the rotarod test for the assessment of motor deficits in the 6-OHDA model. J Neurosci Methods *158*, 219-223.

Moreland, J.L., Gramada, A., Buzko, O.V., Zhang, Q., and Bourne, P.E. (2005). The Molecular Biology Toolkit (MBT): a modular platform for developing molecular visualization applications. BMC Bioinformatics *6*, 21.

Morens, D.M., Grandinetti, A., Reed, D., White, L.R., and Ross, G.W. (1995). Cigarette smoking and protection from Parkinson's disease: false association or etiologic clue? Neurology *45*, 1041-1051.

Morgenstern, J.P., and Land, H. (1990). ADVANCED MAMMALIAN GENE-TRANSFER - HIGH TITER RETROVIRAL VECTORS WITH MULTIPLE-DRUG SELECTION MARKERS AND A COMPLEMENTARY HELPER-FREE PACKAGING CELL-LINE. Nucleic Acids Research *18*.

Nagy, A. (2000). Cre recombinase: the universal reagent for genome tailoring. Genesis *26*, 99-109.

Nalepa, G., Rolfe, M., and Harper, J.W. (2006). Drug discovery in the ubiquitin-proteasome system. Nature reviews Drug discovery *5*, 596-613.

Narendra, D., Walker, J.E., and Youle, R. (2012). Mitochondrial quality control mediated by PINK1 and Parkin: links to parkinsonism. Cold Spring Harb Perspect Biol *4*.

Narendra, D.P., Jin, S.M., Tanaka, A., Suen, D.F., Gautier, C.A., Shen, J., Cookson, M.R., and Youle, R.J. (2010). PINK1 is selectively stabilized on impaired mitochondria to activate Parkin. PLoS Biol *8*, e1000298.

Nelson, D.E., and Laman, H. (2011). A Competitive binding mechanism between Skp1 and exportin 1 (CRM1) controls the localization of a subset of F-box proteins. J Biol Chem *286*, 19804-19815.

Nelson, D.E., Randle, S.J., and Laman, H. (2013). Beyond ubiquitination: the atypical functions of Fbxo7 and other F-box proteins. Open Biol *3*, 130131.

Nichols, R.J., Dzamko, N., Morrice, N.A., Campbell, D.G., Deak, M., Ordureau, A., Macartney, T., Tong, Y., Shen, J., Prescott, A.R*., et al.* (2010). 14-3-3 binding to LRRK2 is disrupted by multiple Parkinson's disease-associated mutations and regulates cytoplasmic localization. Biochem J *430*, 393-404.

Ohta, A., Schumacher, F.R., Mehellou, Y., Johnson, C., Knebel, A., Macartney, T.J., Wood, N.T., Alessi, D.R., and Kurz, T. (2013). The CUL3-KLHL3 E3 ligase complex mutated in Gordon's hypertension syndrome interacts with and ubiquitylates WNK isoforms: disease-causing mutations in KLHL3 and WNK4 disrupt interaction. Biochem J *451*, 111-122.

Olanow, C.W., and McNaught, K.S. (2006). Ubiquitin-proteasome system and Parkinson's disease. Movement disorders : official journal of the Movement Disorder Society *21*, 1806-1823.

Osaka, H., Wang, Y.L., Takada, K., Takizawa, S., Setsuie, R., Li, H., Sato, Y., Nishikawa, K., Sun, Y.J., Sakurai, M*., et al.* (2003). Ubiquitin carboxy-terminal hydrolase L1 binds to and stabilizes monoubiquitin in neuron. Hum Mol Genet *12*, 1945-1958.

Paisan-Ruiz, C., Bhatia, K.P., Li, A., Hernandez, D., Davis, M., Wood, N.W., Hardy, J., Houlden, H., Singleton, A., and Schneider, S.A. (2009). Characterization of PLA2G6 as a locus for dystonia-parkinsonism. Annals of neurology *65*, 19-23.

Paisan-Ruiz, C., Guevara, R., Federoff, M., Hanagasi, H., Sina, F., Elahi, E., Schneider, S.A., Schwingenschuh, P., Bajaj, N., Emre, M.*, et al.* (2010). Early-onset L-dopa-responsive parkinsonism with pyramidal signs due to ATP13A2, PLA2G6, FBXO7 and spatacsin mutations. Movement disorders : official journal of the Movement Disorder Society *25*, 1791-1800.

Paisan-Ruiz, C., Jain, S., Evans, E.W., Gilks, W.P., Simon, J., van der Brug, M., Lopez de Munain, A., Aparicio, S., Gil, A.M., Khan, N.*, et al.* (2004). Cloning of the gene containing mutations that cause PARK8-linked Parkinson's disease. Neuron *44*, 595-600.

Pankratz, N., Pauciulo, M.W., Elsaesser, V.E., Marek, D.K., Halter, C.A., Wojcieszek, J., Rudolph, A., Shults, C.W., Foroud, T., and Nichols, W.C. (2006). Mutations in DJ-1 are rare in familial Parkinson disease. Neuroscience letters *408*, 209-213.

Park, J., Lee, S.B., Lee, S., Kim, Y., Song, S., Kim, S., Bae, E., Kim, J., Shong, M., Kim, J.M.*, et al.* (2006). Mitochondrial dysfunction in Drosophila PINK1 mutants is complemented by parkin. Nature *441*, 1157-1161.

Parkinson, J. (2002). An essay on the shaking palsy. 1817. The Journal of neuropsychiatry and clinical neurosciences *14*, 223-236; discussion 222.

Parsons, J.L., Tait, P.S., Finch, D., Dianova, II, Edelmann, M.J., Khoronenkova, S.V., Kessler, B.M., Sharma, R.A., McKenna, W.G., and Dianov, G.L. (2009). Ubiquitin ligase ARF-BP1/Mule modulates base excision repair. Embo J *28*, 3207-3215.

Pelzer, C., Kassner, I., Matentzoglu, K., Singh, R.K., Wollscheid, H.P., Scheffner, M., Schmidtke, G., and Groettrup, M. (2007). UBE1L2, a novel E1 enzyme specific for ubiquitin. J Biol Chem *282*, 23010-23014.

Peng, J., Schwartz, D., Elias, J.E., Thoreen, C.C., Cheng, D., Marsischky, G., Roelofs, J., Finley, D., and Gygi, S.P. (2003). A proteomics approach to understanding protein ubiquitination. Nat Biotechnol *21*, 921-926.

Periquet, M., Latouche, M., Lohmann, E., Rawal, N., De Michele, G., Ricard, S., Teive, H., Fraix, V., Vidailhet, M., Nicholl, D.*, et al.* (2003). Parkin mutations are frequent in patients with isolated early-onset parkinsonism. Brain : a journal of neurology *126*, 1271-1278.

Pettan-Brewer, C., and Treuting, P.M. (2011). Practical pathology of aging mice. Pathobiol Aging Age Relat Dis *1*.

Pichler, A., Gast, A., Seeler, J.S., Dejean, A., and Melchior, F. (2002). The nucleoporin RanBP2 has SUMO1 E3 ligase activity. Cell *108*, 109-120.

Pickart, C.M. (2001). Mechanisms underlying ubiquitination. Annu Rev Biochem *70*, 503-533.

Polymeropoulos, M.H., Higgins, J.J., Golbe, L.I., Johnson, W.G., Ide, S.E., Di Iorio, G., Sanges, G., Stenroos, E.S., Pho, L.T., Schaffer, A.A.*, et al.* (1996). Mapping of a gene for Parkinson's disease to chromosome 4q21-q23. Science *274*, 1197-1199.

Polymeropoulos, M.H., Lavedan, C., Leroy, E., Ide, S.E., Dehejia, A., Dutra, A., Pike, B., Root, H., Rubenstein, J., Boyer, R.*, et al.* (1997). Mutation in the alpha-synuclein gene identified in families with Parkinson's disease. Science *276*, 2045-2047.

Poole, A.C., Thomas, R.E., Yu, S., Vincow, E.S., and Pallanck, L. (2010). The mitochondrial fusion-promoting factor mitofusin is a substrate of the PINK1/parkin pathway. PLoS One *5*, e10054.

Puffenberger, E.G., Jinks, R.N., Wang, H., Xin, B., Fiorentini, C., Sherman, E.A., Degrazio, D., Shaw, C., Sougnez, C., Cibulskis, K.*, et al.* (2012). A homozygous missense mutation in HERC2 associated with global developmental delay and autism spectrum disorder. Human mutation *33*, 1639-1646.

Ramirez, A., Heimbach, A., Grundemann, J., Stiller, B., Hampshire, D., Cid, L.P., Goebel, I., Mubaidin, A.F., Wriekat, A.L., Roeper, J.*, et al.* (2006). Hereditary parkinsonism with dementia is caused by mutations in ATP13A2, encoding a lysosomal type 5 P-type ATPase. Nature genetics *38*, 1184-1191.

Ramser, J., Ahearn, M.E., Lenski, C., Yariz, K.O., Hellebrand, H., von Rhein, M., Clark, R.D., Schmutzler, R.K., Lichtner, P., Hoffman, E.P.*, et al.* (2008). Rare missense and synonymous variants in UBE1 are associated with X-linked infantile spinal muscular atrophy. American journal of human genetics *82*, 188-193.

Rao, D.S., Chang, J.C., Kumar, P.D., Mizukami, I., Smithson, G.M., Bradley, S.V., Parlow, A.F., and Ross, T.S. (2001). Huntingtin interacting protein 1 Is a clathrin coat binding protein required for differentiation of late spermatogenic progenitors. Mol Cell Biol *21*, 7796-7806.

Redman, K.L., and Rechsteiner, M. (1989). Identification of the long ubiquitin extension as ribosomal protein S27a. Nature *338*, 438-440.

Rose, I. (2005). Ubiquitin at Fox Chase (Nobel lecture). Angewandte Chemie *44*, 5926-5931.

Ross, C.A., and Poirier, M.A. (2004). Protein aggregation and neurodegenerative disease. Nature medicine *10 Suppl*, S10-17.

Rostovtseva, T., and Colombini, M. (1997). VDAC channels mediate and gate the flow of ATP: implications for the regulation of mitochondrial function. Biophys J *72*, 1954-1962.

Rotin, D., and Kumar, S. (2009). Physiological functions of the HECT family of ubiquitin ligases. Nature reviews Molecular cell biology *10*, 398-409.

Samaranch, L., Lorenzo-Betancor, O., Arbelo, J.M., Ferrer, I., Lorenzo, E., Irigoyen, J., Pastor, M.A., Marrero, C., Isla, C., Herrera-Henriquez, J.*, et al.* (2010). PINK1-linked parkinsonism is associated with Lewy body pathology. Brain : a journal of neurology *133*, 1128-1142.

Sanchez, I., Hughes, R.T., Mayer, B.J., Yee, K., Woodgett, J.R., Avruch, J., Kyriakis, J.M., and Zon, L.I. (1994). ROLE OF SAPK/ERK KINASE-1 IN THE STRESS-ACTIVATED PATHWAY REGULATING TRANSCRIPTION FACTOR C-JUN. Nature *372*.

Sarraf, S.A., Raman, M., Guarani-Pereira, V., Sowa, M.E., Huttlin, E.L., Gygi, S.P., and Harper, J.W. (2013). Landscape of the PARKIN-dependent ubiquitylome in response to mitochondrial depolarization. Nature *496*, 372-376.

Scaglione, K.M., Zavodszky, E., Todi, S.V., Patury, S., Xu, P., Rodriguez-Lebron, E., Fischer, S., Konen, J., Djarmati, A., Peng, J.*, et al.* (2011). Ube2w and ataxin-3 coordinately regulate the ubiquitin ligase CHIP. Mol Cell *43*, 599-612.

Schneider, S.A., Paisan-Ruiz, C., Quinn, N.P., Lees, A.J., Houlden, H., Hardy, J., and Bhatia, K.P. (2010). ATP13A2 mutations (PARK9) cause neurodegeneration with brain iron accumulation. Movement disorders : official journal of the Movement Disorder Society *25*, 979-984.

Schulman, B.A., Carrano, A.C., Jeffrey, P.D., Bowen, Z., Kinnucan, E.R., Finnin, M.S., Elledge, S.J., Harper, J.W., Pagano, M., and Pavletich, N.P. (2000). Insights into SCF ubiquitin ligases from the structure of the Skp1-Skp2 complex. Nature *408*, 381-386.

Schwab, M.E. (2010). Functions of Nogo proteins and their receptors in the nervous system. Nat Rev Neurosci *11*, 799-811.

Seibler, P., Graziotto, J., Jeong, H., Simunovic, F., Klein, C., and Krainc, D. (2011). Mitochondrial Parkin recruitment is impaired in neurons derived from mutant PINK1 induced pluripotent stem cells. The Journal of neuroscience : the official journal of the Society for Neuroscience *31*, 5970-5976.

Shang, J., Wang, G., Yang, Y., Huang, X., and Du, Z. (2013). Expression, purification and crystallization of the FP domain of the human F-box protein Fbxo7. Acta crystallographica Section F, Structural biology and crystallization communications *69*, 1097-1099.

Shimizu, S., Narita, M., and Tsujimoto, Y. (1999). Bcl-2 family proteins regulate the release of apoptogenic cytochrome c by the mitochondrial channel VDAC. Nature *399*, 483-487.

Shin, J.H., Ko, H.S., Kang, H., Lee, Y., Lee, Y.I., Pletinkova, O., Troconso, J.C., Dawson, V.L., and Dawson, T.M. (2011). PARIS (ZNF746) repression of PGC-1alpha contributes to neurodegeneration in Parkinson's disease. Cell *144*, 689-702.

Shojaee, S., Sina, F., Banihosseini, S.S., Kazemi, M.H., Kalhor, R., Shahidi, G.A., Fakhrai-Rad, H., Ronaghi, M., and Elahi, E. (2008). Genome-wide linkage analysis of a Parkinsonian-pyramidal syndrome pedigree by 500 K SNP arrays. American journal of human genetics *82*, 1375-1384.

Sievers, F., Wilm, A., Dineen, D., Gibson, T.J., Karplus, K., Li, W., Lopez, R., McWilliam, H., Remmert, M., Soeding, J.*, et al.* (2011). Fast, scalable generation of high-quality protein multiple sequence alignments using Clustal Omega. Molecular Systems Biology *7*.

Singh, B.B., Patel, H.H., Roepman, R., Schick, D., and Ferreira, P.A. (1999). The zinc finger cluster domain of RanBP2 is a specific docking site for the nuclear export factor, exportin-1. J Biol Chem *274*, 37370-37378.

Singleton, A.B., Farrer, M., Johnson, J., Singleton, A., Hague, S., Kachergus, J., Hulihan, M., Peuralinna, T., Dutra, A., Nussbaum, R.*, et al.* (2003). alpha-Synuclein locus triplication causes Parkinson's disease. Science *302*, 841.

Singleton, A.B., Farrer, M.J., and Bonifati, V. (2013). The genetics of Parkinson's disease: progress and therapeutic implications. Movement disorders : official journal of the Movement Disorder Society *28*, 14-23.

Skaar, J.R., D'Angiolella, V., Pagan, J.K., and Pagano, M. (2009a). SnapShot: F Box Proteins II. Cell *137*, 1358, 1358 e1351.

Skaar, J.R., D'Angiolella, V., Pagan, J.K., and Pagano, M. (2009b). SnapShot: F Box Proteins II. Cell *137*, 1358-U1100.

Skaar, J.R., Pagan, J.K., and Pagano, M. (2009c). SnapShot: F box proteins I. Cell *137*, 1160-1160 e1161.

Skaar, J.R., Pagan, J.K., and Pagano, M. (2013). Mechanisms and function of substrate recruitment by F-box proteins. Nature reviews Molecular cell biology *14*, 369-381.

Soucy, T.A., Smith, P.G., Milhollen, M.A., Berger, A.J., Gavin, J.M., Adhikari, S., Brownell, J.E., Burke, K.E., Cardin, D.P., Critchley, S.*, et al.* (2009). An inhibitor of NEDD8-activating enzyme as a new approach to treat cancer. Nature *458*, 732-736.

Spangler, S.A., and Hoogenraad, C.C. (2007). Liprin-alpha proteins: scaffold molecules for synapse maturation. Biochem Soc Trans *35*, 1278-1282.

Spillantini, M.G., Schmidt, M.L., Lee, V.M., Trojanowski, J.Q., Jakes, R., and Goedert, M. (1997). Alpha-synuclein in Lewy bodies. Nature *388*, 839-840.

Tan, F., Lu, L., Cai, Y., Wang, J., Xie, Y., Wang, L., Gong, Y., Xu, B.E., Wu, J., Luo, Y.*, et al.* (2008). Proteomic analysis of ubiquitinated proteins in normal hepatocyte cell line Chang liver cells. Proteomics *8*, 2885-2896.

Tanaka, A., Cleland, M.M., Xu, S., Narendra, D.P., Suen, D.F., Karbowski, M., and Youle, R.J. (2010). Proteasome and p97 mediate mitophagy and degradation of mitofusins induced by Parkin. J Cell Biol *191*, 1367-1380.

Tatham, M.H., Rodriguez, M.S., Xirodimas, D.P., and Hay, R.T. (2009). Detection of protein SUMOylation in vivo. Nat Protoc *4*, 1363-1371.

Taylor, T.N., Greene, J.G., and Miller, G.W. (2010). Behavioral phenotyping of mouse models of Parkinson's disease. Behav Brain Res *211*, 1-10.

Tieu, K. (2011). A guide to neurotoxic animal models of Parkinson's disease. Cold Spring Harb Perspect Med *1*, a009316.

Trinkle-Mulcahy, L., Boulon, S., Lam, Y.W., Urcia, R., Boisvert, F.M., Vandermoere, F., Morrice, N.A., Swift, S., Rothbauer, U., Leonhardt, H.*, et al.* (2008). Identifying specific protein interaction partners using quantitative mass spectrometry and bead proteomes. J Cell Biol *183*, 223-239.

Udeshi, N.D., Mani, D.R., Eisenhaure, T., Mertins, P., Jaffe, J.D., Clauser, K.R., Hacohen, N., and Carr, S.A. (2012). Methods for quantification of in vivo changes in protein ubiquitination following proteasome and deubiquitinase inhibition. Mol Cell Proteomics *11*, 148-159.

Udeshi, N.D., Svinkina, T., Mertins, P., Kuhn, E., Mani, D.R., Qiao, J.W., and Carr, S.A. (2013). Refined preparation and use of anti-diglycine remnant (K-epsilon-GG) antibody enables routine quantification of 10,000s of ubiquitination sites in single proteomics experiments. Mol Cell Proteomics *12*, 825-831.

Ujwal, R., Cascio, D., Colletier, J.P., Faham, S., Zhang, J., Toro, L., Ping, P., and Abramson, J. (2008). The crystal structure of mouse VDAC1 at 2.3 A resolution reveals mechanistic insights into metabolite gating. Proc Natl Acad Sci U S A *105*, 17742-17747.

Valente, E.M., Abou-Sleiman, P.M., Caputo, V., Muqit, M.M., Harvey, K., Gispert, S., Ali, Z., Del Turco, D., Bentivoglio, A.R., Healy, D.G.*, et al.* (2004). Hereditary early-onset Parkinson's disease caused by mutations in PINK1. Science *304*, 1158-1160.

Vasilescu, J., Smith, J.C., Ethier, M., and Figeys, D. (2005). Proteomic analysis of ubiquitinated proteins from human MCF-7 breast cancer cells by immunoaffinity purification and mass spectrometry. J Proteome Res *4*, 2192-2200.

Vertegaal, A.C. (2011). Uncovering ubiquitin and ubiquitin-like signaling networks. Chemical reviews *111*, 7923-7940.

Vijay-Kumar, S., Bugg, C.E., and Cook, W.J. (1987). Structure of ubiquitin refined at 1.8 A resolution. Journal of molecular biology *194*, 531-544.

Von Coelln, R., Thomas, B., Savitt, J.M., Lim, K.L., Sasaki, M., Hess, E.J., Dawson, V.L., and Dawson, T.M. (2004). Loss of locus coeruleus neurons and reduced startle in parkin null mice. Proc Natl Acad Sci U S A *101*, 10744-10749.

Wagner, S.A., Beli, P., Weinert, B.T., Nielsen, M.L., Cox, J., Mann, M., and Choudhary, C. (2011). A proteome-wide, quantitative survey of in vivo ubiquitylation sites reveals widespread regulatory roles. Mol Cell Proteomics *10*, M111 013284.

Wang, H., Qian, W.J., Chin, M.H., Petyuk, V.A., Barry, R.C., Liu, T., Gritsenko, M.A., Mottaz, H.M., Moore, R.J., Camp Ii, D.G.*, et al.* (2006). Characterization of the mouse brain proteome using global proteomic analysis complemented with cysteinyl-peptide enrichment. J Proteome Res *5*, 361-369.

Wang, X., Winter, D., Ashrafi, G., Schlehe, J., Wong, Y.L., Selkoe, D., Rice, S., Steen, J., LaVoie, M.J., and Schwarz, T.L. (2011). PINK1 and Parkin target Miro for phosphorylation and degradation to arrest mitochondrial motility. Cell *147*, 893-906.

Waterhouse, A.M., Procter, J.B., Martin, D.M., Clamp, M., and Barton, G.J. (2009a). Jalview Version 2--a multiple sequence alignment editor and analysis workbench. Bioinformatics *25*, 1189-1191.

Waterhouse, A.M., Procter, J.B., Martin, D.M.A., Clamp, M., and Barton, G.J. (2009b). Jalview Version 2-a multiple sequence alignment editor and analysis workbench. Bioinformatics *25*, 1189-1191.

Waterston, R.H., Lindblad-Toh, K., Birney, E., Rogers, J., Abril, J.F., Agarwal, P., Agarwala, R., Ainscough, R., Alexandersson, M., An, P.*, et al.* (2002). Initial sequencing and comparative analysis of the mouse genome. Nature *420*, 520-562.

Wauer, T., and Komander, D. (2013). Structure of the human Parkin ligase domain in an autoinhibited state. Embo J *32*, 2099-2112.

Welcker, M., and Clurman, B.E. (2008). FBW7 ubiquitin ligase: a tumour suppressor at the crossroads of cell division, growth and differentiation. Nature reviews Cancer *8*, 83-93.

Wenzel, D.M., Lissounov, A., Brzovic, P.S., and Klevit, R.E. (2011). UBCH7 reactivity profile reveals parkin and HHARI to be RING/HECT hybrids. Nature *474*, 105-108.

Werner, A., Flotho, A., and Melchior, F. (2012). The RanBP2/RanGAP1*SUMO1/Ubc9 complex is a multisubunit SUMO E3 ligase. Mol Cell *46*, 287-298.

Wertz, I.E., and Dixit, V.M. (2010). Signaling to NF-kappaB: regulation by ubiquitination. Cold Spring Harb Perspect Biol *2*, a003350.

Whitby, F.G., Xia, G., Pickart, C.M., and Hill, C.P. (1998). Crystal structure of the human ubiquitin-like protein NEDD8 and interactions with ubiquitin pathway enzymes. J Biol Chem *273*, 34983-34991.

Wilkins, M.R., Gasteiger, E., Bairoch, A., Sanchez, J.C., Williams, K.L., Appel, R.D., and Hochstrasser, D.F. (1999). Protein identification and analysis tools in the ExPASy server. Methods Mol Biol *112*, 531-552.

Winston, J.T., Koepp, D.M., Zhu, C., Elledge, S.J., and Harper, J.W. (1999). A family of mammalian F-box proteins. Current biology : CB *9*, 1180-1182.

Wu, G., Xu, G., Schulman, B.A., Jeffrey, P.D., Harper, J.W., and Pavletich, N.P. (2003). Structure of a beta-TrCP1-Skp1-beta-catenin complex: destruction motif binding and lysine specificity of the SCF(beta-TrCP1) ubiquitin ligase. Mol Cell *11*, 1445-1456.

Wu, J., Lee, S.W., Zhang, X., Han, F., Kwan, S.Y., Yuan, X., Yang, W.L., Jeong, Y.S., Rezaeian, A.H., Gao, Y.*, et al.* (2013a). Foxo3a transcription factor is a negative regulator of Skp2 and Skp2 SCF complex. Oncogene *32*, 78-85.

Wu, J., Matunis, M.J., Kraemer, D., Blobel, G., and Coutavas, E. (1995). Nup358, a cytoplasmically exposed nucleoporin with peptide repeats, Ran-GTP binding sites, zinc fingers, a cyclophilin A homologous domain, and a leucine-rich region. J Biol Chem *270*, 14209-14213.

Wu, S., Zhu, W., Nhan, T., Toth, J.I., Petroski, M.D., and Wolf, D.A. (2013b). CAND1 controls in vivo dynamics of the cullin 1-RING ubiquitin ligase repertoire. Nat Commun *4*, 1642.

Xia, C., Ma, W., Stafford, L.J., Liu, C., Gong, L., Martin, J.F., and Liu, M. (2003). GGAPs, a new family of bifunctional GTP-binding and GTPase-activating proteins. Mol Cell Biol *23*, 2476-2488.

Xu, G., Paige, J.S., and Jaffrey, S.R. (2010). Global analysis of lysine ubiquitination by ubiquitin remnant immunoaffinity profiling. Nat Biotechnol *28*, 868-873.

Xu, J. (2005). Preparation, culture, and immortalization of mouse embryonic fibroblasts. Curr Protoc Mol Biol *Chapter 28*, Unit 28 21.

Y, B.Y.H. (1995). Controlling the False Discovery Rate: A practical and powerful approach to multiple testing. Journal of the Royal Statistical Soeciety *57*, 289-300.

Yang, Y., Gehrke, S., Imai, Y., Huang, Z., Ouyang, Y., Wang, J.W., Yang, L., Beal, M.F., Vogel, H., and Lu, B. (2006). Mitochondrial pathology and muscle and dopaminergic neuron degeneration caused by inactivation of Drosophila Pink1 is rescued by Parkin. Proc Natl Acad Sci U S A *103*, 10793-10798.

Yang, Y., Lorick, K.L., Jensen, J.P., and Weissman, A.M. (2005). Expression and evaluation of RING finger proteins. Methods Enzymol *398*, 103-112.

Ye, Y., and Rape, M. (2009). Building ubiquitin chains: E2 enzymes at work. Nature reviews Molecular cell biology *10*, 755-764.

Yen, H.C., and Elledge, S.J. (2008). Identification of SCF ubiquitin ligase substrates by global protein stability profiling. Science *322*, 923-929.

Yen, H.C., Xu, Q., Chou, D.M., Zhao, Z., and Elledge, S.J. (2008). Global protein stability profiling in mammalian cells. Science *322*, 918-923.

Yokoyama, N., Hayashi, N., Seki, T., Pante, N., Ohba, T., Nishii, K., Kuma, K., Hayashida, T., Miyata, T., Aebi, U*., et al.* (1995). A giant nucleopore protein that binds Ran/TC4. Nature *376*, 184-188.

Yoshida, Y., Murakami, A., and Tanaka, K. (2011). Skp1 stabilizes the conformation of F-box proteins. Biochem Biophys Res Commun *410*, 24-28.

Young, M.J., Bay, D.C., Hausner, G., and Court, D.A. (2007). The evolutionary history of mitochondrial porins. BMC Evol Biol *7*, 31.

Yumimoto, K., Matsumoto, M., Oyamada, K., Moroishi, T., and Nakayama, K.I. (2012). Comprehensive Identification of Substrates for F-box Proteins by Differential Proteomics Analysis. J Proteome Res.

Zalman, L.S., Nikaido, H., and Kagawa, Y. (1980). Mitochondrial outer membrane contains a protein producing nonspecific diffusion channels. J Biol Chem *255*, 1771-1774.

Zhao, T., De Graaff, E., Breedveld, G.J., Loda, A., Severijnen, L.A., Wouters, C.H., Verheijen, F.W., Dekker, M.C., Montagna, P., Willemsen, R*., et al.* (2011). Loss of nuclear activity of the FBXO7 protein in patients with parkinsonian-pyramidal syndrome (PARK15). PLoS One *6*, e16983.

Zhao, T., Severijnen, L.A., van der Weiden, M., Zheng, P.P., Oostra, B.A., Hukema, R.K., Willemsen, R., Kros, J.M., and Bonifati, V. (2013). FBXO7 immunoreactivity in alpha-synuclein-containing inclusions in Parkinson disease and multiple system atrophy. Journal of neuropathology and experimental neurology *72*, 482-488.

Zheng, N., Schulman, B.A., Song, L., Miller, J.J., Jeffrey, P.D., Wang, P., Chu, C., Koepp, D.M., Elledge, S.J., Pagano, M*., et al.* (2002). Structure of the Cul1-Rbx1-Skp1-F boxSkp2 SCF ubiquitin ligase complex. Nature *416*, 703-709.

Zhou, H., Falkenburger, B.H., Schulz, J.B., Tieu, K., Xu, Z., and Xia, X.G. (2007). Silencing of the Pink1 gene expression by conditional RNAi does not induce dopaminergic neuron death in mice. Int J Biol Sci *3*, 242-250.

Zimprich, A., Biskup, S., Leitner, P., Lichtner, P., Farrer, M., Lincoln, S., Kachergus, J., Hulihan, M., Uitti, R.J., Calne, D.B.*, et al.* (2004). Mutations in LRRK2 cause autosomal-dominant parkinsonism with pleomorphic pathology. Neuron *44*, 601-607.